JUSTUS-LIEBIG-UNIVERSITÄT GIESSEN

Spatiotemporal initiation and assembly dynamics of polar flagellation in γ-proteobacteria

Dissertation
to attain the degree Doktor rer. nat.

Carried to completion at

Faculty 8 - Biology and Chemistry

Institute of Microbiology and Molecular Biology

Justus-Liebig-University, Gießen

Presented by

John Christopher Hook

Gießen, 01.07.2022

„The peak of attained achievements

is yet another departure

to future triumphs."

-J.C.H.

Abstract

Bacterial motility, more precisely bacterial flagellation, is an extremely complex topic due to the plethora of mechanisms and factors involved in the precise assembly and functioning of flagellar structures. This high complexity in part originates in various flagellation patterns employed by different bacterial species, with some possessing randomly positioned flagellar structures, while others position their flagella in a targeted fashion at the cell pole. A factor, which is essential for this spatially constricted positioning of flagellar structures occurring in many bacterial species, is the SRP-GTPase FlhF. This factor has, in a multitude of publications, been established as the prime element in determining the construction site of the flagellum, as it arrives at the site of flagellar assembly prior to other structural components of the flagellum and the loss of FlhF leads to a randomly positioned flagellar structure. While the positioning of the flagellum has always been attributed to FlhF, the targeting mechanism, utilised by FlhF, to reach the cell pole, has not been determined. This study aimed to shed a light on this insufficiently analysed stage in the establishment process of flagella meditated motility. In line with this goal a novel factor named FipA, which governs the polar targeting behaviour of FlhF through direct interaction in a partially co-dependent manner, was discovered in *Shewanella putrefaciens* CN-32 and *Pseudomonas putida* KT2440. Here FipA is presumed to anchor FlhF at the cell pole through its predicted N-terminal transmembrane domain, while the C-terminal domain of FipA, comprising a DUF2802 domain, appears to interact with the N-terminal B-domain of FlhF. Due to the variability of the FlhF B-domain in different bacterial species and the observed differences in FipA functioning between the monotrichously flagellated *Shewanella putrefaciens* CN-32 and lophotrichously flagellated *Pseudomonas putida* KT2440, this interaction is postulated to account for variations in flagellation occurring in different bacterial species. Additionally, the ability of FipA to interact C-terminally with the C-terminal region of FlhF and the absence of interaction in the context of a FlhF variants, which are incapable of homodimerizing with their C-terminal G-domain, implies FipA requiring FlhF homodimerization prior to FlhF/FipA interaction. Here the ability to interact in this terminus configuration, while FipA also is able to interact with the N-terminal region of FlhG, which contains the activator helix, required for the induction of the FlhF GTPase activity, points towards an additional involvement of FipA in not just the polar recruitment of FlhF but also the disbanding of the FlhF homodimer.

Besides elucidating the mechanisms and factors involved in the initiation phase of flagellar assembly, this study focused on characterising a unique C-terminal motif in the flagellar type 3 secretion system component FlhB in *Shewanella putrefaciens* CN-32 [1]. In the flagellar assembly process FlhB is essential for the export of extracellular flagellum components and, besides, together with FliK, being involved in the determination of the hook length, enables an

export switching from hook associated proteins to filament associated proteins upon hook completion. This switch in export specificity occurs due to autocleavage of the cytoplasmic domain of FlhB, designated as FlhB-C, into the two distinct subdomains FlhB-CN and FlhB-CC. The peculiar motif characterised in this study is positioned in FlhB-CC and distinguishes itself through a high proline density, which is why it was appropriately named "Proline Rich Region" or in short PRR. Through the gathered data it was possible to determine the FlhB PRR an element, which influences hook assembly, the ability of FlhB-C to perform autocleavage and, by enabling an efficient export of filament subunits, the process of filament assembly. While phases downstream from the construction of the basal section of the flagellum, appear affected by the loss of the PRR, the general stability and formation of the C-ring indicated by FliM, unlike in the case of complete *flhB* deletion, is not affected. With the PRR motif being conserved in the FlhB of many β- and γ-proteobacteria, it presents itself as a factor, which enables the efficient assembly of extracellular substructures of the flagellum, while at the same time supporting the ability of FlhB to autocleave.

Zusammenfassung

Bakterielle Motilität, präziser gesagt die bakterielle Flagellierung, ist ein äußerst komplexes Thema, da eine Vielzahl von Mechanismen und Faktoren am korrekten Aufbau und der Funktion der Flagellenstruktur beteiligt sind. Diese hohe Komplexität ist zum Teil auf die unterschiedlichen Flagellierungsmuster, welche von verschiedenen Bakterienarten ausgeprägt werden, zurückzuführen, von denen Einige zufällig angeordnete Flagellen besitzen, während andere ihre Flagellen gezielt am Zellpol positionieren. Ein Faktor, welcher bei vielen Bakterienarten für diese präzise räumliche Positionierung der Flagelle verantwortlich ist, ist die SRP-GTPase FlhF. Dieses Protein wurde in einer Vielzahl von Publikationen als Hauptelement bei der Bestimmung des Assemblierungsortes der Flagelle identifiziert, da er vor anderen strukturellen Komponenten der Flagelle an den späteren Ort der Flagellenassemblierung rekrutiert wird und der Verlust von FlhF zu zufällig positionierten Flagellen führt. Während die Positionierung der Flagelle stets FlhF zugeschrieben wurde, war der Mechanismus, mit welchem FlhF den Zellpol erreicht, nicht bekannt. Ziel dieser Arbeit war es, diese bisher ungenügend untersuchte Phase im Entstehungsprozess der durch Flagellen-vermittelten Motilität zu untersuchen. Hierbei wurde ein neuartiger Faktor, welchem der Name FipA gegeben wurde, der das polare Zielverhalten von FlhF durch direkte Interaktion in einer zum Teil co-abhängigen Weise steuert, in *Shewanella* putrefaciens CN-32 und *Pseudomonas putida* KT2440 entdeckt. Hierbei wird angenommen, dass FipA FlhF durch seine mit bioinformatischen Methoden vorhergesagte N-terminale Transmembrandomäne am Zellpol verankert, während die C-terminale Domäne von FipA, welche eine DUF2802-Domäne beinhaltet, vermutlich mit der B-Domäne von FlhF interagiert. Aufgrund der Variabilität der B-Domäne von FlhF in verschiedenen Bakterienspezies, und der beobachteten Unterschiede in der Funktionsweise von FipA zwischen dem monotrich flagellierten Bakterium *Shewanella putrefaciens* CN-32 und dem lophotrich flagellierten Bakterium *Pseudomonas putida* KT2440, wird angenommen, dass diese Interaktion für die Variationen in der Flagellierung verschiedener Bakterienarten verantwortlich ist. Die Fähigkeit von FipA, C-terminal mit der C-terminalen Region von FlhF zu interagieren, und das Ausbleiben der Interaktion im Zusammenhang mit FlhF-Varianten, welche aufgrund von Aminosäure Substitutionen in der C-terminalen G-Domäne von FlhF nicht mehr homodimerisieren können, deutet darauf hin, dass FlhF homodimerisieren muss bevor eine Interaktion mit FipA stattfinden kann. Die Fähigkeit, in dieser Terminuskonfiguration zu interagieren, während FipA auch in der Lage ist, mit dem N-terminalen Bereich von FlhG zu interagieren, welcher die *activator helix* enthält, die für die Induktion der GTPase-Aktivität von FlhF erforderlich ist, deutet auf eine zusätzliche Beteiligung von FipA nicht nur an der polaren Rekrutierung von FlhF, sondern auch an der Auflösung des FlhF-Homodimers durch FlhG hin.

Neben der Ergründung von Mechanismen und Faktoren, welche an der Initiationsphase der Flagellenassemblierung beteiligt sind, fokussierte sich diese Arbeit auf die Charakterisierung eines bestimmten C-terminalen Motivs in der *flagellar type 3 secretion system*-Komponente FlhB in *Shewanella putrefaciens* CN-32 (Hook et al., 2020). FlhB ist für den Export von Bausteinen der extrazellulär positionierten Flagellenabschnitte essenziell und ermöglicht, zusammen mit FliK, welches an der Bestimmung der Hakenlänge beteiligt ist, nach der Fertigstellung des Hakens, eine Umstellung des Exports von hakenassoziierten Proteinen auf filamentassoziierte Proteine. Dieser Wechsel der Exportspezifität erfolgt durch Selbstspaltung der zytoplasmatischen Domäne von FlhB, welche auch als FlhB-C bezeichnet wird, in die zwei unterschiedlichen Subdomänen FlhB-CN und FlhB-CC. Das in dieser Studie charakterisierte Motiv befindet sich in FlhB-CC und zeichnet sich durch eine hohe Prolin-Dichte aus, weshalb es "*Proline Rich Region*" oder kurz PRR genannt wurde. Durch die in dieser Studie akkumulierten Daten wurde die PRR von FlhB als ein Element bestimmt, welches die Hakenassemblierung, die Fähigkeit von FlhB-C zur Selbstspaltung und, durch die Ermöglichung eines effizienten Exports von Filamentuntereinheiten, den Prozess der Filamentassemblierung beeinflusst. Während Phasen, welche dem Aufbau des basalen Abschnitts des Flagellums folgen, durch den Verlust des PRR beeinträchtigt zu sein scheinen, sind die allgemeine Stabilität und die Bildung des C-Rings, welcher durch FliM angezeigt wird, anders als im Fall einer vollständigen Deletion von *flhB*, nicht betroffen. Da das PRR-Motiv im FlhB vieler β- und γ-Proteobakterien konserviert ist, stellt es einen Faktor dar, der den effizienten Aufbau der extrazellulären Substrukturen der Flagelle ermöglicht und gleichzeitig die Fähigkeit von FlhB zur Selbstspaltung unterstützt.

Table of contents

Statement of authorship

I declare that I have completed this dissertation with the title

"Spatiotemporal initiation and assembly dynamics of polar flagellation in γ-proteobacteria"

single-handedly without the unauthorized help of a second party and only with the assistance acknowledged therein. I have appropriately acknowledged and cited all text passages that are derived verbatim from or are based on the content of published work of others, and all information relating to verbal communications. I consent to the use of an anti-plagiarism software to check my thesis. I have abided by the principles of good scientific conduct laid down in the charter of the Justus-Liebig-University Giessen „Satzung der Justus-Liebig-Universität Gießen zur Sicherung guter wissenschaftlicher Praxis" in carrying out the investigations described in the dissertation.

_____   _____

Date   Signature

1. Introduction

1.1 <u>Targeted motility – a hallmark of life</u>

Of all the characteristics, which define life, motility, even if it is the most obvious and easily observable, does not stand behind any of the other life defining traits, when it comes to complexity. The mechanisms, which result in movement, span from tightly regulated motility factors on a molecular level to the intricate interaction of muscles and tendons perceivable in macroscopic eukaryotes [2]. An important aspect, when it comes to defining motility as a trait associated with life, is that it does not occur randomly through diffusion, but in a targeted demeanour mandated by internal or external stimuli. The ability to wilfully direct locomotion, through the use of motility structures, enables organisms to move away from unfavourable conditions towards more favourable ones ensuring optimised survival and therefore clearly presenting itself as a skill beneficial in avoiding natural selection on an individual and ultimately evolutionary scale [3].

1.2 <u>Motility in bacteria</u>

Bacteria, being one of the earliest organisms to appear on earth, have had a long time to accommodate a plethora of independent motility mechanisms enabling them to move over surfaces or in liquid or semisolid environments. To achieve optimal mobility, these motility methods are employed in accordance with the dominantly occurring physical parameters set by each individual environmental situation, leading to them mostly differing from each other in both speed and utilised motility structure. The modes of motility available to prokaryotes include swimming, swarming, twitching and gliding, with most organisms, due to heterogeneous habitats, possessing the ability to perform multiple kinds of locomotion, enabling them to seamlessly adapt to a changing environment [4–6]. The determination of favourable or unfavourable conditions is achieved through the use of various kinds of bacterial taxis including chemotaxis, phototaxis, thermotaxis, aerotaxis and magnetotaxis [7–13]. Untargeted motility through diffusion or sliding motility, caused by the displacement of cells due to population growth, appears for untethered cells of every bacterial species, as these means of translocation do not require specialised structures or the additional expenditure of energy [4].

When in contact with solid or semisolid surfaces, prokaryotes either employ twitching, gliding or swarming motility to translocate, with the motility modes significantly differing in required motility machinery. Twitching motility, often occurring prior to biofilm formation, requires the use of Type IV pili, which are supramolecular motility and adherence structures traversing the

cell envelope and therefore extending beyond the cell body. They are able to extended from the cell body up to a length of 10 μm in the desired direction of movement until surface contact occurs and then retracted resulting in the cell being dragged along, with a continuous repetition of this leading to cells reaching speeds of up to 1 μm per second [14,15]. In detail, the Type IV pilus comprises 12 - 15 proteins, being divided into proteins required for the structural assembly and proteins involved in the extension and retraction of the pilus [16]. Among the major proteins involved in pilus architecture are PilC and PilM, forming the cytoplasmic base, which in turn is targeted by either of the two ATPases PilB or PilT. These are required for the extension and retraction of the pilus, with PilB being the factor, which polymerises and PilT being the factor which depolymerises the pilus under ATP hydrolysis. The pilus itself is composed from multiple PilA copies, sourced from a pool of membrane bound PilA, which are processed by the prepilin peptidase PilD, enabling polymerization. The nascent pilus, measuring approximately 6 nm in diameter, is then channelled through periplasmic structures consisting of PilF, PilN, PilO and PilP, to ultimately extend beyond the spatial confinements of the cell through the outer membrane pore formed by PilQ.

Another mode of motility employed in conjunction with surface interaction is gliding motility, which does not require extracellular motility structures stretching far from the cell body, but rather relies on cell envelope associated factors forming focal adhesion points to the substratum and moving the cell along its own axis in a helical fashion through the interaction with the cytoskeletal structure of the cell body [17]. The underlying molecular mechanism consists of the GTP-bound G-protein MglA, belonging to the Ras superfamily of proteins, interacting with the bacterial actin MreB at the leading cell pole. This interaction in turn leads to the formation of the Agl-Glt motility complex [18]. This supramolecular complex, which interacts with MreB bound MglA, is subdivided into the Agl and the Glt subcomplex, with the Agl subcomplex consisting of AglR, being a homolog to MotA, and AglQ and AglS, being homologs to MotB. Together the complex formed by the Agl proteins forms a proton channel between the periplasmic space and the cytosol. The Glt subcomplex, which functions as the gliding transducer, in itself is subdivided into a cytoplasmic-inner membrane subcomplex, consisting of GltI, GltG and GltJ, and a periplasmic-outer membrane subcomplex, consisting of GltD, GltE, GltF, GltK, GltB, GltA, GltC and GltH [19]. The motility mechanism functions through proton motive force (PMF) induced activation of the Agl motor complex, leading to a conformational change of the periplasmic GltG proteins, which then are able to stretch through the periplasm and cell wall to interact with the periplasmic-outer membrane associated Glt complex [20]. Upon interaction the GltG protein retracts, pulling the entire Agl-Glt motility complex, excluding the periplasmic-outer membrane Glt subcomplex, with it along the cell envelope. After continuously repeating this process, the entire complex moves away from the

leading cell pole and reaches the area of the cell lying in direct contact with the underlying surface. This causes the periplasmic-outer membrane Glt subcomplex to form a so-called focal adhesion point, which locks the subcomplex in place and offers the remaining Agl-Glt complex a location to push itself off from [18,21]. Due to the Agl-Glt complex being bound to the bacterial cytoskeleton through MreB, the translocation along the focal adhesion forming periplasmic-outer membrane Glt subcomplex leads to the entire cell body being pushed along the cell axis in a helical, screw-like motion [22]. Once the Agl-Glt complex reaches the lagging cell pole, MglB induces the GTPase activity of the GTP bound MglA, which in turn leads to the dissociation of GDP bound MglA from the cell pole and therefore breaking the link between the Agl-Glt protein complex and the cytoskeleton of the cell. This causes the Agl-Glt complex to be disbanded at the lagging cell pole, freeing up the complex to be reassembled at the leading cell pole. The extrusion of polysaccharides has been observed as being beneficial for gliding motility in some bacterial species, as they possibly coat the interaction surface and therefore offer an anchor point for cell surface adhesins [23,24].

Swarming motility is employed by many bacterial species when contacting solid or semisolid surfaces and usually occurs when transitioning from a planktonic to a surface associated lifestyle. It differs from other surface associated modes of locomotion in that it requires flagellation, which is increased by the surface contact [25–27]. This increase is believed to originate in the rising drag enacted by the surface on the main flagellar system, which activates a feedback loop leading to the assembly of more flagellar structures [28]. These additionally constructed flagella, which in some species are separately expressed and regulated from the mainly utilised flagellar system, enable cells to reach speeds of up to 10 µm per second and therefore mark swarming as one of the fastest surface associated types of motility. An additionally morphological characteristic observed in swarming cells is an elongation of individual cell bodies and an overall increase in cell population. When transferring from a motility style associated with a liquid environment to surface associated swarming motility, cells usually form multicellular rafts, consisting of cells contacting each other and causing intercellular bundling of flagella. Expulsion and incorporation of cells into the raft occurs dynamically with the expulsion from such a raft usually leading to discontinued locomotion, while incorporated cells synchronize their speed and heading with that of the raft [29]. Another important aspect of swarming motility is the often-occurring secretion of surfactants preceding the cells at the leading edge of the raft and reducing the overall friction between the cells in the raft and the surface on which it moves.

Apart from twitching, gliding, and swarming, being mostly surface associated motility styles, swimming motility is employed by bacteria in planktonic phase, when facing semisolid or aquatic environments [30]. Swimming enables bacteria to rapidly change their position in a three-

dimensional manner to adapt to the highly dynamic nutritional situation faced, when populating an aquatic habitat. Just like swarming, which occurs as a successive motility style to swimming, a flagellar system is required for cellular propulsion in a liquid environment. To achieve propulsion the flagellum is rotated in either a counterclockwise (CCW) or clockwise (CW) direction, resulting in, as seen from the leading cell pole, forward or backward motion, respectively, indicating the ability for swimming reversal without having to realign the leading pole's position [31,32]. With liquid habitats being highly diverse in for example viscosity and to which degree they are influenced by external factors, different bacterial species have adapted varying swimming strategies to suit their habitational needs. Enteric bacteria, such as *E. coli*, which possesses multiple flagella randomly spread across the envelope of the cell body, employ the so-called run-and-tumble strategy, which enables them to reach speeds of up to 20 µm per second [33]. This strategy is based on the flagella rotating in a CCW fashion, enabling directional movement, which is sequentially interrupted by the flagella changing their rotational direction to CW leading to a tumbling motion, enabling the bacterial cell to reorient its leading cell pole and therefore swimming direction. In the case of this swimming strategy, the run time and tumble frequency are influenced by the chemotaxis system, as an increase in attractant density leads to longer run times and an increased occurrence of repellents leads to more frequent tumbling [34–37]. Many marine bacteria, due to their environment presenting different challenges, such as increased turbulence inside the water body influenced by atmospheric and gravitational factors, employ a technique different from that of enteric bacteria. This approach consists of the bacteria intermittently stopping and reversing, being describable as a stop-and-go style of swimming motility. The employment of this swimming strategy enables swimming speeds of up to 200 µm per second, equipping marine bacteria with the ability to traverse, considering the scale, large distances in a short time. In certain cases this swimming style is accompanied by a hydrodynamically induced buckling of the flagellum when rotational direction of the flagellum is changed, resulting in a slight reorientation of the cell [38]. Swimming in semi solid environments poses the threat of coming across confined spaces capable of trapping bacteria. To counter this many bacterial species are able to wrap their flagellum around their cell body enabling them to reverse out of the confinement and therefore demonstrate the bacterial flagellum as a highly dynamic and versatile motility structure enabling swimming in different environmental situations [39].

1.3 <u>Flagellation in prokaryotes</u>

With being essential in delivering propulsion for many motility styles and therefore enabling bacteria to manoeuvre and survive in a plethora of different habitats, the flagellum is one of

the most important and extensively studied supramolecular structures formed by prokaryotes. Flagellation occurs in both morphologically and numerically highly diverse configurations, with some bacteria such as spirochaetes possessing a periplasmic endoflagellum [40]. This endoflagellum allows individual cells to invade semisolid substrates such as tissue and therefore presents itself as a pathogenicity factor. Flagella reaching into the extracellular space, being the most common configuration of flagellar structures, also fulfil this function, as they enable bacteria to actively colonise liquid filled cavities [41,42].

Flagellation pattern	Flagellation model	Exemplary electron micrographs
monotrichous		*Vibrio parahaemolyticus*
lophotrichous		*Pseudomonas putida*
amphitrichous		*Campylobacter jejuni*
peritrichous		*Lactobacillus capilatus*
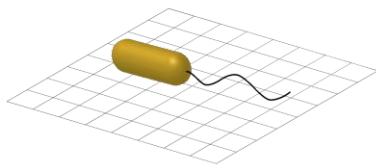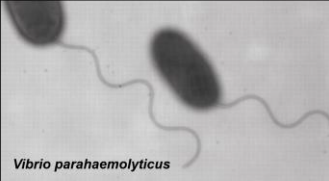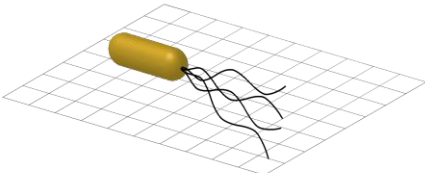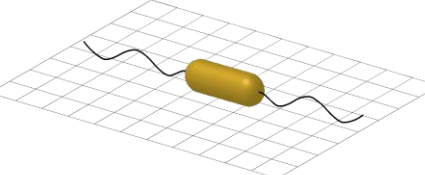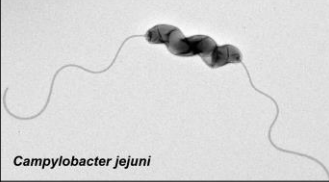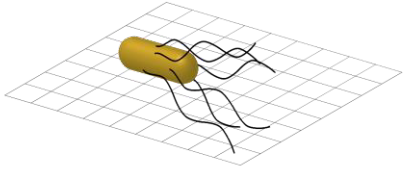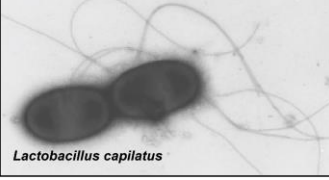
Figure 1. Bacterial flagellation patterns with exemplary micrographs and organisms. Electron micrographs sourced from [43], [44], [45], [46]

The positioning and number of flagella extending from the cell body in itself also is highly diverse, as cells are able to precisely or randomly position either a single flagellum or multiple flagella on the cell body, with individual bacterial species possessing the capacity to express different flagellation styles to perform optimised locomotion in their current environment. Flagellation patterns include monotrichous flagellation, being characterised by a targeted or untargeted positioned single flagellum, amphitrichous flagellation, describing the flagellation pattern of a single flagellum at each cell pole, lophotrichous flagellation, being defined as the formation of a polar tuft of multiple flagella, and peritrichous flagellation, representing the random positioning of multiple flagella along the body of the cell (**Figure 1**) [47,48]. The individual

flagella are powered by an ion gradient, which in flagellar systems associated with swarming motility often is powered by PMF and in flagellar systems used for planktonic swimming motility often is powered by a Na^+ gradient [49,50].

1.4 <u>Structure of the bacterial flagellum</u>

Structurally the flagellum is composed of a helical filament revolved by a rotary motor which is anchored in the cell envelope. Its macrostructure can be broken up into three structural sections consisting of the flagellar base, the cell envelope traversing rod and the extracellularly positioned hook and filament (**Figure 2**).

This overall flagellar macrostructure, consisting of these three substructures, is the same for all bacterial species, with them individually varying in the complexity of the rod, due to the differences in the envelope composition of gram-positive and gram-negative bacteria [51]. Endoflagella, observable in gram-negative spirochaetes, possess a similar rod structure to gram-positive bacteria, due to the endoflagellum only having to pass the inner membrane and the peptidoglycan layer, while not penetrating the outer membrane. Unlike extracellularly positioned flagella, endoflagella do not only function as a structure conferring locomotion, but rather govern cell morphology by bestowing a screw like form on the body of the cell through direct contact with cell membrane and due to the endoflagellum being stiffer than the cell membrane [52–54]. When analysing the bacterial flagellum in the context of targeted positioning at the cell pole, it is important to note that other factors situated in the polar vicinity of the cell are integral for efficient flagellar assembly and targeted motility. One such component playing an important role in flagellar assembly, which also is vital for the assembly of other polar structures and cell segregation, is the polar landmark protein HubP or the orthologously functioning motility hub protein FimV [55–59]. Both proteins, which are anchored to the cell pole through transmembrane domains, are essential for the recruitment of many polar factors and the stabilisation of the polar landscape. Additionally, they assist in chromosome separation, which taken together makes them indispensable for establishment of polar identity and organisation [55,58]. An additional pole integrated structure, of high relevance for effective motility, is the chemotaxis system, which through the utilisation of its components CheA, CheB and CheY, is able to directly influence the rotational direction of the flagellum and therefore can trigger a reorientation of swimming direction [60].
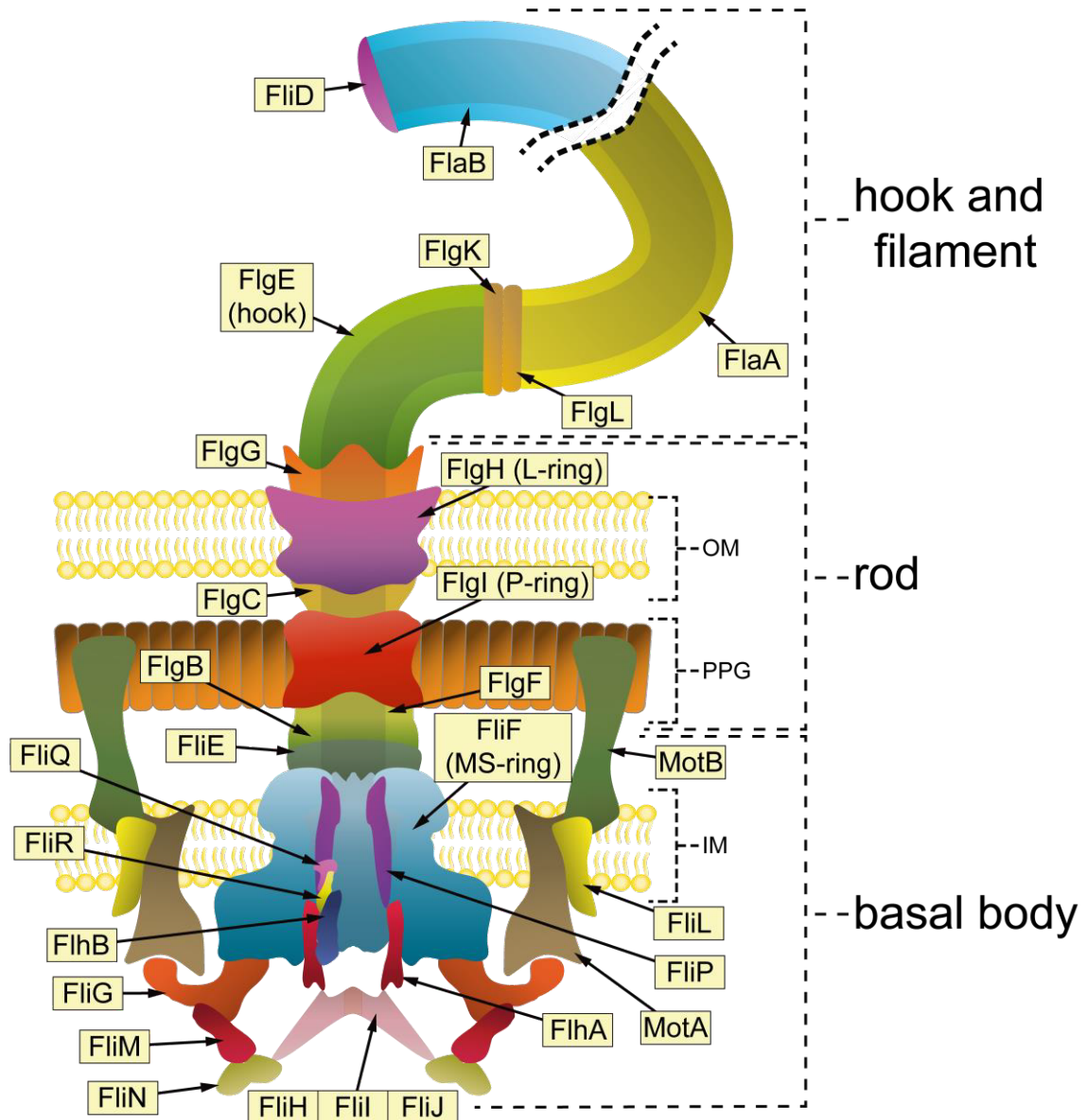
Figure 2. Model of bacterial flagellum (gram-negative) with individually annotated structural proteins. OM = outer membrane, PPG = peptidoglycan layer; IM = inner membrane.

1.4.1 Basal body – flagellar export machinery and torque generator

The flagellar basal body, being the first substructure formed during flagellar assembly, is the most complex unit of the bacterial flagellum as it contains the bi-directional flagellar motor, with its rotor and stator, and the secretion machinery for the export of envelope spanning and extracellular flagellum components [61–65]. More precisely, it consists of the rotor forming MS- and C-ring, with the MotA/MotB motor torque generating complex being the stator and the flagellar type III export gate complex, which possesses striking similarities, both in sequence and function, to the bacterial injectisome [66,67]. The MS-ring, being at the centre of the basal body structure and also the first unit of the basal body to appear, self-assembles out of multiple

copies of the protein FliF, of which the number varies, depending on C-ring composition [68]. The FliF protein contains a periplasmic region enclosed by two trans-membrane domains (TMD) [65]. It forms a two tiered trans-membrane ring (MS-ring), containing the S-ring, which sits on the top of the MS-ring and extends into the periplasm and the M-ring, which is embedded into the inner membrane [69,70]. As the name suggests, the inside of the MS-ring contains an empty space, which forms a pore allowing the passage of flagellar components required for rod, hook and filament assembly. Besides the MS-ring, the cytoplasmic C-ring is part of the rotor complex, which transfers torque to the final flagellar structure and is essential for switching of the rotational direction. It is attached to the MS-ring at its cytoplasmic interface through the interaction of FliF and the C-ring component FliG [71–73]. FliG incorporates three domains $FliG_N$, $FliG_M$ and $FliG_C$, of which the N-terminal $FliG_N$-domain strongly interacts with the C-terminus of FliF and therefore indirectly anchors the C-ring to the cell membrane [74]. The $FliG_M$ and $FliG_C$-domains, both located at the top of the C-ring, are essential for the interaction with FliM, whereas the $FliG_C$-domain plays an important role in the switching of the motor direction [73,75–78]. FliM, through its C-terminal domain, $FliM_C$, forms a complex with tetrameric FliN, which together form the bulk of the C-ring [79]. This complex also appears as the docking point for the phosphorylated chemotaxis signalling factor CheY ($CheY^P$), which binds the intermediary FliM domain ($FliM_M$). This then enables an interaction of $CheY^P$ with FliN, which, through a conformational change of the C-ring, induces a motor reversal from CCW to CW [80,81]. Beside the rotor, the stator, comprising MotA and MotB, is an essential part for motor rotation. Here the C-terminal domain of MotB ($MotB_C$) due to its linkage with the peptidoglycan layer, appears as the anchor of the MotAB stator complex [82]. The complex is linked to the C-ring through the C-terminal cytoplasmic domain of MotA ($MotA_C$) which electrostatically interacts with $FliG_C$, allowing the transfer of torque. For the generation of torque, proton translocation from the periplasm to the cytoplasm is utilised, which induces a conformational change in $MotA_C$ and then enables MotA to transfer the generated torque to the C-ring associated $FliG_C$ and therefore the entire flagellar structure [83,84]. Here an essential component, required for stator assembly, is the integral membrane protein FliL which is assumed to act as a kind of scaffold, assisting efficient MotAB stator complex assembly and function, while it also interacts with the basal body [85,86]. An additional part of the overall basal body essential for the export of rod, hook and filament subunits, is the flagellar type III secretion system (fT3SS) housed in the intrastructural pore formed by the MS-ring. The apparatus itself encompasses two substructures, those being the PMF-powered transmembrane export gate complex containing the structural proteins FlhA, FlhB, FliP, FliQ and FliR and a cytoplasmic ATPase ring-like complex being composed of the structural proteins FliH, FliI and FliJ [87,88]. The protein FliO, even if it is not a structural part of the final export gate complex, appears to only function as a non-essential scaffold on which FliP can form a hexameric ring structure, required for the

recruitment of FliQ, FliR and FlhB. To embed the export gate complex, now consisting of a hexameric FliP-ring, FliQ, FliR and FlhB, in the central pore of the MS-ring, FlhA forms a nonameric ring, which facilitates the structural unification of the export gate complex with the MS-ring [89]. An essential part of the fT3SS is the protein FlhB, which facilitates the switch from hook to filament substrate export during flagellar assembly [90]. FlhB consists of a transmembrane domain interacting with the FliPQR complex and a cytoplasmic domain (FlhB-C) containing a self-cleavage motif required for substrate specificity switching [91,92]. The export of proteins through the export gate complex appears to be coupled with the influx of protons suggesting that the PMF-driven export gate complex functions as a proton-protein antiporter [93]. The export machinery appears to mainly require PMF for the export of proteins, as the ATPase ring-like complex, containing the ATPase FliI, and its two regulators FliH and FliJ, seems to not be essential for the translocation of flagellar components, when the PMF is high enough [94]. The cytoplasmic ATPase ring-like complex rather seems to function as an activator of the export gate complex proton channel, formed by the proteins FlhA and FliP, and therefore enables efficient antiporting of protons and flagellar proteins through the hydrolysis of ATP [95–97]. An essential basal body associated component required for the transfer of force from the rotor/stator complex to the subsequent rod structure, and ultimately the hook and filament, is FliE, which forms a linker section between the MS-ring, through the interaction with FliF, and the subsequent proximal rod section composed of FlgB [98,99]. The intermediately positioned section associated with FliE, being positioned on the periplasmic side of the MS-ring, interacts with components of the export machinery, aiding the export of further flagellar components, due to it being the first protein aggregating at a proximal position relative to the MS-ring [100].

1.4.2   Rod – transmitter of rotational force

The cell envelope traversing flagellar rod functions as a drive shaft transferring torque generated by the basal body to the hook and ultimately filament in the fully assembled flagellum. Besides transferring mechanical energy through the cell envelope, it also serves as a channel through which proteins of flagellar substructures situated distal from the basal body, such as components of the nascent rod, hook and filament are transported. The rod itself, as with all proteins incorporated into the flagellar structure at a position distal from the basal body, requires the utilisation of the fT3SS for the assembly of its central structure [87]. The proximal rod structure as viewed from the basal body is composed of oligomeric FlgB, which has been reported to interact with FliE. Structurally it is presumed to be followed by a FlgF and then FlgC oligomer under the use of FlgJ, which through its muramidase activity allows peptidoglycan penetration of the nascent rod [101,102]. The rod structure ultimately is finalised with FlgG, being the most abundant rod protein, and due to coprecipitating with the hook

structure, has been defined as the distal component of the flagellar rod bordering on the extracellular hook [100,103,104]. The actual formation of a rod like structure has been proposed to be the result of a cooperative process of polymerizing rod components after the addition of FlgF [69]. The rod in itself is nestled into two distinct ring-like structures being the periplasmic P-ring, consisting of FlgI, and the outer-membrane L-ring, consisting of FlgH, with both of the rings acting as bushings for the rotating rod structure and therefore stabilising it in the cell envelope. FlgI and FlgH presumably are present in their respective cell envelope layer prior to rod assembly and form their individual ring-like structures once the central rod structure is complete. Unlike the other rod components FlgB, FlgC, FlgF and FlgG, the P- and L-ring components, FlgI and FlgH, respectively, do not require the fT3SS for export, but rather rely on a signal-dependant pathway [105,106]. The completed rod substructure is capped with a FlgD oligomer, which additionally functions as a cap for the subsequent flagellar hook.

1.4.3 Hook and filament – extracellular propeller and rudder

The flagellar hook and filament form the extracellular segment of the flagellum, where they together function as a screw-like propeller that both enacts force on the cells environment resulting in propulsion and at the same time functions as a rudder steering the cell through its heterogeneous habitat [107–109]. The hook operates as a universal joint which transfers motor torque from the basal body and subsequent rod to the filament, while its curved hollow structure allows the passage of hook and filament associated proteins. A crucial property of the flagellar hook, which allows it to function as a universal joint, is the ability to be flexible when bending but rigid against twisting forces, resulting in optimal physical properties to function as a torque transferring component for locomotion in a diverse environment [110,111]. These physical properties are presumed to be the result of the domain structure inside of the hook subunit FlgE, which through its loose arrangement allows a certain amount of flexibility [112]. FlgE is exported under the utilisation of the fT3SS and integrated into the nascent hook substructure from the distal end and not, like in the case of pilus extension, from the proximal end [113]. As the hook is constructed successive to the distal rod, FlgE directly interacts with the distal rod component FlgG, with both the distal rod and the hook possessing a similar subunit arrangement [114,115]. Here the rod cap, composed of FlgD, also is utilised as a capping structure by the nascent hook and falls off once the required hook length has been reached [116]. Hook length is controlled by both the fT3SS protein FlhB and the protein FliK functioning as a molecular ruler, which signal hook completion once a length of approximately 55 nm has been reached [114,117]. To transition between the hook and filament, which structurally differ from each other, the hook-filament junction structure composed of FlgK, on the hook side, and FlgL, on the filament side, is integrated into the nascent extracellular substructure of the flagellum [103].

The filament, comprising tens of thousands of flagellin subunits, presents itself as a heteromorphic supercoiled structure, which allows it to operate as a helical propeller, able to alter its pitch and handedness according to the utilised motility mode. Different organisms vary in their filament composition, as it in some species is composed of only one kind of flagellin (FliC), while others possess flagellar filaments composed of different kinds of flagellins (minor flagellin = FlaA, major flagellin = FlaB), which are incorporated into the filament in varying stoichiometries. In this case, the proximal section of the filament is constructed from a different flagellin than the distal filament section, giving the entire filament distinct physical properties and therefore allowing it to perform as more than a rotor under specific environmental conditions [39]. Due to the filament also being the largest substructure of the flagellum, the flagellins constitute the bulk of flagellar proteins. The filament substructure, just like the hook, possesses an internal channel and is polymerised from the distal end, at which it retains the filament cap composed of FliD. Unlike FlgD, which only is utilised during flagellar assembly and functions as a scaffold for the nascent hook, FliD is a structural component indefinitely incorporated into the flagellum and, through it functioning as a scaffold, is essential for filament polymerisation [118]. To reach the distal tip of the filament, flagellin monomers, exported via the fT3SS, diffuse through the narrow central channel at the core of the flagellum, and are incorporated into the nascent filament to form a long helical structure [119,120]. Filament growth is ultimately halted by the decreasing rate at which flagellin subunits reach the tip of the growing filament through diffusion [121]. Another factor in which bacterial species differ, when it comes to the flagellar structure, is that they either possess a sheathed or unsheathed flagellum [122]. A sheathed flagellum is defined by the extracellular section of the flagellum being enclosed in an extrusion of the outer membrane, which grows synchronously with the hook and filament. The function of the sheath has not been fully elucidated but is it thought to be involved in surface adherence or host immune response modulation through evasion or LPS-induced overstimulation [122–125].

1.5 <u>FlhF and FlhB in the context of the flagellar assembly mechanism</u>

Besides the static components which make up the flagellar structure, the dynamic mechanisms and factors involved in its construction are of grave importance when analysing bacterial flagellation.

In many bacterial species the signal recognition particle (SRP)-GTPase FlhF is an essential factor involved in the initiation of flagellar assembly through the specifically targeted determination of the assembly start site at the cytoplasmic membrane [126]. Additionally, FlhF

has been observed to influence the expression of flagellar genes, which cumulatively leads to a strongly inhibited motility phenotype that is accompanied by the spatially and numerically randomised occurrence of flagellar structures along the cell body on the single cell level [127–129]. Together with FtsY and Ffh, which function as regulators for the cotranslational insertion of proteins into the cell membrane, FlhF is grouped in the SRP GTPase subfamily, which in itself is categorised under the SIMIBI class of nucleotide triphosphate (NTP)-binding proteins [130–134]. Purification results and the analysis of the crystal structure of FlhF revealed it to either be present as a GDP-bound monomer or a stable GTP-bound homodimer, unlike the SRP-GTPases FtsY and Ffh, which form a heterodimer with each other [135]. The homodimer of FlhF contains one GTP per FlhF and an equal amount of Mg^{2+} ions to aid the GTPase activity. FlhF can be subdivided into three functionally distinct domains, those being the N-terminal B-domain, the intermediate N-domain, and the C-terminal G-domain (**Figure 3**) [135]. The N-terminally situated basic B-domain presents itself in a natively unfolded form and besides being predicted as playing a role in the regulation of GTP dependant homodimerization of FlhF, through interaction with the G-domain, is presumed to contain species-specific functions due its variability between FlhF homologs in different bacterial species. For flagellar assembly the function of the FlhF B-domain appears to be centred on recruiting the MS-ring component FliF to the cell pole for the initiation of basal body construction [136]. Additional in-house studies have shown the B-domain, or rather individual sections, to also be involved in overall protein stability and the localisation of FlhF to the cell pole (unpublished data). The conserved N-domain of FlhF comprising 4 α-helices (N1-4) is situated at an intermediate position in the protein sequence of FlhF and besides being involved in the polar targeting of FlhF is assumed to regulate overall FlhF protein function, such as stabilising the GTP bound state through structurally being positioned adjacent to the similarly conserved G-domain [137–139]. The C-terminal G-domain, together with the N-domain, possesses significant homologies to the domain counterparts in FtsY and FfH indicating the conservation of this structural protein composition inside the family of SRP-GTPases. A feature, which distinguishes the G-domain from the other FlhF domains, is the presence of conserved nucleotide-binding elements (G1-5), indicated by their individual conserved amino acid sequences, and its GTPase activity. These conserved nucleotide-binding elements, also called loops due to their orientation inside the protein structure, have mostly been characterised for G-domains of the other SRP-GTPases. Due to the homology, they are predicted to be essential for transferring FlhF into its active state for which it requires the formation of a GTP bound homodimer. They are subdivided into the G1-loop also called P-loop (phosphate-binding loop), which facilitates main chain hydrogen bonding interactions with the α-, β- and γ-phosphate groups of GTP, followed by the G2-loop, which contains an arginine finger, required for the stimulation of GTPase activity, and, together with the G1-loop, binds the γ-phosphate group of GTP [140]. Additionally

the G2-loop, together with the following G3-loop and the G1-loop, coordinates active site Mg^{2+} [32,141–148]. Between the G2- and the G3-loop the so called I-box (insertion-box) is positioned, which is conserved among SRP-GTPases and characterised by its unique tertiary structure being defined as α-β-α. Together with the G2-loop the first α-helix of the I-box forms a functional unit, which is indispensable for the overall GTPase activity of FlhF [133]. The sequentially following G4-loop is located downstream from the G3-loop with the G4-loop being structurally positioned on the opposite side from the previous loops on the GTP binding pocket. Here it enables interactions with the guanine base through two hydrogen bonds and is responsible for nucleotide specificity. The final G5-loop interacts with the bound guanine through a single hydrogen bond, enhancing the overall nucleotide binding, and additionally functions as the closing loop of the GTP binding pocket [130,149].
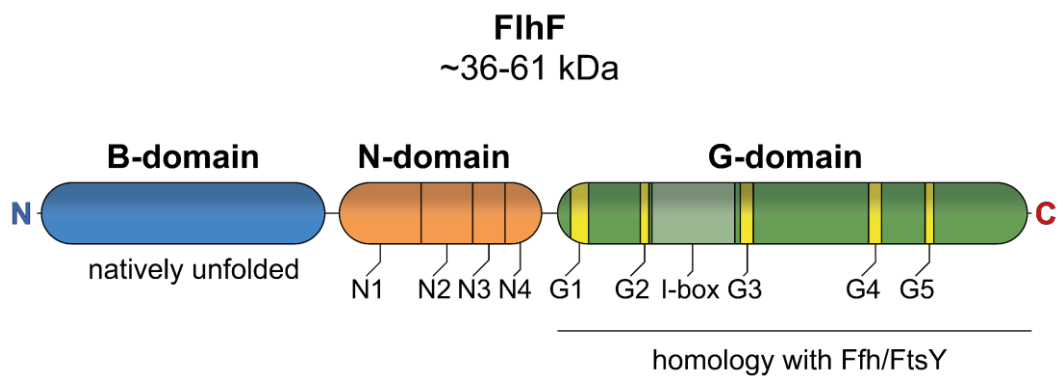
Figure 3. Domain structure model of the SRP-GTPase FlhF. N1-4 = N-domain helices, G1-5 = conserved nucleotide binding motifs (loops), G1 = P-loop (phosphate-binding loop), G4 = nucleoside specificity-loop G5 = closing-loop, I-box = insertion box.

In the context of flagellar positioning and assembly homodimeric GTP-bound FlhF appears to independently target or be transported to the unflagellated cell pole through a so far unknown mechanism or factor, where it initiates flagellar assembly through the recruitment of the MS-ring component FliF [150]. As, with most structural components of the flagellum, the expression of FliF is regulated by the flagellar master regulator FlrA and the sigma factor RpoN ($σ^{54}$) [151–153]. In the late stages of the subsequent basal body construction, following the formation of the fT3SS and initiation of C-ring assembly through the polar recruitment of FliG, the ATPase FlhG, which functions as a regulator of FlhF and therefore is an essential factor for functional flagellation, is transferred to the nascent basal body [154,155]. FlhG, just like FlhF, is grouped inside the SIMIBI class of NTPases and possesses strong homology to the ATPase MinD, which is essential for Z-ring formation during cellular division [156]. The polar recruitment of monomeric FlhG is thought to be facilitated through its intrinsic C-terminal membrane targeting site and the C-ring components FliM and FliN, which already appear as an oligomer prior to integration into the growing C-ring structure [157]. Here the interaction of FlhG with FliM is

facilitated by the conserved N-terminal motif of FliM consisting of the residues "EIDAL" [158]. Besides the mentioned factors involved in the polar targeting behaviour of FlhG, the polar landmark protein HubP, as another pole associated component, has been determined as essential in the polar recruitment of FlhG in the context of flagellar synthesis [57]. At the cell pole FlhG, possibly induced by membrane interaction of its C-terminally positioned MTS, forms an ATP-bound homodimer, which is presumed to induce the GTPase activity of the FlhF homodimer through the formation of an activator complex in which the N-terminally located activator helix of FlhG interacts with the FlhF N- and G-domain [141,159]. The close association of FlhF and FlhG is reiterated by their genes consistently being positioned adjacent to each other on the chromosome in various bacterial species, highlighting their strong connection not only on a functional but also transcriptional level. The induction of the FlhF GTPase activity, as has been observed for other NTPases, causes the bound GTP to be hydrolysed, leading to the transition of FlhF from an active GTP-bound homodimeric state to an inactive apo- or GDP-bound monomeric state, with the FlhF monomers subsequently dissociating from the nascent flagellar structure and being incapable of recruiting further flagellar components to the cell pole [160].
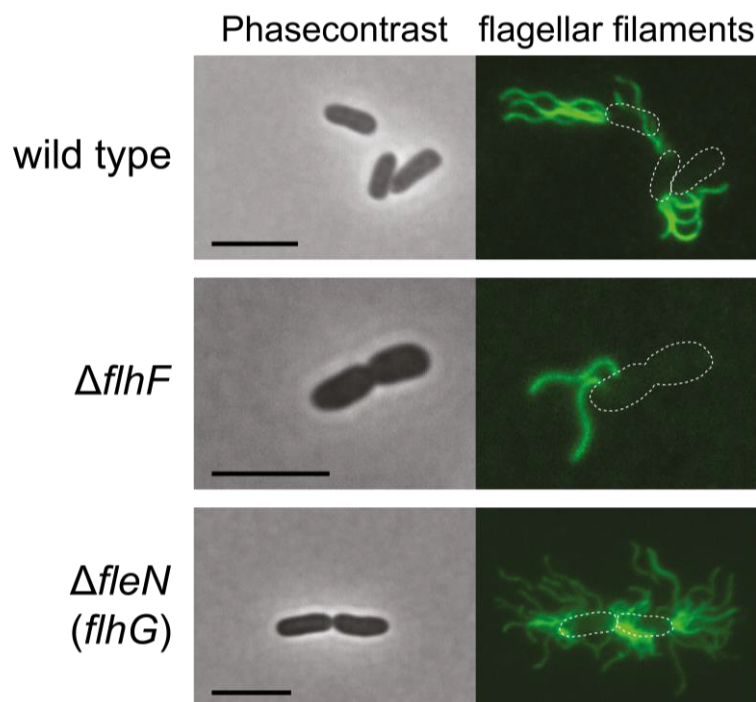
Figure 4. Flagellation phenotypes caused by either the absence of FlhF or the FlhG homolog FleN in the lophotrichously flagellated bacterium *Pseudomonas putida* KT2440. Scalebar: 5 µm.

FlhG, as an ATP-bound homodimer, then interacts with the flagellar master regulator FlrA, which leads to the down-regulation of resource intensive flagellar gene expression [157,161,162].

Thus, concerning the functions of FlhF and FlhG the experimentally confirmed conclusions can be drawn that the absence of FlhF, which plays the role of a flagellar positioning factor, leads to a delocalised flagellum, and the absence of FlhG leads to hyperflagellation, due to FlhF not being removed from the nascent flagellar structure resulting in the continuous recruitment of flagellar components (**Figure 4**) [163].

During flagellar assembly at a timepoint subsequent to the completion of the basal body and rod, the construction of extracellular flagellum components commences beginning with the flagellar hook. Like most structural components incorporated into the nascent flagellum, following the completion of the basal body, the fT3SS system is utilised for the export of the hook subunit FlgE. An integral factor of the fT3SS involved in this export is FlhB, which through direct interaction with the export gate complex, composed of FliPQR, triggers opening and closing of the export gate [90]. FlhB, which was initially characterised with other components of the fT3SS comprises two structural regions, being the N-terminal TMD and the C-terminal cytoplasmic domain (FlhB-C) [164,165]. The TMD is presumed to be involved in the formation of the FlhB/export gate complex, while FlhB-C, which comprises two distinct polypeptides, being FlhB-CN and FlhB-CC, is essential for the substrate specificity switch of the fT3SS [91,166]. Here FlhB-CN has been proposed to be involved in the translocation of flagellar proteins into the central pore of the export gate complex, while FlhB-CC, through a conserved hydrophobic patch, appears as responsible for the interaction with the export signal containing N-terminus of hook associated proteins, which is recognised by the flagellar protein export mechanism [167]. The subdomains of FlhB-C are connected by a highly conserved NP(T/E)H loop containing an intrinsic auto cleavage site between the Asn and Pro and remain strongly associated after autocleavage, standing at the core of the export substrate specificity switch, has commenced [168]. An important factor, involved in flagellar assembly up to the auto-cleavage of FlhB-C, is FliK, which, prior to the switching of substrate specificity acts as an "infrequent molecular ruler" in conjunction with FlhB, to determine the final length of the hook [114,117]. The mechanism governing hook length determination is thought to function through the export of FliK, which, with its N-terminal region, is able to interact with FlgE and the hook cap FlgD, while its C-terminal region is involved in the auto-cleavage of FlhB-C (**Figure 5**). Both of these regions of FliK are connected with a long and natively unstructured linker, enabling FliK to span the distance between the tip of the nascent hook and the export complex located in the basal body [169]. FliK is intermittently secreted during the synthesis of the still incomplete hook, which interrupts hook assembly and leads to the N-terminal region of FliK interacting with FlgE and FlgD prior to secretion. This interaction is presumed to lead to a conformational change in FliK, which causes the C-terminal region of FliK, previously residing in the cytoplasm below the fT3SS, to pass FlhB in a velocity unfavourable to FlhB-C/FliK interaction [170]. Once the

flagellar hook has reached the defined length of approximately 55 nm and the export of another FliK molecule commences, FliK moves slower towards the distal end of the completed hook for FlgD interaction and secretion due to frequent interactions with FlgE. These interactions cause the extended FliK molecule to pass FlhB with its C-terminal region in a velocity favourable to interaction [171]. This leads to FlhB-C auto-cleaving and, accompanying the finalisation of the hook, the export switch from hook assembly associated substrates such as FlgE, FlgD and FliK to the class of substrates enabling filament construction such as FlgM, FlgK, FlgL, FliD and FliC or FlaA and FlaB [172,173]. While this is the widely accepted mechanism integral to substrate specificity switching, the involvement of other factors of the fT3SS and rod structure have been confirmed experimentally [174].
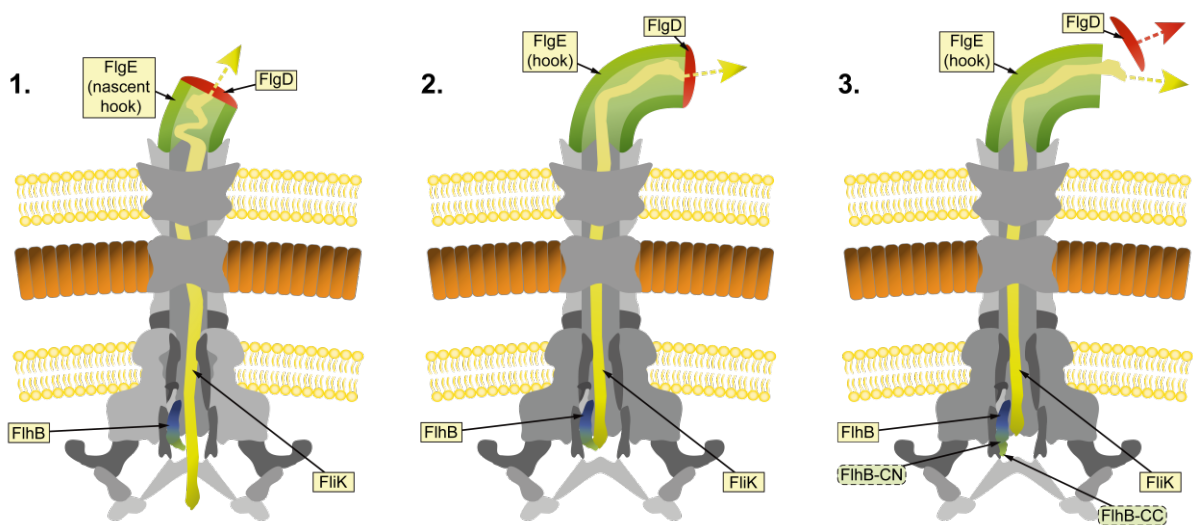
Figure 5. Model of hook assembly and substrate specificity switching under the influence of FlhB and FliK. 1. Early stage of hook assembly; No interaction between FliK and FlhB. **2.** Target hook length has been reached; FliK C-terminus interacts with FlhB-C. **3.** Interaction between FliK and FlhB-C leads to autocleavage of FlhB-C into FlhB-CN and FlhB-CC; Substrate specificity of export machine switches from hook to filament substrates.

Following the completion of the hook, the anti-sigma factor FlgM, which supresses FliA (σ^{28}), functioning as the sigma factor responsible for flagellin expression, is secreted and therefore opens up the way for flagellin gene expression, which leads to the assembly of the last flagellar substructure, being the filament.

1.6 <u>γ-proteobacterial model organisms for bacterial motility</u>

The results described in this study, concerning the spatiotemporal mechanisms involved in flagellar assembly, were generated through the utilisation of two flagellated species from the γ-proteobacterial class of bacteria [175].

1.6.1   *Shewanella putrefaciens*

The organism, which was used for the majority of generated data, is the γ-proteobacterium *Shewanella putrefaciens* and more precisely the strain CN-32. It is a member of the *Shewanellaceae* family and was isolated from an anaerobic subsurface sample obtained through drilling of a shale-sandstone sequence at the Morrison Formation in north western New Mexico (USA) [176]. As the members of the *Shewanellaceae* mostly appear in marine habitats, it can be assumed that the progenitor of the now isolated *S. putrefaciens* CN-32 lived in an aquatic environment and was trapped in sediment depositions in the Late Jurassic period approximately 163 to 145 million years ago. *S. putrefaciens* CN-32 is physiologically characterised by being a rod-shaped, Gram-negative bacterium, which forms light salmon-coloured colonies when grown on LB-medium agar plates. Besides other members of the *Shewanella*ceae, *S. putrefaciens* CN-32 has been observed to utilise metals, metalloids and radionuclides, as terminal electron acceptors, enabling it to thrive in anaerobic conditions. This characteristic is deemed to be a driving factor in the formation of mineable depositions of metal ores, as soluble metallic ions are converted into insoluble forms, which precipitate and over time form substantial deposits [177]. Besides playing an important role in the formation of resource deposits, *S. putrefaciens* CN-32 has become of interest for the construction of microbial fuel cells and therefore is involved in the development of alternative energy sources [178]. What however makes *S. putrefaciens* CN-32 an interesting model organism for the analysis of bacterial motility, is that it is a peritrichously flagellated bacterium, which possesses two distinct flagellar systems. These flagellar systems are separately regulated and expressed from two individual gene clusters, being the *ClusterI*, or polar flagellar gene cluster, which encodes components for the polar flagellar system, and the *ClusterII*, or lateral flagellar gene cluster, which encodes the factors for the lateral flagellar system [179,180]. The primary flagellar system, which in part depends on HubP for correct functioning, comprises a single polar flagellum, which is mainly used for planktonic locomotion in marine or semi-solid habitats and the secondary flagellar system is composed of up to 6 lateral flagella, which are utilised in environments with high viscosity or nutrient density for swarming motility and directional persistence [57]. Interestingly only the position and quantity of the polar flagellum is regulated by the interplay of FlhF and FlhG, of which the genes are also positioned in the polar gene cluster [158,179,180]. An additional feature through which the flagellar systems in *S. putrefaciens* CN-32 distinguish themselves is that the filaments are composed of two distinct flagellins, minor flagellin FlaA and major flagellin FlaB, which bestow the individual filament sections with distinct physical properties [39].

1.6.2 *Pseudomonas putida*

To corroborate some of the data acquired for *Shewanella putrefaciens* CN-32 and secure the newly developed model for the initiation of flagellar assembly, the *Pseudomonas putida* strain KT2440 was utilised. *Pseudomonas putida* is a member of the *Pseudomonadaceae* and just like *Shewanella putrefaciens*, with which it shares a similar cell morphology and the feature of being Gram-negative, belongs to the class of γ-proteobacteria. While the overall species *P. putida* firstly was mentioned in 1889 under the name *Bacillus putidus*, the KT2440 strain was established in 1982 as a plasmid-free derivative from the toluene-degrading bacterium *Pseudomonas putida* mt-2 [181]. In spite of being a strain developed in a laboratory *P. putida* KT2440 still is capable of thriving in the wild, most likely making it one of the best characterised saprophytic bacteria, which are capable of doing so. Its metabolic versatility also makes it an excellent model organism for both the study of genetic and physiological aspects of prokaryotes, as well as the development of biotechnological applications [182]. Physiologically *P. putida* KT2440 distinguishes itself by forming tea green-coloured colonies on agar plates, which exhibit strong fluorescence when exposed to UV radiation. A trait often observed in other species belonging to the *Pseudomonadaceae* family [183]. *P. putida* KT2440 qualifies itself to be utilised as a model organism for bacterial flagellation and motility, by being lophotrichously flagellated, with *P. putida* KT2440, unlike *S. putrefaciens* CN-32, however only possessing genes for one flagellar system (**Figure 1**, **Figure 4**) [184,185]. Concerning flagellation and the general governance of the polar landscape, additional differences between these two organisms are that the flagellar quantity in *P. putida* KT2440 is not regulated by FlhG but instead the homologously functioning FleN and that *P. putida* KT2440 does not possess HubP, but rather the homologously functioning FimV, while the filament in *P. putida* KT2440 also is composed of only one flagellin being FliC [58,59,186,187].

2. Project aim

2.1 Mechanisms involved in polar targeting of FlhF

The mechanisms involved in the establishment and regulation of bacterial flagellation have been the focus of many studies [136,188–190]. So far, these studies have revealed the SRP-GTPase FlhF to be a prime targeting factor for flagellar assembly in a plethora of bacterial species, which possess precisely positioned flagellar systems. The mechanisms and factors involved in the regulation of FlhF have however only been characterised in a more detailed manner downstream of the actual polar targeting of FlhF and the recruitment of basal body components. With the activities related to the polar localisation of FlhF being poorly understood and rife with speculation, an untapped source of discoveries concerning the

initiation of flagellar assembly presents itself. This study therefore is focused on the elucidation of both in- and extrinsic elements involved in the polar targeting of FlhF. Accordingly, the specific topics of investigation in the context of polar FlhF recruitment are polar cell morphology, factors associated with polarity and motility and distinct domain features of FlhF. Once promising targets have been acquired for the primary model organism, *S. putrefaciens* CN-32, select findings will be replicated in *P. putida* KT2440, to on the one hand broaden and strengthen the base of these discoveries and on the other hand, due to *P. putida* KT2440 possessing a different flagellation pattern than *S. putrefaciens* CN-32, to show the conservation of the mechanism across species boundaries. With the help of the resulting revelations, it should then be possible to shift the spatiotemporal starting point of the polar flagellar assembly mechanism away from the polar recruitment of basal body components through FlhF, to the factor(s) and mechanisms involved in the polar targeting of FlhF.

2.2 Involvement of FlhB-C motif in export specificity switching

The fT3SS component FlhB has been widely established to be an essential factor in the assembly of the flagellar structure, with its role being the facilitation of hook and filament subunit export. At the core of this function stands the ability of FlhB to autocleave its cytoplasmic domain (FlhB-C), initiated with the assistance of other factors involved in the export of flagellar factors located at a distal position, if viewed from the basal body [191]. This autocleavage of FlhB-C into the subdomains FlhB-CN and FlhB-CC enables the substrate specificity switch from hook- to filament-associated proteins. For FlhB-C various features have been identified as vital for autocleavage activity. This study aims to investigate a motif distinguishing itself by being rich in prolines and positioned in the FlhB-CC region of FlhB, which was briefly touched upon in a previous publication [168]. To characterise this motif and determine its role in the overall function of FlhB in *S. putrefaciens* CN-32, the effects of its absence on hook, filament and C-ring formation as well as autocleavage ability of FlhB-C are the topic of investigation. With the resulting insights it should be possible to create an even clearer picture concerning the functioning of intrinsic FlhB-C features in the switching of substrate specificity during flagellar assembly.

3. Results

The SRP-GTPase FlhF has repeatedly been experimentally verified as the prime initiation factor required for polar flagellar targeting and assembly. The upstream mechanisms and possible factors involved in the targeting of FlhF to the cell pole have however so far not been determined. The primary goal of this study therefore is focused on discovering how FlhF initially targets the membrane at the cell pole in both *S. putrefaciens* CN-32 and *P. putida* KT2440.

The secondary goal of this study is to examine the fT3SS protein FlhB, which plays a crucial role in the specificity switching of flagellar substrate export. Here a distinct C-terminal motif of FlhB, alongside additional residues is at the centre of features targeted for analysis to determine their involvement in the overall function of FlhB in *S. putrefaciens* CN-32.

3.1 Determination of polar FlhF localisation dependencies

3.1.1 FlhF membrane targeting is not dependent on polar membrane curvature

To initially determine, if the localisation of FlhF is dependent on morphological features, such as the unique membrane curvature at the pole of the cell, the placement of FlhF was analysed in a strain treated to be deficient of wild type cell morphology. This was achieved by cultivating a *S. putrefaciens* CN-32 strain which had its naturally occurring ampicillin resistance inducing *bla* gene (*Sputcn32_3157*) deleted and both a fluorescently tagged variant of FlhF and HubP, in medium supplemented with ampicillin at a dosage sublethal to the bacterial culture. After reaching exponential phase a sample was harvested from the culture and briefly treated with lysozyme, after which the outgrowth of the cells was observed with the help of time lapse microscopy.

The resulting micrographs (**Figure 6**) show what appear to be two cells with a morphology distinctly resembling spheroplasts [192], which initially are mostly spherical and over time seem to form outgrowths with morphological features more closely related to a wild type cell. There however is no apparent separation of newly formed daughter cells from the initial mother cell spheroplasts, leading to the emergence of two individual unusually large cell bodies. Concerning the localisation behaviour of the mVenus tagged FlhF, it can be observed that fluorescent mVenus foci are located at fixed positions both at the cell membrane and at a position most likely situated inside of the cell body, with, in the case of the mVenus signal in the top left quadrant of the 0 and 10 min timepoints, a FlhF localisation to occur at a negatively curved stretch of cell membrane. Over the course of the time lapse the initial FlhF foci can be

seen moving with the growing cell bodies without altering their position at the membrane. This occurs, while new FlhF foci form, which, among others, appear at locations with morphology more closely resembling a cell pole, indicated here by white arrows (**Figure 6**). In the case of HubP a similar localisation behaviour can be observed, in which the membrane is targeted independently of curvature. The absence of random membrane targeting of either FlhF or HubP is indicated by the colocalisation of both proteins, observable over the entire timespan of the micrograph series.
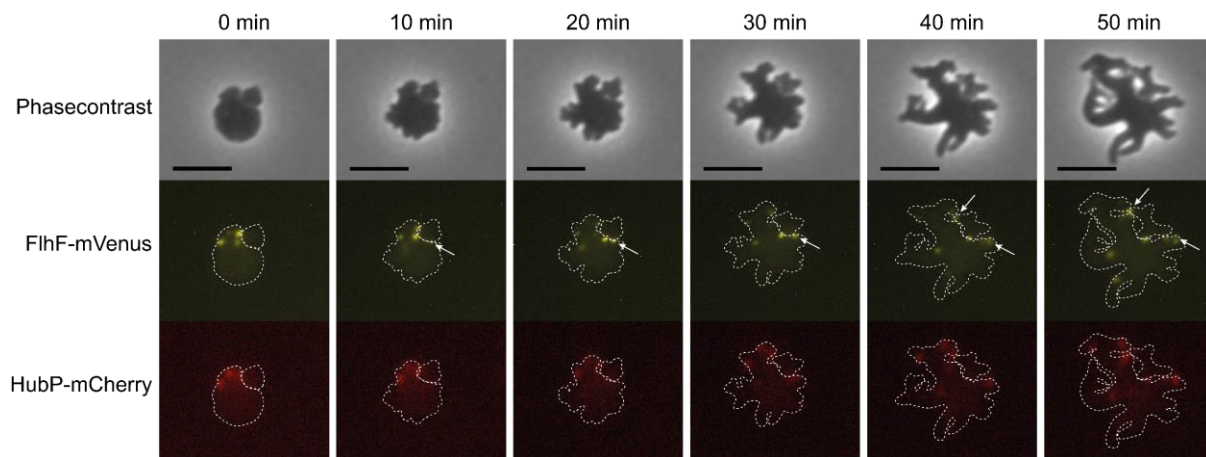
Figure 6. Timelapse of spheroplast outgrowth with localisation of FlhF (Sputcn32_2561) and HubP (Sputcn32_2442). Micrographs of spheroplasts taken in 10 min intervals showing mVenus tagged FlhF and mCherry tagged HubP localisation behaviour. White arrows indicate foci formation at membrane sections with wild type-like positive polar membrane curvature. **Scalebar: 5 μm**.

3.1.2   Polar targeting of FlhF is affected by motility associated factor(s)

As cell morphology could mostly be ruled out as playing a role in polar FlhF localisation, the focus was moved to factors associated with overall motility.

To get a general sense of to what degree FlhF is dependent on motility related factors, for its ability to localise to the cell pole, mVenus tagged FlhF was expressed from an arabinose inducible promoter in a strain devoid of all motility-associated genes (*ClusterI = Sputcn32_2548-2608, ClusterII = Sputcn32_3444-3485*) and the gene of the polar landmark protein *hubP* (*Sputcn32_2442*) (^{ara}FlhF-mVenus Δ*hubP* Δ*ClusterI* Δ*ClusterII*). In this instance mVenus tagged FlhF had to be expressed from a non-native promoter, as the entire polar gene cluster (*Sputcn32_2548-2608*) including the native *flhF* (*Sputcn32_2561*) gene and its promoter were deleted. To confirm a wild type-like localisation behaviour, mVenus tagged FlhF was additionally expressed from an arabinose inducible promoter in a strain with an otherwise unaltered genomic structure (^{ara}FlhF-mVenus) and a strain devoid of a wild type *flhF* copy (^{ara}FlhF-mVenus Δ*flhF*). The stable expression of the protein of interest was determined via Western blot (**Supplemental figure 38.A**). When observing the micrographs of all the

mentioned strains, one can see clear mVenus foci, forming abundantly at the cell poles in all strains except for the strain in which all motility related genes and *hubP* were deleted (**Figure 7.A**). In this multi-deletion strain the formation of unusually intense fluorescent foci can only rarely be seen, whereas besides localising at the cell pole, some of these foci localise at the membrane in subpolar positions.
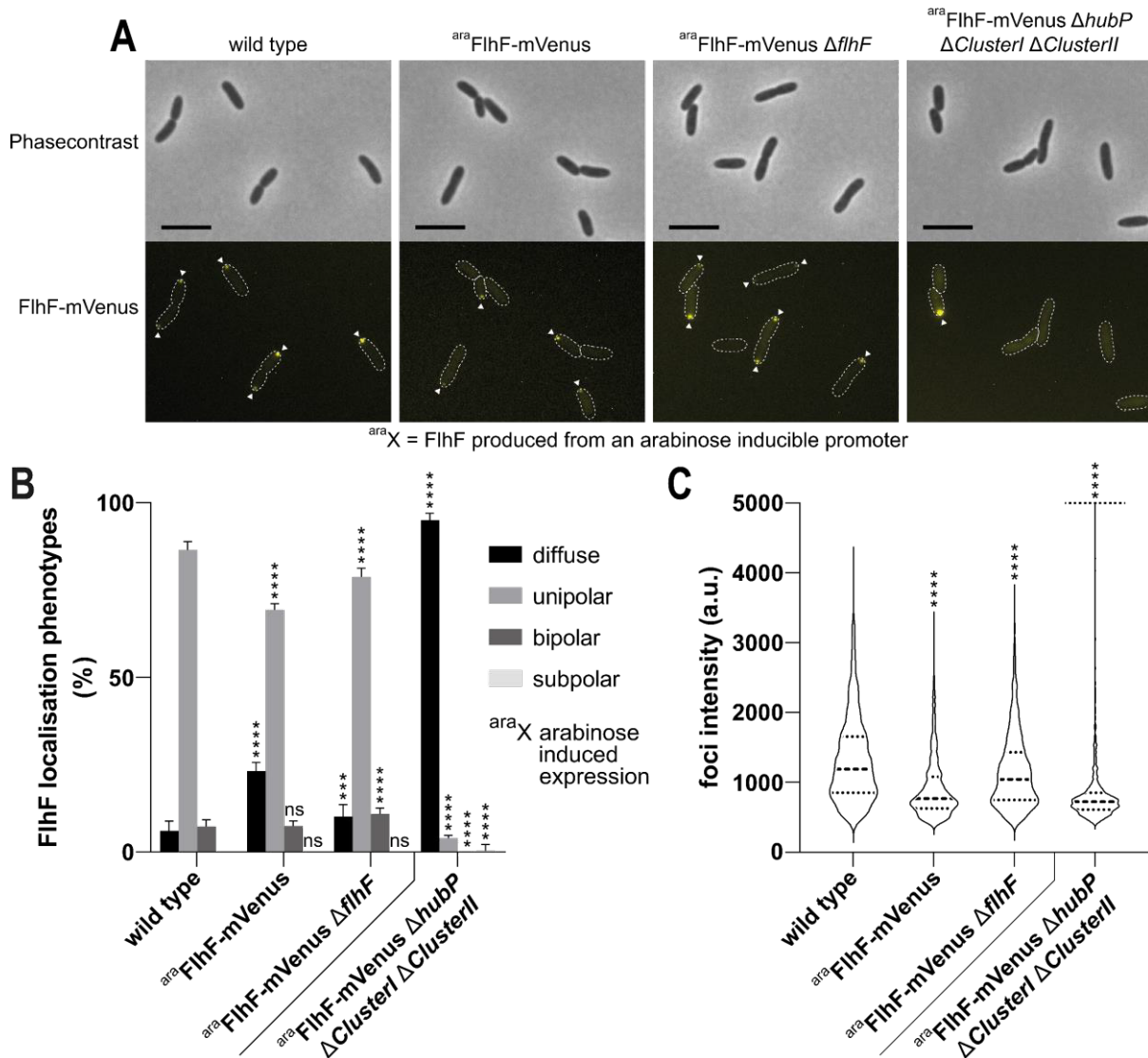
Figure 7. Localisation and foci intensity quantification of FlhF (Sputcn32_2561) under the absence of motility related factors. (A) Micrographs showing cells with mVenus tagged FlhF, **(B)** quantification of mVenus tagged FlhF localisation phenotypes and **(C)** foci fluorescence intensities of mVenus tagged FlhF in the context of various expression conditions and mutational backgrounds. White triangles indicate fluorescent foci formation. **Scalebar: 5 µm**. ***** = P value < 0.001, **** = P value < 0.0001. n ≥ 900 cells**.

When observing the overall abundance of mVenus foci, the quantification data shows a significant difference in localisation behaviour between the wild type and all additional strains of interest for both diffuse, unipolar, and bipolar localisation phenotypes (**Figure 7.B**). For

diffuse fluorescence, indicated by cells devoid of fluorescent foci, compared to the wild type (6 ± 3 % of cells), the most significant difference can be seen in the [ara]FlhF-mVenus Δ*hubP* Δ*ClusterI* Δ*ClusterII* strain (95 ± 2 % of cells) and the least significant difference being presented by the data of the [ara]FlhF-mVenus Δ*flhF* strain (10 ± 3 % of cells), with the [ara]FlhF-mVenus strain (23 ± 2 % of cells) lying in between these two but quantitatively closer to the [ara]FlhF-mVenus Δ*flhF* strain. The abundance of unipolar localisation, marked by a single polar fluorescent focus per cell, shows an equally significant difference between all analysed strains and the wild type (87 ± 2 % of cells) with the [ara]FlhF-mVenus Δ*hubP* Δ*ClusterI* Δ*ClusterII* strain (4 ± 1 % of cells) displaying the least cells with unipolar fluorescence and the [ara]FlhF-mVenus Δ*flhF* strain (79 ± 2 % of cells) showing the most. Just like with the diffuse fluorescence the [ara]FlhF-mVenus (69 ± 2 % of cells) strain is quantitively positioned between these two strains. Concerning bipolar localisation, indicated by cells possessing one fluorescent focus per cell pole, the [ara]FlhF-mVenus strain (7 ± 1 % of cells) does not significantly differ from the wild type (7 ± 2 % of cells). The other two strains however exhibit a significant difference to the wild type with the [ara]FlhF-mVenus Δ*flhF strain* (11 ± 2 %of cells) having a significantly increased bipolar localisation and the [ara]FlhF-mVenus Δ*hubP* Δ*ClusterI* Δ*ClusterII* strain (0 % of cells) lacking bipolar localisation altogether. An additional localisation phenotype, being the subpolar formation of fluorescent foci, is another, in which the [ara]FlhF-mVenus Δ*hubP* Δ*ClusterI* Δ*ClusterII* strain (1 ± 2 % of cells) significantly differs from the wild type and all other analysed strains. These overall localisation phenotypes are reflected in the intensity data of fluorescent foci, which is measured in arbitrary units (a.u.) (**Figure 7.C**). Here the fluorescence intensity of all analysed strains is significantly decreased compared to the wild type (1317 ± 612 a.u.) with the fluorescence intensity profile of the [ara]FlhF-mVenus Δ*flhF* strain (1153 ± 537 a.u.) having the most and that of the [ara]FlhF-mVenus Δ*hubP* Δ*ClusterI* Δ*ClusterII* strain (983 ± 1271 a.u.), with its large standard deviation, the least resemblance to the wild type, while the [ara]FlhF-mVenus strain (918 ± 449 a.u.) just exhibits an overall decline in fluorescence intensity. The generally large standard deviation of fluorescence intensity in the [ara]FlhF-mVenus Δ*hubP* Δ*ClusterI* Δ*ClusterII* strain appears to be reflected in the strong accumulation of fluorescence appearing at the pole of individual cells (**Figure 7.A**).

This highly significant effect on FlhF localisation observed in the [ara]FlhF-mVenus Δ*hubP* Δ*ClusterI* Δ*ClusterII* strain was then analysed more precisely by specifically deleting motility associated factors essential for specific assembly stages of the polar flagellar system and previously uncharacterised genes inside of the polar flagellar gene cluster. Among the deleted factors known to be required for the facilitation of flagellar assembly, were the genes encoding the master regulator for polar flagellar gene expression, FlrA (Sputcn32_2580), the structural MS-ring component FliF (Sputcn32_2576) and C-ring protein FliG (Sputcn32_2575), the

fT3SS protein FlhB (Sputcn32_2563) and the antagonistically to FlhF acting ATPase FlhG (Sputcn32_2560). When observing the micrographs of the strains lacking these individual genes, fluorescent foci, are present at the cell poles in all analysed samples, with the fluorescent mVenus foci being strongly pronounced in the ΔfliFG double deletion and ΔflhG single deletion strain, if compared to the wild type. Unlike the ΔfliFG and the ΔflhG strain, the ΔflrA and ΔflhB strain appear to not differ much from the wild type in the abundance of exhibited polar foci (**Figure 8.A**). The localisation quantification data shows partially highly significant differences between the wild type and the analysed strains, with the ΔflhB strain displaying no significant difference from the wild type in any of the main three localisation phenotype categories (**Figure 8.B**). Compared to the wild type (6 ± 3 % of cells), the strain which shows the most significant difference, concerning the display of diffuse fluorescence, is the of ΔflrA strain (24 ± 3 % of cells) with an increase in diffuse fluorescence, while the ΔflhG strain (1 ± 2 % of cells) exhibits the most significant decrease in diffuse fluorescence. The least significant difference in diffuse fluorescence compared to the wild type is displayed by the ΔfliFG strain (83 ± 1 % of cells), with the ΔflhB strain (5 ± 2 % of cells) showing no significant difference. The unipolar localisation of FlhF, indicated by one fluorescent focus per cell at the cell pole, does not significantly differ from the wild type (86 ± 3 % of cells) in any of the analysed strains except for the ΔflrA strain (72 ± 2 % of cells), in which it is significantly decreased. As mentioned, there is no significant observable difference between the wild type and the ΔfliFG (87 ± 2 % of cells), ΔflhB (87 ± 2 % of cells) and ΔflhG strain (87 ± 2 % of cells). Like the diffuse localisation phenotype, the bipolar formation of fluorescent foci again is significantly different in most strains compared to the wild type (8 ± 2 % of cells). With the ΔflhG strain (13 ± 2 % of cells) showing the most significant increase in bipolar accumulation of fluorescence and the ΔflrA strain (4 ± 1 % of cells) displaying the most significant decrease in bipolar fluorescence, while the ΔfliFG strain (11 ± 2 % of cells) presents a significant increase in fluorescence equal to that of the ΔflhG strain (13 ± 2 % of cells). A rarely observable localisation phenotype is the additional formation of a subpolar fluorescent focus in cells already expressing wild type-like positioning of SpFlhF, which in this case only is observable in the ΔflhG strain (9 ± 2 % of cells). The fluorescent foci intensity phenotypes were already partially distinguishable when examining the micrographs (**Figure 8.A**), with there being a highly significant difference between the wild type (1153 ± 542 a.u.) and the ΔfliFG (7068 ± 6124 a.u.) and ΔflhG (8799 ± 7349 a.u.) strains with their strongly increased fluorescence reaching beyond the borders of the graph (**Figure 8.C**), while the ΔflrA strain (794 ± 447 a.u.) shows an overall significant decline in fluorescent foci intensity and the ΔflhB strain (1765 ± 988 a.u.), still being significantly different from the wild type, exhibits a wild type-like fluorescence intensity profile. In the context of all these observations it also is important to refer to the expression control performed for mVenus tagged FlhF with a Western blot

(**Supplemental figure 38.B**), in which a strong decrease of mVenus tagged FlhF signal can be seen in the Δ*flrA* strain and a strong increase is visible in the Δ*fliFG* and Δ*flhG* strain, whereas the Δ*flhB* strain appears to express mVenus tagged FlhF in wild type-like levels.
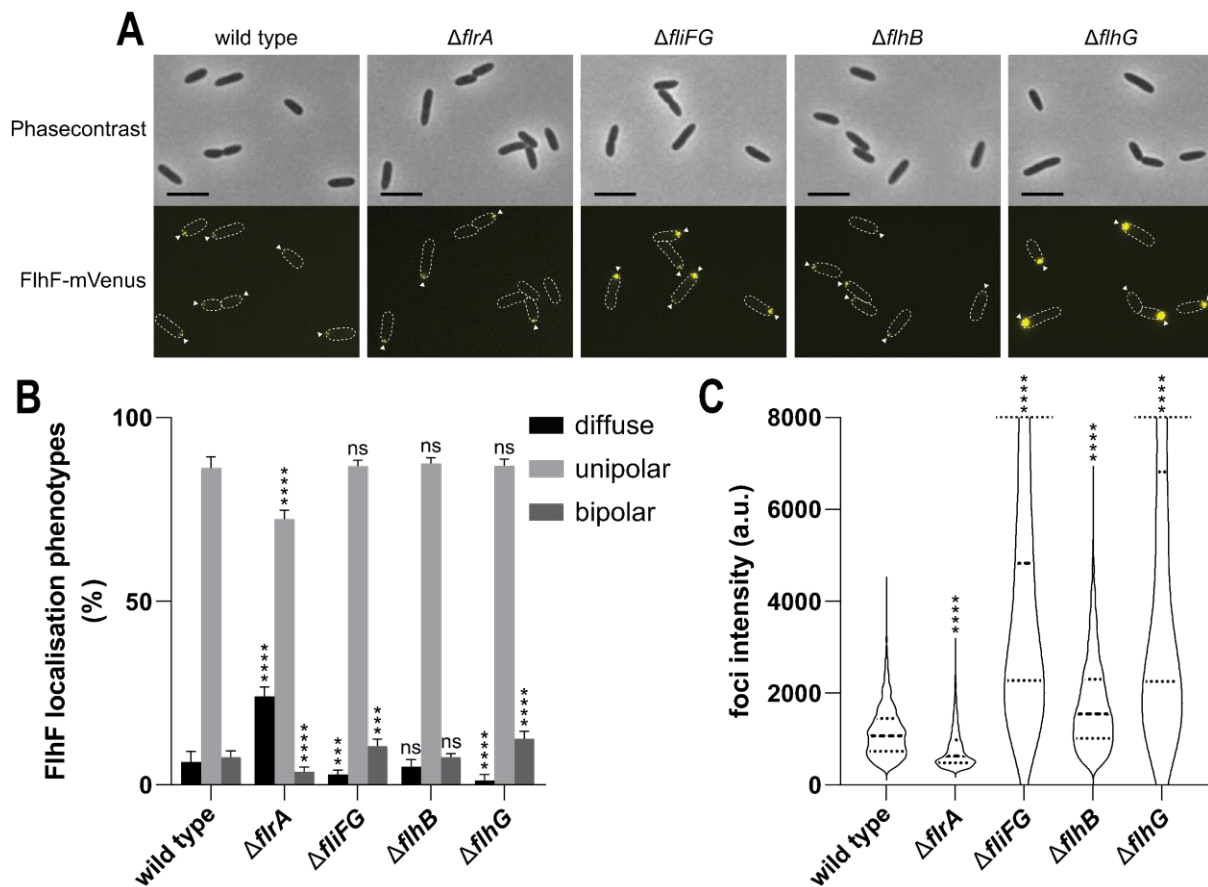
Figure 8. Localisation and foci intensity quantification of *Sp*FlhF under the absence of cell pole associated motility factors in *S. putrefaciens* CN-32. (A) Micrographs showing cells with mVenus tagged *Sp*FlhF, **(B)** quantification of mVenus tagged *Sp*FlhF and **(C)** foci fluorescence intensities of mVenus tagged *Sp*FlhF in the context of cell pole associated motility factor absence. White triangles indicate fluorescent foci formation. **Scalebar: 5 μm**. ***** = P value < 0.001**, ****** = P value < 0.0001**. **n ≥ 900 cells**.

3.1.3   FipA directly affects polar targeting of FlhF

In addition to the factors essential for flagellar synthesis, the products previously uncharacterized genes, associated with the polar flagellar gene cluster by genomic proximity, were analysed for their effect on polar FlhF localisation. Here the deletion of one of these genes had the single most significant effect on the ability of FlhF to target the cell pole of all analysed single deletions and therefore was investigated more closely in this context. The discovered gene *Sputcn32_2550* was named *fipA*, being an abbreviation for "**F**lhF **i**nteracting **p**rotein **A**", and firstly was analysed in a single deletion context for its involvement in polar

FlhF localisation and in conjunction with the deletion of *hubP* (*Sputcn32_2442*), due to the increased impact the double deletion had on polar FlhF localisation.

The micrographs of the *fipA* and *hubP* single and double deletion strains all show cells with polar fluorescent foci. In addition to generally exhibiting weaker foci compared to the wild type, individual cells of strains carrying a *fipA* deletion possess fluorescent foci in subpolar positions (**Figure 9.A**). The Δ*hubP* strain, judging from the micrographs, appears to resemble the wild type more closely concerning the positioning and intensity of foci fluorescence. The localisation phenotype quantification data (**Figure 9.B**) reveals that, in the context of diffuse fluorescence, the Δ*fipA* (35 ± 3 % of cells) and the Δ*fipA* Δ*hubP* strain (53 ± 3 % of cells) display the most significant difference compared to the wild type (6 ± 3 % of cells), whereas the single deletion of *hubP* (7 ± 2 % of cells) has no significant effect on diffuse fluorescence. A similar distribution of significances can be observed for the unipolar localisation phenotype of FlhF, with the Δ*fipA* (63 ± 2 % of cells) and the Δ*fipA* Δ*hubP* strain (45 ± 2 % of cells) showing a highly significant decline in unipolar localisation compared to the wild type (86 ± 3 of cells), while the unipolar localisation of FlhF appears to remain mainly unaffected in the Δ*hubP* strain (86 ± 2 % of cells). The bipolar localisation phenotype follows a similar pattern, with the Δ*fipA* (2 ± 1 % of cells) and the Δ*fipA* Δ*hubP* strain (2 ± 1 % of cells) again exhibiting a significant decrease compared to the wild type (8 ± 2 %of cells), whereas the Δ*hubP* strain (7 ± 2 of cells) shows no such effect. As observed in the micrographs, subpolar localisation of fluorescent foci, on the level of the entire cell population, can only be detected in the Δ*fipA* (5 ± 3 % of cells) and the Δ*fipA* Δ*hubP* strain (15 ± 3 % of cells). The foci fluorescence intensity (**Figure 9.C**) for these two strains also appears to be significantly different, when taking the wild type (1317 ± 612 a.u.) as reference, as both the Δ*fipA* (1069 ± 486 a.u.) and the Δ*fipA* Δ*hubP* strain (1055 ± 505 a.u.) exhibit a significant loss in fluorescent mVenus foci intensity, whereas the Δ*hubP* strain (1486 ± 666 a.u.) displays a significant increase in foci fluorescence intensity, in relation to the wild type.

S. putrefaciens
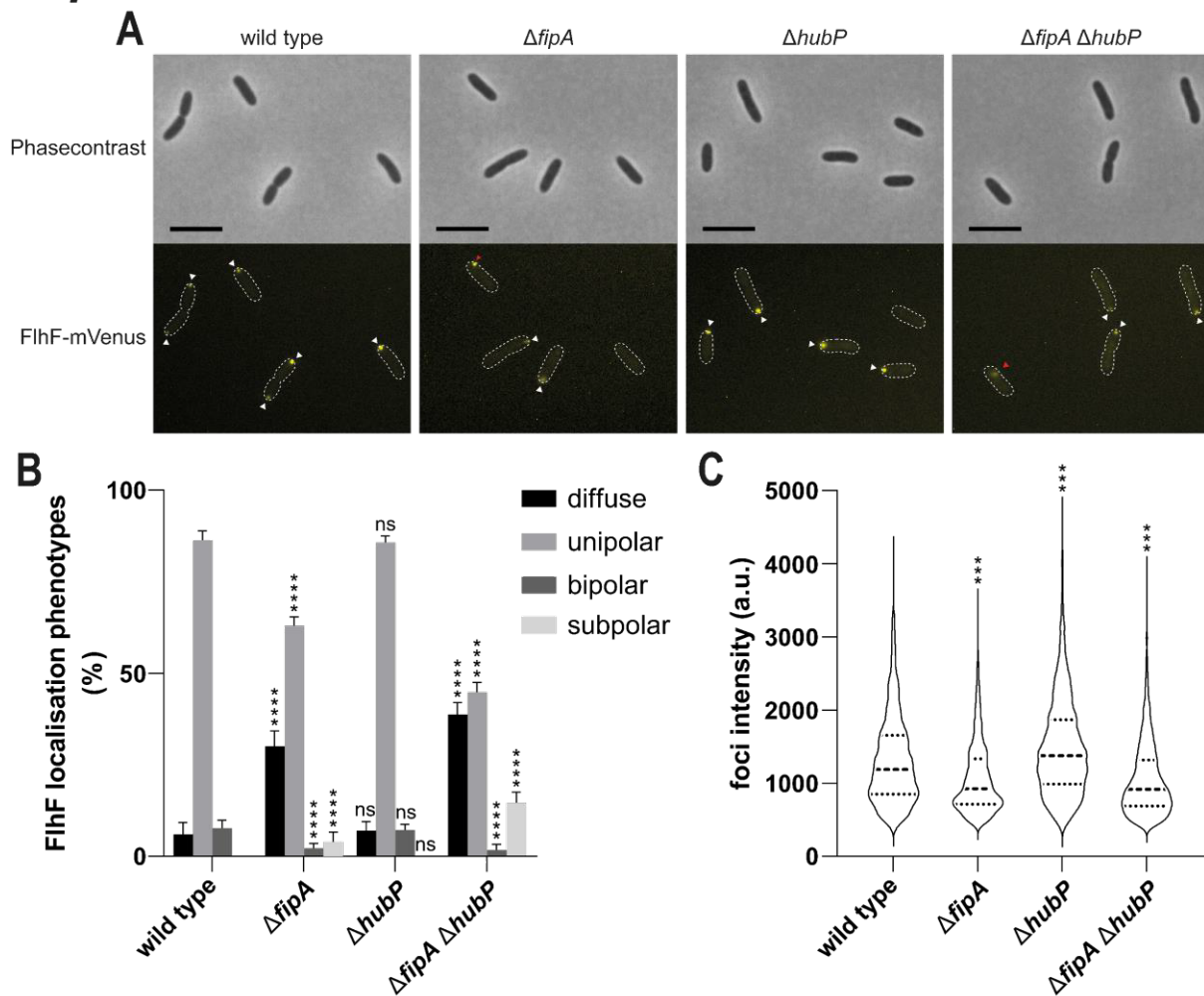
Figure 9. Localisation and foci intensity quantification of *Sp*FlhF in *S. putrefaciens* CN-32 in Δ*fipA* (*Sputcn32_2550*) and Δ*hubP* (*Sputcn32_2442*) backgrounds. (A) Micrographs of localisation phenotypes of mVenus tagged FlhF (subpolar foci indicated by red triangles), **(B)** quantification of mVenus tagged FlhF localisation phenotypes and **(C)** foci fluorescence intensities of mVenus tagged FlhF in the absence of *fipA* and *hubP*. White triangles indicate fluorescent foci formation. **Scalebar: 5 μm**. *** = P value < 0.001, **** = P value < 0.0001. n ≥ 900 cells.

To confirm the conservation of this dependency of FlhF on FipA for polar localisation and to broaden the base and increase the impact of these findings, the experiment to localise FlhF in a Δ*fipA* strain was replicated in *Pseudomonas putida* KT2440, which possesses an ortholog to *Sputcn32_2550* with the gene number *PP_4331*. Additionally, the gene of the orthologously to HubP functioning *Pp*FimV (PP_1992) was deleted in the context of the double deletion.

To be able to more clearly separate the data acquired for both organisms, proteins related to *S. putrefaciens* CN-32 will receive the prefix *Sp* and proteins related to *P. putida* KT2440 will receive the prefix *Pp* in the text, while figures will clearly display the organism of which the data originates from here on out.

The micrographs display a strong decrease in fluorescent *Pp*FlhF-mCherry foci in the Δ*fipA* and in the Δ*fimV* strain, with only a few cells possessing polar mCherry signals, while the formation of fluorescent foci is completely absent in the Δ*fipA* Δ*fimV* strain (**Figure 10.A**). Despite *Pp*FlhF not visibly accumulating in the Δ*fipA* Δ*fimV* strain, the expression was confirmed via Western blot (**Supplemental figure 43**). Overall, the mCherry foci appear much weaker than the mVenus foci previously observed in *S. putrefaciens* CN-32 (**Figure 9.A**) with there being a stronger fluorescent background in the cytoplasm of the *P. putida* KT2440 cells. The single and double gene deletions generally had a highly significant effect on the localisation of mCherry tagged *Pp*FlhF, with the Δ*fipA* Δ*fimV* strain not exhibiting any formation of fluorescent foci (**Figure 10.B**).

P. putida
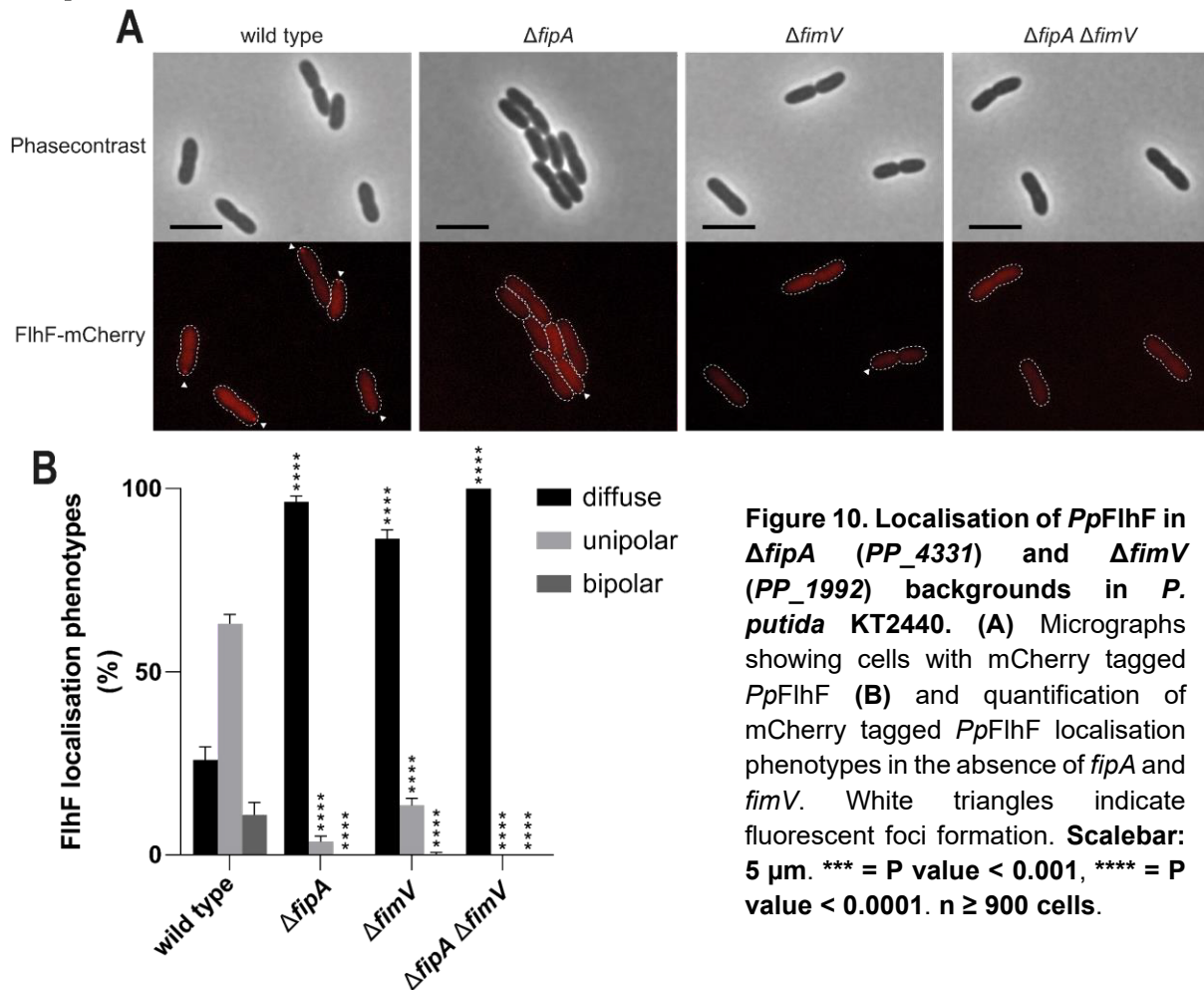
Figure 10. Localisation of *Pp*FlhF in Δ*fipA* (*PP_4331*) and Δ*fimV* (*PP_1992*) backgrounds in *P. putida* KT2440. (A) Micrographs showing cells with mCherry tagged *Pp*FlhF (B) and quantification of mCherry tagged *Pp*FlhF localisation phenotypes in the absence of *fipA* and *fimV*. White triangles indicate fluorescent foci formation. **Scalebar: 5 μm. *** = P value < 0.001, **** = P value < 0.0001. n ≥ 900 cells**.

In comparison to the wild type (26 ± 2 % of cells) the Δ*fipA* strain (96 ± 2 % of cells) and the Δ*fimV* strain (86 ± 2 % of cells) showed a significant increase in diffuse fluorescence, with the increase of the Δ*fipA* strain being stronger than that of the Δ*fimV* strain. Unipolar foci formation is almost absent in the Δ*fipA* strain (4 ± 2 % of cells) and, in contrast to the wild type (63 ± 3

% of cells), significantly reduced in the Δ*fimV* strain (13 ± 2 % of cells). The bipolar localisation phenotype observable in a few of the wild type cells (11 ± 3 % of cells), is not detectable in the Δ*fipA* strain and almost non-existent in the Δ*fimV* strain (2 ± 1 % of cells).

It was not possible to perform the foci intensity analysis for these strains, due to the fluorescence of the mCherry fluorophore being much weaker than that of the mVenus fluorophore and the *P.* putida KT2440 cells possessing a strong background fluorescence in the mCherry fluorescence channel.

3.1.4   FlhF and FipA display heterologous interaction

With having established that FipA plays a significant cross-species role in polar FlhF localisation, the next step was to determine, if this effect possibly was the result of a direct interaction between FlhF and FipA or if FipA rather regulated a still unknown factor that facilitated polar FlhF recruitment. To determine, if FlhF and FipA directly interact, a bacterial adenylate cyclase two-hybrid (BACTH) assay was conducted, in which firstly the ability for homologous interaction and secondly the ability for heterologous interaction were analysed.

The BACTH assay results, showing the homologous interaction phenotypes of *S. putrefaciens* CN-32 FlhF (*Sp*FlhF), indicate a strong intrinsic ability of *Sp*FlhF to interact with itself in all possible terminus configurations (**Figure 11.A**). In the case of *S. putrefaciens* CN-32 FipA (*Sp*FipA) there appears to be the ability to interact in an N- to C-terminal and a C- to C-terminal configuration, while the N- to C-terminal interaction appears to only function if the T25 fragment is fused to the N-terminus and the T18 fragment is fused to the C-terminus of *Sp*FipA (**Figure 11.B**). The BACTH assay performed to confirm a possible heterologous interaction between *Sp*FlhF and *Sp*FipA displays a clear ability to perform protein-protein interaction, with both the N- and C-terminal region of *Sp*FlhF interacting with the C-terminal region of *Sp*FipA (**Figure 11.C**).

S. putrefaciens
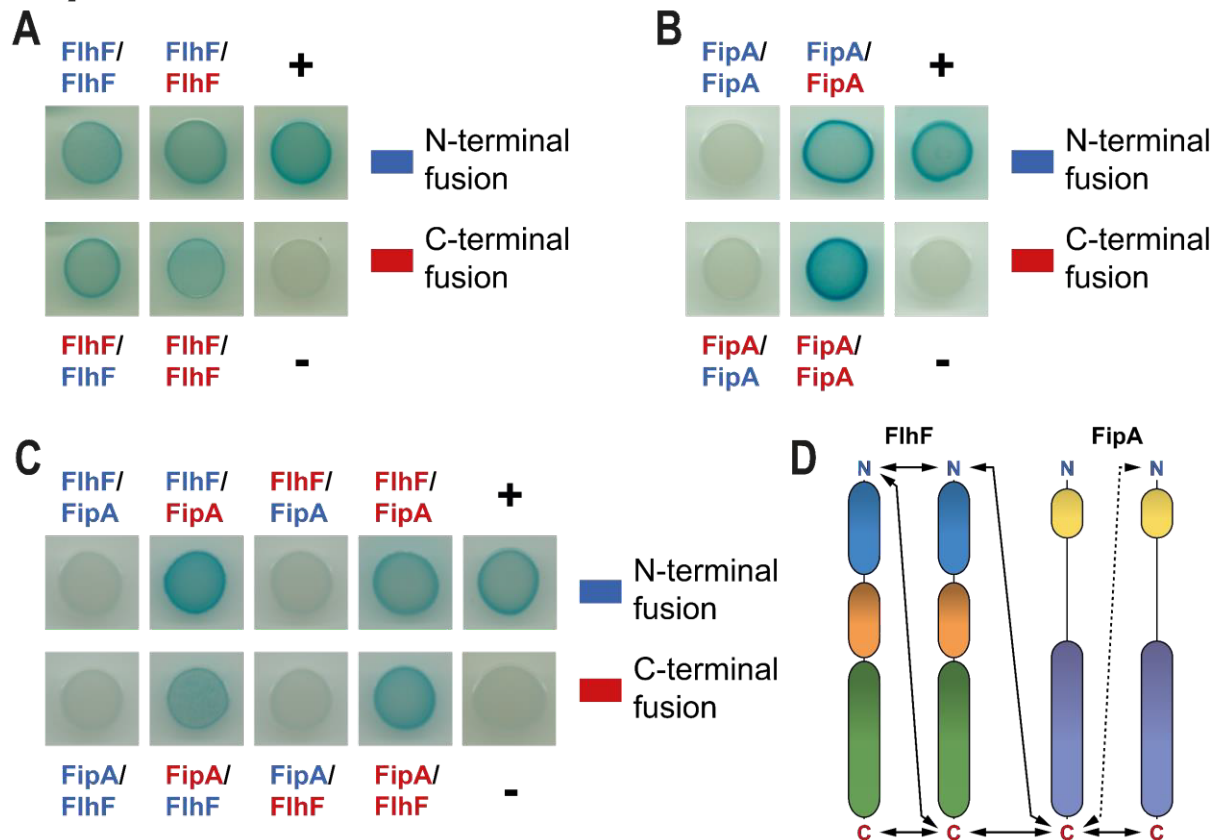
Figure 11. Homo- and heterologous interactions of *S. putrefaciens* CN-32 *Sp*FlhF and *Sp*FipA.
(A) Homologous BACTH assay with wild type *Sp*FlhF. **(B)** Homologous BACTH assay with wild type *Sp*FipA. **(C)** Heterologous BACTH assay with wild type *Sp*FlhF and wild type *Sp*FipA. **(D)** Model of observed homo- and heterologous interaction phenotypes of *Sp*FlhF and *Sp*FipA. In each interaction the protein named first is fused to T25 and the second protein is fused to T18, while N-terminal fusion indicates a fusion of the respective catalytic domain to the N-terminus of the protein of interest and C-terminal fusion indicates a fusion of the respective catalytic domain to the C-terminus of the protein of interest.

For the FlhF ortholog in *P. putida* KT2440 (*Pp*FlhF), the same interaction profile can be seen in the bacterial adenylate cyclase two-hybrid (BACTH) assay, with all termini of *Pp*FlhF being able to homologously interact (**Figure 12.A**). The FipA ortholog in *P. putida* KT2440 (*Pp*FipA), unlike *Sp*FipA, only appears to homologously interact in a C-terminal manner, with no visible indication for N- to C-terminal interaction (**Figure 12.B**), while the heterologous interaction profile of *Pp*FlhF and *Pp*FipA matches the one of *Sp*FlhF and *Sp*FipA with both the *Pp*FlhF N-terminal region being able to interact with the *Pp*FipA C-terminal region and the *Pp*FlhF C-terminal region being able to interact with the *Pp*FipA C-terminal region (**Figure 12.C**).
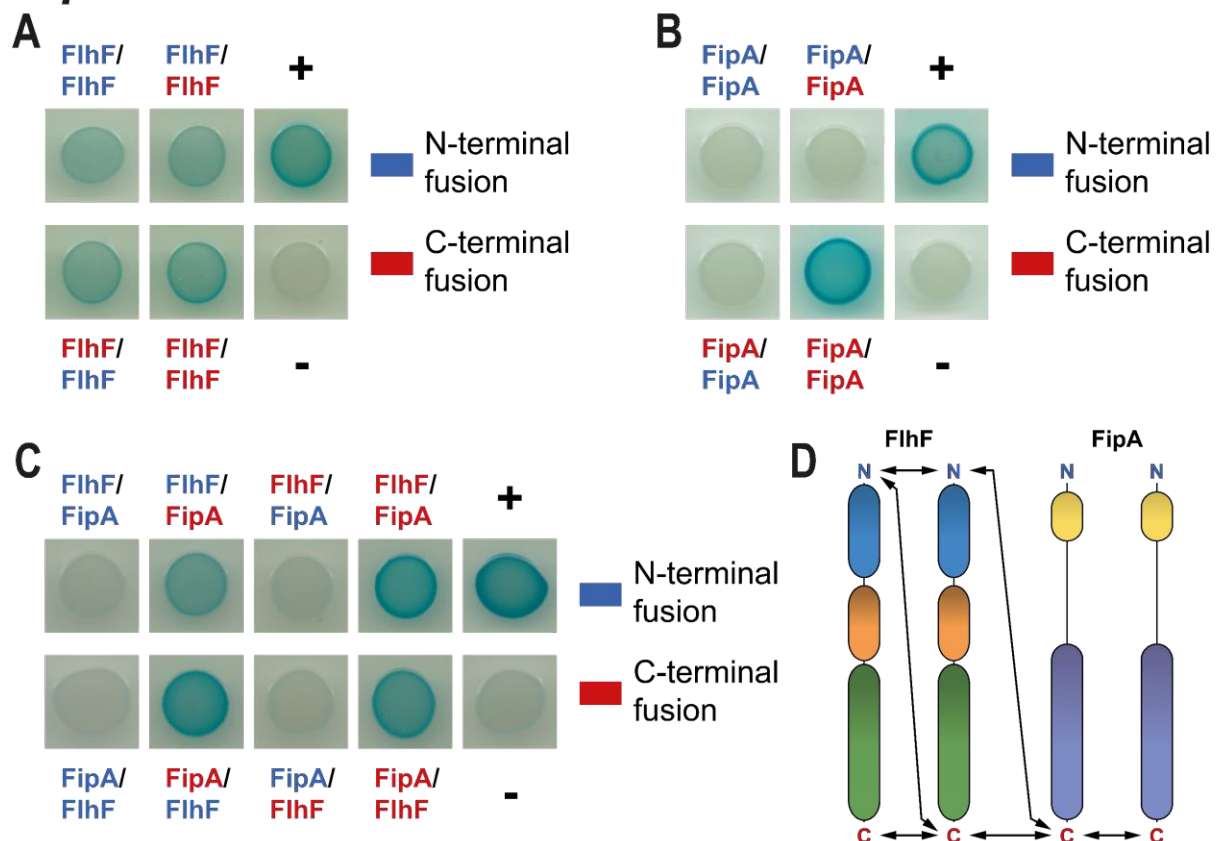
Figure 12. Homo- and heterologous interactions of *P. putida* KT2440 *Pp*FlhF and *Pp*FipA. (A) Homologous BACTH assay with wild type *Pp*FlhF. **(B)** Homologous BACTH assay with wild type *Pp*FipA. **(C)** Heterologous BACTH assay with wild type *Pp*FlhF and wild type *Pp*FipA. **(D)** Model of observed homo- and heterologous interactions of *Pp*FlhF and *Pp*FipA. In each interaction the protein named first is fused to T25 and the second protein is fused to T18, while N-terminal fusion indicates a fusion of the respective catalytic domain to the N-terminus of the protein of interest and C-terminal fusion indicates a fusion of the respective catalytic domain to the C-terminus of the protein of interest.

3.2 Characterisation of the novel FlhF localisation factor FipA

After having confirmed FipA as a major factor, involved in the polar localisation behaviour of FlhF through a possible direct interaction, in both *S. putrefaciens* CN-32 and *P. putida* KT2440, the focus was shifted towards more closely analysing FipA both for its conservation among bacterial species and its effects on other motility related processes.

3.2.1 FipA is conserved among bacteria with polar flagellation regulated by FlhF and HubP/FimV

The in-silico investigation to classify the conservation level of FipA among various bacterial species resulted in FipA orthologs being discovered in many members of γ-proteobacterial genera, such as *Shewanella*, *Pseudomonas*, *Vibrio* and *Aeromonas* (**Figure 13**). Here FipA appeared exclusively in genera possessing a polar landmark protein such as HubP or FimV

and polar flagellation regulated by FlhF and FlhG. Orthologs for FipA could not be detected in genera lacking directed positioning of flagellar structures, such as *Escherichia* and *Rhodobacter* or genera missing a HubP/FimV ortholog such as *Clostridium*, *Campylobacter* and *Bacillus*.

	FlhF	FlhG	FipA	HubP/(FimV)	Flagellation
Shewanella	✓	✓	✓	✓	
Pseudomonas	✓	✓	✓	(✓)	
Vibrio	✓	✓	✓	✓	
Aeromonas	✓	✓	✓	(✓)	
Clostridium	✓	✓	✗	✗	
Campylobacter	✓	✓	✗	✗	
Escherichia	✗	✗	✗	✗	
Rhodobacter	✗	✗	✗	✗	
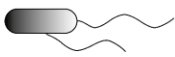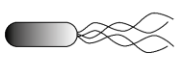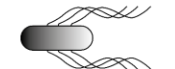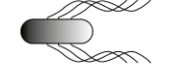
Figure 13. Occurrence of FipA orthologs among various bacterial genera in relation to the presence or absence of essential motility related factors.

In accordance with these findings, a synteny analysis was performed for *fipA* in the *Shewanella, Pseudomonas* and *Vibrio* genera (**Supplemental figure 47**), which revealed a strong association of all *fipA* orthologs with flagellar genes in each individual genome. Here *fipA* always appeared in close vicinity downstream from the gene cluster encoding the main flagellar system and always approximately 8-11 genes downstream from *flhF*, while consistently possessing the gene encoding the chemotaxis protein CheW in its immediate upstream proximity.

The bioinformatically determined domain composition of FipA was acquired through running multiple FipA sequences through the Simple Modular Architecture Research Tool (SMART), which revealed that most FipA protein orthologs are composed of an N-terminal transmembrane domain and a C-terminal DUF2802 domain (**Figure 14**), while a few FipA orthologs, possess either a putative intermediate low complexity region, such as orthologs from the *Aliivibrio* genus, or an intermediate coiled coil region, such as orthologs from the *Aeromonas* genus.
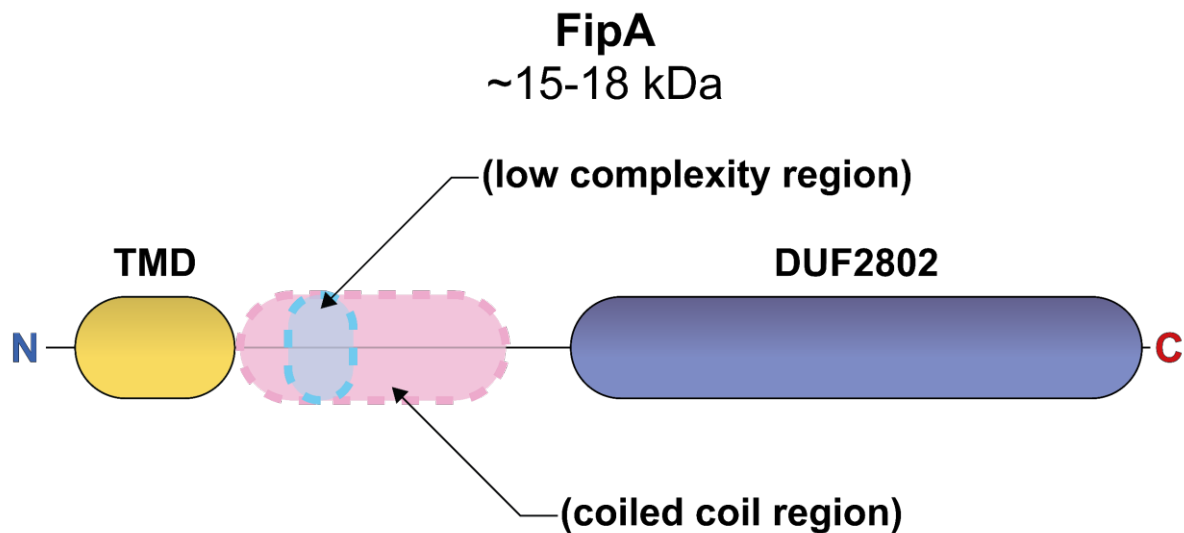
FipA
~15-18 kDa

Figure 14 Conserved bioinformatically determined domain structure of the FipA protein. Solid domains are conserved among all FipA orthologs, whereas domains encircled by dashed lines only appear in a few FipA orthologs. **TMD = transmembrane domain**.

3.2.2 FipA significantly affects motility but not chemotaxis and requires cell pole associated factors for localisation

For the analysis of which cellular mechanisms, besides the polar localisation behaviour of FlhF, are influenced by FipA, the effects, which the deletion of *fipA* has on cellular growth, overall motility and the localisation of motility related factors and structures, were investigated in both *S. putrefaciens* CN-32 and *P. putida* KT2440.

In *S. putrefaciens* CN-32 the deletion of *fipA* (*Sputcn32_2550*) did not affect the overall growth of bacteria, demonstrated by the lack of difference in comparison to the wild type growth curve, with both strains expressing an identical change in optical density through all supposed growth phases (**Figure 15.A**). Overall motility, indicated by spreading on soft agar plates, is significantly reduced in the Δ*fipA* strain (44 ± 2 % of WT spreading area), if it is compared to the spreading area of the wild type, which is set as reference. The Δ*flhF* strain (44 ± 2 % of WT spreading area) exhibits a spreading decrease with similar significance to the Δ*fipA* strain but with an overall stronger impact on motility (**Figure 15.B**). The localisation of the C-ring component *Sp*FliM (Sputcn32_2569) (wild type: 62 ± 9 % of cells; Δ*fipA*: 51 ± 4 % of cells) and the flagellar hook structure composed of *Sp*FlgE (Sputcn32_2594) (wild type: 45 ± 6 % of cells; Δ*fipA*: 34 ± 4 % of cells) appears to be significantly affected by the deletion of *fipA*, indicated by the localisation quantification data for each individual protein (**Figure 15.C**). In a strain with the same Δ*fipA* background an effect on the localisation behaviour of the chemotaxis system, represented by *Sp*CheA (wild type: 71 ± 5 % of cells; Δ*fipA*: 69 ± 5 % of cells), is not detectable.

S. putrefaciens

Figure 15. Effects of *fipA* (*Sputcn32_2550*) deletion on overall growth, motility and the localisation of motility and chemotaxis associated factors and structures in *S. putrefaciens* CN-32. (A) Growth curve of wild type and Δ*fipA* strain measured over 24 h. **(B)** Spreading area of Δ*flhF* and Δ*fipA* strain relative to the wild type spreading phenotype. **(C)** Quantification of polar localisation of C-ring component *Sp*FliM, flagellar hook (*Sp*FlgE) structure and chemotaxis factor *Sp*CheA in a wild type and Δ*fipA* background. **(D)** Micrographs of flagellar filament morphology and localisation phenotypes in a wildtype, Δ*flhF* and Δ*fipA* background. **(E)** Quantification of flagellar filament phenotypes in a wildtype, Δ*flhF* and Δ*fipA* background. **Scalebar: 5 μm. * = P value < 0.1, ** = P value < 0.01, *** = P value < 0.001, **** = P value < 0.0001. n ≥ 900 cells**.

Formation of flagellar filaments at the cell pole can be seen in the micrographs of all analysed strains, with the Δ*flhF* and Δ*fipA* strain demonstrating flagellation phenotypes not observed in

the wild type (**Figure 15.D**). Those flagellation configurations are subpolar localisation of the flagellum associated with the polar flagellar system and, in the Δ*fipA* strain, hyperflagellation, indicated by the formation of more than one flagellum comprising components related to the polar flagellar system. Quantification of the polar flagellation reveals it to appear to a significantly lower degree in the Δ*flhF* (7 ± 2 % of cells) and the Δ*fipA* strain (42 ± 3 % of cells) if compared to the wild type (57 ± 2 % of cells), with the Δ*flhF* strain showing overall less polar filaments than the Δ*fipA* strain (**Figure 15.E**). Subpolar formation of flagella, unlike in the wild type, is exhibited by both the Δ*flhF* (28 ± 2 % of cells) and the Δ*fipA* strain (1 ± 1 % of cells), with, despite it appearing to a significant degree in both strains, being more pronounced in the Δ*flhF* strain. The hyperflagellation phenotype only appears in the Δ*fipA* strain (1 ± 1 % of cells) and therefore significantly differs from the wild type, even if it only occurs in a subpopulation of cells.

Due to the observed hyperflagellation phenotype in the Δ*fipA* mutant strain of *S. putrefaciens* CN-32, a possible interaction between *Sp*FipA and *Sp*FlhG, as a loss of FlhG causes a similar flagellation pattern, was assessed via BACTH (**Figure 16**). Here an interaction was observable in one of the assay constellations in which the N-terminal region of *Sp*FlhG interacted with the C-terminal region of *Sp*FipA, which also functions as a target for *Sp*FlhF (**Figure 16.A**).
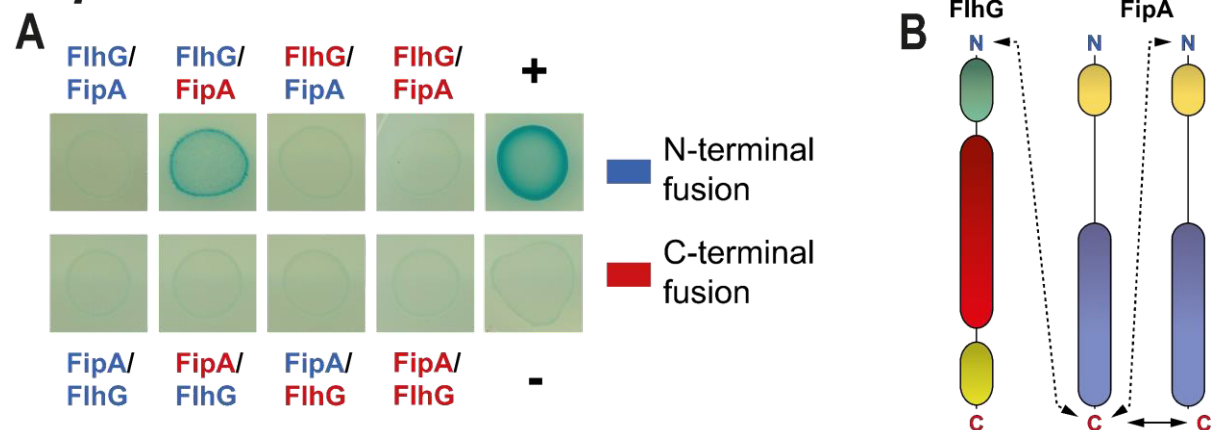
Figure 16. Heterologous interactions of *S. putrefaciens* CN-32 *Sp*FlhG and S*p*FipA. (A) Heterologous BACTH assay with wild type *Sp*FlhG and wild type *Sp*FipA. **(B)** Model of observed heterologous interaction of *Sp*FlhG and *Sp*FipA. In each interaction the protein named first is fused to T25 and the second protein is fused to T18, while N-terminal fusion indicates a fusion of the respective catalytic domain to the N-terminus of the protein of interest and C-terminal fusion indicates a fusion of the respective catalytic domain to the C-terminus of the protein of interest.

The deletion of *fipA* (*PP_4331*) in *P. putida* KT2440 appears to have a similarly low effect on cellular growth as the deletion of *fipA* in *S. putrefaciens* CN-32. Here the wild type and Δ*fipA*

strain growth progresses in a comparable manner throughout almost all growth phases, with there being a slight peak in the growth behaviour of the wild type in comparison to the Δ*fipA* strain, when transitioning from the exponential to the stationary phase (**Figure 17.A**). General motility appears to be largely affected by the deletion of *flhF* (17 ± 3 % of WT spreading area) and *fipA* (55 ± 6 % of WT spreading area), as the quantification of the spreading area of both these *P. putida* KT2440 mutant strains reveals a highly significant defect in their ability to spread on soft agar in comparison to the wild type, with the Δ*flhF* strain showing a greater drop in area occupied through motility than the Δ*fipA* strain **(Figure 17.B)**.

P. putida
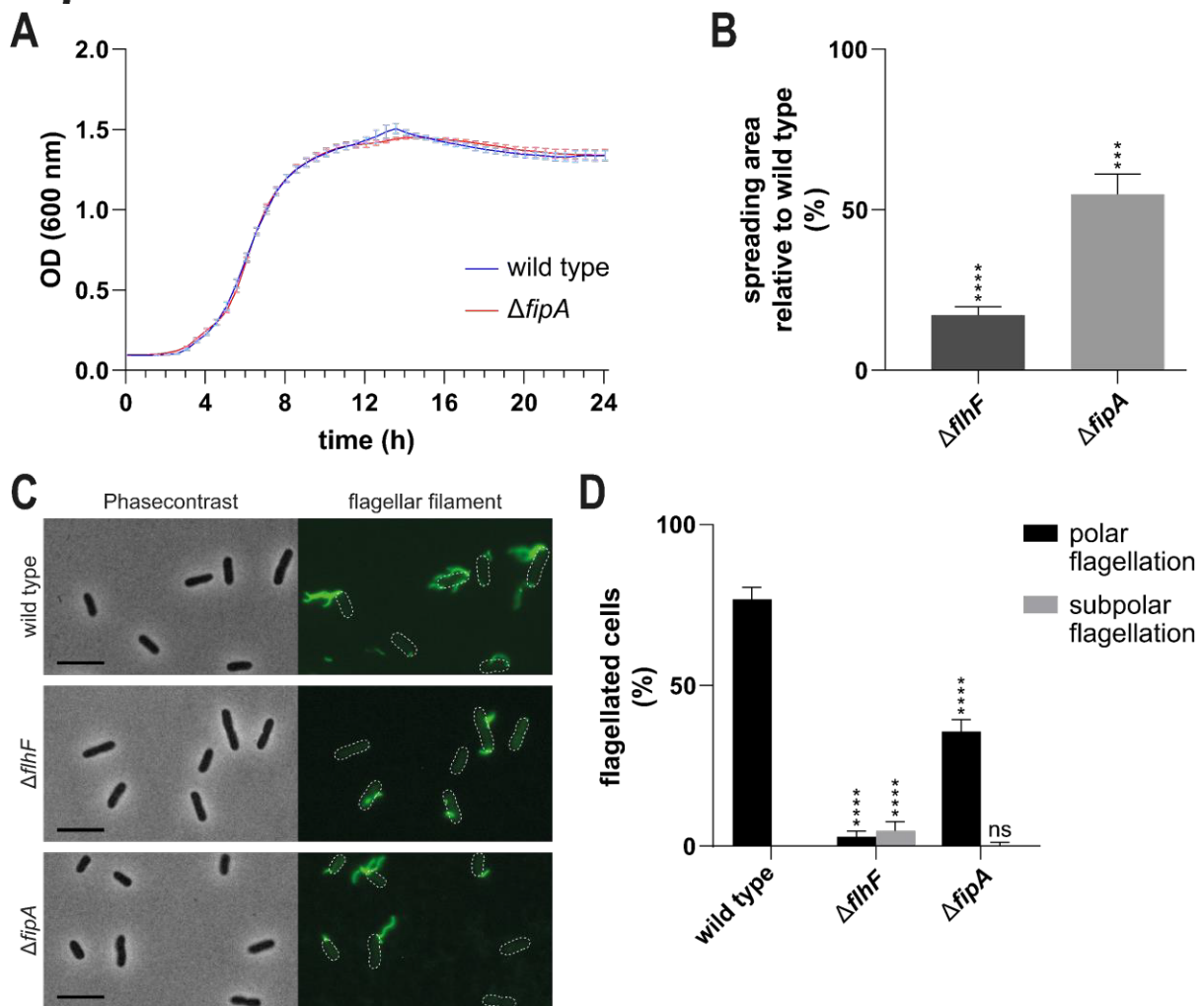
Figure 17. Effects of *fipA* (*PP_4331*) deletion on overall growth and motility and flagellar filament formation in *P. putida* KT2440. (A) Growth curve of wild type and Δ*fipA* strain measured over 24 h. **(B)** Spreading area of Δ*flhF* and Δ*fipA* strain relative to the wild type spreading phenotype. **(C)** Micrographs of flagellar filament morphology and localisation phenotypes in a wildtype, Δ*flhF* and Δ*fipA* background. **(D)** Quantification of flagellar filament phenotypes in a wildtype, Δ*flhF* and Δ*fipA* background. **Scalebar: 5 µm**. *** = P value < 0.001**, **** = P value < 0.0001**. **n ≥ 900 cells**.

Polar formation of flagella, in the lophotrichously flagellated *P. putida* KT2440, is observable in the micrographs of all strains, with the Δ*fipA* and the Δ*flhF* strain showing an obvious decrease in polar flagellation and an increase of subpolar flagellar assembly, which does not occur in the wild type (**Figure 17.C**). The quantification of the flagellation phenotypes reveals an overall highly significant decrease in polar flagellation in both the Δ*flhF* (3 ± 2 % of cells) and the Δ*fipA* strain (36 ± 4 % of cells) if compared to the wild type (77 ± 4 % of cells), with the Δ*flhF* strain displaying a greater drop in polar flagellation than the Δ*fipA* strain (**Figure 17.D**). Subpolar flagellation, which, dissimilarly to the wild type, only appears in the Δ*flhF* and Δ*fipA* strain, therefore also is significantly increased in both these strains, with the Δ*flhF* (5 ± 3 % of cells) strain showing more subpolarly flagellated cells than the Δ*fipA* strain (1 ± 1 % of cells).

To further characterise FipA, its own cellular positioning and possible localisation dependencies on other factors, such as FlhF and HubP, were studied.

Here it was possible to observe sf-GFP tagged *Sp*FipA forming unipolar and bipolar foci in individual cells of an appropriately modified *S. putrefaciens* CN-32 strain (**Figure 18.A**). The formation of these foci, even though in varying degrees, also was present in strains carrying an additional deletion of either *flhF* or *hubP*. By quantifying the occurrence of the various *Sp*FipA localisation behaviours, it was possible to reveal a significant decline in overall abundance of diffuse fluorescence in the Δ*flhF* (21 ± 5 % of cells) and Δ*hubP* strain (91 ± 2 % of cells) in comparison to the wild type (14 ± 6 of cells) (**Figure 18.B**). The unipolar localisation of *Sp*FipA also was impacted in a significant manner in the Δ*flhF* (53 ± 4 % of cells) and Δ*hubP* strain (9 ± 2 % of cells), with the deletions, in contrast to the wild type (61 ± 3 % of cells), causing a significant decrease in unipolar localisation, which was much more severe in the Δ*hubP* strain than the Δ*flhF* strain. No significant effect, concerning the bipolar localisation of *Sp*FipA, was observable in the Δ*flhF* strain (26 ± 2 % of cells), while the deletion of *hubP* led to a total absence of bipolar *Sp*FipA localisation observed in approximately a quarter of wild type cells (25 ± 5 % of cells). Through the analysis of the fluorescent *Sp*FipA-sfGFP foci intensity it was possible to detect a significant difference between the wild type (1796 ± 365 a.u.) and both the Δ*flhF* (1904 ± 313 a.u.) and Δ*hubP* strain (1767 ± 167 a.u.), with the foci fluorescence intensity profile of the *ΔhubP* strain being much more constricted, if compared to that of the wild type, than the one of the Δ*flhF* strain (**Figure 18.C**).

S. putrefaciens
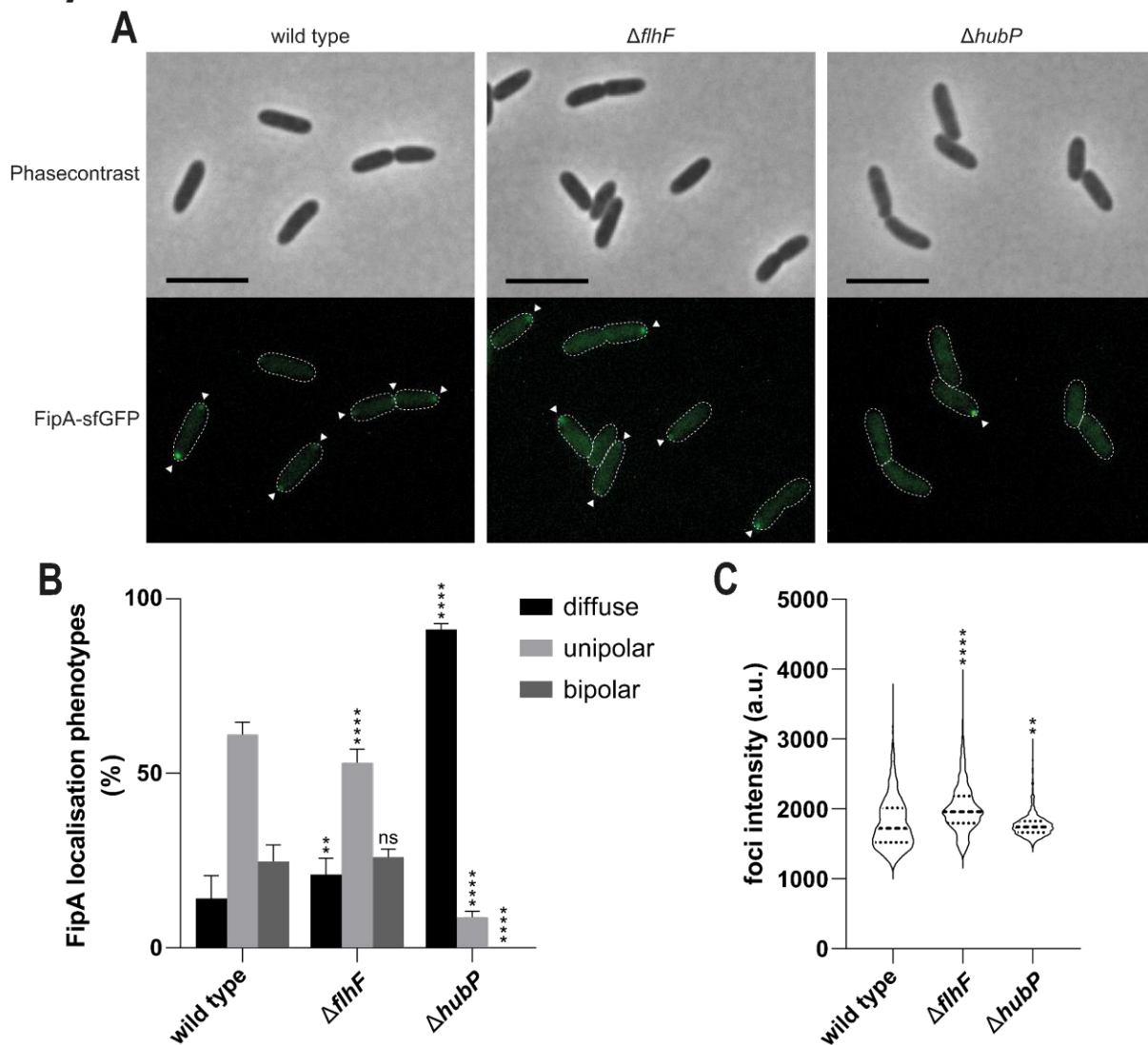
Figure 18. Localisation and foci intensity quantification of *Sp*FipA-sfGFP in *S. putrefaciens* CN-32 in Δ*flhF* (*Sputcn32_2561*) and Δ*hubP* (*Sputcn32_2442*) backgrounds. (A) Micrographs showing cells with sfGFP tagged *Sp*FipA, **(B)** quantification of sfGFP tagged *Sp*FipA localisation phenotypes and **(C)** foci fluorescence intensities of sfGFP tagged *Sp*FipA in the absence of *flhF* and *hubP*. White triangles indicate fluorescent foci formation. **Scalebar: 5 μm. ** = P value < 0.01, *** = P value < 0.001, **** = P value < 0.0001. n ≥ 900 cells**.

The FipA ortholog in *P. putida* KT2440, *Pp*FipA, which also was C-terminally tagged with sfGFP, followed the same localisation pattern as *Sp*FipA in a wild type background, with there being fluorescent *Pp*FipA-sfGFP foci forming in a unipolar and bipolar manner (**Figure 19.A**). Unlike *Sp*FipA, *Pp*FipA appears to be much more dependent on FlhF than HubP, or in the case of *P. putida* KT2440, *Pp*FimV, as almost no fluorescent foci are visible in the Δ*flhF* strain, while the deletion of *fimV* does not appear to severely impact the ability of *Pp*FipA to target the cell pole. When observing the quantification data (**Figure 19.B**), the differences become

more apparent, with diffuse fluorescence being significantly increased in the Δ*flhF* strain (93 ± 2 % of cells), when taking the wild type (1 ± 2 % of cells) as reference. Diffuse fluorescence also appears to be significantly increased, even though to a lesser degree, in the Δ*fimV* strain (25 ± 6 % of cells).

P. putida
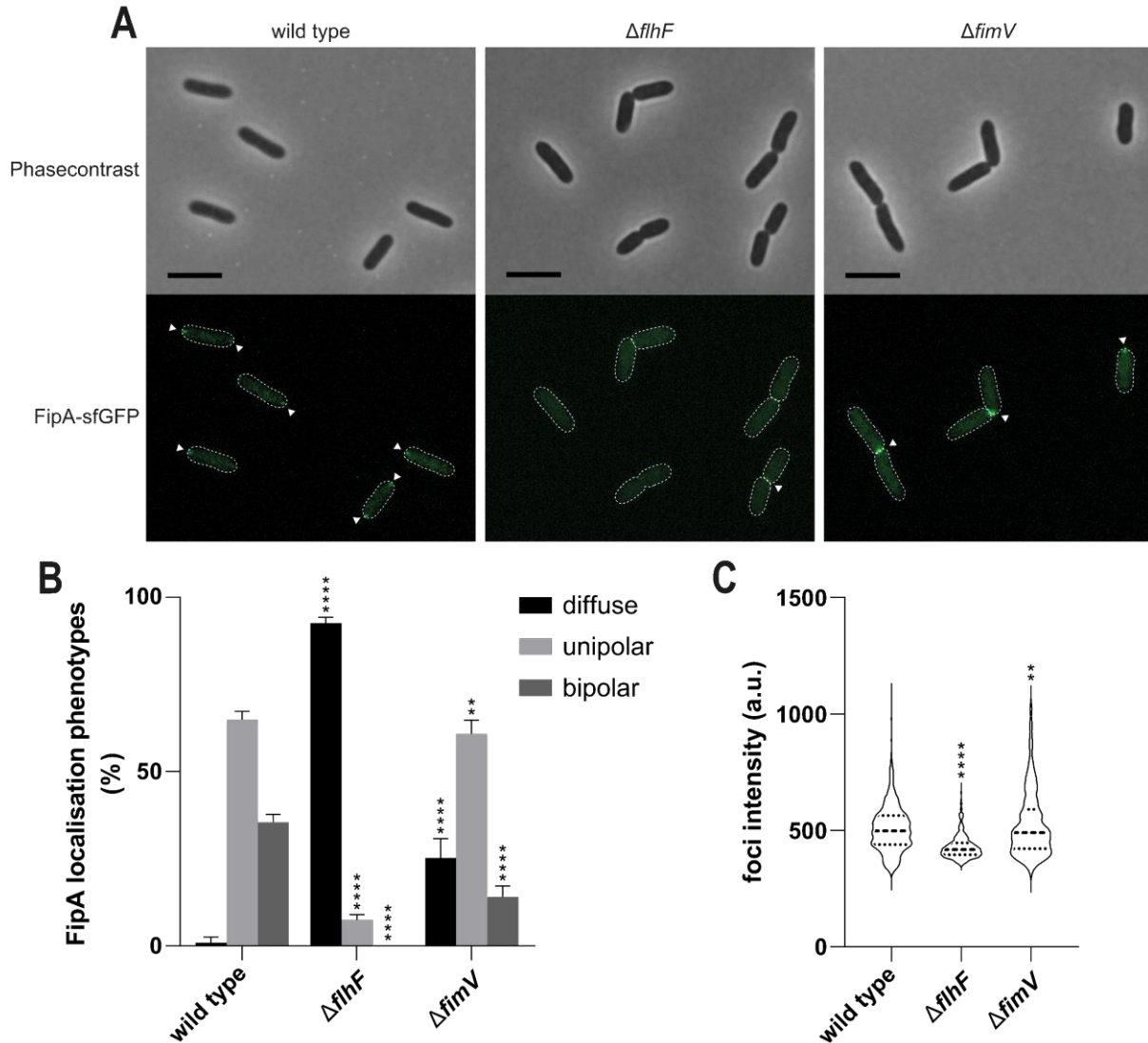
Figure 19. Localisation and foci intensity quantification of *Pp*FipA-sfGFP in *P. putida* KT2440 in Δ*flhF* (*PP_4343*) and Δ*fimV* (*PP_1992*) backgrounds. (A) Micrographs showing cells with sfGFP tagged *Pp*FipA, **(B)** quantification of sfGFP tagged *Pp*FipA localisation phenotypes and **(C)** foci fluorescence intensities of sfGFP tagged *Pp*FipA in the absence of *flhF* and *fimV*. White triangles indicate fluorescent foci formation. **Scalebar: 5 μm**. **** = P value < 0.01**, ***** = P value < 0.001**, ****** = P value < 0.0001**. **n ≥ 900 cells**.

Like the diffuse fluorescence, the unipolar localisation of *Pp*FipA is significantly affected by the deletion of Δ*flhF* (7 ± 2 % of cells) and the deletion of Δ*fimV* (61 ± 4 % of cells), with the absence of *fimV* causing a much smaller decrease than the deletion of *flhF*, if compared to

the wild type (65 ± 2 % of cells). The bipolar localisation phenotype, observable in the wild type (35 ± 2 % of cells), is totally absent in the Δ*flhF* strain, whereas it occurs in significantly reduced abundance in the Δ*fimV* strain (14 ± 3 % of cells). The fluorescence intensity of *Pp*FipA-sfGFP foci is affected by the individual deletions, to a similar extent, as the overall localisation phenotypes, with the determined foci intensity exhibiting the strongest decrease in the Δ*flhF* (429 ± 51 a.u.) strain. In the data gathered for the foci intensity of the Δ*fimV* strain (527 ± 140 a.u.), despite showing a significant difference to the wild type (507 ± 99 a.u.), a profile, not dissimilar to that of the wild type, is visible (**Figure 19.C**).

Having investigated FipA for its general localisation behaviour in a wild type background and in strains carrying specific gene deletions, it became of interest to view the positioning of FipA throughout a cell's life cycle in a higher spatiotemporal resolution and its localisation in relation to other motility factors and factors associated with the cell pole.

In *S. putrefaciens* CN-32 *Sp*FipA mostly colocalised with *Sp*HubP, whereas all cells possessing *Sp*HubP-mCherry foci did not always exhibit *Sp*FipA-sfGFP foci (**Figure 20.A**). When looking at the micrograph showing maleimide stained filaments of the polar flagellar system, and comparing it with the corresponding micrograph showing *Sp*FipA localisation, it can be observed that *Sp*FipA is positioned at the pole of cells devoid of or not possessing a fully formed filament. The cells retaining fully formed filaments do not exhibit *Sp*FipA-sfGFP foci at the flagellated pole, while *Sp*HubP always is associated with the flagellated pole. When observing the localisation behaviour of *Sp*FipA in a spatiotemporal context, it appears to be a rather dynamic protein not locked to a certain position, with the displayed cell switching between bipolar to unipolar *Sp*FipA localisation in the final stages of cell separation, until it is completed (**Figure 20.B**). The resulting daughter cells then each possess one fluorescent focus at the old cell poles, being the cell poles already existing in the mother cell. Here *Sp*FipA also accumulates at the cell pole prior to mCherry tagged *Sp*CheA, which only starts appearing at the cell pole just before cell separation. *Sp*FlhF tagged with mCherry, as can be seen in the micrographs, colocalises with *Sp*FipA, while *Sp*FlhF only appears at cell poles, at which *Sp*FipA is present (**Figure 20.C**). Both *Sp*FlhF and *Sp*FipA appear to be associated with cell poles, at which the flagellar assembly has not been fully completed and *Sp*FipA is also present at cell poles with no visible flagellar filament. The micrographs displaying, the colocalisation behaviour of *Sp*FlhF and *Sp*FipA, in a spatiotemporal context, show *Sp*FipA appearing at the cell pole prior to *Sp*FlhF (**Figure 20.D**). Here *Sp*FlhF seem to disappear from the cell pole, when *Sp*FipA leaves the cell pole, and does not reappear, even when *Sp*FipA intermittently returns to the cell pole. These returns of *Sp*FipA however are characterised by exhibiting much weaker fluorescent foci, than in conjunction with *Sp*FlhF.

S. putrefaciens
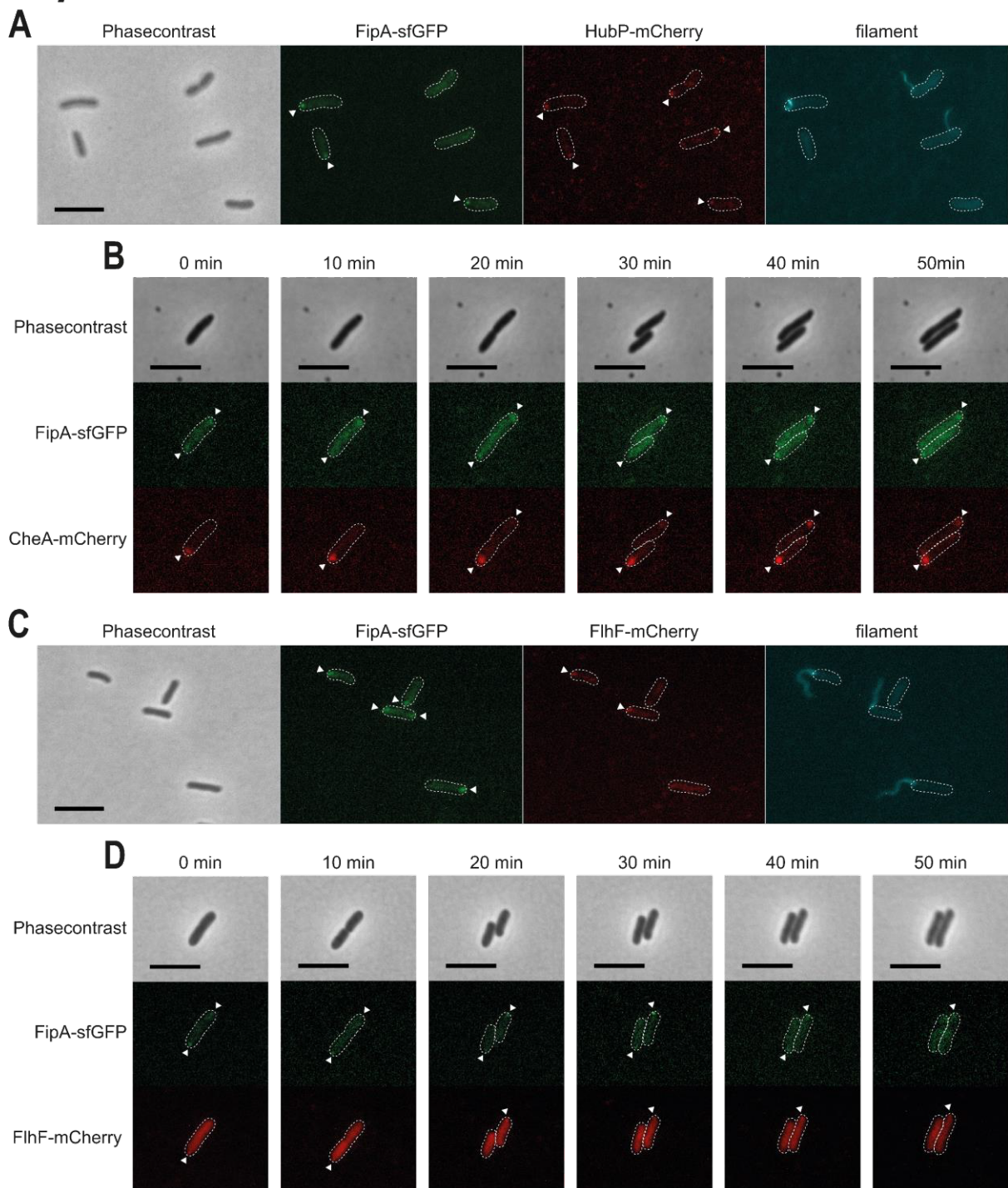
Figure 20. *Sp*FipA localisation and colocalisation with polar factors in a spatiotemporal manner in *S. putrefaciens* CN-32. (A) Micrographs showing colocalisation of sfGFP tagged *Sp*FipA with mCherry tagged *Sp*HubP and maleimide stained flagellar filament. **(B)** Micrographs taken in 10 min intervals showing spatiotemporal colocalisation of sfGFP tagged *Sp*FipA with the mCherry tagged chemotaxis factor *Sp*CheA (Sputcn32_2556). **(C)** Micrographs showing colocalisation of sfGFP tagged *Sp*FipA with mCherry tagged *Sp*FlhF and maleimide stained flagellar filament. **(D)** Micrographs taken in 10 min intervals showing spatiotemporal colocalisation of sfGFP tagged *Sp*FipA with mCherry tagged *Sp*FlhF. White triangles indicate fluorescent foci formation. **Scalebar: 5 µm**.

In comparison to *S. putrefaciens* CN-32, *P. putida* KT2440 exhibits a slight variation in its *Pp*FipA localisation behaviour, when viewed in a spatiotemporal context.

Here sfGFP tagged *Pp*FipA dynamically accumulates at the cell poles, with there being a stronger and more persistent fluorescent focus at the old cell pole, indicated by being the pole, at which the first *Pp*FipA focus is formed, than the new pole (**Figure 21.A**). Unlike *Sp*FipA, the *P. putida* KT2440 ortholog *Pp*FipA appears to target newly forming cell poles faster, as clear *Pp*FipA foci are visible at the septum just before cellular separation, which increase in intensity after the cells separate and the *Pp*FipA foci at the old cell poles dissipate.
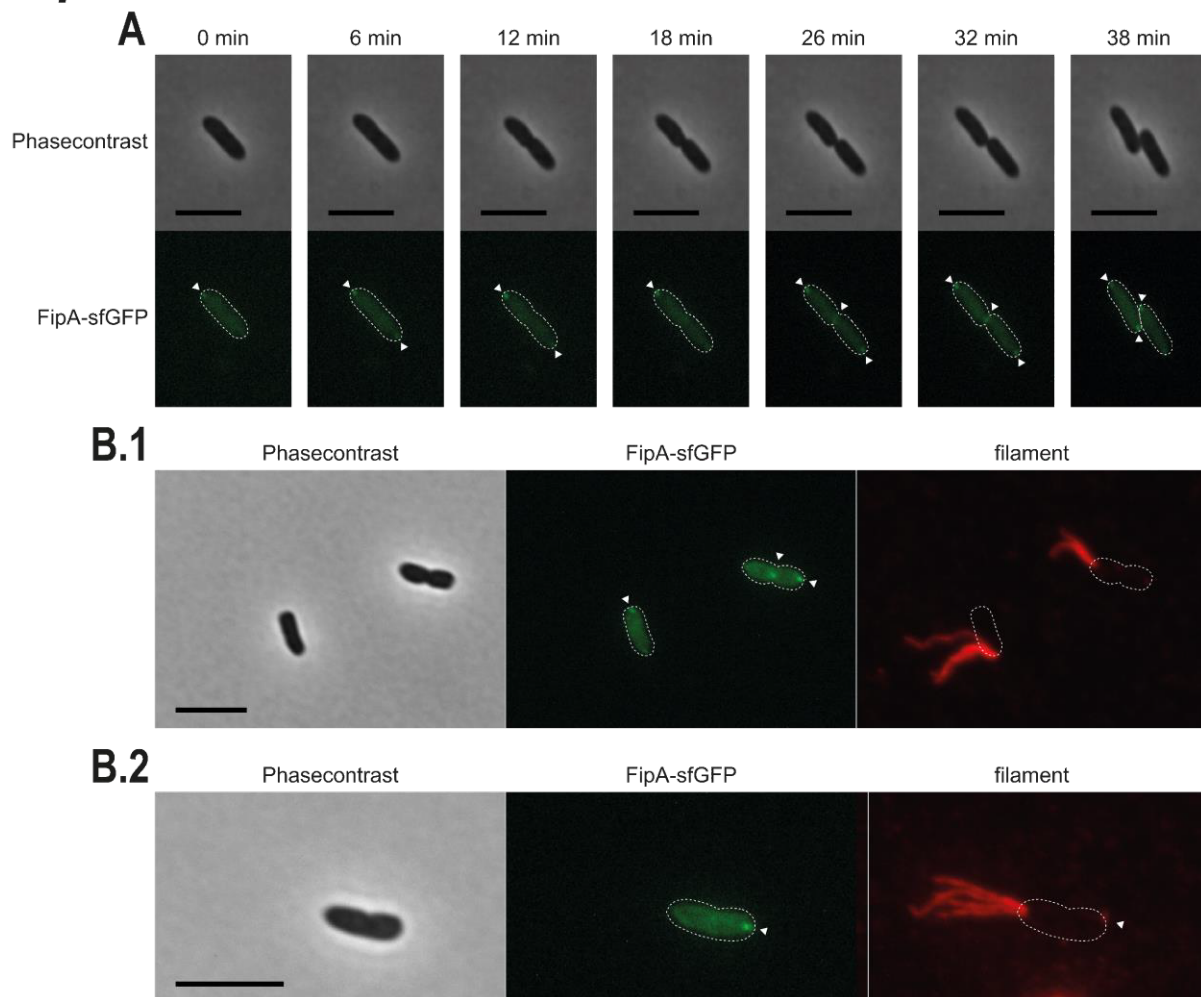
Figure 21. *Pp*FipA localisation in a spatiotemporal manner and colocalisation with the polar filament bundle in *P. putida* KT2440. (A) Micrographs taken in 10 min intervals showing spatiotemporal localisation of sfGFP tagged *Pp*FipA. **(B.1/B.2)** Micrographs showing colocalisation of sfGFP tagged *Pp*FipA with maleimide stained flagellar filament. White triangles indicate fluorescent foci formation. **Scalebar: 5 μm**.

When observing *Pp*FipA in conjunction with the filament bundle, the micrographs show *Pp*FipA mainly being associated with the opposing cell pole, when a fully formed filament bundle is present at the flagellated cell pole (**Figure 21.B.1**). Here *Pp*FipA also is positioned at the cell pole with a nascent filament bundle (white arrow in the filament channel), while the other pole, which possesses a fully formed flagellar system does not display a *Pp*FipA accumulation (**Figure 21.B.2**).

3.3 <u>Localisation and interaction phenotypes of FlhF and FipA mutant variants</u>

After having analysed FipA and its effects on cell physiology to a certain extent, it became of interest, to focus on the relation it has with FlhF and which residues are required for individual protein function, demonstrated by the effect a substitution has on localisation and motility and on homo- and heterologous interaction.

3.3.1 FlhF G-domain residues play critical role in both localisation and homo- and heterologous interaction

Firstly, FlhF residues, partially defined as functionally indispensable through previous publications [135,136] and protein sequence conservation analysis (**Supplemental figure 48**), were substituted with the amino acid alanine, while simultaneously maintaining optimised codon usage for each respective species. All residues which were targeted for substitution are contained in the G-domain of FlhF, which is indispensable for the correct functioning of FlhF.

In *S. putrefaciens* CN-32 the conserved G-domain residues K^{256}, which is contained in the G1-loop and predicted to interact with phosphate groups β and γ of GTP, D^{328}, which is contained in the G3-loop and predicted to stabilise Mg^{2+} in the FlhF homodimer and D^{390} and E^{391}, which are contained in the G4-loop and are predicted to be essential for nucleoside binding, were substituted. When observing the effects caused by these substitutions, the micrographs of most of the FlhF mutant strains show FlhF-mVenus foci, with the *Sp*FlhF K^{256}A, the *Sp*FlhF D^{390}A and the *Sp*FlhF $D^{390}\_E^{391}$A mutants exhibiting an apparent decrease in FlhF localisation (**Figure 22.A**).

Here the analysis of the localisation phenotype quantification data, reveals that all substitution mutants show overall significant changes in their localisation behaviour if compared to the wild type (**Figure 22.B**). Here all mutant strains, in contrast to the wild type (6 ± 3 % of cells), show a significant increase in diffuse fluorescence starting with the *Sp*FlhF D^{328}A strain (9 ± 2 % of cells), with the smallest increase, followed by the *Sp*FlhF E^{391}A (18 ± 5 % of cells), the *Sp*FlhF D^{390}A (25 ± 4 % of cells), the *Sp*FlhF K^{256}A (32 ± 2 % of cells) and the *Sp*FlhF D^{390}A_E^{391}A strain (92 ± 2 % of cells), which also exhibited the strongest increase in diffuse fluorescence.

Opposingly, the unipolar localisation of the individual FlhF mutants is significantly decreased in a similar pattern, with the SpFlhF D^{328}A strain (84 ± 2 % of cells), exhibiting the least decrease, followed by the SpFlhF E^{391}A (75 ± 3 % of cells), the SpFlhF D^{390}A (65 ± 3 % of cells), the SpFlhF K^{256}A (65 ± 1 % of cells) and the SpFlhF D^{390}A_E^{391}A strain (8 ± 2 % of cells) almost displaying no unipolar localisation, if compared to the wild type (87 ± 3 % of cells).
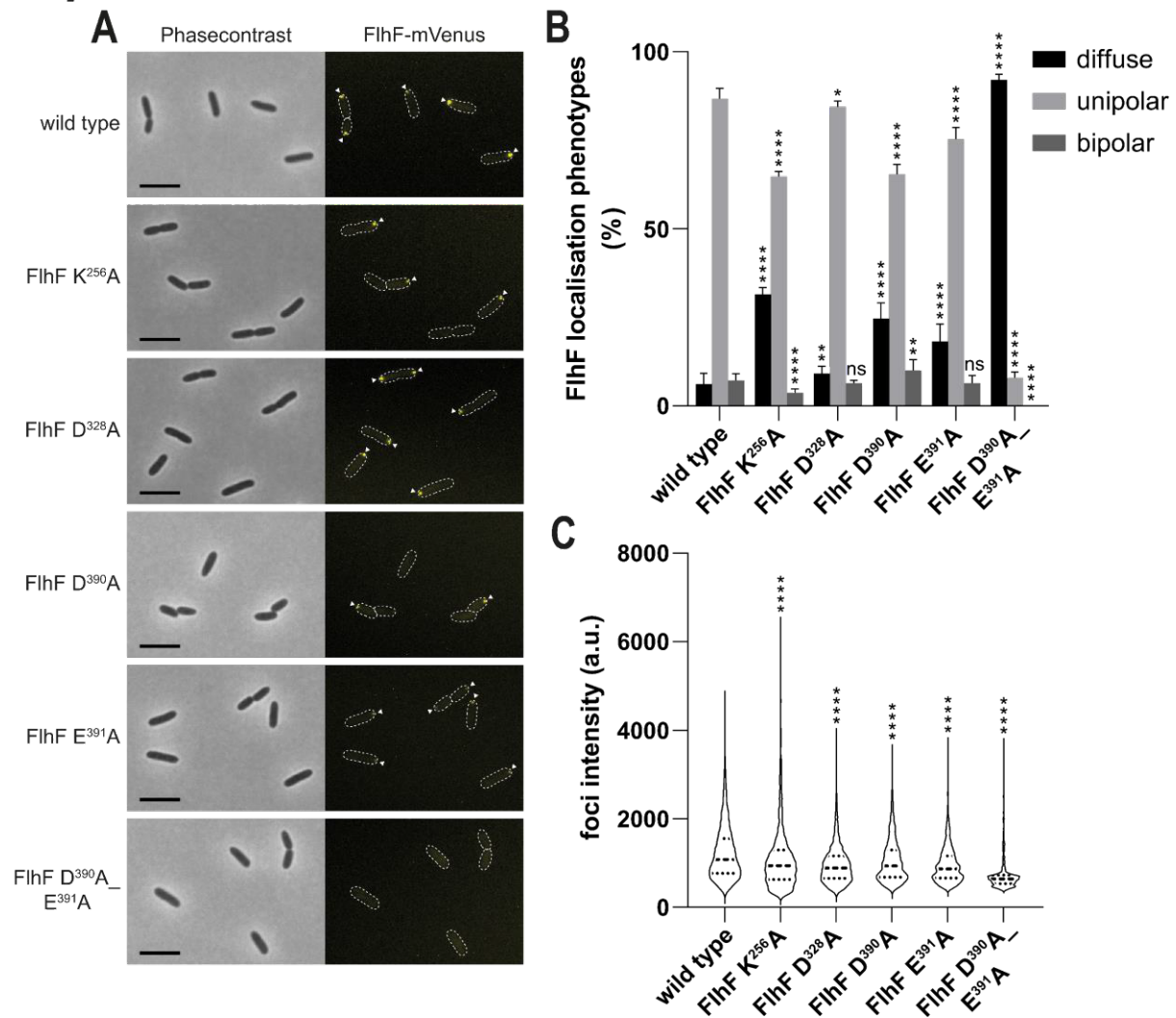
Figure 22. Effects of select residue substitutions in SpFlhF on localisation and foci intensity in S. putrefaciens CN-32. (A) Micrographs showing localisation phenotypes, **(B)** quantification of localisation phenotypes and **(C)** foci fluorescence intensities of mVenus tagged wild type and mutant variants of SpFlhF. White triangles indicate fluorescent foci formation. **Scalebar: 5 µm**. * = P value < 0.1, ** = P value < 0.01, *** = P value < 0.001, **** = P value < 0.0001. n ≥ 900 cells.

The SpFlhF D^{390}A_E^{391}A strain also does not show any bipolar localisation, observable in the wild type (7 ± 2% of cells) and other mutant strains, such as the SpFlhF D^{328}A (6 ± 1 % of cells) and SpFlhF E^{391}A strain (6 ± 2 % of cells), which do not significantly differ from the wild

type. The SpFlhF K^{256}A strain (4 ± 1 % of cells) expresses a significantly decreased bipolar localisation and the SpFlhF D^{390}A strain (10 ± 3 % of cells) a significantly increased localisation. The foci fluorescence intensity data displays a difference between the wild type (1235 ± 632 a.u.) and all analysed SpFlhF mutant strains, with all strains possessing a significantly decreased mean foci intensity (**Figure 22.C**). This drop in foci intensity appears to the least extent in the SpFlhF K^{256}A strain (1112 ± 763 a.u.), which also exhibits foci with a stronger intensity than the wild type, followed by the SpFlhF D^{390}A strain (1048 ± 478 % of cells). The SpFlhF D^{328}A (971 ± 448 a.u.) and SpFlhF E^{391}A strain (961 ± 448 a.u.) show a similar decrease in mean foci intensity, with the SpFlhF D^{390}A_E^{391}A strain (729 ± 377 a.u.), which unlike the wild type and other mutant strains, possesses a strongly condensed foci intensity profile, ultimately having the strongest decrease in mean foci intensity.

With having inspected the effects of the individual residue substitutions on the localisation behaviour of SpFlhF, the influence on overall motility was assessed (**Figure 23.A**). Naturally, in comparison to the wild type, the complete deletion of flhF (41 ± 1 % of WT spreading area) resulted in a highly significant decrease in overall motility, indicated by the ability to cover a certain area through spreading on soft agar. The SpFlhF D^{390}A_E^{391}A strain (41 ± 3 % of WT spreading area) exhibited a similar spreading phenotype, while the other mutant strains, albeit showing a significant decrease in spreading, if compared to the wild type, still showed a stronger ability to spread on soft agar than the ΔflhF and the SpFlhF D^{390}A_E^{391}A strain, with the SpFlhF D^{390}A strain (82 ± 4 % of WT spreading area), in comparison to the wild type, displaying the least decrease in spreading ability, followed by the SpFlhF E^{391}A (81 ± 2 % of WT spreading area), then the SpFlhF D^{328}A (80 ± 2 % of WT spreading area) and finally the SpFlhF K^{256}A strain (70 ± 2 % of WT spreading area). As confirmed by BACTH assay, homologous interaction between wild type SpFlhF and these SpFlhF mutants, appears to be mostly possible in a N- to C-terminal manner, with there being a decrease in interactivity between SpFlhF K^{328}A and wild type SpFlhF and an absence of interaction between both SpFlhF D^{390}A and SpFlhF D^{390}A_E^{391}A mutant with the wild type SpFlhF (**Figure 23.B**). The results are much less clear concerning the interaction in a C- to C-terminal manner with there being an inconsistent colour pattern in the previously interacting protein pairs, and a strong interaction for the previously not interacting protein pairs.

S. putrefaciens
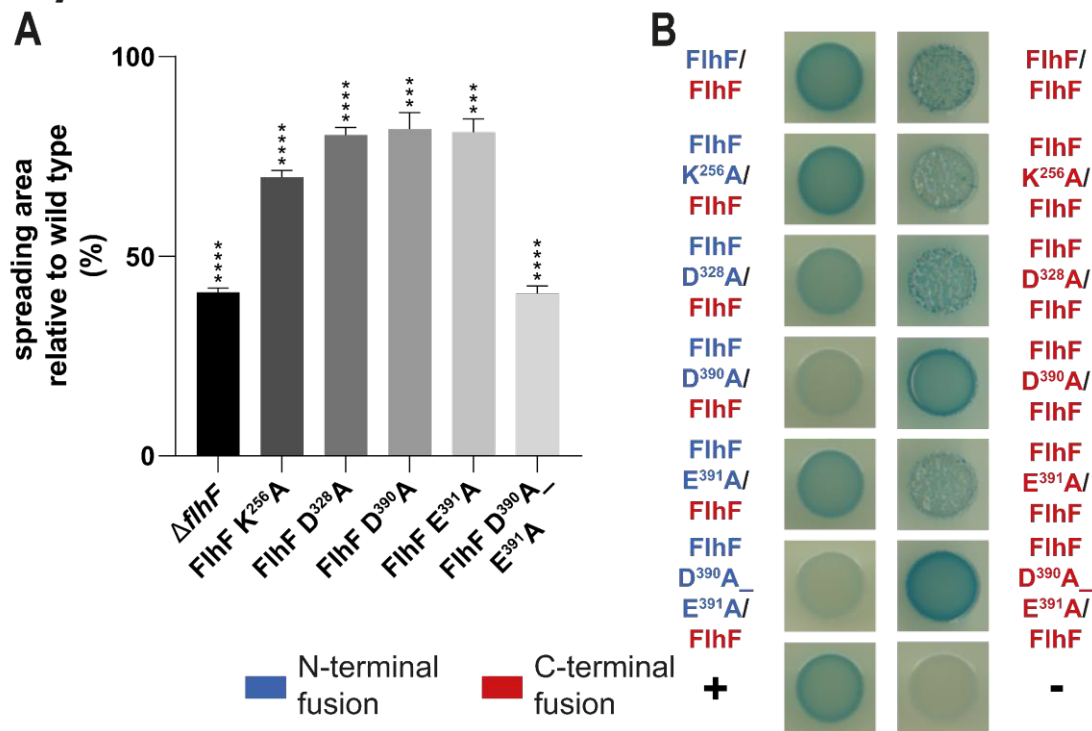
Figure 23. Effects of select residue substitutions in *Sp*FlhF on overall motility and homologous interaction in *S. putrefaciens* CN-32. (A) Spreading area of *Sp*FlhF mutant strains relative to the wild type spreading phenotype. **(B)** BACTH assay of FlhF mutants with wild type *Sp*FlhF. In each interaction the protein named first is fused to T25 and the second protein is fused to T18, while N-terminal fusion indicates a fusion of the respective catalytic domain to the N-terminus of the protein of interest and C-terminal fusion indicates a fusion of the respective catalytic domain to the C-terminus of the protein of interest. ***** = P value < 0.001**, ****** = P value < 0.0001**.

In *P. putida* KT2440 the orthologous *Pp*FlhF residues K^{229} (G1-loop), D^{301} (G3-loop) and D^{362} (G4-loop), with the addition of the residue K^{235} (positioned approximately 5 residues downstream from G1-loop), were substituted. For these strains, the micrographs show a clear absence of *Pp*FlhF localisation, in the *Pp*FlhF K^{229}A, the *Pp*FlhF D^{301}A and the *Pp*FlhF D^{362}A mutants, while the *Pp*FlhF K^{235}A strain still displays *Pp*FlhF-mCherry foci (**Figure 24.A**). When quantifying the *Pp*FlhF localisation phenotypes, all mutant strains exhibit a significant increase in diffuse fluorescence if compared to the wild type (26 ± 4 % of cells), with the *Pp*FlhF K^{235}A strain (39 ± 3 % of cells) showing a moderate increase in diffuse fluorescence and the other *Pp*FlhF substitution strains, as neither uni- nor bipolar foci formation can be observed, possess diffuse fluorescence in 100% of cells (**Figure 24.B**). Unipolar *Pp*FlhF localisation on the other hand is significantly decreased in the *Pp*FlhF K^{235}A strain (51 ± 2 % of cells), if compared to the wild type (63 ± 2 % of cells), while bipolar localisation in the *Pp*FlhF K^{235}A strain (10 ± 2 % of cells) does not show any significant difference from the wild type (11 ± 3 % of cells).

P. putida
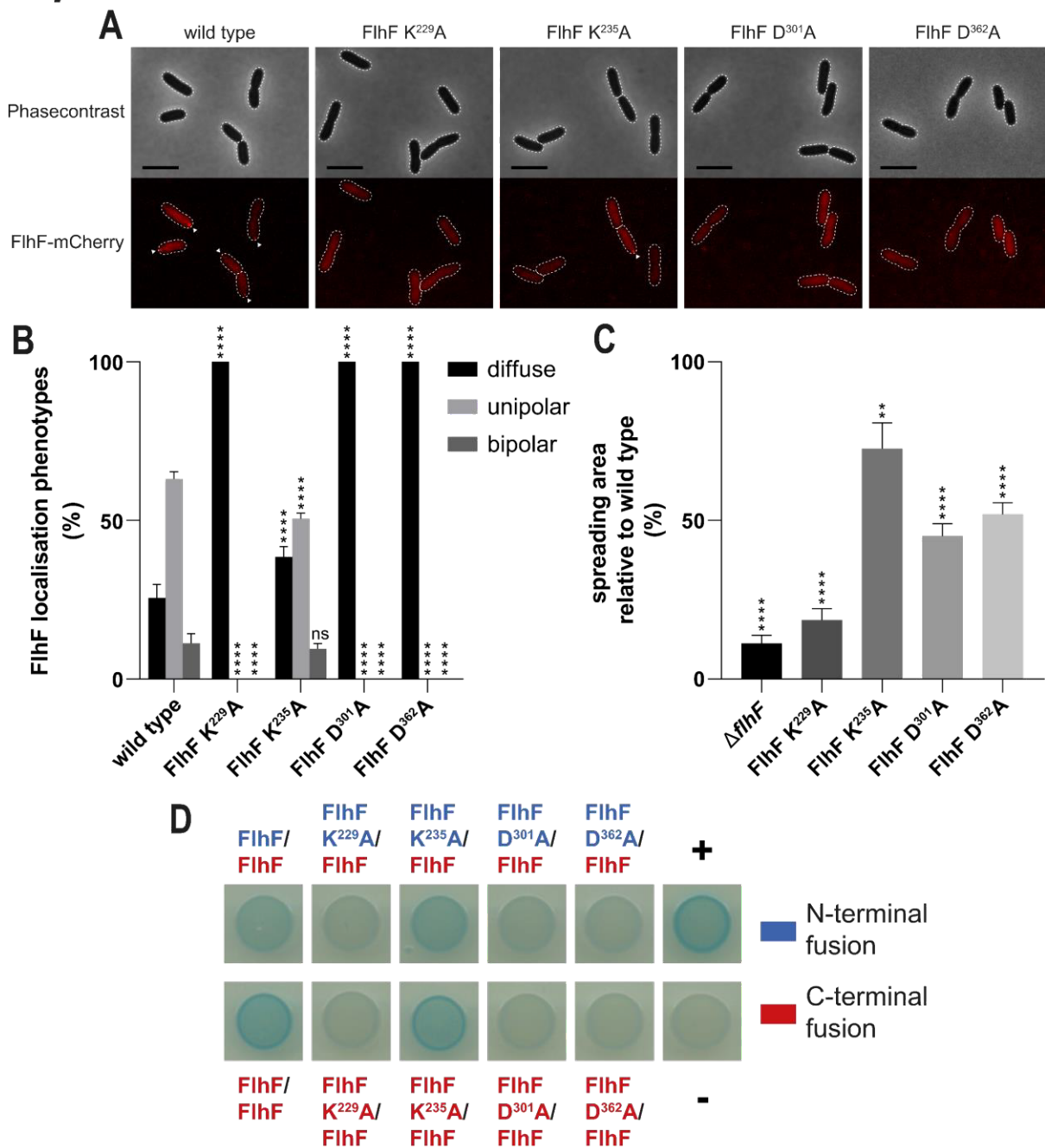
Figure 24. Effects of select residue substitutions in *Pp*FlhF on localisation, foci intensity, overall motility, and homologous interaction in *P. putida* KT2440. (A) Micrographs showing localisation phenotypes and **(B)** quantification of localisation phenotypes of mCherry tagged wild type and mutant variants of *Pp*FlhF. **(C)** Spreading area of *Pp*FlhF mutant strains relative to the wild type spreading phenotype. **(D)** BACTH assay of FlhF mutants with wild type *Pp*FlhF. In each interaction the protein named first is fused to T25 and the second protein is fused to T18, while N-terminal fusion indicates a fusion of the respective catalytic domain to the N-terminus of the protein of interest and C-terminal fusion indicates a fusion of the respective catalytic domain to the C-terminus of the protein of interest. White triangles indicate fluorescent foci formation. **Scalebar: 5 μm**. **** = P value < 0.01**, ****** = P value < 0.0001**. **n ≥ 900 cells**.

Motility, as indicated by the ability to spread on soft agar, is significantly impacted by the deletion of *flhF* (11 ± 2 % of WT spreading area), with the *Pp*FlhF K^{229}A (19 ± 4 % of WT spreading area) strain showing a similar decrease in spreading ability (**Figure 24.C**). The remaining *Pp*FlhF substitution strains all show a significantly decreased spreading phenotype, if compared to the wild type, with the *Pp*FlhF K^{235}A strain (73 ± 8 % of WT spreading area) showing the least decrease, followed by the *Pp*FlhF D^{362}A strain (52 ± 4 % of WT spreading area) and then the *Pp*FlhF D^{301}A (45 ± 4 % of WT spreading area) strain. Homologous protein-protein interaction between the *Pp*FlhF mutant variants and the *Pp*FlhF wild type protein, like the localisation, is strongly impacted by the K^{229}A, the D^{301}A as well as the D^{362}A substitution, as indicated by the BACTH assay (**Figure 24.D**). Here none of these *Pp*FlhF mutants can interact with wild type *Pp*FlhF in neither a N- nor a C-terminal manner, while the *Pp*FlhF K^{235}A substitution mutant still is able to interact with wild type *Pp*FlhF in both terminus configurations.

As FlhF, to varying degrees, affected FipA in its ability to target the cell pole, the impact, which these substitutions in FlhF have on the localisation behaviour of FipA and on the heterologous interaction between FlhF and FipA, became the successive target of investigation.

For *S. putrefaciens* CN-32 the microscopical analysis of these *Sp*FlhF substitution strains showed *Sp*FipA-sfGFP foci still forming at cell poles, with there being a slight noticeable decrease in some strains (**Figure 25.A**). Here the quantification of the *Sp*FipA localisation, displays a significant increase in diffuse fluorescence, occurring in varying degrees, observable in the Δ*flhF* (21 ± 5 % of cells), the *Sp*FlhF K^{256}A (19 ± 4 % of cells), the *Sp*FlhF D^{390}A (20 ± 4 % of cells) and the *Sp*FlhF D^{390}A_E^{391}A strain (20 ± 3 % of cells), while the *Sp*FlhF D^{328}A (13 ± 2 % of cells) and the *Sp*FlhF E^{391}A strain (15 ± 4 % of cells) show no significant difference to the wild type (14 ± 6 % of cells) (**Figure 25.B**). The occurrence of unipolar *Sp*FipA localisation is similarly affected by the residue substitutions, with the Δ*flhF* (53 ± 4 % of cells), the *Sp*FlhF K^{256A}A (56 ± 2 % of cells), the *Sp*FlhF D^{390}A (56 ± 2 % of cells) and the *Sp*FlhF D^{390}A_E^{391}A strain (56 ± 2 % of cells) possessing significantly less unipolar *Sp*FipA than the wild type (61 ± 3 % of cells), while the unipolar localisation in the *Sp*FlhF D^{328}A (62 ± 2 % of cells) and the *Sp*FlhF E^{391}A strain (60 ± 3 % of cells) is not significantly different from the one observed in the wild type. Unlike the other two localisation phenotypes, the appearance of bipolar *Sp*FipA localisation in the Δ*flhF* (26 ± 2 % of cells), the *Sp*FlhF K^{256A}A (25 ± 2 % of cells), the *Sp*FlhF D^{328}A (25 ± 1 % of cells), the *Sp*FlhF D^{390}A (24 ± 2 % of cells), the *Sp*FlhF E^{391}A (25 ± 3 % of cells) and the *Sp*FlhF D^{390}A_E^{391}A strain (24 ± 2 % of cells) does not significantly differ from the bipolar localisation phenotype observable in the wild type (25 ± 5 % of cells).

S. putrefaciens
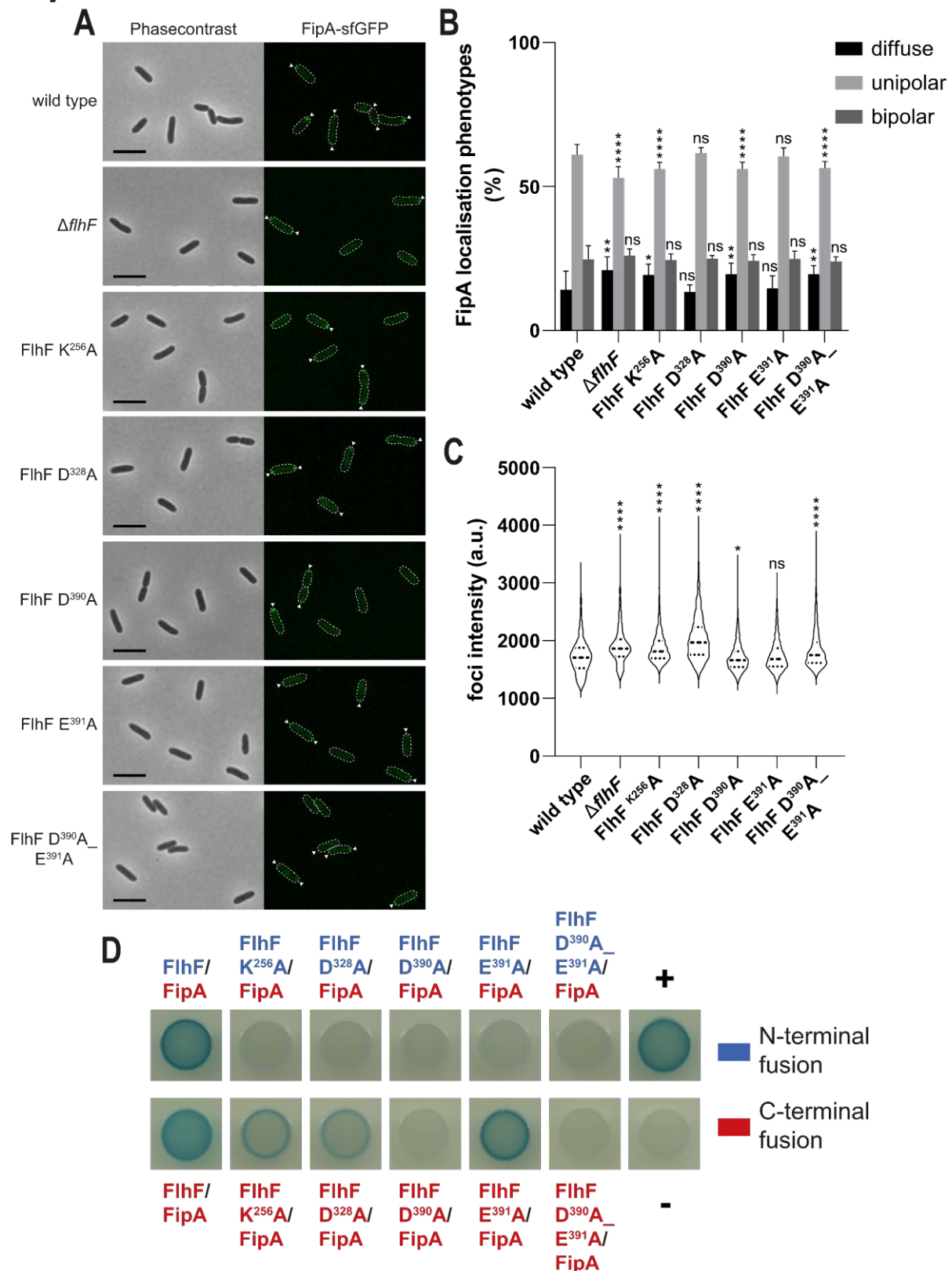
Figure 25. Effects of select residue substitutions in *Sp*FlhF on *Sp*FipA localisation, foci intensity and heterologous interaction in *S. putrefaciens* CN-32. (A) Micrographs showing localisation phenotypes, **(B)** quantification of localisation phenotypes of sfGFP tagged *Sp*FipA in *Sp*FlhF mutant strains and **(C)** foci fluorescence intensities of sfGFP tagged *Sp*FipA in *Sp*FlhF mutant strains. **(D)**

BACTH assay of *Sp*FlhF mutants with wild type *Sp*FipA. In each interaction the protein named first is fused to T25 and the second protein is fused to T18, while N-terminal fusion indicates a fusion of the respective catalytic domain to the N-terminus of the protein of interest and C-terminal fusion indicates a fusion of the respective catalytic domain to the C-terminus of the protein of interest. White triangles indicate fluorescent foci formation. **Scalebar: 5 µm**. * = P value < 0.1, ** = P value < 0.01, *** = P value < 0.001, **** = P value < 0.0001. n ≥ 900 cells.

The intensity of *Sp*FipA-sfGFP foci fluorescence also is affected by the *Sp*FlhF residue substitutions in all strains except for the $E^{391}A$ strain (1745 ± 285 a.u.), which displays a similar and not significantly different foci fluorescence intensity to that of the wild type (1728 ± 312 a.u.) (**Figure 25.C**). A significant increase in foci intensity, from strongest to weakest increase, is observable in the *Sp*FlhF $D^{328}A$ strain (2036 ± 381 a.u.), followed by the Δ*flhF* (1904 ± 313 a.u.), the *Sp*FlhF $K^{256}A$ (1874 ± 268 a.u.) and the *Sp*FlhF $D^{390}A\_E^{391}A$ strain (1843 ± 333 a.u.), while the *Sp*FlhF $D^{390}A$ strain (1710 ± 253 a.u.) exhibits an overall decrease in foci intensity if compared to the wild type. Regarding the ability of *Sp*FipA to interact with the *Sp*FlhF mutants, it clearly appears to be influenced by most substitutions, as none of the *Sp*FlhF substitution variants are able to heterologously interact with *Sp*FipA in a N- to C-terminal manner (**Figure 25.D**). In a C- to C-terminal configuration wild type-like interaction only is observable in the case of the *Sp*FlhF $E^{391}A$ protein variant, while the *Sp*FlhF $K^{256A}A$ and the *Sp*FlhF $D^{328}A$ protein variants show a weak interaction. Finally, no interaction is visible in the C- to C-terminal combination of *Sp*FipA with *Sp*FlhF $D^{390}A$ and *Sp*FlhF $D^{390}A\_E^{391}A$.

In *P. putida* KT2440, as observable in the according micrographs, the insertion of the various *Pp*FlhF residue substitutions, with exemption of the *Pp*FlhF $K^{235}A$ substitution, lead to a clear decrease in overall *Pp*FipA-sfGFP localisation, with there still being *Pp*FipA-sfGFP foci present at the poles of cells in all mutant strains (**Figure 26.A**). Through the analysis of the *Pp*FipA localisation quantification data a significant effect, caused by the deletion of *flhF* and many of the substitutions, is revealed for most of the localisation phenotypes (**Figure 26.B**). Diffuse fluorescence is, to a significant degree, positively affected by the deletion of *flhF* (93 ± 2 % of cells) followed, in decreasing occurrence, by the *Pp*FlhF $D^{362}A$ (71 ± 4 % of cells), the *Pp*FlhF $D^{301}A$ (70 ± 5 % of cells) and the *Pp*FlhF $K^{229}A$ strain (61 ± 3 % of cells), while the diffuse fluorescence exhibited by the *Pp*FlhF $K^{235}A$ strain (1 ± 2 % of cells) does not significantly differ from that of the wild type (1 ± 2 % of cells). Unipolar localisation of *Pp*FipA on the other hand is significantly affected in all observed strains, in comparison to the wild type (65 ± 3 % of cells), with the Δ*flhF* strain (7 ± 2 % of cells) exhibiting the strongest decrease, followed by the *Pp*FlhF $D^{301}A$ (24 ± 3 % of cells), the *Pp*FlhF $D^{362}A$ (25 ± 3 % of cells) and the *Pp*FlhF $K^{229}A$ strain (29 ± 2 % of cells), while the *Pp*FlhF $K^{235}A$ strain (74 ± 3 % of cells) shows a significant increase in unipolar localisation.
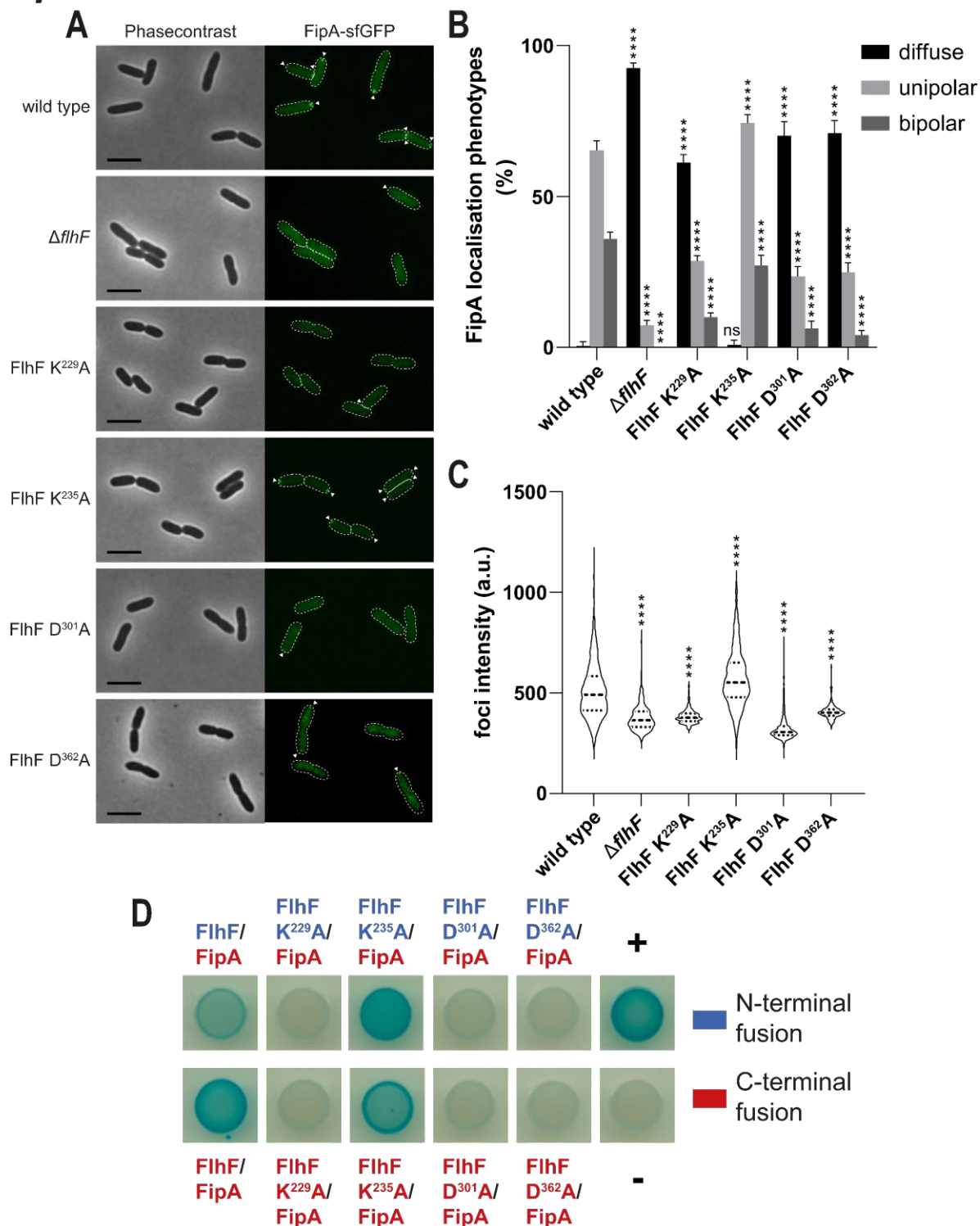
Figure 26. Effects of select residue substitutions in *Pp*FlhF on *Pp*FipA localisation, foci intensity and heterologous interaction in *P. putida* KT2440. (A) Micrographs showing localisation phenotypes, **(B)** quantification of localisation phenotypes and **(C)** foci fluorescence intensities of sfGFP tagged *Pp*FipA in *Pp*FlhF mutant strains. **(D)** BACTH assay of *Pp*FlhF mutants with wild type *Pp*FipA. In each interaction the protein named first is fused to T25 and the second protein is fused to T18, while N-terminal fusion indicates a fusion of the respective catalytic domain to the N-terminus of the protein

of interest and C-terminal fusion indicates a fusion of the respective catalytic domain to the C-terminus of the protein of interest. White triangles indicate fluorescent foci formation. **Scalebar: 5 µm**. ****** = P value < 0.0001**. **n ≥ 900 cells**.

The bipolar distribution of PpFipA also is negatively affected by the deletion of $flhF$ and the insertion of residue substitutions into PpFlhF to a significant degree, when taking the wild type (36 ± 2 % of cells) as reference. Following the $\Delta flhF$ strain, which does not possess any bipolarly localising PpFipA, the sharpest decline in bipolar localisation is observable in the PpFlhF D^{362}A strain (4 ± 2 % of cells) accompanied, with increasing bipolar occurrence, by the PpFlhF D^{301}A (6 ± 2 % of cells), the PpFlhF K^{229}A (10 ± 1 % of cells) and finally the PpFlhF K^{235}A strain (27 ± 2 % of cells). Significant effects on foci fluorescence intensity, caused by either the deletion of $flhF$ or the substitution of individual residues in PpFlhF, are shown by the foci intensity quantification data, for all analysed strains (**Figure 26.C**). The PpFlhF K^{235}A strain (572 ± 142 a.u.), albeit exhibiting a significant increase in mean foci intensity, displays a similar foci intensity profile to that of the wild type (510 ± 137 a.u.), while the D^{301}A strain (324 ± 63 a.u.), which also shows the strongest decline in foci intensity, followed by the $\Delta flhF$ (377 ± 68 a.u.), the PpFlhF K^{229}A (383 ± 35 a.u.) and the PpFlhF D^{362}A strain (405 ± 36 a.u.), possesses a foci intensity profile dissimilar to that of the wild type, but comparable to that of the PpFlhF K^{229}A and PpFlhF D^{362}A strain.

Concerning the ability of SpFlhF to heterologously interact with SpFipA, it can be observed that most of the residue substitution mutants of PpFlhF appear to severely be affected (**Figure 26.D**). The residue substitutions K^{229}A, D^{301}A and D^{362}A in PpFlhF lead to an inability of PpFipA to interact with PpFlhF in either a N- to C-terminal or a C- to C-terminal manner, while the PpFlhF K^{235}A substitution mutant still is able to interact with PpFipA in both termini configurations.

3.3.2 C-terminal FipA residues are mostly essential for both polar localisation and homo- and heterologous interaction

Following the investigation of residues in FlhF, supposedly playing a role in the heterologous interaction between FlhF and FipA, the focus was shifted towards FipA and its amino acid sequence to determine possible residues required for its interaction with FlhF. Residues were targeted according to conservation and putatively being of functional importance, as predicted by a ConSurf analysis of multiple orthologous FipA sequences (**Supplemental figure 49**). In this context, the effect, which the deletion of the predicted N-terminal transmembrane domain would have on the overall function of FipA, also was analysed.

In *S. putrefaciens* CN-32, the targets chosen for substitution, were the three residues G^{106}A, L^{118}A and L^{125}A, which all are contained in the predicted C-terminal DUF2802 domain of

*Sp*FipA. When observing the localisation of these *Sp*FipA variants, the micrographs clearly show a decrease in *Sp*FipA abundance in the *Sp*FipA ΔTMD, the *Sp*FipA G^{106}A and the *Sp*FipA L^{118}A strain, while the *Sp*FipA L^{125}A strain still shows a wild type-like amount of *Sp*FipA foci (**Figure 27.A**). This initial observation is confirmed, when viewing the localisation phenotype quantification data, as the three strains showing clear defects in overall *Sp*FipA localisation in the micrographs, also have a significantly altered *Sp*FipA localisation behaviour, if compared to the wild type (**Figure 27.B**). Here diffuse fluorescence appears significantly increased in the *Sp*FipA ΔTMD strain (93 ± 2 % of cells), followed by the *Sp*FipA L^{118}A (49 ± 6 % of cells) and the *Sp*FipA G^{106}A strain (48 ± 5 % of cells), while the diffuse fluorescence quantified for the *Sp*FipA L^{125}A strain (15 ± 3 % of cells) is not significantly different from the one observed in the wild type (14 ± 6 % of cells).

S. putrefaciens
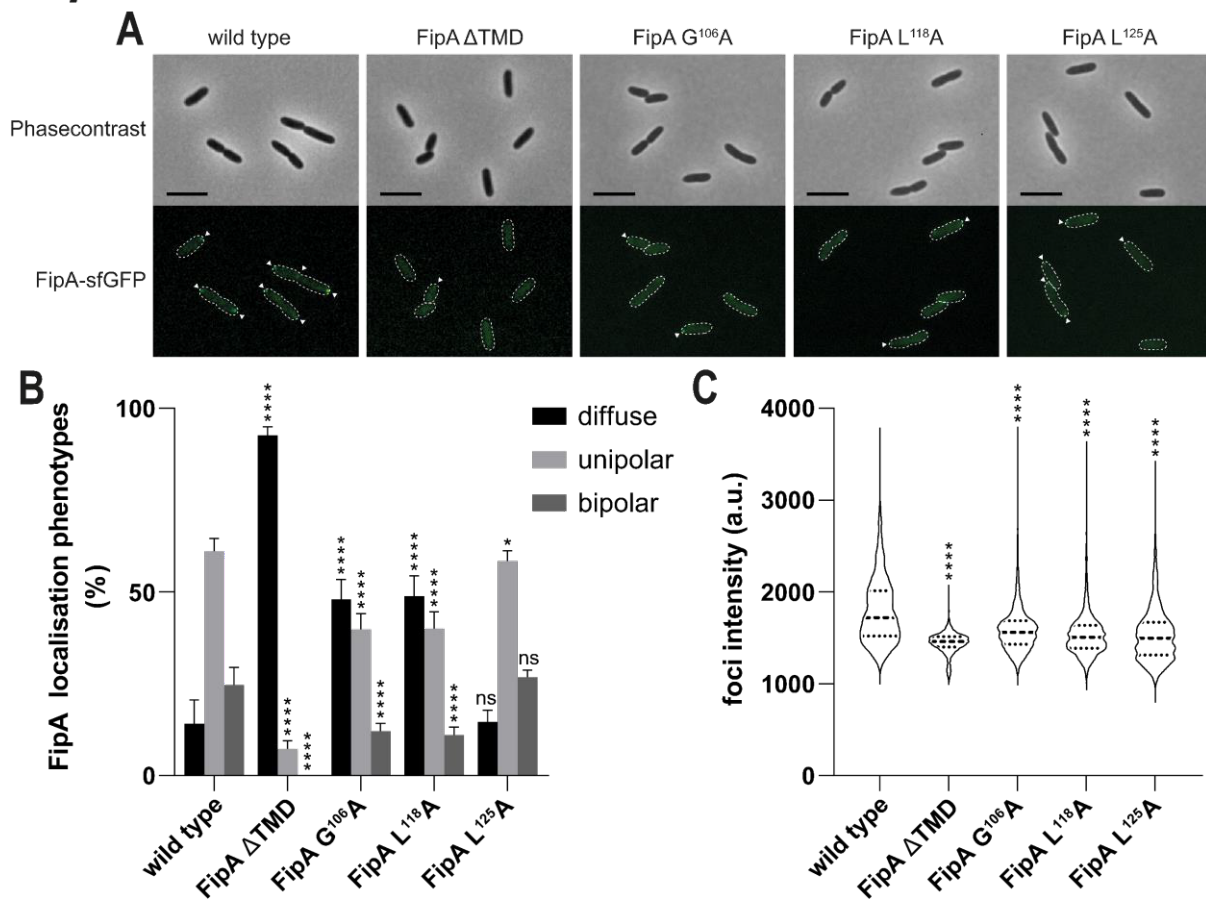
Figure 27. Effects of select residue substitutions in *Sp*FipA on localisation and foci intensity in *S. putrefaciens* CN-32. (A) Micrographs showing localisation phenotypes, **(B)** quantification of localisation phenotypes and **(C)** foci fluorescence intensities of sfGFP tagged wild type and mutant variants of *Sp*FipA. White triangles indicate fluorescent foci formation. **Scalebar: 5 µm**. * = P value < 0.1, **** = P value < 0.0001. n ≥ 900 cells.

To a similar order of magnitude, to how the diffuse fluorescence is increased in most of the observed mutant strains, a decrease in unipolar localisation of SpFipA is exhibited by all SpFipA mutant strains and therefore significantly differs from the unipolar SpFipA localisation phenotype seen in the wild type (61 ± 3 % of cells). Here the strongest decrease is visible in the SpFipA ΔTMD strain (7 ± 2 % of cells), followed, with decreasing severity, by the SpFipA $G^{106}A$ (40 ± 4 % of cells) and the SpFipA $L^{118}A$ strain (40 ± 5 % of cells), while the SpFipA $L^{125}A$ strain (58 ± 3 % of cells) displays a unipolar localisation phenotype of SpFipA, which is only slightly, but still significantly different from the one observed for the wild type. Bipolar localisation of SpFipA appears similarly affected by the TMD deletion and residue substitutions, with there being no bipolar SpFipA localisation in the SpFipA ΔTMD strain. The SpFipA $G^{106}A$ (12 ± 2% of cells) and SpFipA $L^{118}A$ strain (11 ± 2 % of cells) still, albeit being significantly decreased in comparison to the wild type (25 ± 5 % of cells), possess bipolar accumulations of SpFipA, while the $L^{125}A$ (27 ± 2 % of cells) substitution does not significantly affect SpFipA in its bipolar localisation behaviour. The intensity of foci fluorescence also appears to be significantly affected by all modifications introduced into SpFipA, with the SpFipA ΔTMD strain (1447 ± 116 a.u.) differing the most from the wild type (1796 ± 365 a.u.) both in mean intensity and foci intensity profile (**Figure 27.C**). Though exhibiting a significantly decreased mean foci intensity, the SpFipA $G^{106}A$ (1594 ± 257 a.u.), the SpFipA $L^{118}A$ (1541 ± 247 a.u.) and the SpFipA $L^{125}A$ strain (1532 ± 294 a.u.) possess a foci intensity profile similar to that of the wild type, with the only exception being a decreased abundance of foci with intensities above 1800 a.u..

Motility, indicated by the ability to spread on soft agar, also appears significantly affected by both the entire deletion of Δ$fipA$ and the deletion of the SpFipA TMD and the introduction of residue substitutions (**Figure 28.A**). With the wild type as reference, the Δ$fipA$ strain (88 ± 1 % of WT spreading area) exhibits the strongest decline in spreading ability, followed by the SpFipA ΔTMD (90 ± 4 % of WT spreading area), the SpFipA $L^{118}A$ (92 ± 2 of WT spreading area), the SpFipA $G^{106}A$ (93 ± 1 % of WT spreading area) and the SpFipA $L^{125}A$ strain (93 ± 1 % of WT spreading area), with decreasing severity. The capacity to homologously interact with wild type SpFipA also appears affected in the case of the $G^{106}A$ and $L^{118}A$ substitution variants of SpFipA, as they display only a weak interaction in the N- to C-terminal interaction configuration and an almost none existent interaction when interacting in a C- to C-terminal manner (**Figure 28.B**). SpFipA $L^{125}A$ on the other hand is still able to interact with wild type SpFipA in both an N- to C-terminal and C- to C-terminal manner.

S. putrefaciens
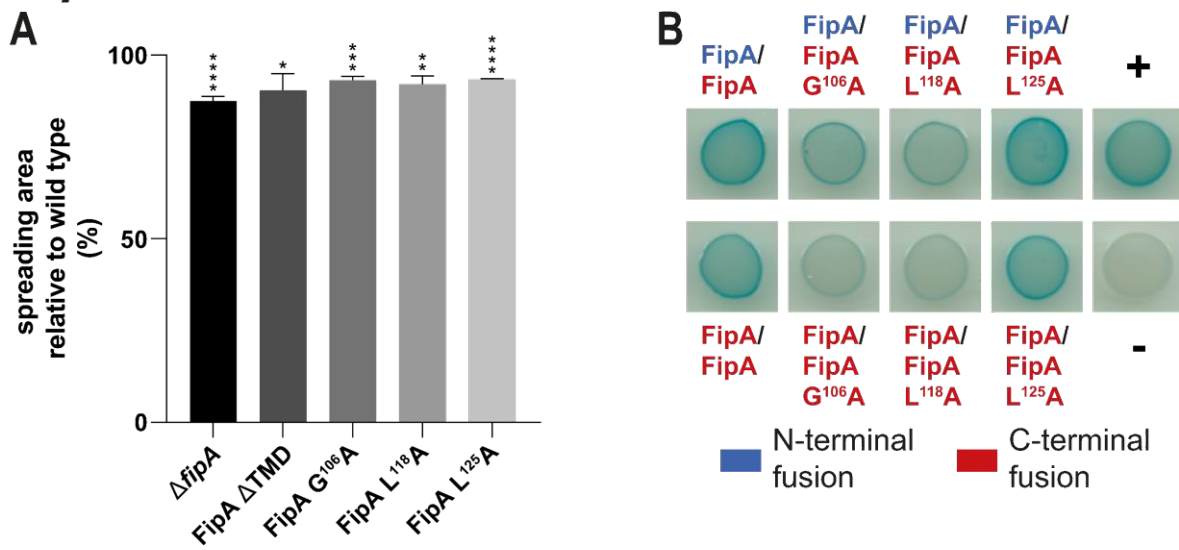
Figure 28 Effects of select residue substitutions in *Sp*FipA on overall motility and homologous interaction in *S. putrefaciens* CN-32. (A) Spreading area of *Sp*FipA mutant strains relative to the wild type spreading phenotype. **(B)** BACTH assay of *Sp*FipA mutants with wild type FipA. In each interaction the protein named first is fused to T25 and the second protein is fused to T18., while N-terminal fusion indicates a fusion of the respective catalytic domain to the N-terminus of the protein of interest and C-terminal fusion indicates a fusion of the respective catalytic domain to the C-terminus of the protein of interest. *** = P value < 0.1, ** = P value < 0.01, *** = P value < 0.001, **** = P value < 0.0001**.

In *P. putida* KT2440 the orthologous residues G^{104}, L^{116} and L^{123} of *Pp*FipA (**Supplemental figure 49**) were targeted for substitution, while the effects, caused by the deletion of the *Pp*FipA TMD, also were analysed.

Here, when viewing the micrographs, showing cells of each of the *Pp*FipA mutant strains, the localisation appears strongly affected in the *Pp*FipA ΔTMD, the *Pp*FipA L^{116}A and the *Pp*FipA L^{123}A strain, while the *Pp*FipA G^{104}A strain still shows abundant *Pp*FipA localisation (**Figure 29.A**). The localisation phenotype quantification data reveals a significant affect caused by all of the *Pp*FipA modifications on the overall ability of *Pp*FipA to target the cell pole, with the most severe effect being visible in the *Pp*FipA ΔTMD mutant strain, which only possesses diffuse fluorescence and no localising *Pp*FipA ΔTMD-sfGFP foci (**Figure 29.B**). Diffuse fluorescence also is significantly increased in the *Pp*FipA G^{104}A (25 ± 5 % of cells), the *Pp*FipA L^{116}A (94 ± 1 % of cells) and the *Pp*FipA L^{125}A strain (93 ± 2 % of cells) if compared to the wild type (1 ± 2 % of cells), with the increase occurring to the strongest degree, while also being highly similar, in the *Pp*FipA L^{116}A and the *Pp*FipA L^{123}A strain. The unipolar localisation of *Pp*FipA G^{104}A (63 ± 3 % of cells), even though still being significantly different, almost appears on the same level as the unipolar localisation of wild type *Pp*FipA (65 ± 2 % of cells). In the *Pp*FipA L^{116}A (6 ± 1 % of cells) and the *Pp*FipA L^{123}A strain (7 ± 2 % of cells) unipolar

localisation is significantly decreased and only observable in a few cells. Not being observable and therefore significantly different to the wild type (35 ± 2 % of cells), the bipolar localisation of PpFipA does not appear in the PpFipA L^{116}A and the PpFipA L^{123}A strain. Unlike these two mutant strains, the PpFipA G^{104}A strain (12 ± 3 % of cells) still possesses bipolar PpFipA localisation, with it however appearing to a significantly reduced degree if compared to the wild type. Even though PpFipA G^{104}A (517 ± 85 a.u.) appears to be significantly affected in its ability to target the cell pole, its mean foci fluorescence intensity does not significantly differ from that of the wild type (529 ± 110 a.u.), while still not matching the foci intensity profile of the wild type (**Figure 29.C**). The mean foci fluorescence intensities of the PpFipA L^{116}A (479 ± 62 a.u.) and the PpFipA L^{123}A strain (501 ± 67 a.u.) also are significantly decreased in comparison to the wild type, while also showing strongly condensed foci intensity profiles.

P. putida
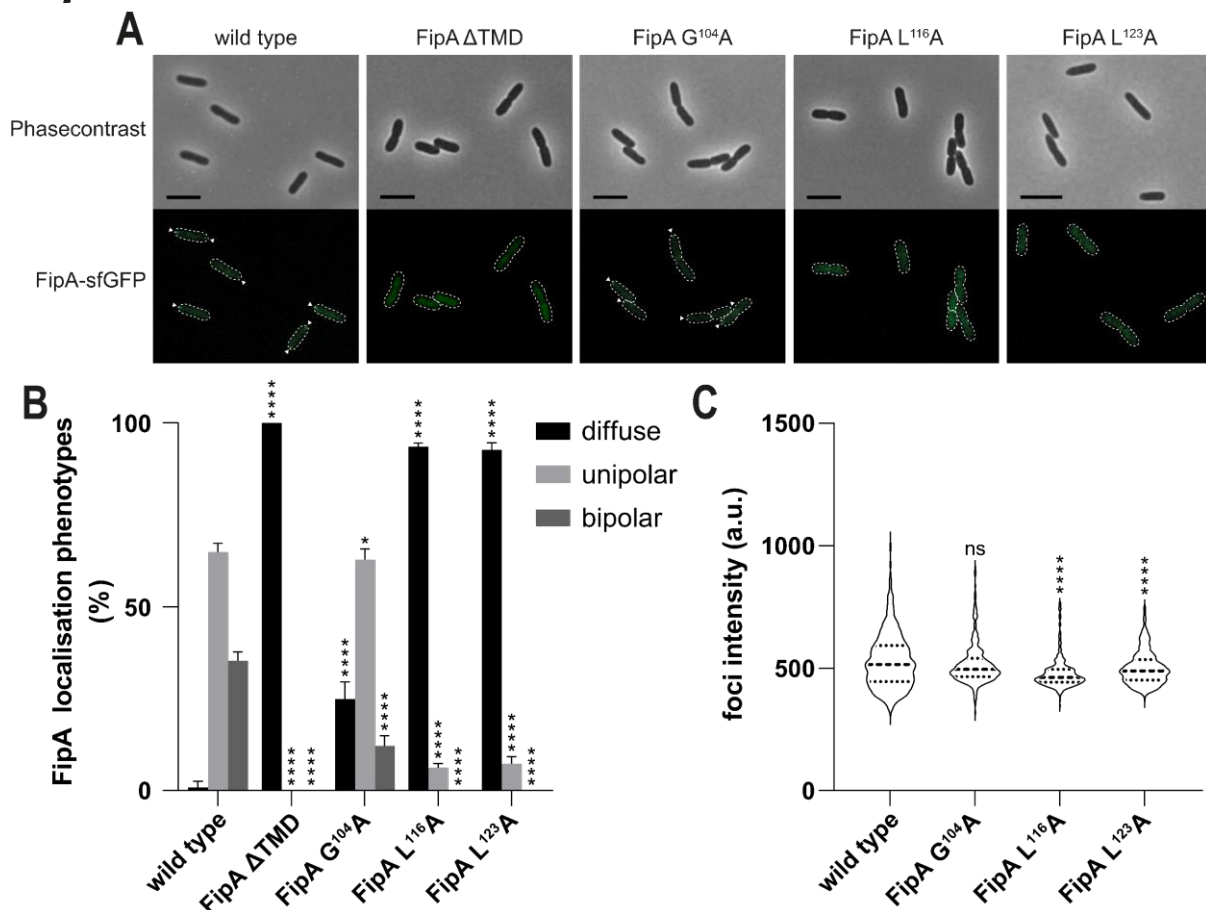
Figure 29. Effects of select residue substitutions in *Pp*FipA on localisation and foci intensity in *P. putida* KT2440. (A) Micrographs showing localisation phenotypes, **(B)** quantification of localisation phenotypes and **(C)** foci fluorescence intensities of sfGFP tagged wild type and mutant variants of *Sp*FipA. White triangles indicate fluorescent foci formation. **Scalebar: 5 µm**. * = P value < 0.1, **** = P value < 0.0001. n ≥ 900 cells.

Overall motility appears significantly affected by the introduction of modifications into the *Pp*FipA protein structure, when taking the wild type as reference, with the *Pp*FipA L^{116}A (59 ± 5 % of WT spreading area), Δ*fipA* (54 ± 5 % of WT spreading area), the *Pp*FipA ΔTMD (53 ± 3 % of WT spreading area) and the *Pp*FipA L^{123}A strains (49 ± 3 % of WT spreading area) exhibiting the strongest decrease in spreading ability (**Figure 30.A**). The reduction in spreading area observable in the *Pp*FipA G^{104}A strain (70 ± 5 % of WT spreading area), even though it is significantly reduced in comparison to that of the wild type, appears to a less severe degree than in the other corresponding strains of interest. While the localisation of *Pp*FipA and the overall motility mostly appears to be significantly affected by the insertion of residue substitutions, *Pp*FipA, as indicated by the BACTH assay, still is able to homologously interact in a C- to C-terminal manner with *Pp*FipA mutant variants carrying residue substitutions (**Figure 30.B**).
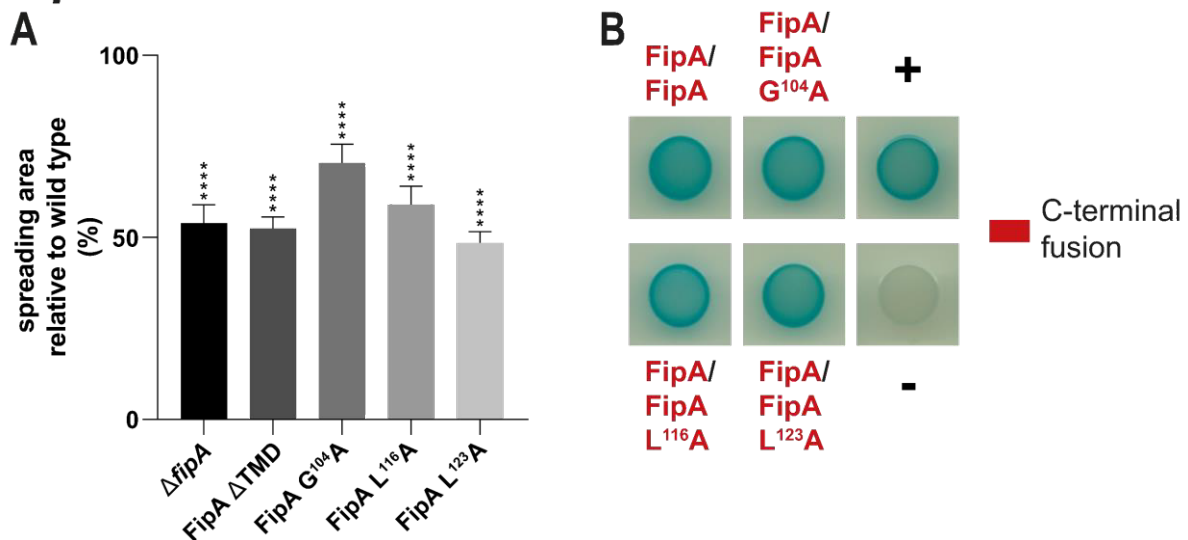
Figure 30. Effects of select residue substitutions in *Pp*FipA on overall motility and homologous interaction in *P. putida* KT2440. (A) Spreading area of FipA mutant strains relative to the wild type spreading phenotype. **(B)** BACTH assay of *Pp*FipA mutants with wild type *Pp*FipA. In each interaction the protein named first is fused to T25 and the second protein is fused to T18, while C-terminal fusion indicates a fusion of the respective catalytic domain to the C-terminus of the protein of interest. ****** = P value < 0.0001**.

Subsequently to having analysed the role, which certain protein structure features of FipA play for its overall ability to function, the effects which the modifications of FipA have on the ability of FlhF to target the cell pole and interact heterologously with FipA were investigated.

When observing the micrographs showing the appropriate *S. putrefaciens* CN-32 strains, even with all strains still displaying polar *Sp*FlhF-mVenus foci, there is a noticeable reduction in *Sp*FlhF localisation, accompanied by the occasional subpolar accumulation of *Sp*FlhF (**Figure**

31.A). The quantification of diffuse fluorescence caused by mainly cytoplasmic mVenus tagged *Sp*FlhF, only occurring in a fraction of wild type cells (5 ± 4 % of cells), yields a significant increase in all analysed strains, with the Δ*fipA* strain showing the strongest increase, followed by the *Sp*FipA L^{125}A strain (26 ± 2 % of cells), then the *Sp*FipA L^{118}A strain (24 ± 3 % of cells), the *Sp*FipA ΔTMD strain (24 ± 4 % of cells) and finally the *Sp*FipA G^{106}A strain (23 ± 3 % of cells) (**Figure 31.B**). The ability of *Sp*FlhF to localise in a unipolar manner is, in contrast to the diffuse fluorescence, significantly impeded in all analysed *Sp*FipA residue substitution strains if compared to the wild type (86 ± 3 % of cells). Here the Δ*fipA* strain (63 ± 2 % of cells) exhibits the strongest decrease, pursued closely by the *Sp*FipA L^{125}A strain (68 ± 1 % of cells), then the *Sp*FipA L^{118}A (71 ± 3 % of cells), the *Sp*FipA G^{106}A (73 ± 2 % of cells) and lastly the *Sp*FipA ΔTMD strain (73 ± 4 % of cells). Similarly, the ability of *Sp*FlhF to localise bipolarly is impeded in the *Sp*FipA mutant strains, with the strongest decrease, in comparison to the wild type (8 ± 2 % of cells), appearing to an equal degree in the Δ*fipA* (3 ± 1 % of cells) and the *Sp*FipA ΔTMD strain (3 ± 2 % of cells), followed, in decreasing severity, by the *Sp*FipA L^{125}A (4 ± 1 % of cells), the *Sp*FipA L^{118}A (5 ± 1 % of cells) and ultimately the *Sp*FipA G^{106}A strain (5 ± 2 % of cells). As already observed in the Δ*fipA* single deletion strain (4 ± 2 % of cells) (**Figure 9B**), the modifications introduced into *Sp*FipA lead to a subpopulation of *Sp*FlhF localising in a subpolar position, being a phenotype not observed in the wild type. Here the *Sp*FipA L^{125}A strain (4 ± 3 % of cells) shows the strongest phenotype, followed by the *Sp*FipA L^{118}A (3 ± 2 % of cells), the *Sp*FipA ΔTMD (2 ± 2 % of cells) and lastly the *Sp*FipA G^{104}A strain (1 ± 1% of cells). *Sp*FlhF foci fluorescence intensity profiles appear to mostly not differ from the wild type in a strong way, with the profile of the *Sp*FipA L^{125}A strain (819 ± 418 a.u.) however being the most dissimilar, while also having a significantly different mean value of foci fluorescence intensity to that of the wild type (1105 ± 538 a.u.) (**Figure 31.C**). Following, the *Sp*FipA L^{125}A strain, the Δ*fipA* (882 ± 386 a.u.), the *Sp*FipAL^{118}A (917 ± 423 a.u.) and finally the *Sp*FipA G^{106}A strain (957 ± 446 a.u.) possess a significantly decreased mean foci intensity, if compared to the wild type, while however still exhibiting a foci intensity profile similar to that of the wild type. The *Sp*FipA ΔTMD strain (1076 ± 452 a.u.) however does not significantly differ from the wild type in its mean value of foci fluorescence intensity, while also displaying a similar foci fluorescence intensity profile. Concerning the ability to heterologously interact, the *Sp*FipA L^{125}A mutant is mostly still able to interact with *Sp*FlhF in both a C-to C-terminal and a C- to N-terminal manner, which however appears much weaker than observed in the interaction of the wild type proteins. For the *Sp*FipA G^{106}A and the *Sp*FipA L^{118}A mutant variants of *Sp*FipA, the ability to interact with *Sp*FlhF in a *Sp*FlhF-N- to *Sp*FipA-C-terminal configuration is not possible.

S. putrefaciens
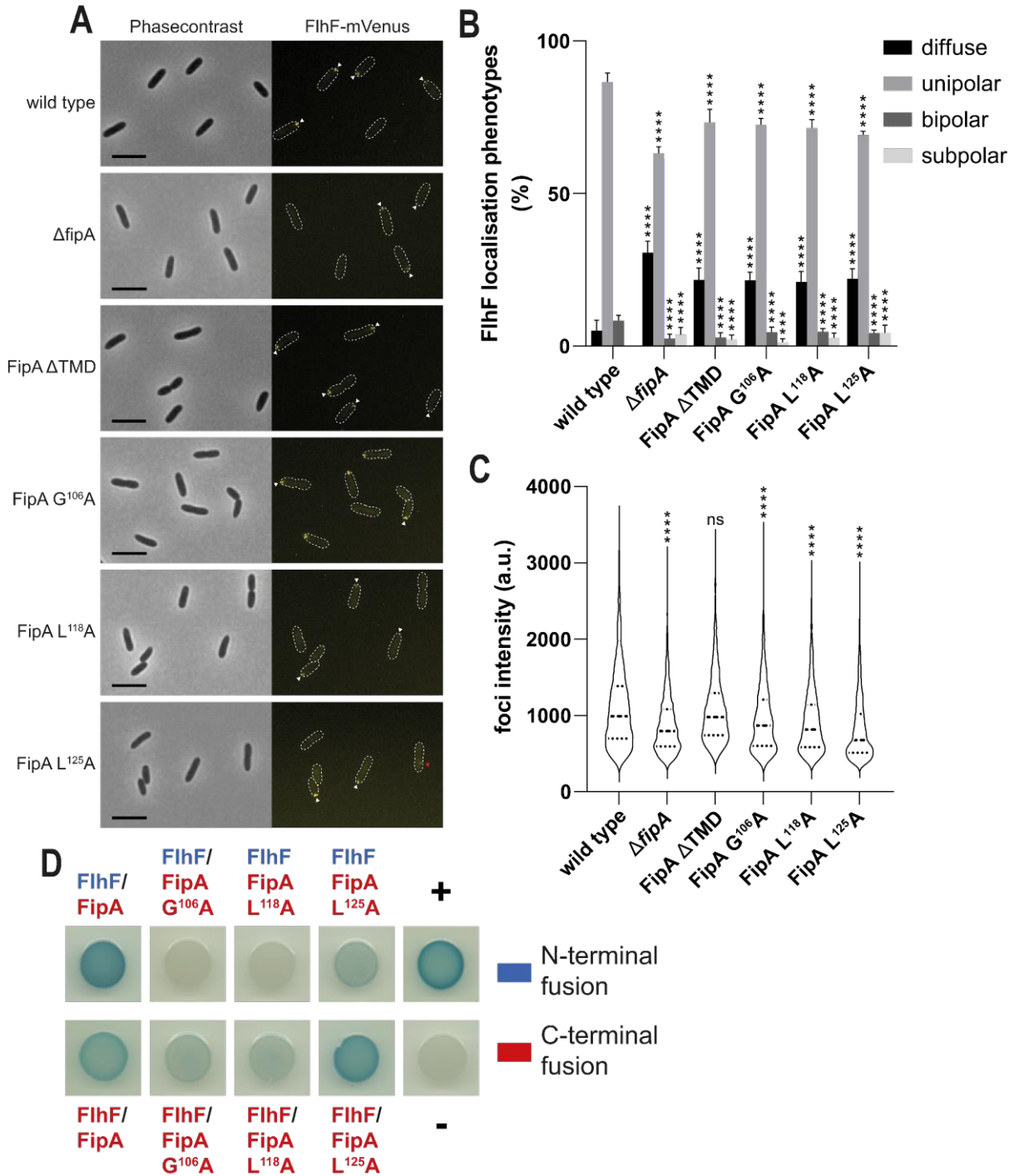
Figure 31. Effects of select residue substitutions in *Sp*FipA on *Sp*FlhF localisation, foci intensity and heterologous interaction in *S. putrefaciens* CN-32. (A) Micrographs showing localisation phenotypes, **(B)** quantification of localisation phenotypes and **(C)** foci fluorescence intensities of mVenus tagged *Sp*FlhF in *Sp*FipA mutant strains. **(D)** BACTH assay of *Sp*FipA mutants with wild type *Sp*FlhF. In each interaction the protein named first is fused to T25 and the second protein is fused to T18, while N-terminal fusion indicates a fusion of the respective catalytic domain to the N-terminus of the protein of interest and C-terminal fusion indicates a fusion of the respective catalytic domain to the C-terminus of the protein of interest. White triangles indicate fluorescent foci formation. **Scalebar: 5 µm. *** = P value < 0.001**, ***** = P value < 0.0001**. **n ≥ 900 cells**.

The capacity to heterologously interact in a C- to C-terminal manner also is strongly affected for these two *Sp*FipA mutant proteins, as they only show a very low interaction with *Sp*FlhF, if compared to the control performed with the corresponding wild type proteins (**Figure 31.D**).

In *P. putida* KT2440 the introduction of modifications into *Pp*FipA had an effect on *Pp*FlhF localisation comparable with the entire deletion of the *fipA* gene, as the formation of *Pp*FlhF-mCherry foci was strongly inhibited in all of the analysed strains (**Figure 32.A**). When viewing the quantification data, a similar picture is presented, as the diffuse fluorescence, in comparison to the wild type (26 ± 4 % of cells), is significantly increased in all of the *Pp*FipA mutant strains, with the *Pp*FipA ΔTMD (99 ± 1 % of cells) and the Δ*fipA* strain (96 ± 2 % of cells) showing the strongest increase in diffuse fluorescence (**Figure 32.B**). The strains carrying residue substitutions in *Pp*FipA are, with the most severe defect in *Pp*FlhF-mCherry foci formation, led by the *Pp*FipA L^{123}A strain (92 ± 1 % of cells) followed by the *Pp*FipA L^{104}A (92 ± 2 % of cells) and the *Pp*FipA G^{116}A strain (88 ± 2 % of cells) with decreasing amounts of diffuse fluorescence. Opposingly to the strong increase in diffuse fluorescence, the *Pp*FipA mutant strains show a significant decrease in unipolarly localising *Pp*FlhF, strongly differing from the phenotype observable in the wild type (63 ± 2 % of cells). Here the least cells with unipolar aggregation of *Pp*FlhF are observable for the *Pp*FipA ΔTMD strain (1 ± 1 % of cells), which is followed by the Δ*fipA* (4 ± 2 % of cells), the *Pp*FipA G^{104}A (8 ± 1 % of cells), the *Pp*FipA L^{123}A (8 ± 1 % of cells) and lastly the *Pp*FipA L^{116}A strain (11 ± 1 % of cells) with an increasing unipolar localisation of *Pp*FlhF. Bipolar accumulation of *Pp*FlhF, which is observable in a subpopulation of the wild type (11 ± 2 % of cells), is not exhibited for any of the *Pp*FipA mutant strains, except for the *Pp*FipA L^{116}A (1 ± 1 % of cells) strain, in which the amount of bipolarly localising *Pp*FlhF is significantly reduced. The ability to heterologously interact with wild type *Pp*FlhF appears to in part be strongly affected by the introduction of residue substitutions into *Pp*FipA, as *Pp*FipA L^{116}A and the *Pp*FipA L^{123}A mutant proteins are not able to interact with *Pp*FlhF in a *Pp*FlhF-N- to *Pp*FipA-C-terminal manner (**Figure 32.C**). The substitution of G^{104} in *Pp*FipA also appears to severely affect the ability of *Pp*FipA to interact with *Pp*FlhF in this manner, with there however still being a weak capacity to interact in the N- to C-terminal configuration. A C- to C-terminal interaction with *Pp*FlhF still appears to be achievable for all *Pp*FipA residue substitution mutants, as observable in the BACTH assay.
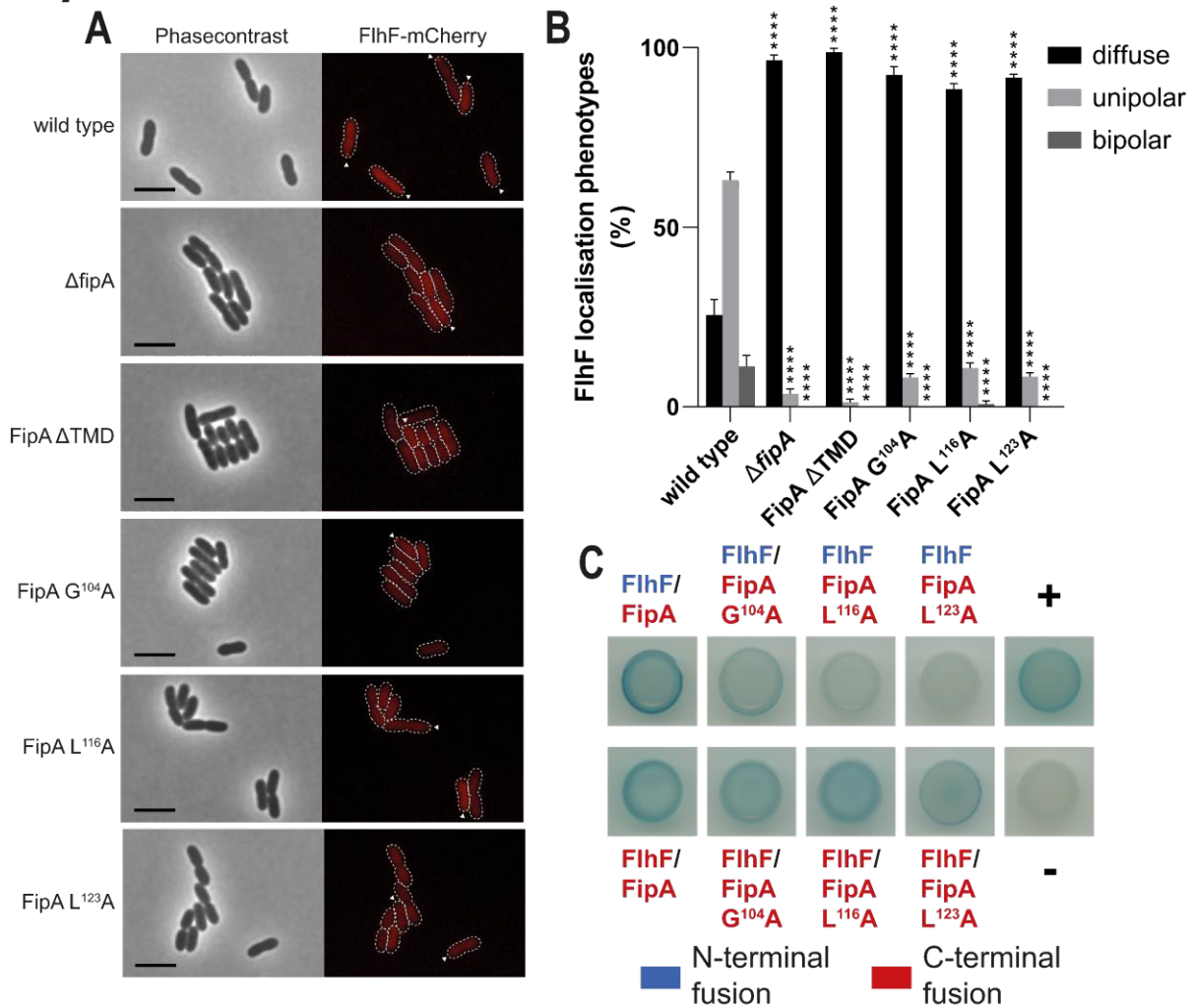
Figure 32. Effects of select residue substitutions in *Pp*FipA on *Pp*FlhF localisation and heterologous interaction in *P. putida* KT2440. (A) Micrographs showing localisation phenotypes and **(B)** quantification of localisation phenotypes of mCherry tagged *Pp*FlhF in *Pp*FipA mutant strains. **(C)** BACTH assay of *Pp*FipA mutants with wild type *Pp*FlhF. In each interaction the protein named first is fused to T25 and the second protein is fused to T18, while N-terminal fusion indicates a fusion of the respective catalytic domain to the N-terminus of the protein of interest and C-terminal fusion indicates a fusion of the respective catalytic domain to the C-terminus of the protein of interest. White triangles indicate fluorescent foci formation. **Scalebar: 5 µm**. ****** = P value < 0.0001**. **n ≥ 900 cells**.

3.4 FlhB "Proline Rich Region" (PRR) is essential for flagellar hook and filament but not C-ring assembly

Besides investigating the localisation dynamics of FlhF and its targeting factor FipA, this study aimed to characterise a C-terminal feature of the fT3SS protein FlhB in *S. putrefaciens* CN-32 (*Sp*FlhB) and its involvement in the flagellin export and the assembly of additional flagellar substructures of the polar flagellar system. This peculiar element positioned at the C-terminus of the cytoplasmic domain of *Sp*FlhB (*Sp*FlhB-C; residues 252-376) consists of an amino acid motif rich in prolines and was therefore appropriately name "**P**roline **R**ich **R**egion" (PRR). Besides the deletion of this motif, the effects on the formation of the polar flagellar structure, caused by substitution of the *Sp*FlhB-C auto cleavage site N^{269} and a substitution of the residue Y^{376}, required for the facilitation of hydrophobic interactions between the PRR and the *Sp*FlhB-C core domain, were investigated [165]. The results obtained from this study were published in the journal frontiers in Microbiology [1].

As *Sp*FlhB, in the later stages of flagellar assembly, is essential for the export of flagellins, required for the assembly of the flagellar filament, the effects, which modifications to the protein structure of *Sp*FlhB have on this function, were the first thing to be analysed. Here, as clearly seen in the micrographs, the cells in the *Sp*FlhB ΔPRR and the *Sp*FlhB Y^{376}A strain still form wild type-like flagellar filaments, whereas the cells in the *Sp*FlhB N^{269}A and the Δ*flhB* strain are devoid of filament structures (**Figure 33.A**). The quantification of filaments shows that the deletion of the PRR motif of *Sp*FlhB (46 ± 5 % of cells) leads to a significant decrease in flagellation, as indicated by the decline in stainable filaments, while the substitution of Y^{376} (64 ± 7 % of cells) does not cause a significant reduction of filament formation, in comparison to the wild type (67 ± 7 % of cells) (**Figure 33.B**). As observed in the micrograph data, both the Δ*flhB* and the *Sp*FlhB N^{269}A strain significantly differ from the wild type, as they are incapable of forming flagellar filaments. With the *Sp*FlhB ΔPRR strain showing a clear defect in filament formation, the overall efficiency and stability of the flagellin export mechanism of *Sp*FlhB ΔPRR was investigated by quantifying the abundance of flagellar filaments according to their length, in relation to the wild type (**Figure 33.C**). Here the *Sp*FlhB ΔPRR strain, in comparison to the wild type and the *Sp*FlhB Y^{376}A strain, which does not differ from the wild type, shows a clear deficit in abundance, across the entire range of measured filament lengths, with a much larger portion of filaments being shorter than 1 μm, 2 μm, 3 μm and 4 μm than in the corresponding categories of the wild type and the *Sp*FlhB Y^{376}A strain.
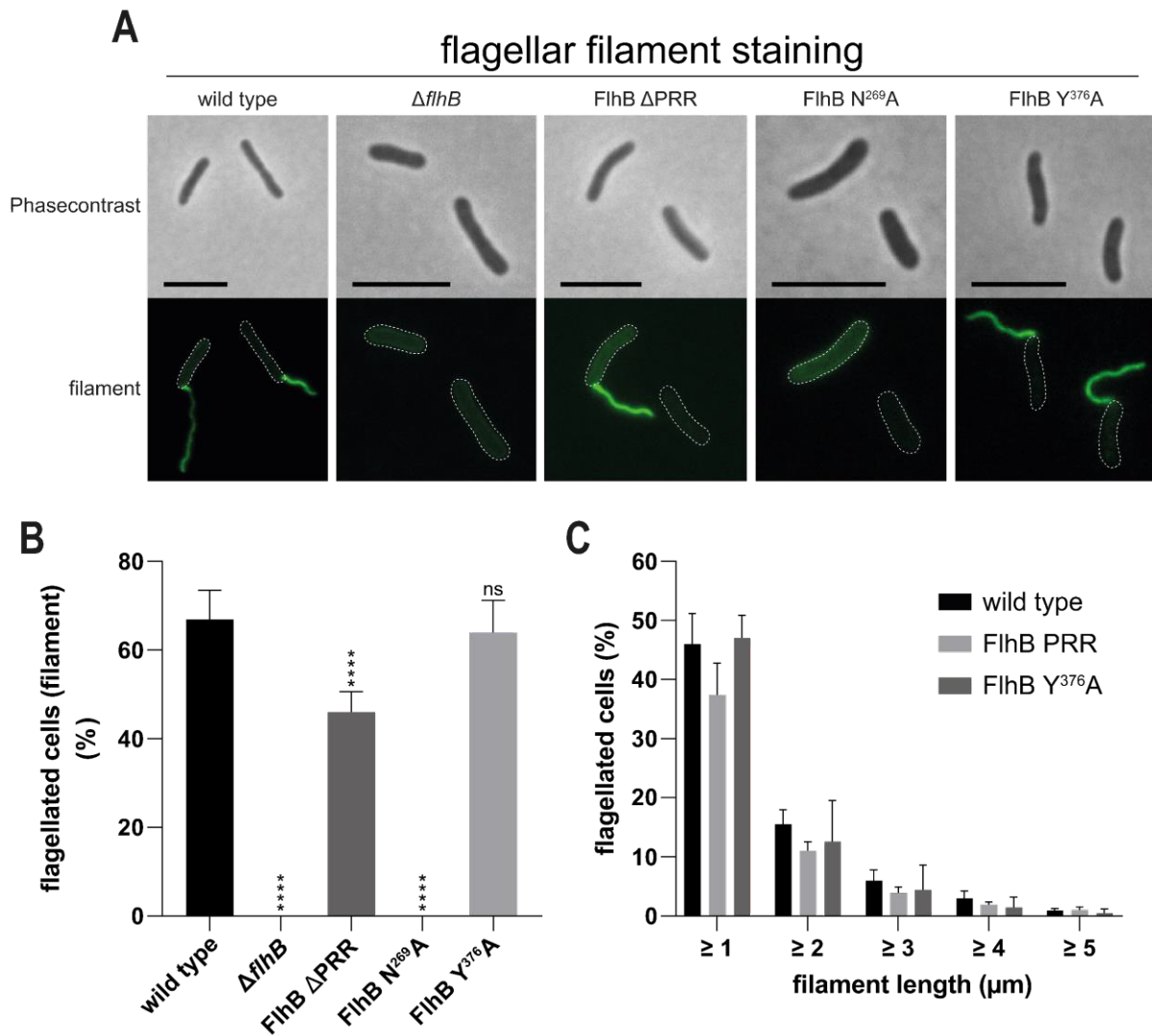
Figure 33. Flagellar filament (FlaAB) phenotype analysis in *Sp*FlhB (Sputcn32_2563) mutant strains in *S. putrefaciens* CN-32. (A) Micrographs showing maleimide stained filaments and **(B)** quantification of filament formation in *Sp*FlhB mutant strains with a wild type control. **(C)** Filament length analysis of flagellated *Sp*FlhB mutant strains with a wild type control. **Scalebar: 5 µm. **** = P value < 0.0001. n ≥ 900 cells**.

Prior to the export of flagellins, the flagellar hook, mostly comprising multiple *Sp*FlgE copies, is assembled. As *Sp*FlhB, through the interaction with the molecular ruler *Sp*FliK, is directly involved in the assembly of the flagellar hook, it was investigated, if the modification of *Sp*FlhB influences the assembly and therefore overall abundance of the flagellar hook, of which the formation was observed and quantified in the appropriate *Sp*FlhB mutant strains, in both a wild type and a Δ*fliK* background.

The micrographs of the *Sp*FlhB mutant strains in a wild type background, with the exception of the Δf*lhB* strain, clearly show stained hook structures comparable to those of the wild type (**Figure 34.A**), whereas a similar distribution of flagellar hook assembly is visible in the *Sp*FlhB

mutant strains in a Δ*fliK* background, with the overall size of stained flagellar hook structures however being much larger, presenting a so called polyhook phenotype [173], than in the appropriate strains in a wild type background (**Figure 34.E**).
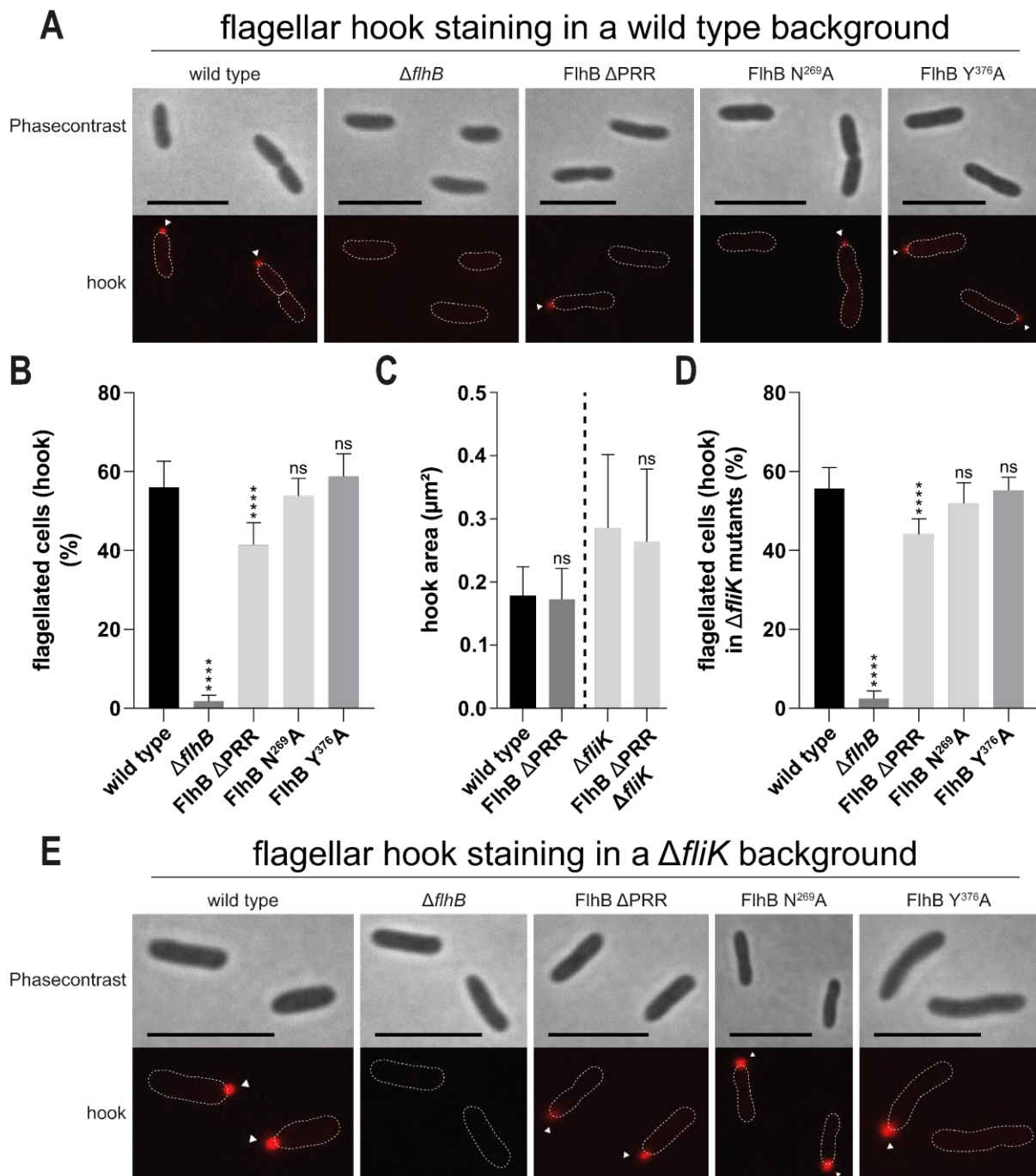
Figure 34. Flagellar hook (*Sp*FlgE) phenotype analysis in *Sp*FlhB mutant strains in both a wild type and Δ*fliK* (*Sputcn32_2571*) background in *S. putrefaciens* CN-32. (A) Micrographs showing maleimide stained flagellar hooks and **(B)** quantification of flagellar hook formation phenotypes in *Sp*FlhB mutant strains with a wild type control. **(C)** Quantification of flagellar hook formation phenotypes and **(D)** micrographs showing maleimide stained flagellar hooks in *Sp*FlhB mutant strains in a Δ*fliK* background with an appropriate control. White triangles indicate fluorescently stained flagellar hook structures. **Scalebar: 5 µm**. ****** = P value < 0.0001**. **n ≥ 900 cells**.

When quantified, it is revealed that the abundance of flagellar hooks is similarly distributed independently of *fliK* presence or absence, with the deletion of *flhB* (WT: 2 ± 1 % of cells; Δ*fliK*: 2 ± 2 % of cells) leading to a highly significant and the strongest decrease in overall hook formation in both the wild type and the Δ*fliK* background, if compared to the appropriate control strains (WT:56 ± 7 % of cells; Δ*fliK*: 56 ± 5 % of cells) (**Figure 34.B,D**). The deletion of the *Sp*FlhB PRR motif (WT: 41 ± 6 % of cells; Δ*fliK*: 44 ± 4 % of cells) also leads to a significant decrease in hook formation occurring equally in both backgrounds, which appears much weaker in severity than in the corresponding Δ*flhB* strains. No significant difference to the appropriate controls, concerning the formation of hook structures, is observable in the *Sp*FlhB $N^{269}A$ (WT: 54 ± 4 % of cells; Δ*fliK*: 52 ± 5 % of cells) and the *Sp*FlhB $Y^{376}A$ strains (WT: 59 ± 6 % of cells; Δ*fliK*: 55 ± 3 % of cells). As the overall hook size, indicated by the measurable area, which the stained hook structure occupies as a fluorescent focus, is strongly affected by the absence of regulation through FliK, leading to the formation of polyhooks, it was indirectly analysed, if the *Sp*FlhB PRR is required for the interaction of *Sp*FlhB with *Sp*FliK. For this the hook areas were measured in the absence of the *Sp*FlhB PRR in both a wild type and a Δ*fliK* background and compared with their respective background strains. Here, if compared to the appropriate control strain (WT: 0.18 ± 0.05 µm²; Δ*fliK*: 0.29 ± 0.12 µm²), no significant difference was visible in any of the *Sp*FlhB ΔPRR strains (WT: 0.17 ± 0.05 µm²; Δ*fliK*: 0.26 ± 0.12 µm²) as they formed similarly sized hook structures (**Figure 34.C**).

Besides analysing to what degree, the modification of *Sp*FlhB affects the formation and abundance of extracellular flagellar structures, the construction of the cytoplasmic C-ring, through the localisation of *Sp*FliM, was examined in each of the *Sp*FlhB mutant strains in both a wild type and a Δ*fliK* background.

As observable in the micrographs, polar *Sp*FliM-sfGFP foci are present in all analysed strains independent of *Sp*FlhB modification or *fliK* presence, with there being the possibility of a slight reduction of abundance in the Δ*flhB* strain (**Figure 35.A,D**). The quantification of *Sp*FliM in all analysed strains reveals, that only the deletion of *flhB*, with its strongly increased diffuse fluorescence (WT: 68 ± 5 % of cells; Δ*fliK*: 70 ± 5 % of cells), has a significant effect on unipolar *Sp*FliM localisation (WT: 32 ± 5 % of cells; Δ*fliK*: 30 ± 5 % of cells), independent of *Sp*FliK presence, with the appropriate control strains comparatively possessing both a decreased diffuse fluorescence (WT: 23 ± 5 % of cells; Δ*fliK*: 31 ± 6 % of cells) and an increased unipolar (WT: 77 ± 5 % of cells; Δ*fliK*: 69 ± 6 % of cells) presence of *Sp*FliM (**Figure 35.B,C**).
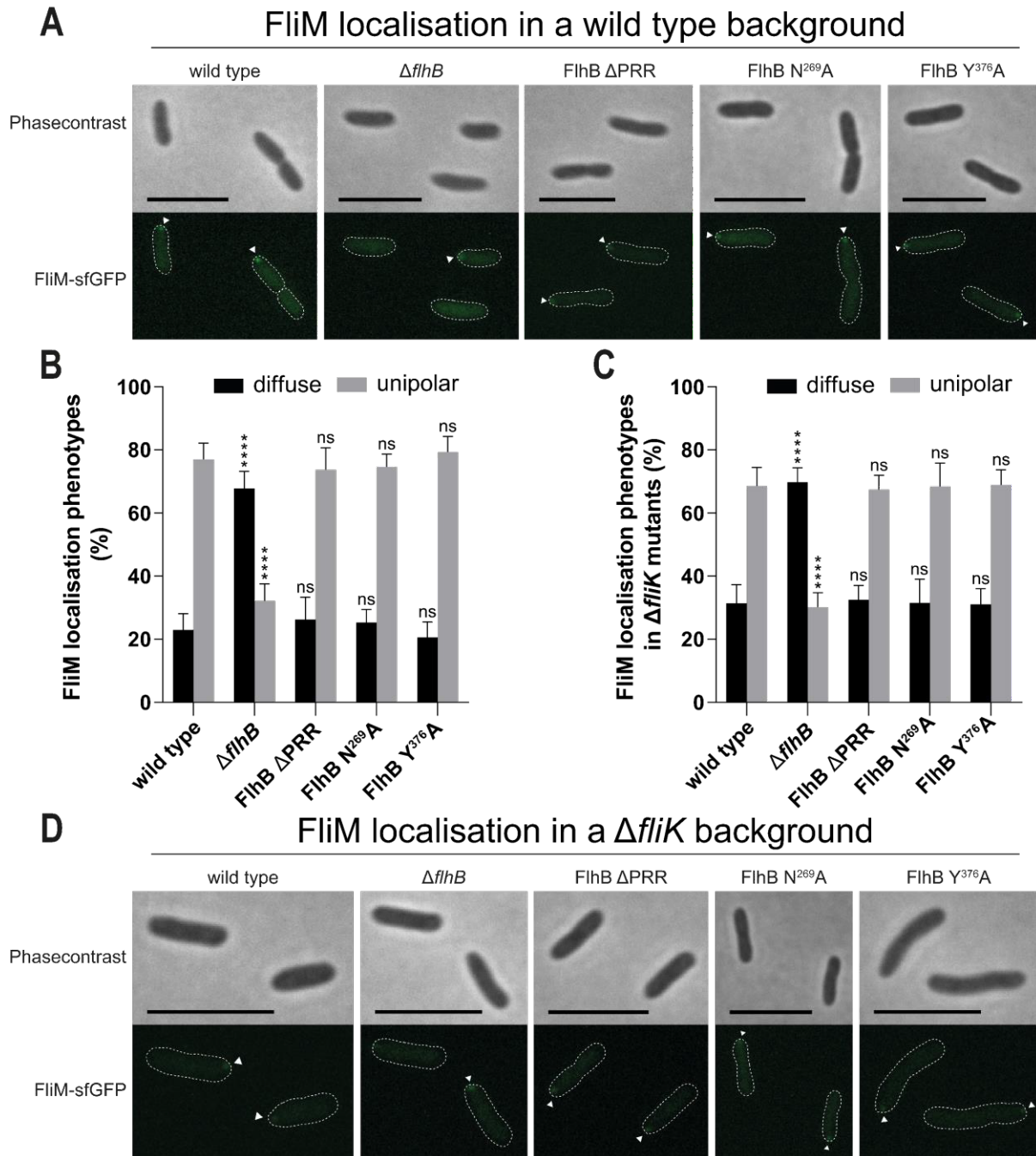
Figure 35 *Sp*FliM (Sputcn32_2569) localisation phenotype analysis in *Sp*FlhB mutant strains in a wild type and a Δ*fliK* (*Sputcn32_2571*) background in *S. putrefaciens* CN-32. (A) Micrographs showing sfGFP tagged *Sp*FliM and **(B)** quantification of sfGFP tagged *Sp*FliM in *Sp*FlhB mutant strains with a wild type control. **(C)** Quantification of sfGFP tagged *Sp*FliM **(D)** micrographs showing sfGFP tagged *Sp*FliM in *Sp*FlhB mutants in a Δ*fliK* background with an appropriate control. White triangles indicate fluorescent foci formation. **Scalebar: 5 µm**. ****** = P value < 0.0001**. **n ≥ 900 cells**.

Independent of *Sp*FliK, diffuse fluorescence is not significantly altered in the *Sp*FlhB ΔPRR (WT: 26 ± 7 % of cells; Δ*fliK*: 33 ± 5 % of cells), the *Sp*FlhB N^{269}A (WT: 25 ± 4 % of cells; Δ*fliK*: 32 ± 7 % of cells) and the *Sp*FlhB Y^{376}A strains (WT: 21 ± 5 % of cells; Δ*fliK*: 31 ± 5 % of cells),

with unipolar localisation of *Sp*FliM also not being significantly affected in the three *Sp*FlhB mutant strains, if compared to the appropriate background strains. Unipolar localisation of *Sp*FliM, in both the wild type and Δ*fliK* backgrounds, also appears to not be significantly affected in the *Sp*FlhB ΔPRR (WT: 74 ± 7 % of cells; Δ*fliK*: 67 ± 5 % of cells), the *Sp*FlhB N^{269}A (WT: 75 ± 4 % of cells; Δ*fliK*: 68 ± 7 % of cells) and the *Sp*FlhB Y^{376}A strain (WT: 79 ± 5 % of cells; Δ*fliK*: 69 ± 5 % of cells). Overall, the quantification data also reveals that the abundance of *Sp*FliM generally appears to be positively affected by the deletion of *fliK* in all analysed strains.

With the deletion of the *Sp*FlhB PRR motif having a strong effect on filament and to a lesser, but still significant, degree hook abundance, the question arose, if the observed effects are caused by an obstruction of the substrate specificity switch, occurring after the completion of the hook, when *Sp*FlhB-C autocleaves itself at the position of N^{269}. This autocleavage facilitates a substrate switch from hook to filament substrates and therefore marks an important waypoint in the overall flagellar assembly. To determine, if the auto cleavage ability of *Sp*FlhB-C primarily in the *Sp*FlhB ΔPRR mutant is impeded, a Western blot was performed to analyse the abundance of C-terminally 3xFLAG tagged cleaved, as determined by the presence of the *Sp*FlhB-C C-terminal region (*Sp*FlhB-CC), and uncleaved *Sp*FlhB for the strains of interest carrying modifications in *Sp*FlhB. The Western blot shows a strong decrease in *Sp*FlhB-CC for the sample of the *Sp*FlhB ΔPRR strain, with an accompanying increase in full length uncleaved *Sp*FlhB if compared to the wild type 3xFLAG tagged *Sp*FlhB, while the sample of the *Sp*FlhB Y^{376}A strain appears to still possess a capacity to auto cleave as the sample of the *Sp*FlhB Y^{376}A strain expresses an abundance of both uncleaved and cleaved *Sp*FlhB comparable to that of the wild type sample (**Figure 36.A**). The observed, in comparison to the wild type sample, increased abundance of uncleaved *Sp*FlhB in the sample of the *Sp*FlhB ΔPRR strain, still occurs to a much weaker degree than the abundance of uncleaved *Sp*FlhB in the sample of the *Sp*FlhB N^{269}A strain, which does not exhibit cleaved *Sp*FlhB. To quantify the observed protein band strengths, the individual amounts of uncleaved and cleaved *Sp*FlhB were determined via measuring the mean grey value of the appropriate bands (**Figure 36.B**). Here, while the sample of the *Sp*FlhB Y^{376}A strain (*Sp*FlhB uncleaved: 44 ± 9 a.u.; *Sp*FlhB-CC: 68 ± 15 a.u.) shows no noticeable difference to the positive control (*Sp*FlhB uncleaved: 44 ± 1 a.u.; *Sp*FlhB-CC: 69 ± 15 a.u.), the sample of the *Sp*FlhB ΔPRR strain (*Sp*FlhB uncleaved: 73 ± 21 a.u.; *Sp*FlhB-CC: 33 ± 8 a.u.) shows both a clear increase in uncleaved *Sp*FlhB and a clear decrease in *Sp*FlhB-CC. The sample of the *Sp*FlhB N^{269}A strain, due to its excess in uncleaved *Sp*FlhB, observable in the Western blot, was not included in the protein quantification.
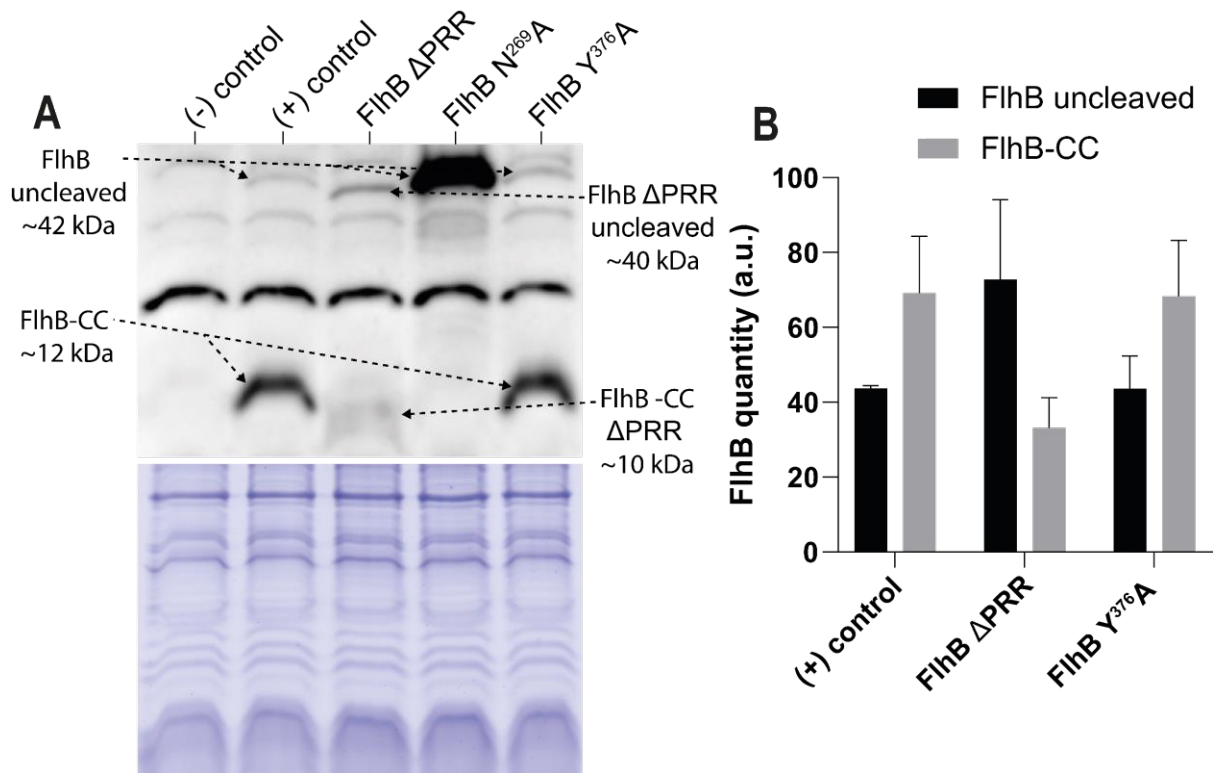
Figure 36. Expression, stability, and quantification analysis of various *Sp*FlhB mutants in *S. putrefaciens* CN-32. (A) Western blot and Coomassie stained SDS-PAGE with samples of individual *Sp*FlhB mutant strains carrying a C-terminally 3xFLAG tagged *Sp*FlhB variant and appropriate controls. **(B)** Protein amount quantification of *Sp*FlhB variants according to mean grey value analysis with a wild type control.

4. Discussion

4.1 FlhF dependencies on the path to polarity in the context of FipA characterisation

With no clear target initially presenting itself for investigation as a possible factor required for the polar recruitment of FlhF, the group of features chosen for analysis comprised elements selected from a rather broad spectrum of cellular characteristics and factors. With the cell pole being a cellular compartment known to house FlhF, the specific curvature imparted on the cell pole membrane was predicted to be a possible morphological feature either directly or indirectly involved in the polar targeting of FlhF. With the SRP-GTPase FtsY, which possesses strong homology to FlhF, being determined as a possible candidate to facilitate membrane-curvature sensing, this theory appeared promising [193]. As both the cytoskeletal structure and the cell envelope possess a positive curvature at the cell pole their cytoplasm exposed components and sections, being MreB and the cytoplasmic membrane, respectively, could through a their curving structure form a unique target structure enabling FlhF to either directly or indirectly interact [194–197]. Therefore, cells lacking poles, as observed in spheroplasts, would not possess a targetable structure for FlhF leading to a strictly cytoplasmic fluorescence in appropriately tagged mutant strains. The localisation behaviour of *Sp*FlhF in outgrowing *S. putrefaciens* CN-32 cells devoid of wild type-like polar morphology however do not support this assumption as *Sp*FlhF still appears to localise at the cell membrane. This localisation also occurs in sections of the cell envelope, which do not possess positive but rather negative curvature indicating an irrelevance of polar curvature for successful membrane targeting. The fact that *Sp*HubP appears to be equally independent of cell pole morphology for its membrane targeting behaviour suggests that both *Sp*FlhF and *Sp*HubP might follow a similar path in determining where to accumulate. This is additionally supported by their continuously observable colocalisation throughout the micrographically displayed timespan. With HubP as the polar landmark protein being a prime factor in determining polarity, the dependence of *Sp*FlhF for polar localisation might in part even require *Sp*HubP or another factor, which depends on *Sp*HubP for localisation, to efficiently target the cell pole.

These assumptions are partially confirmed when observing the localisation behaviour of *Sp*FlhF in a mutant devoid of all motility related genes and *hubP*. Tagged *Sp*FlhF expressed from an arabinose inducible promoter appears to be severely affected in its pole targeting behaviour as polar fluorescent foci are virtually absent in this mutant strain, with the bulk of fluorescence appearing diffuse in the cytoplasm. This result clearly indicates a dependence of *Sp*FlhF on *Sp*HubP including one or more factors, which most likely are expressed from the

polar flagellar gene cluster, as no connection between *Sp*FlhF and the lateral flagellar system has been observed [158,179,180].

The deletion of select known and characterised polar motility factors showed interesting results, but the absence of none of them had a significant effect comparable with the previously conducted entire deletion of motility related genes and *hubP*. The observed effects concerning the localisation phenotypes of *Sp*FlhF can rather be explained to different effects than the overall inability of *Sp*FlhF to target the cell pole successfully. In the case of the Δ*flrA* mutant the decrease in localisation rather appears to be the result of a decreased abundance of *Sp*FlhF proteins as can be seen when comparing the FlhF-mVenus protein amount in the Δ*flrA* mutant with that of the wild type. The decreased diffuse fluorescence and increase in bipolar *Sp*FlhF-mVenus foci formation in the Δ*fliFG* and Δ*flhG* mutants here also appears due to the fact that on the one hand FlhG, which acts antagonistically to *Sp*FlhF, cannot be recruited to the pole due to the absence of the nascent basal body, caused by the absence of the MS-ring component FliF and the integral C-ring component FliG, and on the other hand FlhG is absent altogether, as its gene had been deleted [158,163]. These two deletion constellations also appear to cause an increase in *Sp*FlhF abundance, as it seems to be continuously expressed while GTP-bound *Sp*FlhF homodimers accumulate at the cell pole. Unsurprisingly the deletion of *flhB* had no effect on the localisation behaviour of *Sp*FlhF as FlhB is a component of the flagellar structure, which is known to be recruited to the pole and incorporated into the nascent flagellum at a timepoint downstream of initial flagellar assembly initiation [87,88].

Besides the known factors involved in the flagellar assembly and function of *S. putrefaciens* CN-32, other, yet uncharacterised proteins were tested for their involvement in the polar localisation behaviour of *Sp*FlhF by deleting their respective genes, which are positioned in close proximity to known genes of the polar flagellar system. By doing so a target was discovered, which, when its gene was deleted, led to the strongest observed decrease in *Sp*FlhF localisation of all analysed single gene deletions and, without affecting *Sp*FlhF protein abundance, led to the formation of polar foci with weaker intensity than in the wild type. This gene, with the number *Sputcn32_2550,* was annotated as "conserved hypothetical protein" and interestingly is positioned only 10 genes downstream from *flhF* in *S. putrefaciens* CN-32. Due to the putative direct involvement in the polar localisation behaviour of *Sp*FlhF and the ability of Sputcn32_2550 to directly interact with *Sp*FlhF, as confirmed via BACTH assay, the gene was named *fipA*, being an acronym for "**F**lhF **i**nteracting **p**rotein **A**".

While the single deletion of *hubP* did not significantly affect *Sp*FlhF in its overall ability to accumulate at the cell pole, the double deletion of *fipA* and *hubP* led to an exacerbated

decrease of *Sp*FlhF localisation if compared to the single *fipA* deletion. This decrease might be a cumulative effect caused by an increased instability of the polar landscape or an indication for *Sp*FlhF being dependant on the presence of *Sp*FipA, in combination with HubP, for efficient polar targeting. Interestingly only the mutants carrying at least the single deletion of *fipA* showed *Sp*FlhF localising at subpolar positions, which implies a disruption of *Sp*FlhF being able to confidently target the cell pole. The observed insignificance of *Sp*HubP for the overall polar presence of *Sp*FlhF might in part be due to *Sp*FlhG not being able to target the cell pole and deplete *Sp*FlhF from the assembly site of the nascent flagellum in the absence of HubP [57]. This might cause an overcompensation and therefore could lead to a polar accumulation of *Sp*FlhF, even if its ability to target the cell pole through a *Sp*HubP dependant factor, like *Sp*FipA, is partially inhibited.

These findings were confirmed by duplicating the experiments concerning *fipA* with the lophotrichously flagellated *P. putida* KT2440. The deletion of the gene *PP_4331*, which encodes an ortholog to Sputcn32_2550, led to an even more severe decrease in *Pp*FlhF localisation than observed in *S. putrefaciens* CN-32. Here *Pp*FlhF additionally appears to be much more dependent on the protein *Pp*FimV, which generally possesses a similar function to *Sp*HubP in *S. putrefaciens* CN-32, as the absence of *Pp*FimV shows an immense decrease in polar *Pp*FlhF-mCherry foci formation. As expected, the double deletion of *fipA* and *fimV* therefore leads to a total absence of *Pp*FlhF localisation in *P. putida* KT2440, indicating a stronger dependence of *Pp*FlhF on *Pp*FipA than *Sp*FlhF on *Sp*FipA. This might either originate in the different flagellation patterns the analysed species employ or on other factors involved in the architecture of the polar landscape, as hinted by the differently levelled influence *Pp*FimV and *Sp*HubP have on the localisation of FlhF in their corresponding organisms.

FipA, which like FlhF accumulates at the cell pole, as confirmed via microscopically observing tagged FipA variants in both *S. putrefaciens* CN-32 and *P. putida* KT2440, appears to not influence overall growth but rather only affects the abundance and localisation of motility factors and structures. While the deletion of *fipA* leads to a decrease in *Sp*FliM localisation and hook formation in *S. putrefaciens* CN-32, the localisation of the chemotaxis component *Sp*CheA, which is known to be dependent on HubP for polar accumulation, does not appear affected [55]. This observation furthermore signifies FipA to be a factor associated with and focused on the establishment of motility. Interestingly the flagellation phenotypes observed in the Δ*fipA* strain of each organism show striking similarities to the flagellation exhibited by strains lacking FlhF, albeit to a less severe degree, such as the delocalisation of flagella, which usually are positioned at the cell pole in a wild type setting. An additional phenotype, which was only observable accompanying the absence of *Sp*FipA in *S. putrefaciens* CN-32, as it, unlike *P. putida* KT2440, possesses only one polar flagellum, was the occurrence of

hyperflagellation. This phenotype commonly only occurs when *flhG* has been deleted and the FlhF facilitated recruitment of flagellar components is not halted, pointing towards a possible involvement of FipA in this process. The subsequently performed BACTH assay with *Sp*FipA and *Sp*FlhG showed an interaction between the C-terminal region of *Sp*FipA and the N-terminal region of *Sp*FlhG. As both the C-terminal region of FipA and the N-terminal region of FlhG, containing the activator helix required for the induction of the GTPase activity of FlhF, interact with the C-terminal region of FlhF, the made observations strongly suggest a likely involvement of FipA in the interaction process of FlhF and FlhG and the accompanying induction of the FlhF GTPase activity [141,159]. These findings imply FipA to not only be involved in the polar recruitment of FlhF but rather also in the overall function of FlhF up until the disbanding of the FlhF homodimer through FlhG.

Another difference between the two organisms, observable when analysing the localisation behaviour of FipA is that *Sp*FipA rather relies on *Sp*HubP than *Sp*FlhF and *Pp*FipA rather relies on *Pp*FlhF than FimV for polar accumulation. This variation further highlights the differences in the functioning of FipA exhibited by both analysed species. At this point it is interesting to see that the deletion of *hubP* has nowhere near the same effect on the localisation behaviour of *Sp*FlhF as the deletion of *fipA*, even though the absence of *Sp*HubP leads to a strong decrease of polarly observed *Sp*FipA. Perhaps the absence of *Sp*HubP only leads to a decreased polar persistence of *Sp*FipA and not a total inability of *Sp*FipA to target the cell pole. This would still enable polar recruitment of *Sp*FlhF, which most likely only requires a small timeframe at the pole for successful initiation of flagellar assembly. *Sp*FipA therefore might not require HubP for actual localisation at the cell pole but rather requires it to maintain a prolonged presence. Here preliminary observations have shown SpFipA to neither directly interact with full-length nor various truncated versions of HubP, suggesting the involvement of an additional factor (data not shown). The mutual dependence of *Pp*FlhF and *Pp*FipA to accumulate at the cell pole might also originate in these two proteins stabilising each other's presence at the cell pole. With the absence of the one protein leading to a decreased persistence and stability of the other protein at the pole of the cell. This assumption, speaking against total absence of FlhF from the cell pole in strains devoid of FipA, might be supported by wild type-like flagellation being much more prevalent in a Δ*fipA* strain than in the corresponding Δ*flhF* strain, which is observable in both *S. putrefaciens* CN-32 and *P. putida* KT2440. This decrease in polar stability and persistence of *Sp*FlhF, in the context of a *fipA* deletion, might also be hinted at by the generally lower foci fluorescence intensity, indicating a smaller number of *Sp*FlhF molecules at the visible foci, being a possible result of a higher turnover or inability to efficiently anchor at the cell pole.

The idea of FipA being a dynamic protein is supported by the timelapse micrographs, which show FipA shifting its position throughout the cell cycle in both *S. putrefaciens* CN-32 and *P. putida* KT2440. Here FipA can be observed cycling between accumulation and dispersion at the cell pole. It also is possible to draw the conclusion from the time lapse microscopy that FipA localises at the cell pole prior to other polar factors such as FlhF and CheA, which only accumulate in the presence of FipA, while HubP appears to target the cell pole independently from FipA, as observed in *S. putrefaciens* CN-32. That HubP localises at the cell pole prior to and independent from FipA also is supported by the presence of *Sp*FipA at the cell pole being decreased in the absence of *Sp*HubP. When colocalising FipA with the polar flagellar filament(s), it seems like the old cell pole, possessing a completed flagellar structure, does not harbour FipA, while the new cell pole, at which filament polymerisation has not yet commenced or only slightly progressed, shows an increased abundance of FipA. This observation, taken together with *Sp*FipA localising at the pole before *Sp*FlhF, furthermore promotes the idea that FipA is involved in flagellar construction from the point of assembly site determination and initiation onwards.

To further analyse the nature of the FlhF/FipA relationship the interaction configurations of FlhF and FipA were scrutinised. Here the interactions occur with both the N- and C-terminus of FlhF being able to interact with the C-terminus of FipA. Additionally, both *Sp*FipA and *Pp*FipA are able to self-interact, with both of the analysed FipA orthologs however slightly varying in their interaction profiles. While *Sp*FipA expresses the ability to interact in both a C- to C-terminal manner and a N- to C-terminal manner, *Pp*FipA only can interact in a C- to C-terminal manner. The observed additional interaction configuration exhibited by *Sp*FipA might hint at why the mechanism, which stands behind the polar recruitment of FlhF under the involvement of FipA appears to function differently from each other in the analysed organisms. *Sp*FipA seems to be able to facilitate different homologous interaction arrangements indicating a difference in its functioning from that of *Pp*FipA. These differences might influence heterologous interaction with *Sp*FlhF and lead to additional factors being involved in and required for the polar targeting mechanism of *Sp*FlhF, which could therefore alter its dependency on *Sp*FipA. This elusive factor might be encoded among the genes deleted in the strain devoid of all motility related genes and *hubP* as polar accumulation of FlhF was, to the furthest extent, inexistant in this strain. Perhaps this elusive additional factor stabilises *Sp*FlhF at the cell pole under the direct or indirect utilisation of *Sp*HubP. In *P. putida* KT2440 this mechanism appears to function in a simpler manner as *Pp*FlhF only seems to require *Pp*FipA and *Pp*FimV for successful polar recruitment.

The fact that FipA C-terminally interacts with the G-domain-harbouring C-terminus of FlhF, suggests, as the homodimerization of FlhF is essential for function and polar targeting, a

possible involvement of FipA in the formation of these homodimers or the necessity of prior FlhF homodimerization for successful interaction with FipA. While the N-terminus of FipA possesses a predicted TMD, the interaction between the B-domain harbouring N-terminus of FlhF with the most likely cytoplasmic C-terminus of FipA, might strengthen the idea of FipA functioning as a membrane anchor for FlhF.

As FipA interacts with the C-terminus of FlhF, which contains the G-domain and therefore presents itself as a region of FlhF vital for homodimerization and polar accumulation, specific conserved residues were substituted to assess their overall role in the function of FlhF and its interaction with FipA in both *S. putrefaciens* CN-32 and *P. putida* KT2440. These conserved residues are positioned in the G1-, G3- and G4-loop and consequently play a role in the nucleotide binding ability of FlhF [135]. Interestingly the substitutions appear to have a stronger effect on *Pp*FlhF than on *Sp*FlhF as the mutant variants of *Pp*FlhF, except for the *Pp*FlhF K^{235}A variant, which still is able to localise and homologously interact with wild type *Pp*FlhF, neither are able to localise at the pole nor interact with a wild type variant of *Pp*FlhF. The residue K^{235} in *Pp*FlhF, albeit being conserved at a position 5 residues downstream from the G1-loop and might structurally stabilise the G5-loop, does not impact the functioning of FlhF to a degree, at which polar localisation and homologous interaction are completely abolished. The residue substitution in the G1- (K^{229}A), G3- (D^{301}A) and G4-loop (D^{362}A) however, as conclusion to the made observations, are presumed to impact the GTP binding ability of *Pp*FlhF in such a way that efficient homodimerization can no longer be established. Concerning the overall capacity of *P. putida* KT2440 to be motile in the context of *Pp*FlhF residue substitution, the ability to interact with GTP phosphate groups and the binding of Mg^{2+} appears to be more important than efficient nucleotide recognition. Oddly, despite *Pp*FlhF not being observable at the cell pole in the *Pp*FlhF D^{301}A and the *Pp*FlhF D^{362}A strain, the motility phenotypes do not signify a total absence of *Pp*FlhF regulation in the establishment of motility, while the substitution of *Pp*FlhF K^{229} appears to lead to an equal motility phenotype as an *flhF* deletion. This highlights the possibility of FlhF being required either not in high quantities or only for a short timespan at the cell pole for the initiation of flagellar assembly. This previously mentioned prioritisation of phosphate group and Mg^{2+} binding over nucleotide recognition, appears to occur in a similar manner in *S. putrefaciens* CN-32, where however the additional substitution of a G4-loop residue (D^{390}A_E^{391}A) leads to a complete functional breakdown of *Sp*FlhF, with *Sp*FlhF being mostly absent from the cell pole and the motility phenotype of the respective strain matching the Δ*flhF* strain. This phenotype most likely occurs due to the residue E^{391} functioning as an additional nucleoside interacting residue for the G4-loop, which also facilitates trans binding of the two *Sp*FlhF monomers. For general robust polar accumulation, *Sp*FlhF however appears to rather require interaction with the phosphate

groups of GTP and nucleoside specificity, facilitated by the substituted residues in G1- and G4-loop, respectively, than the binding of Mg^{2+} through the substituted residue in the G3-loop. To be able to form a stable SpFlhF homodimer, the nucleoside specificity facilitated by the D^{390} residue, contained in the G4-loop, understandably appears to be more critical, as it most likely occurs as an initial step of homodimerization, than the interaction with GTP phosphate groups or the binding of Mg^{2+}. The reduced motility observed in the SpFlhF D^{328}A strain might be caused by the GTPase ability of SpFlhF being impeded, which could cause a prolonged recruitment of flagellar components resulting in hyperflagellation. The observation that wild type FlhF displays a homologous interaction in an N- to C-terminal manner, also observed in all SpFlhF mutant variants still possessing the ability to specifically bind GTP, might originate in the putatively unstructured N-terminal B-domain, which has been predicted to regulate homodimerization, interacting with the C-terminal G-domain in a cis or trans configuration, when an FlhF homodimer is formed. Concerning the C- to C-terminal interaction of SpFlhF mutant variants, the results either allow no clear conclusion or rather oppose the additional data and current understanding of FlhF functioning, therefore warranting further investigation. Overall, the observations confirm a strong dependence of FlhF on its ability to efficiently bind the nucleoside and phosphate regions of GTP to form stable homodimers and localise at the cell pole in both $S.$ $putrefaciens$ CN-32 and $P.$ $putida$ KT2440, while also allowing the hypothesis of FlhF not requiring a strong prolonged polar presence for the initiation of flagellar assembly, ultimately resulting in motility, which requires further investigation for absolute confirmation.

To substantiate or refute a possible link between these residues in FlhF and the FipA-mediated localisation of FlhF to the cell pole, the effects, which the substitutions in FlhF have on the localisation behaviour of FipA and its ability to heterologously interact were quantified. Here SpFipA exhibits a severely decreased ability to interact with the SpFlhF mutant variants, as it with its C-terminus is not able to interact with the N-terminus of the SpFlhF residue substitution mutants but still able to interact with the C-terminus of the SpFlhF E^{391}A variant and to a strongly decreased degree with the C-terminus of the SpFlhF K^{256}A and the SpFlhF D^{328}A variant. With SpFipA only being dependant on SpFlhF for its polar presence to a lesser degree, the putative inability of SpFlhF K^{256}A to efficiently interact with GTP phosphate groups and the probable absence of nucleoside binding in SpFlhF D^{390}A and SpFlhF D^{390}A_E^{391}A appears to have a similar effect on the localisation behaviour of SpFipA, as the complete deletion of $flhF$ in $S.$ $putrefaciens$ CN-32. Unimpeded localisation of SpFipA however seems to occur in strains, which possess either the D^{328}A or the E^{391}A variant of SpFlhF. These variants have previously been observed to only affect SpFlhF functioning to a lesser degree, indicating that even a weak C- to C-terminal interaction between SpFlhF and SpFipA is sufficient for wild

type-like polar anchoring of SpFipA, with the efficient interaction of SpFlhF with the phosphate groups of GTP and the ability to bind the nucleoside section of GTP being the most important of all analysed SpFlhF functions, if viewed from both the SpFipA and SpFlhF side. In *P. putida* KT2440, with PpFipA being much more dependent on PpFlhF than SpFipA on SpFlhF, PpFipA, while being able to interact with non-other than the $K^{235}A$ variant of PpFlhF, is still able to maintain a stronger polar presence in all the PpFlhF mutant strains than in the total absence of PpFlhF. Here PpFipA appears to rather require PpFlhF to be able to efficiently interact with the nucleoside section of GTP and successfully bind Mg^{2+} than interact with the phosphate groups of GTP, albeit still requiring this ability in PpFlhF to attain wild type-like levels of localisation. Interestingly the substitution of the putatively G5-loop stabilising residue K^{235}, of which the substitution does not impact the ability of PpFlhF and PpFipA to interact, rather led to an increase in unipolar localisation and a decrease in bipolar localisation indicating an involvement in the timing of the proposed dynamic behaviour of FipA at the cell pole. Taken together these observations furthermore allow the assumption that PpFipA directly depends on PpFlhF and select residues in its G-domain for polar attachment and persistence, while SpFlhF also appears to, even if to a lesser degree than in *P. putida* KT2440, modulate the function of SpFipA directly through interaction with G-domain residues.

To equally assess residues and putative domain features on the FipA side, possessing functional significance for FipA and additionally might play a role in the FlhF/FipA interaction, the conserved putative TMD at the N-terminus of FipA and residues sequentially positioned in a highly conserved region of the C-terminal DUF2802 domain were deleted and substituted, respectively, while the effect, which a deletion of the TMD had on homo- and heterologous interaction, was not analysed and remains to be evaluated. Here the predicted N-terminal TMD of FipA was determined as vital for protein stability and the pole targeting capability of FipA in both *S. putrefaciens* CN-32 and *P. putida* KT2440, with also the motility phenotype being identical with the one observed in the strains lacking *fipA* altogether. Concerning the substituted conserved residues in FipA, SpFipA and PpFipA however appear to diverge from each other in dependence on individual residues, when it comes to the ability of FipA to target the cell pole. While the residue L^{118} in SpFipA and the heterologous L^{116} in PpFipA appear to both be vital for FipA functioning, the substitution of residue G^{106} in SpFipA affects localisation and overall motility more than the substitution of the orthologous residue G^{104} in PpFipA in comparison to each corresponding control. Similarly, the substitution of the residue L^{125} in SpFipA does not affect SpFipA localisation and motility to a similar degree as the substitution of its conserved counterpart, L^{123}, in PpFipA, additionally indicating a general difference in the functioning of FipA in *S. putrefaciens* CN-32 and *P. putida* KT2440. The observed dysfunctions in both SpFipA localisation and overall motility are mirrored in the interaction phenotypes of

wild type SpFipA with individual mutant variants, as the G^{106}A and L^{118}A residue substitutions strongly affect the ability of SpFipA to homologously interact, while the L^{125}A substitution has no effect on either the N- to C-terminal or C- to C-terminal interaction ability of SpFipA. While the residue substitutions in PpFipA significantly affect localisation and overall motility to varying degrees, they have no impact on the previously observed capacity of PpFipA to homologously interact in a C- to C-terminal manner. This suggests that the residue substitutions introduced into PpFipA, despite not influencing the ability to C-terminally self-interact, are crucial for polar targeting. This proposes a possibility for most of these residues to be important for heterologous interaction(s) or a homologous interaction, which was not discovered by the performed assays.

Having firstly determined the effects of the TMD deletion and the substitution of select residues in FipA on its general function, the impact, which these modifications have on the functioning of FlhF were analysed. Additionally, to the deletion of the TMD, which equated in a phenotype more or less similar to the one observed when $fipA$ was completely deleted, as the stability of FipA ΔTMD was severely impacted, the role of the SpFipA residues G^{106} and L^{118} as well as the PpFipA residues L^{116} and L^{123}, in spite of the strains displaying clear defects in polar FlhF localisation and the inability of these FipA variants to interact with FlhF, could not be accurately assessed. This stemmed from the individual FipA variants in $S. putrefaciens$ CN-32 and $P. putida$ KT2440 themselves being significantly hindered in their functioning and polar targeting behaviour by these residue alterations. Therefore, all observed effects on FlhF were preliminarily classified as downstream effects caused by the disfunction of FipA. To determine, how these residues of FipA affect the polar targeting of FlhF, as well as their exact role in the establishment of motility, therefore remains to be elucidated by future studies. The observation of how the substitution of SpFipA residue L^{125} affected both the localisation behaviour of SpFipA and SpFlhF, made this residue a prime candidate implicated in facilitation of the SpFipA/SpFlhF interaction, as its substitution comparatively has a minimal effect on SpFipA localisation, while SpFlhF localisation is dissimilarly strongly affected. This assumption is equally reflected in the ability of SpFipA L^{125}A to interact with SpFlhF, as a wild type-like interaction is no longer possible in a SpFlhF-N- to SpFipA-C-terminal manner, which is predicted to be the interaction of choice to indirectly anchor FlhF to the inner membrane through FipA. Due to this SpFipA variant still being able to interact with SpFlhF in a C- to C-terminal manner, this termini interaction constellation appears as not that necessary for polar recruitment of FlhF but rather plays a role in the later stages of the FipA/FlhF interaction. This theory is further supported by the effects, which the introduction of residue substitutions into PpFipA had on the capacity of PpFipA to interact with PpFlhF in a C- to C-terminal manner, as the establishment of this interaction configuration still was possible with all PpFipA variants,

while *Pp*FlhF was significantly affected in its ability to target the cell pole. The *Pp*FlhF-N- to *Pp*FipA-C-terminal interaction configuration however is mostly completely absent in all tested *Pp*FipA mutant variants, additionally reinforcing the idea of FlhF interacting with its N-terminal B-domain with the C-terminus of FipA at the initial targeting of the pole, as the *Pp*FipA G^{104}A strain only exhibits a mild defect in polar *Pp*FipA localisation, while the ability of *Pp*FlhF to accumulate at the cell pole appears strongly compromised. Here the interaction also appears strong enough to likely initiate membrane anchoring of *Pp*FipA, as a total inability to interact would presumably have the same effect on *Pp*FipA as the absence of *Pp*FlhF, leading to *Pp*FipA being mostly dispersed in the cytoplasm. The faint observable N- to C-terminal interaction of *Pp*FlhF with the *Pp*FipA G^{104}A variant in the BACTH assay, respectively, and the motility and FipA localisation phenotype caused by *Pp*FipA G^{104}A, which appears inequal to a total absence of *Pp*FlhF mediated regulation of flagellar assembly, suggests that an interaction between *Pp*FipA G^{104}A and *Pp*FlhF still occurs, but with a significantly decreased efficiency than in the wild type. This therefore only allows limited establishment of flagellar structures, causing diminished overall motility.

All considered, the observations made, surrounding the novel motility factor FipA, characterised for both *S. putrefaciens* CN-32 and *P. putida* KT2440, allow the assumption that it is a prime factor involved in the ability of FlhF to target the cell pole and therefore participates in the initial steps of polar flagellar assembly. Despite this study only analysing FipA of the two γ-proteobacteria *S. putrefaciens* CN-32 and *P. putida* KT2440, FipA orthologs, sharing vast conserved stretches in the amino acid sequence, have been discovered for many other bacterial species, with the protein domain structure being universally conserved as an N-terminal TMD and a C-terminal DUF2802 domain. Here FipA always occurs in conjunction with a flagellation pattern characterised by flagellar structures precisely being positioned at the cell pole, through the regulation by FlhF and FlhG, with the addition of a polar landmark protein, such as HubP or the orthologously functioning FimV being present. Furthermore, the genomic position of *fipA* generally also is conserved adjacent to the gene cluster encoding the polar flagellar system, directly adjacent to *cheW* and approximately 10 genes downstream from *flhF* (**Supplemental figure 47**).

Due to the mostly overlapping observations made in *S. putrefaciens* CN-32 and *P. putida* KT2440 the proposition can be made that FipA, through its TMD, functions as an anchor at the inner membrane, which aids efficient polar attachment of FlhF. This hypothesis partially opposes the previously published notion that FlrD, which is the ortholog to FipA in *Vibrio cholerae*, only acts as an element, that indirectly regulates the expression of late flagellar genes through the transcriptional factors FlrB and FlrC [198,199]. The observed effects caused by the deletion of *flrD* could therefore mostly be attributed to a disturbed feedback loop, blocking

the transcription of late flagellar genes due to the flagellar assembly not being able to move past a distinct waypoint, at which FlrD might be released from the cell pole so that it can positively interact with FlrB and FlrC to indirectly induce the expression of late flagellar genes. This effect on FlrB and FlrC, which remains to be investigated for FipA of *S. putrefaciens* CN-32 and *P. putida* KT2440, might rather be an additional function of FipA, which, like FlhG regulating flagellar gene expression through the interaction with FlrA, could play a role in the complete flagellar assembly mechanism besides just being involved in the polar recruitment of FlhF [157,161,162]. The proposed anchoring of FlhF to the inner membrane most likely occurs through the interaction of the FipA DUF2802 domain and the FlhF B-domain, which in turn positively affects the polar persistence and stability of FipA. Here it appears plausible that either FlhF must be in a homodimeric state to achieve this docking or FipA plays a role in the facilitation of FlhF homodimerization through interaction with the FlhF G-domain either in the cytoplasm or at the membrane. An additional function of FipA, besides the initial recruitment of FlhF to the cell pole, might be an involvement in the ultimate disbanding of the FlhF homodimer by assisting the interaction of FlhF with FlhG. This theory is based on the observation made for the flagellation phenotype in the Δ*fipA* strain of *S. putrefaciens* CN-32, which exhibited hyperflagellation, being indicative for a dysfunction of FlhG and on the fact that FipA and FlhG are able to interact. Overall FipA does not appear as essential as FlhF in the mechanism governing the establishment of motility, while it does however appear to greatly enhance the efficiency of flagellar assembly. The putative mode of interaction between the B-domain of FlhF and the DUF2802 domain of FipA and the observed variations concerning the proposed interaction residues on both the FlhF and FipA side in both utilised model organisms, might point towards the assumed species-specific function of the variable FlhF B-domain playing a role in the development of unique species-specific flagellation patterns. Variations in FlhF/FipA interaction might therefore have an impact on the polar presence of FlhF, which in turn could lead to a variation in the abundance of assembled flagellar structures. This theory makes it essential to analyse individual stretches of the FlhF B-domain for their function in the facilitation of an FlhF/FipA interaction. With the witnessed diversity of FipA functioning in *S. putrefaciens* CN-32 and *P. putida* KT2440, FipA has an impact on the formation of motility structures, which varies in intensity depending on the organism. The underlying broad mechanisms however appear to be the same. For the utilised model organisms this might originate in *S. putrefaciens* CN-32 natively possessing only a single flagellum at the cell pole, of which the assembly mechanism might be more robust and have more redundancies instead of heavily relying on individual factors for essential waypoints in the construction process, as the disruption of a single factor would lead to an immotile cell. In *P. putida* KT2440, which is lophotrichously flagellated, the mechanism might not need to be as robust, as an error in the assembly of one polar flagellum would not lead to total immobility

due to the sheer number of polar flagella, which are assembled. The validity of this hypothesis and the exact relationship of FlhF and FipA concerning the involvement and timing of their interaction in the flagellar assembly process remains to be analysed by future studies.
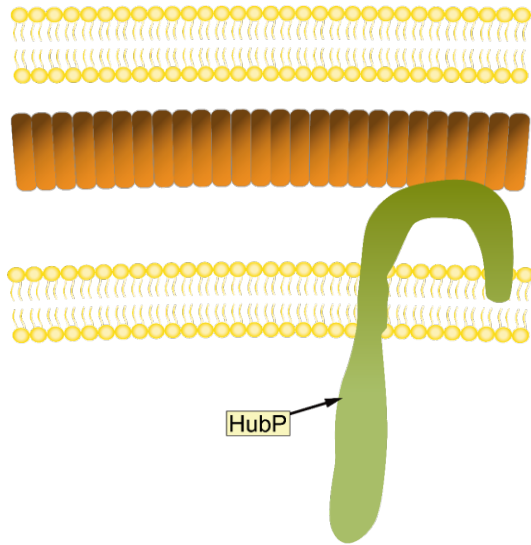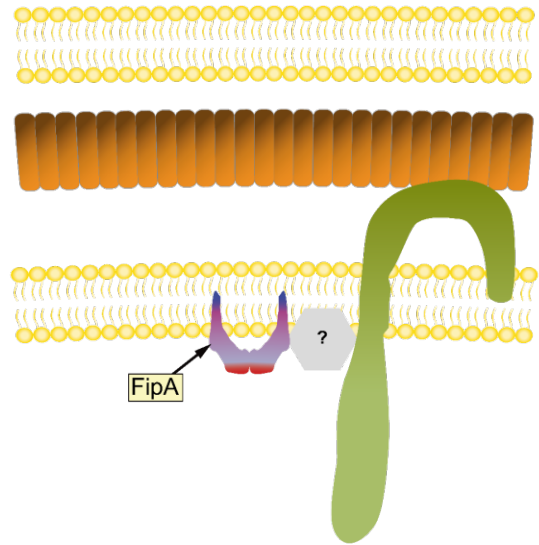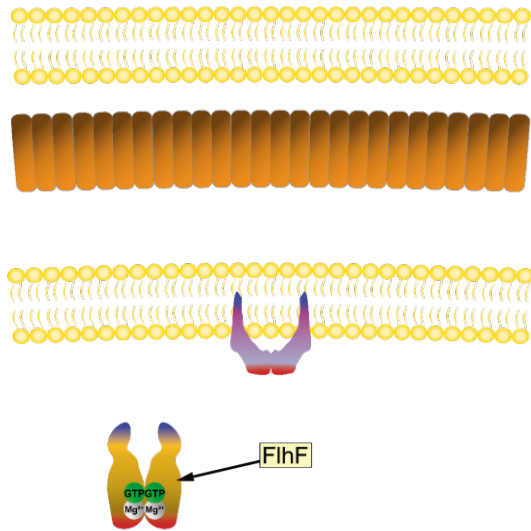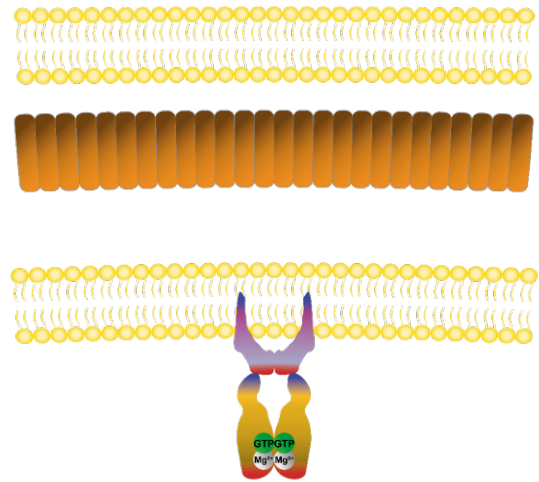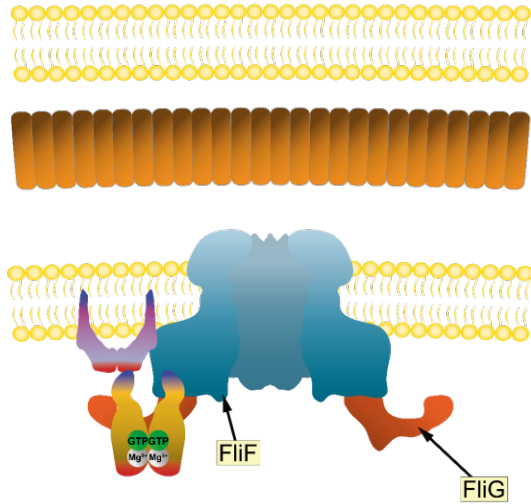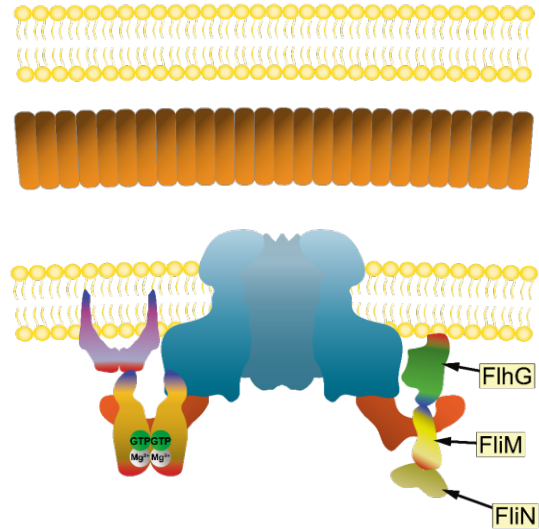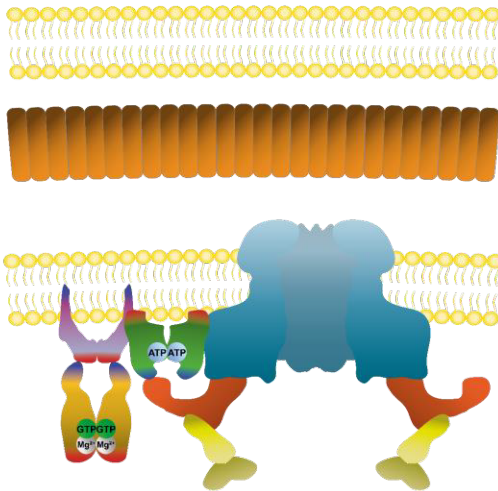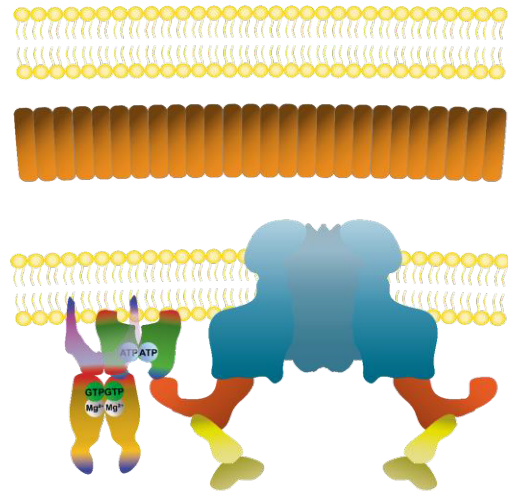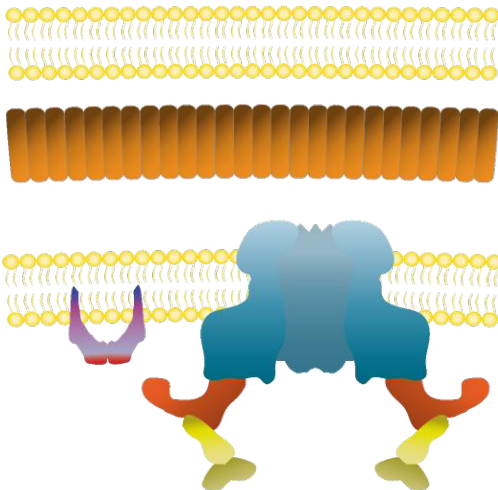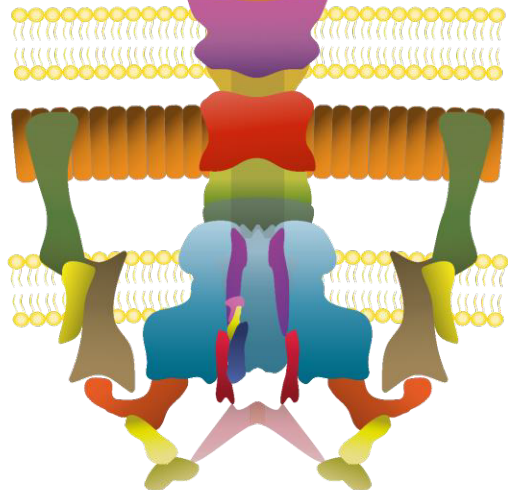
Figure 37. Preliminary model of flagellar assembly in *S. putrefaciens* CN-32. 1. HubP is recruited to the cell pole. **2.** FipA is recruited to the pole in an indirect HubP-dependant manner. **3.** FlhF homodimerizes in the cytoplasm under the utilisation of GTP and Mg^{2+} and travels to the cell pole. **4.** The FlhF homodimer is anchored at the pole through an interaction between the B-domain and the C-terminal region of FipA. **5.** The FlhF homodimer, with its B-domain, accumulates components of the basal body such as FliF and FliG, which are incorporated into the nascent flagellar structure. **6.** FlhG bound to the FliMN complex through an interaction with the EIDAL motif of FliM migrates to the pole. **7.** Upon membrane contact with its C-terminal MTS FlhG homodimerizes under the utilisation of ATP. **8.**

The FlhG homodimer interacts with both the C-terminal region of FipA and the G-domain of FlhF enabling GTPase activity induction. **9.** This induction leads to the disbanding of the FlhF homodimer and an end of the polar recruitment of MS- and C-ring components. The FlhG homodimer leaves the pole and represses FlrA activity, blocking further expression of early flagellar genes, while FipA remains present at the pole in a dynamic manner. **10.** Once the flagellar structure has been completed FipA leaves the cell pole. (N-termini of protein models are highlighted in blue and C-termini are highlighted in red.)

4.2 Role of *Sp*FlhB PRR in overall flagellar assembly and export specificity switching

The characterisation contained in this study covering the "Proline Rich Region" (residues 358-376), located at the very C-terminal end of *Sp*FlhB, offers a new insight into the overall functioning of FlhB. Its spatial proximity to the *Sp*FlhB-C autocleavage site, N^{269}, previously described for *Salmonella sp.*, suggested an involvement in the autocleavage ability of *Sp*FlhB and therefor the switching of substrate specificity upon hook completion from hook to filament subunits [165,168]. This assumption was supported by the filament staining results, with the deletion of the PRR leading to a significant decrease in filament occurrence. Additionally, the deletion of the complete *flhB* gene and the substitution of the autocleavage site N^{269} in the conserved NPEH motif caused the absence of filament formation, confirming the necessity of *Sp*FlhB and the distinct conserved autocleavage feature for native flagellum formation in *S. putrefaciens* CN-32. The residue Y^{376} positioned at the C-terminal end of the PRR motif, which through substitution also was assessed for its effect on flagellation, does not appear to play a vital role in the functioning of *Sp*FlhB related to substrate specificity switching, as its deletion only had an insignificant effect on the formation of flagella in the respective strain. With the flagellation being significantly impacted but not completely abolished by the deletion of the PRR in *Sp*FlhB, the overall export efficiency of filament subunits was assessed in the strains still forming observable filaments. This was achieved by measuring the length of the produced filament structures in the *Sp*FlhB ΔPRR, as well as the accompanying strains of interest. Here, just like on the overall abundance of flagella, the substitution of *Sp*FlhB Y^{376} did not affect the length of the observable flagella, as the *Sp*FlhB Y^{376}A strain still formed filaments that matched those of the wild type across all analysed filament lengths. The *Sp*FlhB ΔPRR strain however clearly displayed a strong decrease in flagella across all quantified filament lengths, indicating a clear decrease in not just overall filament quantity but also assembly quality in the absence of the *Sp*FlhB PRR. This observation suggests the *Sp*FlhB PRR to be involved in overall export efficiency of filament subunits rather than export specificity switching, as its absence does not totally negate filament assembly, but rather severely impacts the length of formed filaments.

To assess, if these observed phenotypes are possible downstream effects caused by a disruption of the hook assembly process, in which the *Sp*FlhB PRR might also play a role, the

abundance of hook structures was quantified. While the SpFlhB Y^{376}A strain, again mirrored the wild type phenotype, concerning the hook formation, and the SpFlhB N^{269}A strain, lacking the ability to autocleave FlhB-C, also showed a hook abundance phenotype similar to that of the wild type, the SpFlhB ΔPRR strain significantly differed from the wild type in the amount of displayed hook structures. This indicates that the SpFlhB PRR does not only affect filament formation, but also the assembly of the flagellar hook. As this step in flagellar assembly is governed by the interaction of FlhB and the hook length measuring FliK, the occurrence of hook structures was analysed in strains lacking $fliK$ additionally to the introduced SpFlhB modifications [169]. This added deletion, besides predictably causing a polyhook phenotype, due to the hook length not being measured during the assembly process, did not lead to an abundance of hook structures differing from the strains with functioning FliK, proposing that the PRR does not play a role in the SpFlhB/FliK interaction, but rather is involved in the export process of hook subunits. Furthermore, these findings show that the ability to autocleave is not instrumental in the export process of hook subunits.

With having assessed the involvement of the SpFlhB PRR in late stages of the flagellar assembly, such as the construction of the hook and filament, the effects, which a deletion of the PRR has on early stages of the flagellar assembly, precisely the C-ring assembly, was analysed. The formation of the C-ring was assessed via the localisation behaviour of the C-ring component SpFliM at the cell pole. While the complete deletion of $flhB$ lead to a significant decrease in SpFliM localisation, none of the other modifications of SpFlhB including the deletion of the PRR influenced SpFliM localisation. The decline of localising SpFliM in the context of Δ$flhB$ here most likely was caused by a general destabilisation of the entire basal body of which SpFlhB is an integral structural and functional component. The absence of effects on SpFliM localisation in the individual strains carrying modifications in SpFlhB shows that the correct functioning of the substituted or deleted features of SpFlhB is not required for the assembly and stability of the basal body, but rather, as proposed by the previous observations, is involved in the export of flagellar components, required at a later point in time as seen from the basal body assembly stage. Even with the additional absence of SpFliK, the previously observed lack of effect on SpFliM localisation, caused by SpFlhB modifications, did not change, reiterating that the functioning of SpFlhB and SpFliK, which plays an essential role in the assembly of extracellular flagellar components, does not affect the assembly of the C-ring and basal body altogether.

The witnessed effects on the assembly of extracellular substructures of the flagellum, such as the hook and filament, caused by the deletion of the SpFlhB PRR, which at the same time did not affect C-ring assembly, raised the question if the decrease in filament formation and apparent assembly efficiency is a downstream effect of the hook formation being affected by

the deletion of the PRR, or a direct consequence of the PRR being involved in the autocleavage ability of SpFlhB. This effect was assessed via Western blot performed with samples from all SpFlhB mutant strains of interest, in which the SpFlhB variant was tagged with a triple FLAG tag at the C-terminal end. This tagging constellation allows to quantification of uncleaved SpFlhB and cleaved SpFlhB, represented by SpFlhB-CC. As expected, and suggested by the previous observations, the SpFlhB autocleavage residue mutant SpFlhB $N^{269}A$ was incapable of performing autocleavage leading to an excessive build-up of uncleaved SpFlhB, while at the same time no FlhB-CC was detectable. The substitution of Y^{376} in SpFlhB predictably, as this substitution also had no effect on the assembly of flagellar substructures, did not influence the ability of SpFlhB to autocleave, with the abundance of uncleaved SpFlhB and SpFlhB-CC matching those exhibited by the positive control sample. When observing and comparing the sample of the SpFlhB ΔPRR variant with the positive control sample, a strong increase in uncleaved SpFlhB and a sharp decline in SpFlhB-CC is detectable. Even though these effects aren't as strong as in the non-cleaver variant of SpFlhB, the deletion of the PRR clearly affects the ability of SpFlhB to perform autocleavage. This result suggests that the PRR of SpFlhB is involved in the autocleavage ability of SpFlhB, which would explain the effects observed on the terminal stages of flagellar assembly.

Summarised, while the residue Y^{376} at the C-terminal end of the PRR motif in SpFlhB does not play an essential role in the overall activity of SpFlhB and the cleavage site at residue N^{269}, just like in $Salmonella$ $sp.$ is essential for substrate specificity switching, the PRR itself is involved in a multitude of SpFlhB functions [165]. These range from the observed export substrate specificity switching, indicated by the decline in export efficiency of filament substrates and a decreased autocleavage activity, to a general reduction of flagellar hook substructures. These effects occur independently from FliK presence or absence, therefore promoting the assumption that the PRR, besides all the other analysed SpFlhB residues, is not part of the FlhB/FliK interaction, which is essential for functional flagellum assembly. These results derived from in vivo experiments generally suggest that the SpFlhB PRR, besides assisting the autocleavage ability of SpFlhB, enables an efficient export of hook and filament substrates. The accompanying in vitro data and structural analysis, accumulated and performed for this publication by the co-author, revealed the PRR to possess a "wave"-shaped linear motif capable of interacting with the SpFlhB-C core domain in a strongly defined manner and therefore might function as a distinct interaction site for a factor involved in the export mechanism or cover a binding region at the core domain for an unknown interaction partner of SpFlhB. This putative interaction partner might be part of the basal section of the flagellum, with the two known interaction partners of SpFlhB, SpFlhA and SpFliK, not requiring the PRR to interact with SpFlhB as confirmed via pulldown assay [97,171,200]. The unknown factor, which

interacts with the PRR of *Sp*FlhB might however assist the export of extracellular flagellum components and raise the overall efficiency of the export process. That the PRR is not directly involved in the binding efficiency of export substrates is implied by a hydrophobic patch comprising four residues in FlhB, required for the binding of proteins targeted for export, as characterised in a previous study, not being near the PRR as confirmed by the structural analysis performed in this study [167]. The fact that the PRR appears widely conserved in β- and γ-proteobacteria, indicates that it is involved in efficient filament substrate export in a wide variety of bacterial species and therefore can be understood as an integral part to overall flagellar assembly [1]. Nevertheless, the exact mechanism of how it is involved in flagellar assembly and influences the efficiency of extracellular flagellum substructure construction, through a possible yet unknown interaction partner, remains to be elucidated by future studies.

5. Materials and methods

5.1 Materials

5.1.1   Microorganisms

Table 5-1 Microorganisms used in this study.

Strain	Genotype	Purpose/description	Source/reference
***Escherichia coli* strains**			
DH5α λpir	φ80d*lacZ* ΔM15 Δ(*lacZYA-argF*) U169 *recA1 hsdR17 deoR thi-I supE44 gyrA96 relA1*/λpir	cloning strain	[201]
BL21 (DE3)	*fhuA2 [lon] ompT gal (λ DE3) [dcm] ΔhsdS λ DE3 = λ sBamHIo ΔEcoRI-B int::(lacI::PlacUV5::T7 gene1) i21 Δnin5*	cloning strain	NEB
WM3064	*thrB1004 pro thi rpsL hsdS lacZ* ΔM15 RP4-1360 Δ(*araBAD*) 567Δ*dapA* 1341: [*erm pir*(wt)]	conjugation strain for *S. putrefaciens* CN-32 and *P. putida* KT2440	W. Metcalf, University of Illinois, Urbana-Champaign
BTH101	*F⁻, cya-99, araD139, galE15, galK16, rpsL1 (Str*ʳ*), hsdR2, mcrA1, mcrB1.*	host strain for two-hybrid assay	Euromedex, France
***Shewanella putrefaciens* CN-32 strains**			
S757	wild type	wild type strain of *S. putrefaciens* CN-32	[176]
S3132	Δ*flhF*	deletion of the gene *flhF* (*Sputcn32_2561*)	Rossmann et al.,2015
S3735	CheA-mCherry	C-terminal mCherry tag of CheA (*Sputcn32_2556*)	this study
S3998	Δ*araAD*	deletion of the genes *araA* (*Sputcn32_2066*) and *araD* (*Sputcn32_2067*)	this study
S4063	*flgE₁* T183C	markerless in-frame substitution of Thr183 to Cys in the polar hook	[202]

		protein FlgE$_1$ (Sputcn32_2594), fully functional and suitable for maleimide staining	
S4401	*flaB$_1$* T166C *flaA$_1$* T174C Δ*flagL*	markerless in-frame substitution of Thr166 to Cys in the polar major flagellin protein FlaB$_1$ (Sputcn32_2585) and Thr174 to Cys in the polar minor flagellin protein FlaA$_1$ (Sputcn32_2586), fully functional and suitable for maleimide staining and deletion of the lateral gene cluster (Sputcn32_*3444*-Sputcn32_*3485*)	[39]
S4623	FlhB-FLAG	C-terminal 3x FLAG tag of FlhB (Sputcn32_2563)	[1]
S4890	Δ*fipA*	deletion of the gene *fipA* (*Sputcn32_2550*)	this study
S4891	CheA-mCherry Δ*fipA*	C-terminal mCherry tag of CheA (Sputcn32_2556) and deletion of the gene *fipA* (*Sputcn32_2550*)	this study
S5151	*flaB$_1$* T166C *flaA$_1$* T174C Δ*flagL* Δ*fipA*	markerless in-frame substitution of Thr166 to Cys in the polar major flagellin protein FlaB$_1$ (Sputcn32_2585) and Thr174 to Cys in the polar minor flagellin protein FlaA$_1$ (Sputcn32_2586), fully functional and suitable for maleimide staining, deletion of the lateral gene cluster (Sputcn32_*3444*-Sputcn32_*3485*) and deletion of the gene *fipA* (*Sputcn32_2550*)	this study
S5180	FlhF-GS-mVenus	C-terminal mVenus tag of FlhF (Sputcn32_2561) linked with Gly and Ser	this study
S5286	FipA-DILEL-sfGFP	C-terminal sfGFP tag of FipA (Sputcn32_2550) linked with Asp, Ile, Leu, Glu and Leu	this study
S5294	FlhF-GS-mVenus Δ*fipA*	C-terminal mVenus tag of FlhF (Sputcn32_2561) linked with Gly and Ser and deletion of the gene *fipA* (*Sputcn32_2550*)	this study
S5307	FlhF-GS-mVenus Δ*flhB*	C-terminal mVenus tag of FlhF (Sputcn32_2561) linked with Gly	this study

		and Ser and deletion of the gene *flhB* (*Sputcn32_2563*)	
S5441	Δ*araAD* FlhF-GS-mVenus Ara ind.	deletion of the genes *araA* (*Sputcn32_2066*) and *araD* (*Sputcn32_2067*) and insertion of C-terminal mVenus tagged FlhF (Sputcn32_2561) linked with Gly and Ser upstream from *Sputcn32_2068*	this study
S5607	FlhF-GS-mVenus Δ*flhG*	C-terminal mVenus tag of FlhF (Sputcn32_2561) linked with Gly and Ser and deletion of the gene *flhG* (*Sputcn32_2560*)	this study
S5675	FlhF-GS-mVenus Δ*flrA1*	C-terminal mVenus tag of FlhF (Sputcn32_2561) linked with Gly and Ser and deletion of the gene *flhG* (*Sputcn32_2560*)	this study
S5714	FipA-DILEL-sfGFP Δ*flhF*	C-terminal sfGFP tag of FipA (Sputcn32_2550) linked with Asp, Ile, Leu, Glu and Leu and deletion of the gene *flhF* (*Sputcn32_2561*)	this study
S5806	FlhF-GS-mVenus Δ*hubP*	C-terminal mVenus tag of FlhF (Sputcn32_2561) linked with Gly and Ser and deletion of the gene *hubP* (*Sputcn32_2442*)	this study
S5807	FlhF-GS-mVenus Δ*fipA* Δ*hubP*	C-terminal mVenus tag of FlhF (Sputcn32_2561) linked with Gly and Ser and deletion of the genes *fipA* (*Sputcn32_2550*) and *hubP* (*Sputcn32_2442*)	this study
S5910	*flgE₁* T183C Δ*flagL*	markerless in-frame substitution of Thr183 to Cys in the polar hook protein FlgE₁ (Sputcn32_2594), fully functional and suitable for maleimide staining and deletion of the lateral gene cluster (Sputcn32_*3444-Sputcn32_3485*)	[1]
S6036	FipA-DILEL-sfGFP Δ*hubP*	C-terminal sfGFP tag of FipA (Sputcn32_2550) linked with Asp, Ile, Leu, Glu and Leu and deletion of the gene *hubP* (*Sputcn32_2442*)	this study
S6053	Δ*araAD* FlhF-1xGS-mVenus Ara ind. Δ*Sputcn32_2548-2608* Δ*hubP*	deletion of the genes *araA* (*Sputcn32_2066*) and *araD* (*Sputcn32_2067*), insertion of C-terminal mVenus tagged FlhF	this study

	Δ*Sputcn32_3444-3485*	(Sputcn32_2561) linked with Gly and Ser upstream from *Sputcn32_2068* and deletion of the polar gene cluster (*Sputcn32_2548-2608*), the gene *hubP* (*Sputcn32_2442*) and the lateral gene cluster (Sputcn32_*3444*-Sputcn32_*3485*)	
S6117	HubP-mCherry FlhF-GS-Venus	C-terminal mCherry tag of HubP (Sputcn32_2442) and C-terminal mVenus tag of FlhF (Sputcn32_2561) linked with Gly and Ser	this study
S6128	Δ*araAD* FlhF-GS-mVenus Ara. indu. Δ*flhF*	deletion of the genes *araA* (*Sputcn32_2066*) and *araD* (*Sputcn32_2067*), insertion of C-terminal mVenus tagged FlhF (Sputcn32_2561) linked with Gly and Ser upstream from *Sputcn32_2068* and deletion of the native *flhF* gene (*Sputcn32_2561*)	this study
S6164	FlhF-GS-mVenus Δ*hubP* Δ*Sputcn32_3157*	C-terminal mVenus tag of FlhF (Sputcn32_2561) linked with Gly and Ser and deletion of the genes hubP (*Sputcn32_2442*) and *Sputcn32_3157*	this study
S6305	*flaB*$_1$ T166C *flaA*$_1$ T174C Δ*flagL* Δ*flhB*	markerless in-frame substitution of Thr166 to Cys in the polar major flagellin protein FlaB$_1$ (Sputcn32_2585) and Thr174 to Cys in the polar minor flagellin protein FlaA$_1$ (Sputcn32_2586), fully functional and suitable for maleimide staining, deletion of the lateral gene cluster (Sputcn32_*3444*-Sputcn32_*3485*) and deletion of the gene *flhB* (Sputcn32_*2563*)	[1]
S6306	*flgE*$_1$ T183C Δ*flagL* Δ*flhB*	markerless in-frame substitution of Thr183 to Cys in the polar hook protein FlgE$_1$ (Sputcn32_2594), fully functional and suitable for maleimide staining, deletion of the lateral gene cluster and deletion of the gene *flhB* (Sputcn32_*2580*)	[1]

S6327	*flaB₁* T166C *flaA₁* T174C Δ*flagL* Δ*flhB* FlhB Δ358-376[+]	markerless in-frame substitution of Thr166 to Cys in the polar major flagellin protein FlaB₁ (Sputcn32_2585) and Thr174 to Cys in the polar minor flagellin protein FlaA₁ (Sputcn32_2586), fully functional and suitable for maleimide staining, deletion of the lateral gene cluster (Sputcn32_*3444*-Sputcn32_*3485*) and deletion of the gene *flhB* (Sputcn32_*2563*) with subsequent reconstitution of *flhB* with a truncated version (FlhB Δ358-376)	[1]
S6328	*flgE₁* T183C Δ*flagL* Δ*flhB* FlhB Δ358-376[+]	markerless in-frame substitution of Thr183 to Cys in the polar hook protein FlgE₁ (Sputcn32_2594), fully functional and suitable for maleimide staining, deletion of the lateral gene cluster (Sputcn32_*3444*-Sputcn32_*3485*) and deletion of the gene *flhB* (Sputcn32_2563) with subsequent reconstitution of *flhB* with a truncated version (FlhB Δ358-376)	[1]
S6581	*flaB₁* T166C *flaA₁* T174C Δ*flagL* FipA-DILEL-sfGFP	markerless in-frame substitution of Thr166 to Cys in the polar major flagellin protein FlaB₁ (Sputcn32_2585) and Thr174 to Cys in the polar minor flagellin protein FlaA₁ (Sputcn32_2586), fully functional and suitable for maleimide staining, deletion of the lateral gene cluster (Sputcn32_*3444*-Sputcn32_*3485*) and C-terminal sfGFP tag of FipA (Sputcn32_2550) linked with Asp, Ile, Leu, Glu and Leu	this study
S6606	*flaB₁* T166C *flaA₁* T174C Δ*flagL* Δ*flhF*	markerless in-frame substitution of Thr166 to Cys in the polar major flagellin protein FlaB₁ (Sputcn32_2585) and Thr174 to Cys in the polar minor flagellin protein FlaA₁ (Sputcn32_2586), fully functional and suitable for maleimide staining, deletion of the lateral gene cluster (Sputcn32_*3444*-Sputcn32_*3485*)	this study

		and deletion of the gene *flhF* (*Sputcn32_2561*)	
S6671	FlhF-1xGS-mVenus Δ*ybcG* (*Sputcn32_1603*)	C-terminal mVenus tag of FlhF (Sputcn32_2561) linked with Gly and Ser and deletion of the gene *ybcG* (*Sputcn32_1603*)	this study
S6789	Δ*fipA* *fipA* (*Sputcn32_2550*) KI	deletion of the gene *fipA* (*Sputcn32_2550*) and reconstitution of the gene *fipA* (*Sputcn32_2550*)	this study
S6803	FipA L118A	markerless in-frame substitution of Leu118 to Ala in the protein FipA (Sputcn32_2550)	this study
S6804	FipA G106A	markerless in-frame substitution of Gly106 to Ala in the protein FipA (Sputcn32_2550)	this study
S6880	FipA L118-DILEL-sfGFP	markerless in-frame substitution of Leu118 to Ala in the protein FipA (Sputcn32_2550) with a C-terminal sfGFP tag linked with Asp, Ile, Leu, Glu and Leu	this study
S6889	FipA G106A-DILEL-sfGFP	markerless in-frame substitution of Gly106 to Ala in the protein FipA (Sputcn32_2550) with a C-terminal sfGFP tag linked with Asp, Ile, Leu, Glu and Leu	this study
S6920	*flgE₁* T183C Δ*flagL* Δ*flhB* Δ358-376+ FliM₁-GS-GFP	markerless in-frame substitution of Thr183 to Cys in the polar hook protein FlgE₁ (Sputcn32_2594), fully functional and suitable for maleimide staining, deletion of the lateral gene cluster (Sputcn32_*3444-Sputcn32_3485*), C-terminal sfGFP tag of FliM₁ (Sputcn32_2569) linked with Gly and Ser and deletion of the gene *flhB* (Sputcn32_2563) with subsequent reconstitution of *flhB* with a truncated version (FlhB Δ358-376)	[1]
S6994	*flgE₁* T183C Δ*flagL* FliM₁-GS-sfGFP	markerless in-frame substitution of Thr183 to Cys in the polar hook protein FlgE₁ (Sputcn32_2594), fully functional and suitable for maleimide staining, deletion of the lateral gene cluster (Sputcn32_*3444-Sputcn32_3485*)	[1]

		and C-terminal sfGFP tag of FliM$_1$ (Sputcn32_2569) linked with Gly and Ser	
S6995	*flgE$_1$* T183C Δ*flagL* Δ*flhB* FliM$_1$-GS-sfGFP	markerless in-frame substitution of Thr183 to Cys in the polar hook protein FlgE$_1$ (Sputcn32_2594), fully functional and suitable for maleimide staining, deletion of the lateral gene cluster (Sputcn32_*3444*-Sputcn32_*3485*), C-terminal sfGFP tag of FliM$_1$ (Sputcn32_2569) linked with Gly and Ser and deletion of the gene *flhB* (Sputcn32_2563)	[1]
S6996	FipA L125A	markerless in-frame substitution of Leu125 to Ala in the protein FipA (Sputcn32_2550)	this study
S7032	*flaB$_1$* T166C *flaA$_1$* T174C Δ*flagL* Δ*fipA* Δ*hubP*	markerless in-frame substitution of Thr166 to Cys in the polar major flagellin protein FlaB$_1$ (Sputcn32_2585) and Thr174 to Cys in the polar minor flagellin protein FlaA$_1$ (Sputcn32_2586), fully functional and suitable for maleimide staining and deletion of the lateral gene cluster (Sputcn32_*3444*-Sputcn32_*3485*) and the genes *fipA* (*Sputcn32_2550*) and *hubP* (*Sputcn32_2442*)	this study
S7064	FipA L125A-DILEL-sfGFP	markerless in-frame substitution of Leu125 to Ala in the protein FipA (Sputcn32_2550) with a C-terminal sfGFP tag linked with Asp, Ile, Leu, Glu and Leu	this study
S7067	*flaB$_1$* T166C *flaA$_1$* T174C Δ*flagL* Δ*fliK$_1$*	markerless in-frame substitution of Thr166 to Cys in the polar major flagellin protein FlaB$_1$ (Sputcn32_2585) and Thr174 to Cys in the polar minor flagellin protein FlaA$_1$ (Sputcn32_2586), fully functional and suitable for maleimide staining, deletion of the lateral gene cluster (Sputcn32_*3444*-Sputcn32_*3485*) and deletion of the gene *fliK* (*Sputcn32_2571*)	[1]

S7068	$flaB_1$ T166C $flaA_1$ T174C $\Delta flagL$ $\Delta flhB$ $\Delta fliK_1$	markerless in-frame substitution of Thr166 to Cys in the polar major flagellin protein FlaB$_1$ (Sputcn32_2585) and Thr174 to Cys in the polar minor flagellin protein FlaA$_1$ (Sputcn32_2586), fully functional and suitable for maleimide staining, deletion of the lateral gene cluster (Sputcn32_3444-Sputcn32_3485), deletion of the genes $flhB$ (Sputcn32_2563) and $fliK$ (Sputcn32_2571)	1
S7069	$flaB_1$ T166C $flaA_1$ T174C $\Delta flagL$ $\Delta flhB$ FlhB Δ358-376$^+$ $\Delta fliK_1$	markerless in-frame substitution of Thr166 to Cys in the polar major flagellin protein FlaB$_1$ (Sputcn32_2585) and Thr174 to Cys in the polar minor flagellin protein FlaA$_1$ (Sputcn32_2586), fully functional and suitable for maleimide staining, deletion of the lateral gene cluster (Sputcn32_3444-Sputcn32_3485) and deletion of the genes $fliK$ (Sputcn32_2571) and $flhB$ (Sputcn32_2563) with subsequent reconstitution of $flhB$ with a truncated version (FlhB Δ358-376)	1
S7070	$flgE_1$ T183C $\Delta flagL$ $\Delta flhB$ FlhB Δ358-376$^+$ FliM$_1$-GS-GFP $\Delta fliK_1$	markerless in-frame substitution of Thr183 to Cys in the polar hook protein FlgE$_1$ (Sputcn32_2594), fully functional and suitable for maleimide staining, deletion of the lateral gene cluster (Sputcn32_3444-Sputcn32_3485), C-terminal sfGFP tag of FliM$_1$ (Sputcn32_2569) linked with Gly and Ser and deletion of the genes $fliK$ (Sputcn32_2571) and $flhB$ (Sputcn32_2563) with subsequent reconstitution of $flhB$ with a truncated version (FlhB Δ358-376)	1
S7071	$flgE_1$ T183C $\Delta flagL$ FliM$_1$-GS-GFP $\Delta fliK_1$	markerless in-frame substitution of Thr183 to Cys in the polar hook protein FlgE$_1$ (Sputcn32_2594), fully functional and suitable for maleimide staining, deletion of the lateral gene cluster, C-terminal sfGFP tag of FliM$_1$ (Sputcn32_2569)	1

		linked with Gly and Ser and deletion of the gene *fliK* (*Sputcn32_2571*)	
S7072	*flgE₁* T183C *ΔflagL* *ΔflhB* FliM₁-GS-GFP *ΔfliK₁*	markerless in-frame substitution of Thr183 to Cys in the polar hook protein FlgE₁ (Sputcn32_2594), fully functional and suitable for maleimide staining, deletion of the lateral gene cluster (Sputcn32_*3444-Sputcn32_3485*), C-terminal sfGFP tag of FliM₁ (Sputcn32_2569) linked with Gly and Ser and deletion of the genes *flhB* (*Sputcn32_2563*) and *fliK* (*Sputcn32_2571*)	[1]
S7080	*flaB₁* T166C *flaA₁* T174C *ΔflagL* FlhB Y376A	markerless in-frame substitution of Thr166 to Cys in the polar major flagellin protein FlaB₁ (Sputcn32_2585) and Thr174 to Cys in the polar minor flagellin protein FlaA₁ (Sputcn32_2586), fully functional and suitable for maleimide staining, deletion of the lateral gene cluster (Sputcn32_*3444-Sputcn32_3485*) and in-frame substitution of Tyr376 to Ala in FlhB (Sputcn32_2563)	[1]
S7081	*flgE₁* T183C *ΔflagL* FliM₁-GS-sfGFP FlhB Y376A	markerless in-frame substitution of Thr183 to Cys in the polar hook protein FlgE₁ (Sputcn32_2594), fully functional and suitable for maleimide staining, deletion of the lateral gene cluster (Sputcn32_*3444-Sputcn32_3485*), C-terminal sfGFP tag of FliM₁ (Sputcn32_2569) linked with Gly and Ser and in-frame substitution of Tyr376 to Ala in FlhB (Sputcn32_2563)	[1]
S7082	*flaB₁* T166C *flaA₁* T174C *ΔflagL* *ΔfliK₁* FlhB Y376A	markerless in-frame substitution of Thr166 to Cys in the polar major flagellin protein FlaB₁ (Sputcn32_2585) and Thr174 to Cys in the polar minor flagellin protein FlaA₁ (Sputcn32_2586), fully functional and suitable for maleimide staining, deletion of the lateral gene cluster (Sputcn32_*3444-Sputcn32_3485*),	[1]

		in-frame substitution of Tyr376 to Ala in FlhB (Sputcn32_2563) and deletion of *fliK* (*Sputcn32_2571*)	
S7083	*flgE₁* T183C Δ*flagL* FliM₁-GS-GFP Δ*fliK₁* FlhB Y376A	markerless in-frame substitution of Thr183 to Cys in the polar hook protein FlgE₁ (Sputcn32_2594), fully functional and suitable for maleimide staining, deletion of the lateral gene cluster (S*putcn32_3444-Sputcn32_3485*), C-terminal sfGFP tag of FliM₁ (Sputcn32_2569) linked with Gly and Ser, deletion of *fliK* (Sputcn32_*2571*) and markerless in-frame substitution of Tyr376 to Ala in FlhB (Sputcn32_2563)	[1]
S7093	*flaB₁* T166C *flaA₁* T174C Δ*flagL* FlhB N269A	markerless in-frame substitution of Thr166 to Cys in the polar major flagellin protein FlaB₁ (Sputcn32_2585) and Thr174 to Cys in the polar minor flagellin protein FlaA₁ (Sputcn32_2586), fully functional and suitable for maleimide staining, deletion of the lateral gene cluster (Sputcn32_*3444-Sputcn32_3485*) and in-frame substitution of Asn269 to Ala in FlhB (Sputcn32_2563)	[1]
S7094	*flgE₁* T183C Δ*flagL* FliM₁-GS-sfGFP FlhB N269A	markerless in-frame substitution of Thr183 to Cys in the polar hook protein FlgE₁ (Sputcn32_2594), fully functional and suitable for maleimide staining, deletion of the lateral gene cluster (S*putcn32_3444-Sputcn32_3485*), C-terminal sfGFP tag of FliM₁ (Sputcn32_2569) linked with Gly and Ser and in-frame substitution of Asn269 to Ala in FlhB (Sputcn32_2563)	[1]
S7095	*flaB₁* T166C *flaA₁* T174C Δ*flagL* Δ*fliK₁* FlhB N269A	markerless in-frame substitution of Thr166 to Cys in the polar major flagellin protein FlaB₁ (Sputcn32_2585) and Thr174 to Cys in the polar minor flagellin protein FlaA₁ (Sputcn32_2586), fully functional and suitable for maleimide staining, deletion of the	[1]

		lateral gene cluster (Sputcn32_3444-Sputcn32_3485), in-frame substitution of Asn269 to Ala in FlhB (Sputcn32_2563) and deletion of *fliK* (*Sputcn32_2571*)	
S7096	*flgE*$_1$ T183C Δ*flagL* FliM$_1$-GS-sfGFP Δ*fliK*$_1$ FlhB N269A	markerless in-frame substitution of Thr183 to Cys in the polar hook protein FlgE$_1$ (Sputcn32_2594), fully functional and suitable for maleimide staining, deletion of the lateral gene cluster (*Sputcn32_3444-Sputcn32_3485*), C-terminal sfGFP tag of FliM$_1$ (Sputcn32_2569) linked with Gly and Ser, deletion of *fliK* (Sputcn32_2571) and markerless in-frame substitution of Asn269 to Ala in FlhB (Sputcn32_2563)	[1]
S7113	FlhB N269A-FLAG	markerless in-frame substitution of Asn269 to Ala in FlhB (Sputcn32_2563) with C-terminal 3x FLAG tag	[1]
S7116	Δ*flhB* FlhB Δ358-376-FLAG	deletion of the gene *flhB* (Sputcn32_2563) with subsequent reconstitution of *flhB* with a truncated version (FlhB Δ358-376) with C-terminal 3x FLAG tag	[1]
S7117	FlhB Y376A-FLAG	markerless in-frame substitution of Tyr376 to Ala in FlhB (Sputcn32_2563) with C-terminal 3x FLAG tag	[1]
S7362	*flaB*$_1$ T166C *flaA*$_1$ T174C Δ*flagL* FipA-DILEL-sfGFP FliM$_1$-GS-mCherry	markerless in-frame substitution of Thr166 to Cys in the polar major flagellin protein FlaB$_1$ (Sputcn32_2585) and Thr174 to Cys in the polar minor flagellin protein FlaA$_1$ (Sputcn32_2586), fully functional and suitable for maleimide staining, deletion of the lateral gene cluster (Sputcn32_*3444-Sputcn32_3485*), C-terminal sfGFP tag of FipA (Sputcn32_2550) linked with Asp, Ile, Leu, Glu and Leu and C-terminal GFP tag of FliM$_1$ (Sputcn32_2569) linked with Gly and Ser	this study
S7811	FlhF D390A-GS-mVenus	markerless in-frame substitution of Asp390 to Ala in FlhF	this study

		(Sputcn32_2561) with C-terminal mVenus tag linked with Gly and Ser	
S7935	FlhF-GS-mVenus *fliFG₁* KO	C-terminal mVenus tag of FlhF (Sputcn32_2561) linked with Gly and Ser and deletion of the genes *fliF₁* (*Sputcn32_2576*) and *fliG₁* (*Sputcn32_2575*)	this study
S7990	FlhF-mCherry FipA-DILEL-sfGFP	C-terminal mCherry tag of FlhF (Sputcn32_2561) and C-terminal sfGFP tag of FipA (Sputcn32_2550) linked with Asp, Ile, Leu, Glu and Leu	this study
S8002	FipA L118A FlhF-GS-mVenus	markerless in-frame substitution of Leu118 to Ala in the protein FipA (Sputcn32_2550) and C-terminal mVenus tag of FlhF (Sputcn32_2561) linked with Gly and Ser	this study
S8003	FipA G106A FlhF-GS-mVenus	markerless in-frame substitution of Gly106 to Ala in the protein FipA (Sputcn32_2550) and C-terminal mVenus tag of FlhF (Sputcn32_2561) linked with Gly and Ser	this study
S8004	FipA L125A FlhF-GS-mVenus	markerless in-frame substitution of Leu125 to Ala in the protein FipA (Sputcn32_2550) and C-terminal mVenus tag of FlhF (Sputcn32_2561) linked with Gly and Ser	this study
S8017	FipA-DILEL-sfGFP FlhF K256A	C-terminal sfGFP tag of FipA (Sputcn32_2550) linked with Asp, Ile, Leu, Glu and Leu and markerless in-frame substitution of Lys256 to Ala in FlhF (Sputcn32_2561)	this study
S8018	FipA-DILEL-sfGFP FlhF D328A	C-terminal sfGFP tag of FipA (Sputcn32_2550) linked with Asp, Ile, Leu, Glu and Leu and markerless in-frame substitution of Asp328 to Ala in FlhF (Sputcn32_2561)	this study
S8099	FlhF K256A-GS-mVenus	markerless in-frame substitution of Lys256 to Ala in FlhF	this study

		(Sputcn32_2561) with C-terminal mVenus tag linked with Gly and Ser	
S8100	FlhF D328A-GS-mVenus	markerless in-frame substitution of Asp328 to Ala in FlhF (Sputcn32_2561) with C-terminal mVenus tag linked with Gly and Ser	this study
S8156	FipA-DILEL-sfGFP FlhF D390A	C-terminal sfGFP tag of FipA (Sputcn32_2550) linked with Asp, Ile, Leu, Glu and Leu and markerless in-frame substitution of Asp390 to Ala in FlhF (Sputcn32_2561)	this study
S8246	FipA ΔTMD	in-frame deletion of the N-terminal transmembrane domain in the protein FipA (Sputcn32_2550)	this study
S8247	FlhF-GS-mVenus FipA ΔTMD	markerless in-frame deletion of the N-terminal transmembrane domain in the protein FipA (Sputcn32_2550) and C-terminal mVenus tag of FlhF (Sputcn32_2561) linked with Gly and Ser	this study
S8248	FipA ΔTMD-DILEL-sfGFP	in-frame deletion of the N-terminal transmembrane domain in the protein FipA (Sputcn32_2550) and C-terminal sfGFP tag of FipA (Sputcn32_2550) linked with Asp, Ile, Leu, Glu and Leu	this study
Pseudomonas putida KT2440 strains			this study
P3811	wildtype	wild type strain of *P. putida* KT2440	[203]
P4135	FliC S267C	markerless in-frame substitution of Ser267 to Cys in the flagellin protein FliC (PP_4378)	this study
P5405	FliC S267C Δ*fleN*	markerless in-frame substitution of Ser267 to Cys in the flagellin protein FliC (PP_4378) and deletion of the gene *fleN* (*PP_4342*)	this study
P5406	FliC S267C Δ*flhF*	markerless in-frame substitution of Ser267 to Cys in the flagellin protein FliC (PP_4378) and deletion of the gene *flhF* (*PP_4343*)	this study
P6506	Δ*fipA*	deletion of the gene *fipA* (*PP_4331*)	this study
P6507	FliC S267C Δ*fipA*	markerless in-frame substitution of Ser267 to Cys in the flagellin protein FliC (PP_4378) and deletion of the gene *fipA* (*PP_4331*)	this study

P6508	FipA -DILEL-sfGFP	C-terminal sfGFP tag of FipA (PP_4331) linked with Asp, Ile, Leu, Glu and Leu	this study
P6510	FliC S267C ΔflhF FipA-DILEL-sfGFP	markerless in-frame substitution of Ser267 to Cys in the flagellin protein FliC (PP_4378), deletion of the gene flhF (PP_4343) and C-terminal sfGFP tag of FipA (PP_4331) linked with Asp, Ile, Leu, Glu and Leu	this study
P6511	FlhF-GS-mCherry	C-terminal mCherry tag of FlhF (PP_4343) linked with Gly and Ser	this study
P6515	FliC S267C ΔfimV FipA -DILEL-sfGFP	markerless in-frame substitution of Ser267 to Cys in the flagellin protein FliC (PP_4378), deletion of the gene fimV (PP_1992) and C-terminal sfGFP tag of FipA (PP_4331) linked with Asp, Ile, Leu, Glu and Leu	this study
P6529	ΔfipA FlhF-GS-mCherry	deletion of the gene fipA (PP_4331) and C-terminal mCherry tag of FlhF (PP_4343) linked with Gly and Ser	this study
P6908	FliC S267C FipA G104A	markerless in-frame substitution of Ser267 to Cys in the flagellin protein FliC (PP_4378) and in-frame substitution of Gly104 to Ala in the protein FipA (Sputcn32_4331)	this study
P7745	FipA L123A	markerless in-frame substitution of Leu123 to Ala in the protein FipA (Sputcn32_4331)	this study
P7774	FliC S267C FipA L123A	markerless in-frame substitution of Ser267 to Cys in the flagellin protein FliC (PP_4378) and in-frame substitution of Leu123 to Ala in the protein FipA (Sputcn32_4331)	this study
P7775	FliC S267C FipA-DILEL-sfGFP	markerless in-frame substitution of Ser267 to Cys in the flagellin protein FliC (PP_4378) and C-terminal sfGFP tag of FipA (PP_4331) linked with Asp, Ile, Leu, Glu and Leu	this study
P7779	FliC S267C FipA L116A	markerless in-frame substitution of Ser267 to Cys in the flagellin protein FliC (PP_4378) and in-frame substitution of Leu116 to Ala in the protein FipA (Sputcn32_4331)	this study

P7841	FliC S267C FipA G104A-DILEL-sfGFP	markerless in-frame substitution of Ser267 to Cys in the flagellin protein FliC (PP_4378) and in-frame substitution of Gly104 to Ala in the protein FipA (Sputcn32_4331) with C-terminal sfGFP tag linked with Asp, Ile, Leu, Glu and Leu	this study
P7864	FliC S267C FipA L123A-DILEL-sfGFP	markerless in-frame substitution of Ser267 to Cys in the flagellin protein FliC (PP_4378) and in-frame substitution of Leu123 to Ala in the protein FipA (Sputcn32_4331) with C-terminal sfGFP tag linked with Asp, Ile, Leu, Glu and Leu	this study
P7865	FliC S267C FipA L116A-DILEL-sfGFP	markerless in-frame substitution of Ser267 to Cys in the flagellin protein FliC (PP_4378) and in-frame substitution of Leu116 to Ala in the protein FipA (Sputcn32_4331) with C-terminal sfGFP tag linked with Asp, Ile, Leu, Glu and Leu	this study
P7939	FlhF-GS-mCherry ΔfimV	C-terminal mCherry tag of FlhF (PP_4343) linked with Gly and Ser and deletion of the gene *fimV* (*PP_1992*)	this study
P7951	FliC S267C ΔfipA FipA KI	markerless in-frame substitution of Ser267 to Cys in the flagellin protein FliC (PP_4378), deletion of the gene *fipA* (*Sputcn32_4331*) and reconstitution of the gene *fipA* (*Sputcn32_4331*)	this study
P7962	FlhF-GS-mCherry ΔfimV ΔfipA	C-terminal mCherry tag of FlhF (PP_4343) linked with Gly and Ser and deletion of the genes *fimV* (*PP_1992*) and *fipA* (*Sputcn32_4331*)	this study
P8038	FliC S267C FipA-DILEL-sfGFP FlhF K235A	markerless in-frame substitution of Ser267 to Cys in the flagellin protein FliC (PP_4378), C-terminal sfGFP tag of FipA (PP_4331) linked with Asp, Ile, Leu, Glu and Leu and in-frame substitution of Lys235 to Ala in FlhF (PP_4343)	this study
P8039	FliC S267C FipA-DILEL-sfGFP FlhF D301A	markerless in-frame substitution of Ser267 to Cys in the flagellin protein FliC (PP_4378), C-terminal sfGFP	this study

		tag of FipA (PP_4331) linked with Asp, Ile, Leu, Glu and Leu and in-frame substitution of Asp301 to Ala in FlhF (PP_4343)	
P8040	FlhF-GS-mCherry FipA L123A	C-terminal mCherry tag of FlhF (PP_4343) linked with Gly and Ser and markerless in-frame substitution of Leu123 to Ala in the protein FipA (Sputcn32_4331)	this study
P8041	FlhF-GS-mCherry FipA L116A	C-terminal mCherry tag of FlhF (PP_4343) linked with Gly and Ser and markerless in-frame substitution of Leu116 to Ala in the protein FipA (Sputcn32_4331)	this study
P8042	FlhF-GS-mCherry FipA G104A	C-terminal mCherry tag of FlhF (PP_4343) linked with Gly and Ser and markerless in-frame substitution of Gly104 to Ala in the protein FipA (Sputcn32_4331)	this study
P8152	FliC S267C FipA-DILEL-sfGFP FlhF K229A	markerless in-frame substitution of Ser267 to Cys in the flagellin protein FliC (PP_4378), C-terminal sfGFP tag of FipA (PP_4331) linked with Asp, Ile, Leu, Glu and Leu and in-frame substitution of Lys229 to Ala in FlhF (PP_4343)	this study
P8206	FliC S267C FlhF D301A-GS-mCherry	markerless in-frame substitution of Ser267 to Cys in the flagellin protein FliC (PP_4378) in-frame substitution of Asp301 to Ala in FlhF (PP_4343) with C-terminal mCherry tag linked with Gly and Ser	this study
P8207	FliC S267C FlhF D362A-GS-mCherry	markerless in-frame substitution of Ser267 to Cys in the flagellin protein FliC (PP_4378) in-frame substitution of Asp362 to Ala in FlhF (PP_4343) with C-terminal mCherry tag linked with Gly and Ser	this study
P8209	KT2440 FliC S267C FlhF K229A-GS-mCherry	markerless in-frame substitution of Ser267 to Cys in the flagellin protein FliC (PP_4378) in-frame substitution of Lys229 to Ala in FlhF (PP_4343) with C-terminal mCherry tag linked with Gly and Ser	this study

P8210	KT2440 FliC S267C FlhF K235A-GS-mCherry	markerless in-frame substitution of Ser267 to Cys in the flagellin protein FliC (PP_4378) in-frame substitution of Lys235 to Ala in FlhF (PP_4343) with C-terminal mCherry tag linked with Gly and Ser	this study
P8243	FliC S267C FlhF-GS-mCherry FipA ΔTMD	markerless in-frame substitution of Ser267 to Cys in the flagellin protein FliC (PP_4378) and in-frame deletion of the N-terminal transmembrane domain in the protein FipA (Sputcn32_4331)	this study
P8244	FliC S267C FlhF-GS-mCherry FipA ΔTMD	markerless in-frame substitution of Ser267 to Cys in the flagellin protein FliC (PP_4378), C-terminal mCherry tag of FlhF (PP_4343) linked with Gly and Ser and in-frame deletion of the N-terminal transmembrane domain in the protein FipA (Sputcn32_4331)	this study
P8245	FliC S267C FipA ΔTMD-DILEL-sfGFP	markerless in-frame substitution of Ser267 to Cys in the flagellin protein FliC (PP_4378) and in-frame deletion of the N-terminal transmembrane domain in the protein FipA (Sputcn32_4331) with C-terminal sfGFP tag linked with Asp, Ile, Leu, Glu and Leu	this study
P8467	FliC S267C FipA-DILEL-sfGFP FlhF D362A	markerless in-frame substitution of Ser267 to Cys in the flagellin protein FliC (PP_4378), C-terminal sfGFP tag of FipA (PP_4331) linked with Asp, Ile, Leu, Glu and Leu and in-frame substitution of Asp362 to Ala in FlhF (PP_4343)	this study

Abbreviations: KO: knock out; KI: knock in

5.1.2 Plasmids and starter oligonucleotides (primer)

All listed primers were acquired from and synthesized by the company Sigma-Aldrich, Steinheim.

Table 5-2 Plasmids used in this study.

Plasmid	Purpose/description	Reference
pNPTS138-R6KT	mobRP4+ ori-R6K *sacB;* β-galactosidase fragment alpha; suicide vector for in-frame deletions or integrations; Kan[r]	[204]
pKT25	*plac* ori p15A vector for protein-protein interaction analysis; MCS downstream from T25 fragment encoding region; Kan[r]	[205]

pKNT25	*plac* ori p15A vector for protein-protein interaction analysis; MCS upstream from T25 fragment encoding region; Kan[r]	[205]
pUT18	*plac* ori Col E1 vector for protein-protein interaction analysis; MCS downstream from T18 fragment encoding region; Amp[r]	[205]
pUT18C	*plac* ori Col E1 vector for protein-protein interaction analysis; MCS upstream from T18 fragment encoding region; Amp[r]	[205]

Plasmids for *S. putrefaciens* CN-32

pNPTS138-R6KT polar flagellar cluster KO (*Sputcn32_2548-2608*)	plasmid for deletion of the polar flagellar gene cluster (*Sputcn32_2548-2608*) in *S. putrefaciens* CN-32; Kan[r]	this study
pNPTS138-R6KT lateral flagellar cluster KO (*Sputcn32_3444-3485*)	plasmid for deletion of the lateral flagellar gene cluster (*Sputcn32_3444-3485*) in *S. putrefaciens* CN-32; Kan[r]	[180]
pNPTS138-R6KT *flagL* KO (*Sputcn32_3455, Sputcn32_3456*)	plasmid for deletion of the lateral flagellin genes (*Sputcn32_3455, Sputcn32_3456*) in *S. putrefaciens* CN-32; Kan[r]	[57]
pNPTS138-R6KT *hubP* KO (*Sputcn32_2442*)	plasmid for deletion of the *hubP* gene (*Sputcn32_2442*) in *S. putrefaciens* CN-32; Kan[r]	[57]
pNPTS138-R6KT *flrA₁* KO (*Sputcn32_2580*)	plasmid for deletion of the *flrA₁* gene (*Sputcn32_2580*) in *S. putrefaciens* CN-32; Kan[r]	[206]
pNPTS138-R6KT *flhF* KO (*Sputcn32_2561*)	plasmid for deletion of the *flhF* gene (*Sputcn32_2561*) in *S. putrefaciens* CN-32; Kan[r]	[57]
pNPTS138-R6KT *flhG* KO (*Sputcn32_2560*)	plasmid for deletion of the *flhG* gene (*Sputcn32_2560*) in *S. putrefaciens* CN-32; Kan[r]	[158]
pNPTS138-R6KT *fliFG₁* KO (*Sputcn32_2576, Sputcn32_2575*)	plasmid for deletion of the *fliF₁* (*Sputcn32_2576*) and *fliG₁* gene (*Sputcn32_2575*) in *S. putrefaciens* CN-32; Kan[r]	this study
pNPTS138-R6KT *flhB* KO (*Sputcn32_2563*)	plasmid for deletion of the *flhB* gene (*Sputcn32_2563*) in *S. putrefaciens* CN-32; Kan[r]	[1]
pNPTS138-R6KT *fliK₁* KO (Sputcn32_2571)	plasmid for deletion of the *fliK₁* gene (*Sputcn32_2571*) in *S. putrefaciens* CN-32; Kan[r]	[1]
pNPTS138-R6KT *Sputcn32_3157* KO	plasmid for deletion of the gene *Sputcn32_3157* in *S. putrefaciens* CN-32; Kan[r]	this study
pNPTS138-R6KT *ybcG* KO (*Sputcn32_1603*)	plasmid for deletion of the *ybcG* gene (*Sputcn32_1603*) in *S. putrefaciens* CN-32; Kan[r]	this study

pNPTS138-R6KT FlhF K256A (Sputcn32_2561)	plasmid for in frame complementation of *flhF* (*Sputcn32_2561*) with FlhF K256A mutant in *S. putrefaciens* CN-32; Kan[r]	this study
pNPTS138-R6KT FlhF D328A (Sputcn32_2561)	plasmid for in frame complementation of *flhF* (*Sputcn32_2561*) with FlhF D328A mutant in *S. putrefaciens* CN-32; Kan[r]	this study
pNPTS138-R6KT FlhF D390A (Sputcn32_2561)	plasmid for in frame complementation of *flhF* (*Sputcn32_2561*) with FlhF D390A mutant in *S. putrefaciens* CN-32; Kan[r]	this study
pNPTS138-R6KT FlhF-GS-Venus (Sputcn32_2561)	plasmid for in frame complementation of *flhF* (*Sputcn32_2561*) with FlhF-GS-mVenus in *S. putrefaciens* CN-32; Kan[r]	this study
pNPTS138-R6KT FlhF-GS-mVenus arabinose inducible (Sputcn32_2561)	plasmid for insertion of FlhF-GS-mVenus upstream from *Sputcn32_2068* in *S. putrefaciens* CN-32; Kan[r]	this study
pNPTS138-R6KT FlhF K256A-GS-mVenus (Sputcn32_2561)	plasmid for in frame complementation of *flhF* (*Sputcn32_2561*) with FlhF K256A-GS-mVenus mutant in *S. putrefaciens* CN-32; Kan[r]	this study
pNPTS138-R6KT FlhF D328A-GS-mVenus (Sputcn32_2561)	plasmid for in frame complementation of *flhF* (*Sputcn32_2561*) with FlhF D328A-GS-mVenus mutant in *S. putrefaciens* CN-32; Kan[r]	this study
pNPTS138-R6KT FlhF D390A-GS-mVenus (Sputcn32_2561)	plasmid for in frame complementation of *flhF* (*Sputcn32_2561*) with FlhF D390A-GS-mVenus mutant in *S. putrefaciens* CN-32; Kan[r]	this study
pNPTS138-R6KT *fipA* KO (*Sputcn32_2550*)	plasmid for deletion of the *fipA* gene (*Sputcn32_2550*) in *S. putrefaciens* CN-32; Kan[r]	this study
pNPTS138-R6KT *fipA* KI (*Sputcn32_2550*)	plasmid for in frame complementation of *fipA* (*Sputcn32_2550*) with wild type *fipA* in *S. putrefaciens* CN-32; Kan[r]	this study
pNPTS138-R6KT FipA ΔTMD (AS5-23) (Sputcn32_2550)	plasmid for in frame complementation of *fipA* (*Sputcn32_2550*) with FipA ΔTMD mutant in *S. putrefaciens* CN-32; Kan[r]	this study
pNPTS138-R6KT FipA G106A (Sputcn32_2550)	plasmid for in frame complementation of *fipA* (*Sputcn32_2550*) with FipA G106A mutant in *S. putrefaciens* CN-32; Kan[r]	this study
pNPTS138-R6KT FipA L118A (Sputcn32_2550)	plasmid for in frame complementation of *fipA* (*Sputcn32_2550*) with FipA L118A mutant in *S. putrefaciens* CN-32; Kan[r]	this study

pNPTS138-R6KT FipA L125A (Sputcn32_2550)	plasmid for in frame complementation of *fipA* (*Sputcn32_2550*) with FipA L125 mutant in *S. putrefaciens* CN-32; Kan^r	this study
pNPTS138-R6KT FipA-DILEL-sfGFP (Sputcn32_2550)	plasmid for in frame complementation of *fipA* (*Sputcn32_2550*) with FipA-DILEL-sfGFP in *S. putrefaciens* CN-32; Kan^r	this study
pNPTS138-R6KT FipA ΔTMD-DILEL-sfGFP (AS5-23) (Sputcn32_2550)	plasmid for in frame complementation of *fipA* (*Sputcn32_2550*) with FipA ΔTMD-DILEL-sfGFP mutant in *S. putrefaciens* CN-32; Kan^r	this study
pNPTS138-R6KT FipA G106A-DILEL-sfGFP (Sputcn32_2550)	plasmid for in frame complementation of *fipA* (*Sputcn32_2550*) with FipA G106A-DILEL-sfGFP mutant in *S. putrefaciens* CN-32; Kan^r	this study
pNPTS138-R6KT FipA L116A-DILEL-sfGFP (Sputcn32_2550)	plasmid for in frame complementation of *fipA* (*Sputcn32_2550*) with FipA L116A-DILEL-sfGFP mutant in *S. putrefaciens* CN-32; Kan^r	this study
pNPTS138-R6KT FipA L125A-DILEL-sfGFP (Sputcn32_2550)	plasmid for in frame complementation of *fipA* (*Sputcn32_2550*) with FipA L125A mutant in *S. putrefaciens* CN-32; Kan^r	this study
pNPTS138-R6KT FliM₁-GS-sfGFP (Sputcn32_2569)	plasmid for in frame complementation of *fliM₁* (*Sputcn32_2569*) with FliM₁-GS-sfGFP in *S. putrefaciens* CN-32; Kan^r	[1]
pNPTS138-R6KT FlhB Δ358-376⁺ (Sputcn32_2563)	plasmid for in frame complementation of *flhB* (*Sputcn32_2563*) with FlhB Δ358-376⁺ mutant in *S. putrefaciens* CN-32; Kan^r	[1]
pNPTS138-R6KT FlhB N269A (Sputcn32_2563)	plasmid for in frame complementation of *flhB* (*Sputcn32_2563*) with FlhB N269A mutant in *S. putrefaciens* CN-32; Kan^r	[1]
pNPTS138-R6KT FlhB Y376A (Sputcn32_2563)	plasmid for in frame complementation of *flhB* (*Sputcn32_2563*) with FlhB Y376A mutant in *S. putrefaciens* CN-32; Kan^r	[1]
pNPTS138-R6KT FlhB-3xFLAG (Sputcn32_2563)	plasmid for in frame complementation of *flhB* (*Sputcn32_2563*) with FlhB-3xFLAG in *S. putrefaciens* CN-32; Kan^r	[1]
pNPTS138-R6KT FlhB Δ358-376⁺-3xFLAG (Sputcn32_2563)	plasmid for in frame complementation of *flhB* (*Sputcn32_2563*) with FlhB Δ358-376⁺-3xFLAG mutant in *S. putrefaciens* CN-32; Kan^r	[1]
pNPTS138-R6KT FlhB N269A-3xFLAG (Sputcn32_2563)	plasmid for in frame complementation of *flhB* (*Sputcn32_2563*) with FlhB N269A-3xFLAG mutant in *S. putrefaciens* CN-32; Kan^r	[1]

pNPTS138-R6KT FlhB Y376A-3xFLAG (Sputcn32_2563)	plasmid for in frame complementation of *flhB* (*Sputcn32_2563*) with FlhB Y376A-3xFLAG mutant in *S. putrefaciens* CN-32; Kan[r]	[1]

Plasmids for *P. putida* KT2440

pNPTS138-R6KT *flhF* KO (*PP_4343*)	plasmid for deletion of the *flhF* gene (*PP_4343*) in *P. putida* KT2440; Kan[r]	this study
pNPTS138-R6KT FlhF K229A (PP_4343)	plasmid for in frame complementation of *flhF* (*PP_4343*) with FlhF K229A mutant in *P. putida* KT2440; Kan[r]	this study
pNPTS138-R6KT FlhF K235A (PP_4343)	plasmid for in frame complementation of *flhF* (*PP_4343*) with FlhF K235A mutant in *P. putida* KT2440; Kan[r]	this study
pNPTS138-R6KT FlhF D301A (PP_4343)	plasmid for in frame complementation of *flhF* (*PP_4343*) with FlhF D301A mutant in *P. putida* KT2440; Kan[r]	this study
pNPTS138-R6KT FlhF D362A (PP_4343)	plasmid for in frame complementation of *flhF* (*PP_4343*) with FlhF D362A mutant in *P. putida* KT2440; Kan[r]	this study
pNPTS138-R6KT FlhF-GS-mCherry (PP_4343)	plasmid for in frame complementation of *flhF* (*PP_4343*) with FlhF-GS-mCherry in *P. putida* KT2440; Kan[r]	this study
pNPTS138-R6KT FlhF K229A-GS-mCherry (PP_4343)	plasmid for in frame complementation of *flhF* (*PP_4343*) with FlhF K229A-GS-mCherry mutant in *P. putida* KT2440; Kan[r]	this study
pNPTS138-R6KT FlhF K235A-GS-mCherry (PP_4343)	plasmid for in frame complementation of *flhF* (*PP_4343*) with FlhF K235A-GS-mCherry mutant in *P. putida* KT2440; Kan[r]	this study
pNPTS138-R6KT FlhF D301A-GS-mCherry (PP_4343)	plasmid for in frame complementation of *flhF* (*PP_4343*) with FlhF D301A-GS-mCherry mutant in *P. putida* KT2440; Kan[r]	this study
pNPTS138-R6KT FlhF D362A-GS-mCherry (PP_4343)	plasmid for in frame complementation of *flhF* (*PP_4343*) with FlhF D362A-GS-mCherry mutant in *P. putida* KT2440; Kan[r]	this study
pNPTS138-R6KT *fipA* KO (*PP_4331*)	plasmid for deletion of the *fipA* gene (*PP_4331*) in *P. putida* KT2440; Kan[r]	this study
pNPTS138-R6KT *fipA* KI (*PP_4331*)	plasmid for in frame complementation of *fipA* (*PP_4331*) with wild type *fipA* in *P. putida* KT2440; Kan[r]	this study
pNPTS138-R6KT FipA ΔTMD (AS5-22) (PP_4331)	plasmid for in frame complementation of *fipA* (*PP_4331*) with FipA ΔTMD mutant in *P. putida* KT2440; Kan[r]	this study
pNPTS138-R6KT FipA G104A (PP_4331)	plasmid for in frame complementation of *fipA* (*PP_4331*) with FipA G104A mutant in *P. putida* KT2440; Kan[r]	this study
pNPTS138-R6KT FipA L116A (PP_4331)	plasmid for in frame complementation of *fipA* (*PP_4331*) with FipA L116A mutant in *P. putida* KT2440; Kan[r]	this study

pNPTS138-R6KT FipA L123A (PP_4331)	plasmid for in frame complementation of *fipA* (*PP_4331*) with FipA L123A mutant in *P. putida* KT2440; Kan[r]	this study
pNPTS138-R6KT FipA-DILEL-sfGFP (PP_4331)	plasmid for in frame complementation of *fipA* (*PP_4331*) with FipA-DILEL-sfGFP in *P. putida* KT2440; Kan[r]	this study
pNPTS138-R6KT FipA ΔTMD-DILEL-sfGFP (AS5-22) (PP_4331)	plasmid for in frame complementation of *fipA* (*PP_4331*) with FipA ΔTMD-DILEL-sfGFP mutant in *P. putida* KT2440; Kan[r]	this study
pNPTS138-R6KT FipA G104A-DILEL-sfGFP (PP_4331)	plasmid for in frame complementation of *fipA* (*PP_4331*) with FipA G104A-DILEL-sfGFP mutant in *P. putida* KT2440; Kan[r]	this study
pNPTS138-R6KT FipA L116A-DILEL-sfGFP (PP_4331)	plasmid for in frame complementation of *fipA* (*PP_4331*) with FipA L116A-DILEL-sfGFP mutant in *P. putida* KT2440; Kan[r]	this study
pNPTS138-R6KT FipA L123A-DILEL-sfGFP (PP_4331)	plasmid for in frame complementation of *fipA* (*PP_4331*) with FipA L123A-DILEL-sfGFP mutant in *P. putida* KT2440; Kan[r]	this study

S. putrefaciens CN-32
BACTH plasmids

pKT25 FlhF (Sputcn32_2561)	plasmid for BACTH assay carrying T25-FlhF (Sputcn32_2561); Kan[r]	this study
pKNT25 FlhF (Sputcn32_2561)	plasmid for BACTH assay carrying FlhF-T25 (Sputcn32_2561); Kan[r]	this study
pUT18 FlhF (Sputcn32_2561)	plasmid for BACTH assay carrying FlhF-T18 (Sputcn32_2561); Amp[r]	this study
pUT18C FlhF (Sputcn32_2561)	plasmid for BACTH assay carrying T18-FlhF (Sputcn32_2561); Amp[r]	this study
pKT25 FlhF K256A (Sputcn32_2561)	plasmid for BACTH assay carrying T25-FlhF K256A (Sputcn32_2561); Kan[r]	this study
pKNT25 FlhF K256A (Sputcn32_2561)	plasmid for BACTH assay carrying FlhF K256A -T25 (Sputcn32_2561); Kan[r]	this study
pUT18 FlhF K256A (Sputcn32_2561)	plasmid for BACTH assay carrying FlhF K256A -T18 (Sputcn32_2561); Amp[r]	this study
pUT18C FlhF K256A (Sputcn32_2561)	plasmid for BACTH assay carrying T18-FlhF K256A (Sputcn32_2561); Amp[r]	this study
pKT25 FlhF D328A (Sputcn32_2561)	plasmid for BACTH assay carrying T25-FlhF D328A (Sputcn32_2561); Kan[r]	this study
pKNT25 FlhF D328A (Sputcn32_2561)	plasmid for BACTH assay carrying FlhF D328A -T25 (Sputcn32_2561); Kan[r]	this study

pUT18 FlhF D328A (Sputcn32_2561)	plasmid for BACTH assay carrying FlhF D328A -T18 (Sputcn32_2561); Amp^r	this study
pUT18C FlhF D328A (Sputcn32_2561)	plasmid for BACTH assay carrying T18-FlhF D328A (Sputcn32_2561); Amp^r	this study
pKT25 FlhF D390A (Sputcn32_2561)	plasmid for BACTH assay carrying T25-FlhF D390A (Sputcn32_2561); Kan^r	this study
pKNT25 FlhF D390A (Sputcn32_2561)	plasmid for BACTH assay carrying FlhF D390A -T25 (Sputcn32_2561); Kan^r	this study
pUT18 FlhF D390A (Sputcn32_2561)	plasmid for BACTH assay carrying FlhF D390A -T18 (Sputcn32_2561); Amp^r	this study
pUT18C FlhF D390A (Sputcn32_2561)	plasmid for BACTH assay carrying T18-FlhF D390A (Sputcn32_2561); Amp^r	this study
pKT25 FipA (Sputcn32_2550)	plasmid for BACTH assay carrying T25-FipA (Sputcn32_2550); Kan^r	this study
pKNT25 FipA (Sputcn32_2550)	plasmid for BACTH assay carrying FipA-T25 (Sputcn32_2550); Kan^r	this study
pUT18 FipA (Sputcn32_2550)	plasmid for BACTH assay carrying FipA-T18 (Sputcn32_2550); Amp^r	this study
pUT18C FipA (Sputcn32_2550)	plasmid for BACTH assay carrying T18-FipA (Sputcn32_2550); Amp^r	this study
pKT25 FipA G106A (Sputcn32_2550)	plasmid for BACTH assay carrying T25-FipA G106A (Sputcn32_2550); Kan^r	this study
pKNT25 FipA G106A (Sputcn32_2550)	plasmid for BACTH assay carrying FipA G106A -T25 (Sputcn32_2550); Kan^r	this study
pUT18 FipA G106A (Sputcn32_2550)	plasmid for BACTH assay carrying FipA G106A -T18 (Sputcn32_2550); Amp^r	this study
pUT18C FipA G106A (Sputcn32_2550)	plasmid for BACTH assay carrying T18-FipA G106A (Sputcn32_2550); Amp^r	this study
pKT25 FipA L116A (Sputcn32_2550)	plasmid for BACTH assay carrying T25-FipA L116A (Sputcn32_2550); Kan^r	this study
pKNT25 FipA L116A (Sputcn32_2550)	plasmid for BACTH assay carrying FipA L116A -T25 (Sputcn32_2550); Kan^r	this study
pUT18 FipA L116A (Sputcn32_2550)	plasmid for BACTH assay carrying FipA L116A -T18 (Sputcn32_2550); Amp^r	this study
pUT18C FipA L116A (Sputcn32_2550)	plasmid for BACTH assay carrying T18-FipA L116A (Sputcn32_2550); Amp^r	this study
pKT25 FipA L125A (Sputcn32_2550)	plasmid for BACTH assay carrying T25-FipA L125A (Sputcn32_2550); Kan^r	this study

pKNT25 FipA L125A (Sputcn32_2550)	plasmid for BACTH assay carrying FipA L125A -T25 (Sputcn32_2550); Kanr	this study
pUT18 FipA L125A (Sputcn32_2550)	plasmid for BACTH assay carrying FipA L125A -T18 (Sputcn32_2550); Ampr	this study
pUT18C FipA L125A (Sputcn32_2550)	plasmid for BACTH assay carrying T18-FipA L125A (Sputcn32_2550); Ampr	this study

P. putida KT2440
BACTH plasmids

pKT25 FlhF (PP_4343)	plasmid for BACTH assay carrying T25-FlhF (PP_4343); Kanr	this study
pKNT25 FlhF (PP_4343)	plasmid for BACTH assay carrying FlhF-T25 (PP_4343); Kanr	this study
pUT18 FlhF (PP_4343)	plasmid for BACTH assay carrying FlhF-T18 (PP_4343); Ampr	this study
pUT18C FlhF (PP_4343)	plasmid for BACTH assay carrying T18-FlhF (PP_4343); Ampr	this study
pKT25 FlhF K229A (PP_4343)	plasmid for BACTH assay carrying T25-FlhF K229A (PP_4343); Kanr	this study
pKNT25 FlhF K229A (PP_4343)	plasmid for BACTH assay carrying FlhF K229A -T25 (PP_4343); Kanr	this study
pUT18 FlhF K229A (PP_4343)	plasmid for BACTH assay carrying FlhF K229A -T18 (PP_4343); Ampr	this study
pUT18C FlhF K229A (PP_4343)	plasmid for BACTH assay carrying T18-FlhF K229A (PP_4343); Ampr	this study
pKT25 FlhF K235A (PP_4343)	plasmid for BACTH assay carrying T25-FlhF K235A (PP_4343); Kanr	this study
pKNT25 FlhF K235A (PP_4343)	plasmid for BACTH assay carrying FlhF K235A -T25 (PP_4343); Kanr	this study
pUT18 FlhF K235A (PP_4343)	plasmid for BACTH assay carrying FlhF K235A -T18 (PP_4343); Ampr	this study
pUT18C FlhF K235A (PP_4343)	plasmid for BACTH assay carrying T18-FlhF K235A (PP_4343); Ampr	this study
pKT25 FlhF D301A (PP_4343)	plasmid for BACTH assay carrying T25-FlhF D301A (PP_4343); Kanr	this study
pKNT25 FlhF D301A (PP_4343)	plasmid for BACTH assay carrying FlhF D301A -T25 (PP_4343); Kanr	this study
pUT18 FlhF D301A (PP_4343)	plasmid for BACTH assay carrying FlhF D301A -T18 (PP_4343); Ampr	this study

pUT18C FlhF D301A (PP_4343)	plasmid for BACTH assay carrying T18-FlhF D301A (PP_4343); Amp^r	this study
pKT25 FlhF D362A (PP_4343)	plasmid for BACTH assay carrying T25-FlhF D362A (PP_4343); Kan^r	this study
pKNT25 FlhF D362A (PP_4343)	plasmid for BACTH assay carrying FlhF D362A -T25 (PP_4343); Kan^r	this study
pUT18 FlhF D362A (PP_4343)	plasmid for BACTH assay carrying FlhF D362A -T18 (PP_4343); Amp^r	this study
pUT18C FlhF D362A (PP_4343)	plasmid for BACTH assay carrying T18-FlhF D362A (PP_4343); Amp^r	this study
pKT25 FipA (PP_4331)	plasmid for BACTH assay carrying T25-FipA (PP_4331); Kan^r	this study
pKNT25 FipA (PP_4331)	plasmid for BACTH assay carrying FipA-T25 (PP_4331); Kan^r	this study
pUT18 FipA (PP_4331)	plasmid for BACTH assay carrying FipA-T18 (PP_4331); Amp^r	this study
pUT18C FipA (PP_4331)	plasmid for BACTH assay carrying T18-FipA (PP_4331); Amp^r	this study
pKT25 FipA G104A (PP_4331)	plasmid for BACTH assay carrying T25-FipA G104A (PP_4331); Kan^r	this study
pKNT25 FipA G104A (PP_4331)	plasmid for BACTH assay carrying FipA G104A -T25 (PP_4331); Kan^r	this study
pUT18 FipA G104A (PP_4331)	plasmid for BACTH assay carrying FipA G104A -T18 (PP_4331); Amp^r	this study
pUT18C FipA G104A (PP_4331)	plasmid for BACTH assay carrying T18-FipA G104A (PP_4331); Amp^r	this study
pKT25 FipA L116A (PP_4331)	plasmid for BACTH assay carrying T25-FipA L116A (PP_4331); Kan^r	this study
pKNT25 FipA L116A (PP_4331)	plasmid for BACTH assay carrying FipA L116A -T25 (PP_4331); Kan^r	this study
pUT18 FipA L116A (PP_4331)	plasmid for BACTH assay carrying FipA L116A -T18 (PP_4331); Amp^r	this study
pUT18C FipA L116A (PP_4331)	plasmid for BACTH assay carrying T18-FipA L116A (PP_4331); Amp^r	this study
pKT25 FipA L125A (PP_4331)	plasmid for BACTH assay carrying T25-FipA L123A (PP_4331); Kan^r	this study
pKNT25 FipA L125A (PP_4331)	plasmid for BACTH assay carrying FipA L123A -T25 (PP_4331); Kan^r	this study

pUT18 FipA L125A (PP_4331)	plasmid for BACTH assay carrying FipA L123A -T18 (PP_4331); Amp^r	this study
pUT18C FipA L125A (PP_4331)	plasmid for BACTH assay carrying T18-FipA L123A (PP_4331); Amp^r	this study

Table 5-3 Primers used in this study.

Identifier	Name	Sequence (5'→3')	Purpose
	M13	TGT AAA ACG ACG GCC AGT CC	CP/SP
	M13r	CAC ACA GGA AAC AGC TAT GAC C	CP/SP
JH3	**fliE1-fliF1 fwd**	TTT GAA GCG ACG GTA CAA GTG C	CP
JH8	**fliG1-fliH1 rev**	TTT CAG CCA TTG TTG GAG GTG C	CP
JH11	**flil1-fliJ1 fw**	GCG ATG AAT GCC TTC TTA AGG C	CP
JH27	**fliQ1-fliR1 fw**	GCA GTG TTT CAA GCT GCC ACT T	CP
JH36	**flhF1-flhG1 fwd**	GCG CTG AGT GTG TTG ATC CAA A	CP
JH37	**flhG1-fliA1 rev**	CAA CGG AGC ATA CTG TTC AAC G	CP
JH77	**EcoRV-flhB KO-fwd**	GCC AAG CTT CTC TGC AGG AT GCG ATG GGG TTT GTT TCC CAG A	KO
JH78	**OL-flhB KO-rev**	TTT AAT GGG CTG CTC TCT TCA GCC ATA CTG AG	KO
JH79	**OL-flhB KO-fwd**	AGA GAG CAG CCC ATT AAA TCA GCC TAT CCC TGA TGA TTT AAA ATA TTA ATG	KO
JH80	**EcoRV-flhB KO-rev**	GCG AAT CGT GGA TCC AGA T TCC ATC GCA CCA TAG AAA TCT GC	KO
JH81	**Check-flhB KO-rev**	GCA AAT CCA GGG CTA TTG CTG	CP
JH84	**EcoRV-fliK KO-fwd**	GCC AAG CTT CTC TGC AGG AT GAT GGC GAA TGC AGA TCC CTT A	KO
JH85	**OL-fliK KO-rev**	ACC AGA ATG CAT TTG TTG CAT ATC AGC TCC AAC C	KO
JH86	**OL-fliK KO-fwd**	CAA CAA ATG CAT TCT GGT ATA GAT TAT TAC GCT TAA GC	KO
JH87	**EcoRV-fliK KO-rev**	GCG AAT CGT GGA TCC AGA T CCT TAA CCT CTT TAA GGT ACT GAA ATT ACG	KO
JH88	**Check-fliK KO-rev**	TCA AGA TCA TCA TCG TCA TCG ACG	CP
JH98	**EcoRV FliM1 N-term fwd**	GCG AAT CGT GGA TCC AGA T GCT CAT TGA AGA TGC TCT CCT G	KI

JH101	EcoRV FliM1 N-term rev	GCC AAG CTT CTC TGC AGG AT AAT AAA ACT GCG GCC CAC TTC C	KI
JH102	Check-GFP FliM1-fwd	GCA GTT CAG ATG AGT CAT CCT C	CP
JH103	Check-GFP FliM1 KO-rev	GAC ATT TTG GCA GTT GAT GCG AC	CP
JH104	OL FliM1 GFP rev	GAA AAG TTC TTC TCC TTT GCT GCT GCC TAA TTC AGA TAT ATC TCT AGC TTT GCC TTT GC	KI
JH105	OL FliM1 GFP fwd	GGA TGA GCT CTA CAA AGG ATC C TAA GGT GAA GCA AGA TGA GCA CAG AAG ATA	KI
JH148	EcoRV FlhF C-term fwd	GCG AAT TCG TGG ATC CAG AT GCA AGA AAT GGT TGG ACA GCC T	KI
JH151	EcoRV FlhF C-term rev	GCC AAG CTT CTC TGC AGG AT GCC ACA TCT AAA AAT CGG TCG G	KI
JH152	Check-FlhF-FLAG-fwd	GCA TCA GTC AAT GCA AGC AAC C	CP
JH166	EcoRV-2069_GFP-fwd	GCG AAT TCG TGG ATC CAG AT CCG TTT AGC CGT AGA ACA TGA T	KI
JH171	EcoRV-2068-rev	GCC AAG CTT CTC TGC AGG AT GCC GCT TGT CTT ACT TCG GTA T	KI
JH172	Check-ParB-fwd	GCC AAC CTT TGC TTG GTA TCT C	CP
JH173	Check-ParB-rev	GCG GTA ATT GCT GTG CCT CT A	CP
JH199	OL-FlhF-Venus rev	CAC GCT GCC CTC AAA TGC ACA GGC CAT ATT ATC TG	KI
JH200	OL_Venus fwd	GCA TTT GAG GGC AGC GTG AGC AAG GGC GAG GAG CTG TT	KI
JH201	OL_Venus rev	GTC ATA ACT TTA CTT GTA CAG CTC GTC CAT GCC	KI
JH202	OL-FlhF-Venus fwd	TAC AAG TAA AGT TAT GAC CCT GGA TCA AGC AAG	KI
JH211	FlhF-Ven Seq_Primer	GCT GAG TTA GTA CGA GCA CTA C	SP
JH212	FlhG-Ven Seq_Primer	CGA TAT TAT TGT CCG TGG GCC T	SP
JH218	FlhF-Ven Seq_Primer fwd	GCT GTT GTA GTT GTA CTC CAG C	SP

JH151	EcoRV FlhF C-term rev	GCC AAG CTT CTC TGC AGG AT GCC ACA TCT AAA AAT CGG TCG G	KI
JH252	EcoRV-2550-GFP-fwd	GCG AAT TCG TGG ATC CAG AT GCC ATC AAT AAC GGA AAA GGG G	KI/ CP
JH253	OL-2550-GFP-rev	GAA AAG TTC TTC TCC TTT GCT CAG TTC CAG AAT ATC TTT ACG ATG TAA CCG GAT CAA TAA TTC AGC	KI/CP
JH254	OL-2550-GFP-fwd	GGA TGA GCT CTA CAA AGG ATC C TAA CGA AGT GTA GGG GCT AAG ACG	KI
JH255	EcoRV-2550-GFP-rev	GCC AAG CTT CTC TGC AGG AT GCC TTT GTT TAT ATG CTC GAC GG	KI
JH256	Check-2550-GFP-fwd	CGA TGA AGA ATG GGC TGA ACT C	KI/CP
JH257	Check-2550-GFP-rev	CGA AGG ATG CGA GAA TGA CGA A	KI/CP
JH294	OL-2069_FlhF-rev	AAT CTT CAC TAG CAT CCC CGT ACA TTG AAC TC	KI
JH295	OL-FlhF-Ven-fwd	GGG ATG CTA GTG AAG ATT AAA CGA TTT TTT GCC AAA GAC	KI
JH296	OL-FlhF-Ven-rev	AAC ATT AGC TTA CTT GTA CAG CTC GTC CAT GC	KI
JH297	OL-2068-fwd	TAC AAG TAA GCT AAT GTT TTA GGG TCT TAC GCG	KI
JH298	FlhF-Ven Ara ind Seq fwd	GCA CAG GCC ATA TTA TCT GAC C	SP
JH299	FlhF-Ven Ara ind Seq rev	GCA TTG GCG CCT ATG AGC AAT T	SP
JH320	BACTH 2550 pkT25 fwd	CA GGG TCG ACT CTA GAG GGC GAT GAA TTT TTG ATC GCG G	BACTH
JH321	BACTH 2550 pkT25 rev	TTA GTT ACT TAG GTA CCC GGG G TTT ACG ATG TAA CCG GAT CAA TAA TTC AGC	BACTH
JH322	BACTH 2550 fwd	C TGC AGG TCG ACT CTA GAG GGC GAT GAA TTT TTG ATC GCG G	BACTH
JH323	BACTH 2550 rev	GA GCT CGG TAC CCG GGG TTT ACG ATG TAA CCG GAT CAA TAA TTC AGC	BACTH
JH324	EcoRV-flrA1_KO_fwd	GCC AAG CTT CTC TGC AGG AT AGT AAT AGT TTG AAC ATG GAT GAA GG	KO
JH325	EcoRV-flrA1_KO_rev	GCG AAT TCG TGG ATC CAG AT CAG ATA ACC GCT GCA GAT GTG	KO

JH331	OL_FliM1 mCh rev	TTT GTA TAA CTC ATC CAT ACC A	KI
JH339	EcoRV-PolClusTotAdj fwd	GCG AAT TCG TGG ATC CAG AT GCT ACT TGG CTC TTC TAA GTT C	KO
JH340	OL-PolClusTotAdj rev	AGC ATA TGC CGA CTC CAT GGG ATG ACC TTA A	KO
JH341	OL-PolClusTotAdj fwd	ATG GAG TCG GCA TAT GCT AAT GTT CCA TGA ACA C	KO
JH342	EcoRV-PolClusTotAdj rev	GCC AAG CTT CTC TGC AGG AT GCC ATT GGG TCT GAA AAT TGC T	KO
JH343	PolClusTotAdj Check fwd	CGG CCA CAT CAA AAA CGC CTA A	CP
JH344	PolClusTotAdj Check rev	GCA AGA CTT GCA CTA TAG CCG T	CP
JH345	ClusterII KO Check fwd	GCC GAG TAC GAC ACC ATT AAA G	CP
JH346	ClusterII KO Check rev	GCC AGA GGA CAT TTG TCT CCT A	CP
JH349	OL-FlhF_D390A rev	GAC TGA TTC GGC GAG TTT TGT GAG CAC G	KI
JH350	OL-FlhF_D390A fwd	ACA AAA CTC GCC GAA TCA GTC TCC CTC G	KI
JH367	FlhF-Ven Seq_Primer rev	GCT GGA GTA CAA CTA CAA CAG C	SP
JH425	OL-GFP-fwd	AGC AAA GGA GAA GAA CTT TTC	KI
JH426	OL-GFP-rev	GGA TCC TTT GTA GAG CTC ATC C	KI
JH427	OL -mCherry fwd	GTT TCC AAA GGG GAA GAG GAC A	KI
JH460	pKT25-for	CAC TGA CGG CGG ATA TCG ACA TGT T	CP/SP
JH461	pKT25-rev	CCG CCG GAC ATC AGC GCC ATT C	CP/SP
JH462	pUT18-for	CCA GGC TTT ACA CTT TAT GCT TCC	CP/SP
JH463	pUT18-rev	GAC GCG CCT CGG TGC CCA CTG C	CP/SP
JH464	pKNT25-for	CCC AGG CTT TAC ACT TTA TGC TTC C	CP/SP
JH465	pKNT25-rev	GTT TTT TCT TCG CAC GGC CTT G	CP/SP
JH466	pUT18C-for	CGG CGT GCC GAG CGG ACG TTC G	CP/SP
JH467	pUT18C-rev	TCA GCG GGT GTT GGC GGG TGT C	CP/SP

JH501	FlhF Seq_Primer fwd	GCC CAC TTT GGA TCA ACA CAC T	SP
JH502	FlhF Seq_Primer rev	CGT GCT CAC AAA ACT CGA TGA A	SP
JH503	EcoRV FliFG1 KO fwd	GCG AAT TCG TGG ATC CAG AT GCC GAA AAC TTG TGG CTG AAA A	KO
JH504	OL- FliFG1 KO rev	ATC GCC ACC CCC GAC AAT CAT TTC TGT GCT C	KO
JH505	OL- FliFG1 KO fwd	ATT GTC GGG GGT GGC GAT GAG TTC CTC TAA T	KO
JH506	EcoRV FliFG1 KO rev	GCC AAG CTT CTC TGC AGG AT GCA ACC TAA TAG TCA CTG CTT G	KO
JH521	EcoRV-ybcG KO-fwd	GCG AAT TCG TGG ATC CAG AT GCA GTA ACG GTG GCC TAT TGA T	KO
JH522	OL-ybcG KO-rev	TGC ACT GTC CCA ATG AAA CGT CAT TTA ATG AAA GCA AG	KO
JH523	OL-ybcG KO-fwd	TTT CAT TGG GAC AGT GCA AGC TGA TAT GTC G	KO
JH524	EcoRV-ybcG KO-rev	GCC AAG CTT CTC TGC AGG AT GCT GGA ATT GCC GCA AAT AGA C	KO
JH525	Check-ybcG KO-fwd	GCT TCC TGT GGC AAA GTT TTG G	CP
JH526	Check-ybcG KO-rev	GCT TGG CGA TGC AAA ATA CTG G	CP
JH550	OL-fipA L118A rev	AGC TTC AGC TTT GGG CGC TTC ACA	KI
JH551	OL-fipA L118A fwd	ATA AAA GAG TGT GAA GCG CCC AAA	KI
JH552	OL-fipA G106A rev	TTC ATC GAC TCC CGC GGC AAG TCC	KI
JH553	OL-fipA G106A fwd	AAA ATG GTC GGA CTT GCC GCG GGA	KI
JH559	Check-flrA1-KO-rev_new	CCG GAG TTA AAG GAG TAA TGG C	CP
JH560	OL_flrA1_new_rev	AAG ACT ATT C AT CTG TTT GCA TCA TTC AGT AGG C	KO
JH561	OL_flrA1_new_fwd	GCA AAC AGA T GA ATA GTC TTT TGC ATT TTT AGT TAT ATT ATT G	KO
JH566	OL-PPfipA G104A rev	CAT CGA TAC TCG CAG CCA TCC C	KI

JH567	OL-PPfipA G104A fwd	GCT GGT GGG GAT GGC TGC GAG T	KI
JH568	OL-PPfipA L123A rev	ACA CCT TGC TCA TCG CCT CCG C	KI
JH569	OL-PPfipA L123A fwd	GGC CGA GGC GGA GGC GAT GAG C	KI
JH576	EcoRV-flhF KO-fwd	GCC AAG CTT CTC TGC AGG AT GCA TAG GCG TCG GTG ATT GAG G	KO
JH577	OL-flhF KO-rev	TAA GTG AAG GCA TTT GAG TAG AGT TAT GAC CCT GG	KO
JH578	OL-flhF KO-fwd	CTC AAA TGC CTT CAC TTA TGC GTC CTC TAC TGG	KO
JH579	EcoRV-flhF KO-rev	GCG AAT TCG TGG ATC CAG ATG CTA AGC ATT CTC CTA AGC TTG TTG	KO
JH587	OL-fipA L125A rev	TAA CCG GAT CAA GGC TTC AGC TTC	KI
JH588	OL-fipA L125A fwd	GCT GAA GCT GAA GCC TTG ATC CGG	KI
JH598	EcoRV FlhF sub rev	GCC AAG CTT CTC TGC AGG AT GCT CGT CAC ATA CAA CGA CTA G	KI
JH608	BACTH 2550 L125A pkT25 rev	TTA GTT ACT TAG GTA CCC GGG G TTT ACG ATG TAA CCG GAT CAA GGC TTC AGC	BACTH
JH609	BACTH 2550 L125A rev	GA GCT CGG TAC CCG GGG TTT ACG ATG TAA CCG GAT CAA GGC TTC AGC	BACTH
JH634	OL-FipA L125A-GFP-rev	GAA AAG TTC TTC TCC TTT GCT CAG TTC CAG AAT ATC TTT ACG ATG TAA CCG GAT CAA GGC TTC AGC	KI
JH635	EcoRV FlhB C-term fwd	GCG AAT TCG TGG ATC CAG AT GAT TGT GGT CAT TGA TGT GCC A	KI
JH636	OL FlhB Y376A FLAG rev	AAT ATC ATG ATC TTT ATA ATC GCC ATC ATG ATC TTT ATA ATC CGC TTT TAA ATC ATC AGG GAT AGG C	KI
JH637	OL FlhB FLAG fwd	ATT ATA AAG ATC ATG ATA TTG ATT ATA AAG ATG ATG ATG ATA AA TAA TGG CTT GCT CGT TCA CTC TT	KI
JH638	EcoRV FlhB C-term rev	GCC AAG CTT CTC TGC AGG AT GGA TGA TAA ATA CCA CTA AAC CCA C	KI
JH639	Check FlhB C-term fwd	CAC CAT GCG TTA GAT CTG TTG A	CP

JH640	Check FlhB C-term rev	ACT CAC CTC TGC AAT ACG ACC A	CP
JH641	OL FlhB Δ358-376-FLAG rev	AAT ATC ATG ATC TTT ATA ATC GCC ATC ATG ATC TTT ATA ATC CCG TCC CTT TTG GTA TTG ACG CAA	KI
JH642	EcoRV-FlhB N269A-fwd	GCG AAT TCG TGG ATC CAG AT GCG ATG GGG TTT GTT TCC CAG A	KI
JH643	OL FlhB N269A rev	ATA ATG CTC AGG GGC GAC GAC AAT C	KI
JH644	OL FlhB N269A fwd	GTG ATT GTC GTC GCC CCT GAG CAT	KI
JH645	EcoRV-FlhB N269A-rev	GCC AAG CTT CTC TGC AGG AT TCC ATC GCA CCA TAG AAA TCT GC	KI
JH646	Check FlhB N269A fwd	GCC ATG GCG ATT ACC TTT GCA A	CP
JH647	OL FlhB Y376A rev	ACG AGC AAG CCA TTA CGC TTT TAA ATC ATC	KI
JH648	OL FlhB Y376A fwd	CCT GAT GAT TTA AAA GCG TAA TGG CTT GCT	KI
JH649	EcoRV-FlhB dPRR-FLAG-fwd	GCG AAT TCG TGG ATC CAG AT GCG ATG GGG TTT GTT TCC CAG A	KI
JH655	EcoRV FlhB C-term fwd	GCG AAT TCG TGG ATC CAG AT GAT TGT GGT CAT TGA TGT GCC A	KI
JH656	OL FlhB FLAG rev	AAT ATC ATG ATC TTT ATA ATC GCC ATC ATG ATC TTT ATA ATC ATA TTT TAA ATC ATC AGG GAT AGG C	KI
JH657	OL FlhB FLAG fwd	ATT ATA AAG ATC ATG ATA TTG ATT ATA AAG ATG ATG ATG ATA AA TAA TGG CTT GCT CGT TCA CTC TT	KI
JH658	Check FlhB C-term fwd	CAC CAT GCG TTA GAT CTG TTG A	CP
JH659	Check FlhB C-term rev	ACT CAC CTC TGC AAT ACG ACC A	CP
JH687	BACTH FlhF pkT25 fwd	CA GGG TCG ACT CTA GAG AAG ATT AAA CGA TTT TTT GCC AAA GAC A	BACTH
JH688	BACTH FlhF pkT25 rev	TTA GTT ACT TAG GTA CCC GGG G CTC AAA TGC ACA GGC CAT ATT ATC T	BACTH
JH689	BACTH FlhF fwd	C TGC AGG TCG ACT CTA GAG AAG ATT AAA CGA TTT TTT GCC AAA GAC A	BACTH

JH690	**BACTH FlhF rev**	GA GCT CGG TAC CCG GGG CTC AAA TGC ACA GGC CAT ATT ATC T	BACTH
JH691	**BACTH FlhF GTG fwd**	C TGC AGG TCG ACT CTA GAG GTG AAG ATT AAA CGA TTT TTT GCC AAA G	BACTH
JH758	**EcoRV_FipA KO fwd**	GCG AAT TCG TGG ATC CAG AT TTT TAG GTA TCA TTA ACT TAC GTG GTA ATG T	KO
JH759	**OL-FipA KO rev**	ACA CTT CGC TAT TTA CGA TG ATC GCC CAT TAA AAA TCC TTA TGC A	KO
JH760	**OL-FipA KO fwd**	AAG GAT TTT TAA TGG GCG AT CAT CGT AAA TAG CGA AGT GTA GGG	KO
JH761	**EcoRV-FipA KO rev**	GCC AAG CTT CTC TGC AGG AT GAA CTG ATC GCC TTT GTT TAT ATG C	KO
JH762	**Check-FipA KO fwd**	AAG AAA TGT CGC AGC CGT AGC	CP
JH763	**Check-FipA KO rev**	CCA GTT GCG ACA ATC TTC GGA G	CP
JH768	**OL-PPfipA L116A rev**	CAT CAA CTC CGC CTC GGC CTG GGT CGC GCC GCA GCT CTG GGT	KI
JH769	**OL-PPfipA L1164A fwd**	GAG TTG A CCC AGA GCT GCG GCG CGA CCC AGG CC GAG GCG	KI
JH770	**Check-PP_4331 (FipA) fwd**	GCT TAC GAA CAG AAC GCA AGG C	CP
JH771	**Check-PP_4331 (FipA) rev**	GCA ATA CGT GAT TTC GGT GCA G	CP
JH796	**EcoRV-PP_4331 KO-fwd**	GCG AAT TCG TGG ATC CAG AT GCA GAT GCA CGC CAA ACA GAA A	KO
JH797	**PP_4331 KO-OL-rev**	TCA AGG AGC TAG GAT CAA CTC AGA TGT TCT CCA GC	KO
JH798	**PP_4331KO-OL-fwd**	TTG ATC CTA GCT CCT TGA CGG GGT ACC CTC G	KO
JH799	**EcoRV-PP_4331 KO-rev**	GCC AAG CTT CTC TGC AGG AT GCA TGA ATT GCC TGT ACA ACA CCA	KO
JH800	**Check-PP_4331KO-fwd**	GCG AAA CGA TCG ATC AGG TCG A	CP
JH801	**Check-PP_4331KO-rev**	GCA CCG TAA TCG AAC ACA TGT G	CP
JH802	**EcoRV-PP_4331-GFP-fwd**	GCG AAT TCG TGG ATC CAG AT GCA GAT GCA CGC CAA ACA GAA A	KI

JH803	PP_4331-GFP-OL-rev	GAA AAG TTC TTC TCC TTT GCT CAG TTC CAG AAT ATC AGG AGC CCG GTA CAC CTT GCT C	KI
JH804	PP_43310-GFP-OL-fwd	GGA TGA GCT CTA CAA AGG ATC C TGA CGG GGT ACC CTC GGC AGC A	KI
JH805	EcoRV-PP_4331-GFP-rev	GCC AAG CTT CTC TGC AGG AT GCA TGA ATT GCC TGT ACA ACA CCA	KI
JH806	EcoRV-FlhF-mCh-fwd	GCG AAT TCG TGG ATC CAG AT GCA TGG ACA GCT TCC GTA TCG G	KI
JH807	FlhF-mCh-OL-rev	CTC TTC CCC TTT GGA AAC GCT GCC ACC CGC TCG CCG TGG GTT GTG A	KI
JH808	FlhF-mCh-OL-fwd	ATG GAT GAG TTA TAC AAA TGA CCA TGA AGC GTG TGC AAA G	KI
JH809	EcoRV-FlhF-mCh-rev	GCC AAG CTT CTC TGC AGG AT GCC AAC ACA CGG AAA CGG TTC A	KI
JH810	Check-PP_4343 KO-fwd	GCC TGA AAT CGA GCC GAT CGA A	CP
JH811	Check-PP_4343 KO-rev	GCG TCG GTA ATC GAG GTA GGT T	CP
JH812	BACTH PP FipA pkT25 fwd	CA GGG TCG ACT CTA GAG ATC CTA GAG GTT GCT GTC ATC T	BACTH
JH813	BACTH PP FipA pkT25 rev	TTA GTT ACT TAG GTA CCC GGG G AGG AGC CCG GTA CAC CTT GCT C	BACTH
JH814	BACTH PP FipA fwd	C TGC AGG TCG ACT CTA GAG ATC CTA GAG GTT GCT GTC ATC T	BACTH
JH815	BACTH PP FipA rev	GA GCT CGG TAC CGG GGA GGA GCC CGG TAC ACC TTG CTC	BACTH
JH816	BACTH PP FlhF pkT25 fwd	CA GGG TCG ACT CTA GAG CAA GTT AAG CGA TTT TTC GCC GC	BACTH
JH817	BACTH PP FlhF pkT25 rev	TTA GTT ACT TAG GTA CCC GGG G ACC CGC TCG CCG TGG GTT GTG A	BACTH
JH818	BACTH PP FlhF fwd	C TGC AGG TCG ACT CTA GAG CAA GTT AAG CGA TTT TTC GCC GC	BACTH
JH819	BACTH PP FlhF rev	GA GCT CGG TAC CGG GGA CCG CTC GCC GTG GGT TGT GA	BACTH
JH820	EcoRV FlhF sub fwd	GCG AAT TCG TGG ATC CAG AT GCA TCA GTC AAT GCA AGC AAC C	KI
JH821	OL-FlhF K256A rev	AGC TAA TGA GGT CGT GGC ACC CAC GCC	KI

JH822	OL-FlhF K256A fwd	CCT ACT GGC GTG GGT GCC ACG ACC TCA	KI
JH823	Check-FlhF KI/O-fwd	GCC ACT GGG TAG TGT CGT AAA A	CP
JH824	OL-FlhF D328A rev	CCC CAT ACC AGC GGT GGC TAT CAA TAC	KI
JH825	OL-FlhF D328A fwd	AAG CTA GTA TTG ATA GCC ACC GCT GGT	KI
JH826	EcoRV PPFlhF sub fwd	GCG AAT TCG TGG ATC AGA T GCA TGT TCT GGC GTA TCA GGA A	KI
JH827	OL-FlhF K235A rev	GCG CGC GGC CAG CGC GGC CAG GGT	KI
JH828	OL-FlhF K235A fwd	GGC AAG ACC ACC ACC CTG GCC GCG CTG GCC GCG	KI
JH829	EcoRV PPFlhF sub rev	GCC AAG CTT CTC TGC AGG AT GCA TGC TAC CCA TGT CTG TTC T	KI
JH830	Check-PP_4343 KI-fwd	GCT ACC AGT GAT TAC CCT GGA G	CP
JH831	OL-FlhF D301A rev	TTG CAG GCC GGC AGT TGC GAT CAG CAC	KI
JH832	OL-FlhF D301A fwd	CGC GTG GTG CTG ATC GCA ACT GCC GGC	KI
JH833	OL-FlhF D362A rev	AAG GCT TGC CGT TTC TGC GAG TTT GGT	KI
JH834	OL-FlhF D362A fwd	ATC CTG ACC AAA CTC GCA GAA ACG GCA	KI
JH835	EcoRV PPFlhF sub 1 rev	GCC AAG CTT CTC TGC AGG AT GCG TCG GTA ATC GAG GTA GGT T	KI
JH838	KT2440 FlhF Seq primer rev	GCT GGT GAG CAT GGA CAG CTT C	SP
JH839	EcoRV-FipA dTM fwd	GCG AAT TCG TGG ATC AGA T GCC GTA GCT GCA AGT AAA GAT G	KI
JH840	OL-FipA dTM rev	CTG CTT TTG TTC ATC GCC CAT TAA AAA TCC TTA TGC	KI
JH841	OL-FipA dTM fwd	GGC GAT GAA CAA AAG CAG TTG AGT AAA TTA CGT AAT AAA GTT G	KI
JH842	OL-PP_FipA dTM rev	GCT GTA GTT CTC TAG GAT CAA CTC AGA TGT TCT CC	KI

JH843	OL-PP_FipA dTM fwd	ATC CTA GAG AAC TAC AGC AAG CGC CAG CGC G	KI
MS352	EcoRV-FlhB-fwd	GCG AAT TCG TGG ATC CAG ATT TGC GAT GGG GTT TGT TTC CCA	KI
MS353	OL-FlhB KO C20AS rev	AAG CCA TTA CCG TCC CTT TTG GTA TTG ACG C	KI
MS354	OL-FlhB KO C20AS-fwd	AAG GGA CGG TAA TGG CTT GCT CGT TCA CTC TTC	KI
MS355	EcoRV-FlhB-rev	GCC AAG CTT CTC TGC AGG ATA ATC GCC ATT TGC TTA CCA GGC	KI
MS356	Check-FlhB-fwd	AGA GTT CCA GCG TTT AGA TCG G	CP
MS357	Check-FlhB-rev	TCA ATG TCA AGC CGA TGG CTT G	CP

Abbreviations: fwd: forward; rev: reverse; KO: Knock out primer; KI: Knock in primer, CP: Check primer, SP: Sequencing primer, BACTH: Bacterial adenylate cyclase two-hybrid system primer

5.1.3 Reagents

Reagents, which are not listed, were acquired from the companies Sigma-Aldrich, Taufkirchen and Roth, Dautphetal.

5.1.4 Media, buffers, solutions

Acrylamide gels:

➢ 30 % acrylamide/ bisacrylamide-solution 37.5: 1 – Rotiphorese, Roth, Dautphetal

➢ APS: 10 % (w/v) in ddH$_2$O; storage under exclusion of light at -20 °C

➢ SDS-Lösung: 10 % (w/v) in ddH$_2$O

➢ 4x lower buffer (SDS-PAGE stacking gel buffer): 0.4 % SDS, 1.5 M Tris-HCl, pH 8.8; storage at RT

➢ 4x upper buffer (SDS-PAGE separating gel buffer): 0.4 % SDS, 0.5 M Tris-HCl, pH 6.8; storage at RT

➢ 10x SDS-PAGE running buffer: 250 mM Tris-Base, 1.92 M glycine, 0.25 % (w/v) SDS, pH 8.3; storage at RT

➢ SDS-PAGE sample buffer, denaturing (2 x): 125 mM Tris, 4 % SDS, 20 % glycerol, 10 % β-mercaptoethanol, 0.02 % bromophenol blue, pH 6.8; storage at RT

➢ Coomassie staining solution: 0.1 % (w/v) Coomassie, 200 ml methanol, 50 ml acetic acid, 250 ml H$_2$O; storage at RT

➢ Fixing solution: 25 % (v/v) ethanol, 5 % (v/v) acetic acid, 70 % (v/v) H$_2$O; storage at RT

Western blot:

- 10x Western transfer buffer: 0.25 M Tris Base, 1.92 M glycine; storage at RT

- 1x Western transfer buffer: 100 ml 10x Western transfer buffer, 100 ml methanol (100%), add ddH$_2$O up to one litre; storage at RT

- 10x PBS: 80 g NaCl, 2 g KCl, 17.8 g Na$_2$HPO$_4$ x 2 H$_2$O, 2.4 g KH$_2$PO$_4$, add ddH$_2$O up to one litre, pH 7.4; storage at RT

- 1x PBS-T: 100 ml 10x PBS, 1 ml Tween 20, add ddH$_2$O up to one litre; storage at RT

- Blocking solution: 5 % milk powder in PBS-T; storage at 4 °C

- Antibody solution: 2.5 % milk powder in 1x PBS-T; storage at 4°C

Agarose gel electrophoresis:

- 50x TBE-Puffer: 2 M Tris-Base, 4.4 M boric acid (100 %), 50 mM EDTA, pH 8.0; storage at RT

- 1x TBE-Puffer: 89 mM Tris-Base, 89 mM boric acid (100 %), 1 mM EDTA, pH 8.0; storage at RT

- 6x Agarose gel electrophoresis loading buffer: 0.5 % (w/v) xylene cyanole, 0.5 % (w/v) bromophenol blue, 30 % (w/v) glycerine; storage at RT

Spheroplast generation:

- 1 M Tris-HCl (pH 8.0); storage at RT

- 0.5 mg/ml lysozyme: dissolve in 10 - 20 mM Tris-HCl (pH 8.0); storage at -20 °C

- 5 mg/ml DNase: dissolve in DNase buffer (10 mM Tris-HCl (pH 7.5), 25 mM MgCl2, 1 mM CaCl2)]; storage at -20 °C

- 125 mM EDTA-NaOH (pH 8.0); storage at RT

- STOP solution: 10 mM Tris-HCl at pH 8, 0.7 M sucrose, 20 mM MgCl$_2$; storage at 4 °C

Antibiotic und additional media supplement stock solutions:

- Kanamycin-stock solution: 50 mg/ml in ddH$_2$O; storage at -20 °C

  → Working concentration 50 µg/ml

- Ampicillin-stock solution: 50 mg/ml in ddH$_2$O; storage at -20 °C

  → Working concentration 50 µg/ml

- DAP-stock solution: 11.4 mg/ml in ddH$_2$O = 60 mM; storage at -20 °C

  → Working concentration 300 µM

- Arabinose-stock solution: 20% (w/v) in ddH$_2$0; storage at -20 °C

  → Working concentration: 0.08 %

- Sucrose-stock solution: 80 % (w/v) in ddH$_2$O; storage at RT

  → Working concentration 10 %

- IPTG-stock solution: 100 mM in ddH$_2$O; storage at -20 °C

➔ Working concentration 100 µM

➢ X-Gal-stock solution: 50 mg/ml in ddH$_2$O; storage at -20 °C

➔ Working concentration 50 µg/ml

Media:

➢ LB-medium: 10 g tryptone, 5 g yeast extract, 10 g NaCl (readymade medium from Roth, Karlsruhe) add ddH$_2$O up to one litre; storage at RT

➢ LB-agar plates: 1.5 % (w/v) Micro Agar (Roth, Karlsruhe) in LB-Medium; addition of appropriate supplement (e.g., antibiotic) after autoclaving and cooling to approx. 50 °C; storage at 4 °C

➢ LB-swimming plates: 0.3 % (w/v) Micro Agar in LB-Medium; let cool to 35 °C before pouring; storage at 4 °C

Additional solutions:

➢ 5x isothermal reaction buffer: 25 % (w/v) PEG 8000, 500 mM Tris HCl pH 7.5, 50 mM MgCl$_2$, 50 mM DTT, 5 mM NAD, 1 mM of every dNTP, fill up to 1 ml with ddH$_2$O; storage at -20 °C

➢ Gibson Assembly mix: 320 µl 5x isothermal reaction buffer, 0.64 µl T5 exonuclease, 20 µl Phusion DNA polymerase (2 U/µl), 160 µl Taq DNA ligase (40 U/µl), 699,36 µl ddH$_2$O; storage at -20 °C

5.1.5 Enzymes, antibodies, markers, kits, stains

Enzymes:

➢ Phusion polymerase – produced in house

➢ Taq polymerase – produced in house

Antibodies:

➢ Monoclonal Anti-FLAG M2, HRP coupled (1:1000) – Sigma Aldrich, Taufkirchen

➢ Anti-GFP from mouse IgG1κ (1:5000) – Sigma Aldrich, Taufkirchen

➢ Anti-mCherry from rabbit IgG (1:10000) – Biovision, USA

➢ Anti-Mouse IgG from goat, AP coupled (1:5000) – Sigma Aldrich, Taufkirchen

➢ Anti-Rabbit IgG, AP coupled (1:20000) – Sigma Aldrich, Taufkirchen

Marker:

➢ BLUeye Prestained Protein Ladder – GeneDireX Inc., USA

➢ GeneRuler™ 1 kb DNA Ladder – Life Technologies, USA

Kits:

➢ E.Z.N.A. DNA Probe Purification Kit – Omega Bio-tek, USA

➢ E.Z.N.A. Plasmid DNA Mini Kit – Omega Bio-tek, USA

➢ E.Z.N.A. Gel Extraction Kit – Omega Bio-tek, USA

- Western Lightning® Plus-ECL, Enhanced Chemiluminescence Substrate – PerkinElmer, USA

- CDP-Star, Chemiluminescence Substrate – Sigma Aldrich, Taufkirchen

Stain:

- CF™ 405M maleimide dye – Sigma Aldrich, Taufkirchen

- CF™ 488A maleimide dye – Sigma Aldrich, Taufkirchen

- Alexa Fluor™ 568 C5 maleimide dye – Thermo Fisher Scientific GmbH, Dreieich

5.1.6 Consumables

- Immobilon™-P Transfer Membrane (PVDF–membrane) – Merck Chemicals GmbH, Darmstadt

- Filtropur S 0,2 sterile filtre – Sarstedt AG, Nümbrecht

5.1.7 Devices and software

Devices

- Mastercycler nexus gradient – Eppendorf SE, Hamburg

- NanoDrop 1000 Spectrophotometer – PEQLAB Biotechnologie GmbH, Erlangen

- Leica DMI6000 B – Leica Camera AG, Wetzlar

- Intas Photo imager – INTAS science imaging, Göttingen

- TE77 ECL Semi-Dry Transfer Unit – Amersham Biosciences Corp., UK

- Ultrospec 2100 pro – Amersham Biosciences Corp., UK

- Fusion SL4 – PEQLAB Biotechnologie GmbH, Darmstadt

- EPOCH2 microplate spectrophotometer – Biotek Instruments Inc, USA

Software

- ImageJ 1.52e Freeware [207]

- Silverfast 8.5.0r5 – LaserSoft Imaging, Inc., USA

- Prism 9.1.1 – GraphPad Software, USA

- BacStalk 1.7stable [208]

5.2 <u>Methods</u>

5.2.1 DNA cloning for the generation of plasmids

For the creation of plasmids, listed in **Table 5-2**, with the aim of genomic mutation or ectopic expression of proteins, the primers, listed in **Table 5-3**, were utilised. The creation of DNA fragments for insertion into linearised vectors was achieved via PCR for which the Phusion polymerase was used. Depending on the desired aim, the wild type or mutant strain DNA of either *S. putrefaciens* CN-32 or *P. putida* KT2440 or plasmids carrying a fluorophore gene were used as template. The volumes for all PCR components and the temporal and thermic settings for the PCR cycler to run a Phusion-PCR are listed in **Table 5-4.**

Table 5-4. Recipe for 1x Phusion-PCR/ thermal and temporal parameters of the Phusion-PCR.

reagent	amount per PCR		temperature	time	step
10x *High Fidelity* buffer	10 µl		98 °C	1 min 30 s	1. initial denaturing
10 mM dNTPs	1.5 µl		98 °C	15 s	2. denaturing
template-DNA (1:10)	1 µl		65 °C	25 s	3. annealing
50 µM primer 1	0.25 µl		72 °C	15-30 s/ 1 kb	4. extension ➔ return to 2. X-times
50 µM primer 2	0.25 µl		72 °C	5 min	5. final extension
***Phusion* polymerase**	0.25 µl		4 °C	∞	
ddH₂O	add up to 50 µl				

5.2.2 Agarose gel electrophoresis

The analysis of PCR products was conducted via agarose gel electrophoresis. To achieve this 2 µl PCR product was mixed with the appropriate volume of sample buffer and loaded onto a 1 % (w/v) TBE-agarose gel containing 0.005 % (w/v) ($\triangleq$0,05 µg/ml) ethidium bromide (EtBr) and immersed in 0.5x TBE-buffer. To be able to determine the size of the PCR products on the gel, 5 µl GeneRulerTM 1 kb DNA Ladder (Life Technologies, USA) was additionally loaded onto the gel. The gel electrophoresis was run at a constant 120 V for 20-30 min at RT. After the run the DNA products in the agarose gel were detected using UV light.

5.2.3 Purification of PCR products and ligation of plasmids

Following the detection of PCR product DNA bearing the correct size through gel electrophoresis, the remaining PCR product was purified via the E.Z.N.A. DNA Probe Purification Kit according to the accompanying protocol and eluted with ddH₂O. The DNA concentration of the eluate was then measured with the NanoDrop spectrophotometer which had previously been blanked with ddH₂O. Depending on the aim either the linearised pNPTS

vector for the genomic integration of mutations or one of the linearised BACTH (pKT25, pKNT25, pUT18 and pUT18C) vectors was chosen for the next step. Here the ligation of the linearised vector and insert was accomplished by utilisation of the Gibson Assembly method for which the required amount of DNA insert was calculated with the following formula:

$$\frac{vector\ (ng) \times insert\ (bp)}{vektor\ (bp)} \times 10 = required\ DNA\ insert\ amount\ (ng)$$

The amount of linearised vector used for the Gibson Assembly was 1 µl containing 25 ng/µl DNA. If the concentration was higher or lower, the used volume was adjusted accordingly. The calculated volumes of insert and vector were added to 15 µl Gibson Assembly Mix and filled up to 20 µl with ddH$_2$O and incubated at 50 °C for 1 hour.

5.2.4 Bacterial transformation and selection of positive clones

To achieve transformation of bacterial cells 1 µl plasmid DNA or an entire Gibson Assembly mix containing the ligated plasmid (20 µl) were added to 50 µl chemically competent *E. coli* DH5α λpir, *E. coli* WM3064 or *E. coli* BTH101 and incubated on ice or 4 °C for 10 minutes. Following this, a heat shock was performed at 42 °C for 30 s after which 800 µl LB medium were added to the entire mixture. Regeneration of the bacteria then was conducted on a thermoblock shaker at 37 °C (30 °C for BTH101) and 600 rpm for 1 h after which the bacterial cells were precipitated by centrifugation (13000 rpm for 1 min) and 700 µl of the supernatant were discarded. The bacterial pellet then was resuspended in the remaining supernatant and plated on an agar plate, or in the case of the BTH101 strain inoculated into 5 ml LB medium, containing the appropriate selection factor(s) or supplements. The cells then were incubated over night at either 37 °C (DH5α λpir and WM3064) or 30 °C (BTH101). To check if the DH5α λpir cells, which were directly transformed with the plasmid ligated by the Gibson Assembly mix, contained the plasmid carrying the PCR insert used in the Gibson Assembly reaction, a colony PCR **Table 5-5** was conducted with 8 colonies which were streak from the plate. The success of the Gibson Assembly and transformation then was analysed via agarose gel electrophoresis after which a positive colony was inoculated in 10 ml LB medium + Kan and incubated over night at 37 °C for plasmid extraction. For the conjugation, the extracted plasmid was retransformed into WM3064 cells which were plated onto plates containing Kan and DAP and incubated at 37 °C overnight.

5.2.5 Plasmid extraction and sequencing

The plasmid DNA was extracted out of the DH5α λpir cells by usage of the E.Z.N.A. Plasmid DNA Mini Kit I (OMEGA Bio-tek, USA). Approximately 5 ml of overnight culture were used and processed according to the operation manual. At the final step between 30 and 50 µl ddH2O were used to eluate the plasmid DNA. Following this the DNA content of the eluate was

measured by NanoDrop spectrophotometer and 15 µl containing at least 30 ng/µl DNA were sent to the company SEQLAB Sequence Laboratories Göttingen for sequencing. If necessary, appropriate sequencing primers were added to the shipment in the concentration of 10 µM. If the sequencing result of the plasmid showed the expected DNA profile, the DH5α λpir cells carrying the plasmid were inoculated into 10 ml LB + Kan medium and incubated overnight at 37 °C. on the following day 1,8 ml of the culture were mixed with 180 µl DMSO and shock frozen in liquid nitrogen after which the strain then was stored at -80 °C.

5.2.6   Conjugation, colony PCR and strain storage

The conjugation of either *Shewanella putrefaciens* CN-32 or *Pseudomonas putida* KT2440 with the aim of genomic modification was initiated with the unification of equicellular amounts (approximately 1 ml) of an over day culture containing either of the previously mentioned species and of an over day culture, which had been supplemented with Kan and DAP, containing WM3064 carrying the appropriate plasmid. Prior to unification the WM3064 cells were washed, by centrifugation and resuspension in LB or another appropriate medium, to remove any remaining Kan. The unified cells were resuspended in 200 µl LB medium and dropped onto an LB + DAP plate in 4 individual 50 µl drops. Following an overnight incubation at 30 °C the cells were washed from the plate with 2 ml LB + Kan medium. To remove any excess DAP the acquired cells were additionally washed twice with 1 ml LB + Kan medium before they were resuspended in 1 ml LB + Kan medium and diluted by a factor of 1:10 and 1:100, of which 100 µl then were plated on individual LB + Kan agar plates. After an overnight incubation of these plates at 30 °C or over a weekend at RT, which from this step onward alternatively can be done to overnight incubation at 30 °C, 25 Kan resistant colonies were individually restreaked first onto an LB + Suc plate and then with the same toothpick onto an LB + Kan plate. These plates then were incubated overnight at 30 °C and checked for colonies which were resistant to Kan and sensitive to Succ. For the loop out 2 times 3 colonies were selected carrying the previously mentioned traits and inoculated into 2 individual flask containing10 ml LB medium. The inoculated cultures were then incubated for 3 h 30 min at 30 °C on a shaker at 160rpm and subsequently plated onto LB + Suc plates in 1:10 and 1:100 dilutions. After an overnight incubation at 30 °C, a total of 50 colonies (25 colonies per loop out) were individually restreaked first onto an LB + Kan agar plate and then onto an LB + Suc agar plate, which was followed by another overnight incubation at 30 °C. To now determine, if the desired mutation had been achieved, a so-called Colony-PCR, for which the Taq polymerase was utilised, was performed with colonies, which were both sensitive to Kan and insensitive to Suc. The volumes for all PCR components and the temporal and thermic settings for the PCR cycler to run a Colony-PCR are listed in **Table 5-5.**

Table 5-5. Recipe for 1x Taq-PCR/ thermal and temporal parameters of the Taq-PCR.

reagent	amount per PCR		temperature	time	step
10x *Taq-buffer*	2.5 µl		98 °C	1 min 30 s	1. initial denaturing
10 mM dNTPs	0.5 µl		98 °C	15 s	2. denaturing
template-DNA (1:10)	1 µl		65 °C	25 s	3. annealing
50 µM primer 1	0.15 µl		72 °C	15-30 s/ 1 kb	4. extension ➜ return to 2. X-times
50 µM primer 2	0.15 µl		72 °C	5 min	5. final extension
Taq-polymerase	0.9 µl		4 °C	∞	
***High Fidelity Phusion* polymerase**	0.1 µl				
ddH₂O	add up to 25 µl				

The subsequently acquired PCR products were analysed via agarose gel electrophoresis to determine a colony, which was carrying the desired genetic traits. If all the colonies were negative the PCR was repeated. To prepare the positive colony the remaining colony material was inoculated into 10 ml LB and incubated over night at RT while shaking at 116 rpm. Following the incubation 1,8 ml of the culture were mixed with 180 µl DMSO and shock frozen in liquid nitrogen. The strain then was stored at -80 °C.

5.2.7 Preparation of cells for microscopy

The strain of interest was inoculated into 10 ml of LB medium at OD 0.02 from an overnight culture and grown to an approximate OD of 0.5. Once this point was reached 2 µl of the culture were dropped on a slide consisting of 1 % agarose solved in LM medium. Following this a coverslip was placed onto the agarose slide once the drop of culture had dried and the sample was analysed via microscopy. If a time-lapse microscopy analysis was to be performed, a specialised agarose slide was prepared inside an adhesive chamber stuck to a glass microscopy slide, which could be sealed with a coverslip after the culture had been dropped onto the agarose slide.

5.2.8 Staining of hook and filament structure

For the staining of extracellular structures, the stain of interest was always handled with cut off pipet tips. To determine the required amount of exponentially growing culture the following formula was used:

$$\frac{0.2}{OD} * 1000 = required\ amount\ of\ culture\ (\mu l)$$

The appropriate amount of culture the was centrifuged at 3500 rpm for 5 min while the maleimide stain was brought into RT about 1 min before the centrifuge cycle ended. Following

the centrifugation step, the supernatant was discarded, and the pellet was resuspended in 50 µl sterile filtered 1x PBS. Then, depending on the stain used, between 0.5 and 1.5 µl of the maleimide stain were added and everything was mixed by flicking the reaction tube. After a 15 min incubation at RT and under the exclusion of light, during which at the median timepoint the reaction tube was reflicked, the sample was centrifuged at 3500 rpm for 5 min. After discarding the supernatant anew, the resulting pellet was resuspended in 1 ml sterile filtered PBS and again centrifuged at 3500 rpm for 5 min. The resulting supernatant was again discarded, and the pellet was resuspended in 1 ml PBS of which then 2 µl were used for microscopy.

5.2.9 Induction of expression from an L-arabinose inducible promoter

Prior to inoculating the strain of interest into LB medium at OD 0.02 from an overnight culture, 0.08 % sterile filtered L-arabinose was added to the medium for the induction of an L-arabinose inducible promoter. Following this the strains were processed according to the method being next in line of the individual procedure.

5.2.10 Initiation of spheroplast formation

The overnight culture of the strain of interest was inoculated at OD 0.02 and grown until it reached the exponential phase (approx. OD 0.5) while 50 µg/ml Ampicillin were added approximately 30 – 40 min before harvesting. When the desired growth phase was reached 0.5 to 1 ml of culture was harvested and centrifuged at 500 rpm for 1 min. While the supernatant was discarded, the resulting pellet was resuspended in 500 µl of an 800 mM sucrose solution. Following this 30 µl 1 M Tris-HCl (pH 8.0), 24 µl 0.5 mg/ml lysozyme, 6 µl 5 mg/ml DNase, and 6 µl 125 mM EDTA-NaOH (pH 8.0) were added in this exact order and the sample was incubated for 5-20 min at RT after which the reaction was stopped with 100 µl STOP solution (10 mM Tris-HCl at pH 8, 0.7 M sucrose, 20 mM $MgCl_2$). Then 2 µl were pipetted onto an agarose slide and the coverslip was added before the drop dried to prevent the bursting of cells. Following this the sample was ready for microscopy.

5.2.11 Motility/swimming assay

Approximately 2 µl of an exponentially growing over day culture containing a strain of interest were dropped onto a semi solid agar plate containing 0.25 % agar dissolved in LB medium. The plate then was incubated over night at either 30 °C for *S. putrefaciens* CN-32 or RT for *P. putida* KT2440. Following the incubation period, the swimming phenotype was documented by scanning of the plates.

5.2.12 Growth curve assay

The strain of interest was taken from an overnight culture, set to OD 0.02 in LB medium and loaded into a 96 well plate. The plate subsequently was put into the EPOCH2 microplate spectrophotometer (Biotek Instruments Inc, USA), and incubated for 24 h at 30 °C, during which the OD measurements were taken every 5 min.

5.2.13 Bacterial adenylate cyclase two-hybrid assay

The bacterial adenylate cyclase two-hybrid system [205] was utilised in this study to determine if proteins of interest from *S. putrefaciens* CN-32 or *P. putida* KT2440 are able to interact homologously and heterologously with proteins of the same species. To cover various protein interaction constellations, plasmids were used on which the individual proteins of interest were genetically fused to either the N- or the C-terminus of either the T18 or T25 fragment of the adenylate cyclase catalytic domain. For the assay 1 µl of each appropriate plasmid, including the positive and negative control plasmid combinations, were individually cotransformed into 20 µl *E. coli* BTH101. After regeneration at 30 °C for at least 1 h the entire transformation reaction mix was inoculated into 5 ml LB medium containing Kan and Amp. The subsequent incubation step was done overnight at 30 °C. Following the incubation, 10 µl of each cotransformation culture were dropped onto an LB agar plate containing Kan, Amp, IPTG and X-gal, which was incubated at 30 °C overnight after the drops had dried into the plate. After the final incubation the plates were checked for the interaction phenotype of each colony drop according to the colour and scanned. To intensify the colour, the plates were then additionally stored at 4 °C.

5.2.14 SDS-PAGE and Western blot

The individual proteins of interest were expressed in a homologous manner in the appropriate strains and analysed through Coomassie stained polyacrylamide gel and Western blot. The gel electrophoretic analysis was conducted according to the method by Laemlli [209] The individual reagents used for the stacking and separating gel are listed in **Table 5-6**. The samples harvested from exponentially growing cultures containing the strain of interest were taken in such a manner that the resuspension of the cell pellet, resulting from centrifugation, in 2x SDS sample buffer, would reach an OD 10. The sample was subsequently additionally denatured at 95 °C. Approximately 10 µl of each sample were then loaded onto a gel with the additional loading of 5 µl BLUeye Prestained Protein Ladder (GeneDireX Inc., USA) as reference. Empty gel pockets were loaded with 10 µl 2x SDS sample buffer.

Table 5-6. Recipe for two SDS-PAA gels.

reagent	5 % stacking gel	12,5 % separating gel
ddH$_2$O	2.8 ml	3.2 ml
30 % acrylamide (37,5: 1)	825 µl	4.2 ml
4x upper buffer	1.25 ml	- -
4x lower buffer	- -	2.5 ml
10 % APS	50 µl	80 µl
TEMED	3.75 µl	6 µl

If not mentioned otherwise, two gels were prepared for the gel electrophoresis to be able to subsequently stain one gel with Coomassie and use the other gel for Western blotting. The electrophoretic separation was conducted at 70 V and stopped once the bromophenol blue front passed the lower edge of the gel. One of the resulting gels was stained using Coomassie according to Neuhoff [210] and incubated overnight after which it was washed with fixing solution to remove excess Coomassie staining. The second gel was used for the Western blot in a semi-dry system to subsequently detect proteins of interest. The blot stacks consisted of 3 individual layers of blotting paper, soaked in 1x Western transfer buffer, per electrode. The PVDF membrane was initially equilibrated in 100% methanol followed by a 2 min bath in ddH$_2$0 and a final equilibration in Western transfer buffer. The blotting stack then was assembled in the following order: Cathode, 3x blotting paper soaked in 1x Western transfer buffer, PAA-gel, PVDF-membrane equilibrated in 1x Western transfer buffer, 3x blotting paper soaked in 1x Western transfer buffer, anode. The electrical transfer of the proteins from the gel to the membrane took approximately 45 min if a current of 0.8 mA per cm^2 membrane was applied. After blotting the membrane was incubated in a blocking solution for 1-2 h and subsequently washed 3x with 1x PBS-T for 10 min to remove excess blocking solution. Following the washing the membrane was incubate with the appropriately diluted primary antibody for 1-2 h at RT or overnight at 4 °C, which was succeeded by an additional washing step with 1x PBS-T as mentioned previously. If a secondary antibody was required, the membrane additionally was incubated with the appropriately diluted secondary antibody for 1.5 h and again washed to remove excess antibody solution. The final step depended on the enzyme the antibody was conjugated to. If an antibody conjugated with HRP was used, the membrane was treated with 1-2 ml of reagent mixture from the Western Lightning® Plus-ECL, Enhanced Chemiluminescence Substrate Kit (PerkinElmer, USA). If the antibody was conjugated with AP, membrane was equilibrated in 10 ml detection buffer for 5 min after which it was placed in a clear foil with 1 ml CDP-Star (Roche, Switzerland) working solution and incubated for 5 min. The final capturing and analysis of the individual membrane independent of development method was done with the Fusion SL4 (PEQLAB Biotechnologie GmbH, Darmstadt).

5.2.15 In silico data acquisition and processing

Scanning and pre-processing of swimming plates, growth plates and Coomassie stained SDS polyacrylamide gels was achieved with the software Silverfast 8.5.0r5 (LaserSoft Imaging, Inc., USA). Images were analysed and edited with ImageJ 1.52e [207] and Adobe Illustrator CS6 16.0.3 (Adobe Systems Incorporated). The software Prism 9.1.1 (GraphPad Software, USA) was utilized for statistical analysis via unpaired t test and the creation of graphs. Fluorescence intensities and flagellar filaments lengths were measured and analysed through BacStalk 1.7stable [208]. Amino acid sequence homology and conservation analysis was conducted via Jalview 2.11.0 [211] and the webtools Basic Local Alignment Search Tool [212], Consurf [213] and Clustal Omega [214]. The protein structure was determined with the **S**imple **M**odular **A**rchitecture **R**esearch **T**ool [215] and the synteny analysis for *fipA* was performed with EDGAR [216].

6. Appendix
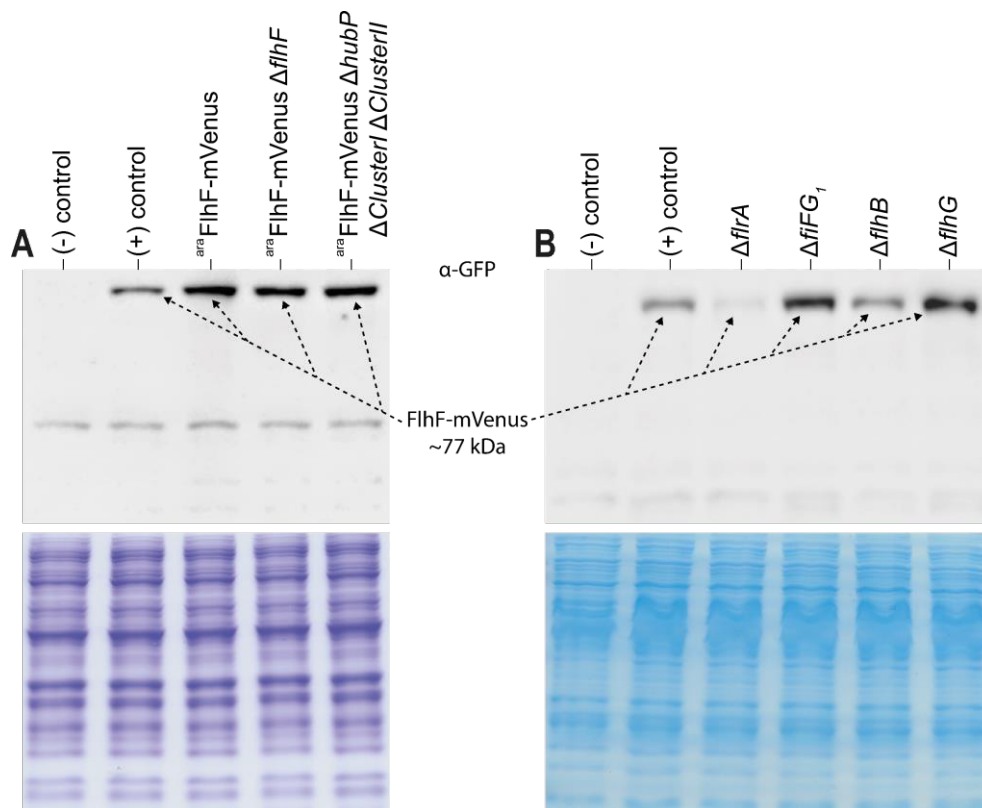
Supplemental figure 38. Expression and stability analysis of *Sp*FlhF (Sputcn32_2561) expressed from an arabinose inducible promoter and in strains carrying motility factor deletions in *S. putrefaciens* CN-32. (A) Western blot and Coomassie stained SDS-PAGE with samples of strains expressing mVenus tagged *Sp*FlhF from an arabinose inducible promoter. **(B)** Western blot and Coomassie stained SDS-PAGE with samples of strains expressing mVenus tagged *Sp*FlhF and carrying motility factor deletions.
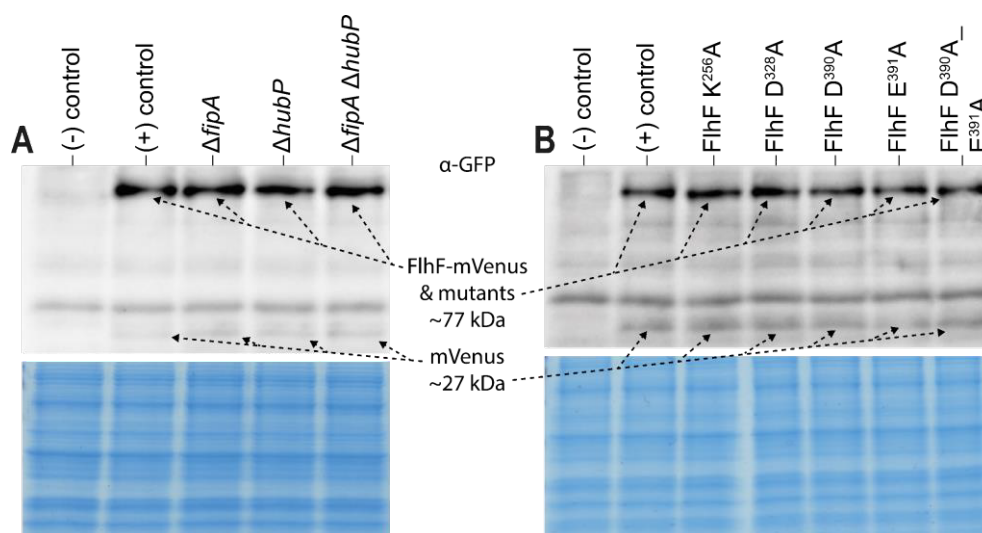
Supplemental figure 39 Expression and stability analysis of *Sp*FlhF (Sputcn32_2561) and *Sp*FlhF mutants in *S. putrefaciens* CN-32. (A) Western blot and Coomassie stained SDS-PAGE with samples of strains expressing mVenus tagged *Sp*FlhF carrying either single gene deletions of *fipA* and *hubP* or a double deletion of both these genes. **(B)** Western blot and Coomassie stained SDS-PAGE with samples of strains expressing mVenus tagged *Sp*FlhF mutants.
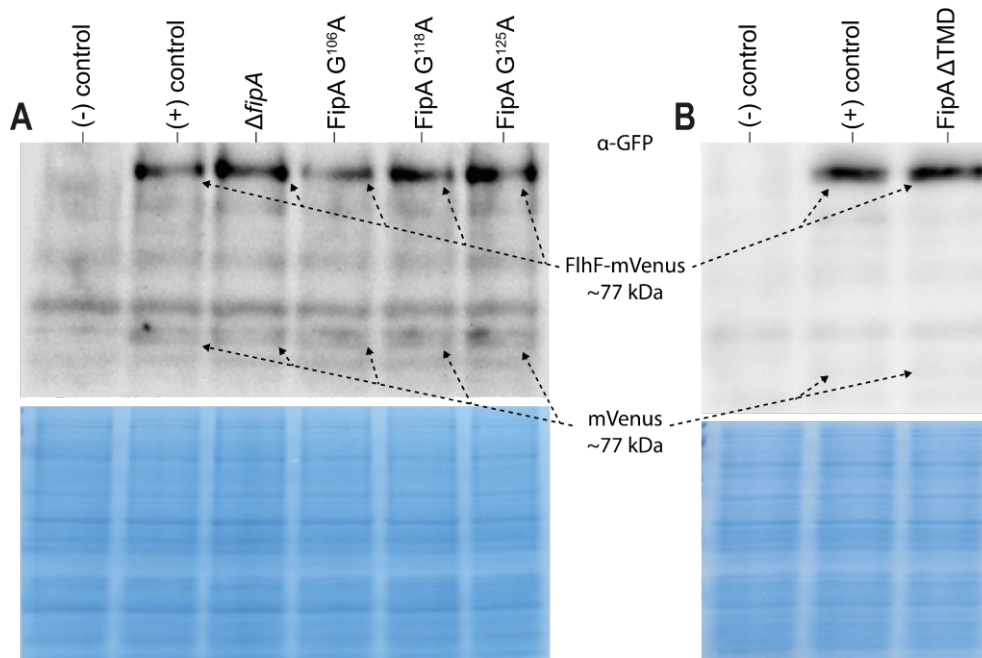
Supplemental figure 40. Expression and stability analysis of wild type *Sp*FlhF (Sputcn32_2561) in Δ*fipA* and *Sp*FipA mutant strains in *S. putrefaciens* CN-32. (A) Western blot and Coomassie stained SDS-PAGE with samples of strains expressing mVenus tagged *Sp*FlhF in a Δ*fipA* and *Sp*FipA mutant strains. **(B)** Western blot and Coomassie stained SDS-PAGE with samples of a strain carrying a *Sp*FipA variant with deleted transmembrane domain and expressing mVenus tagged *Sp*FlhF.
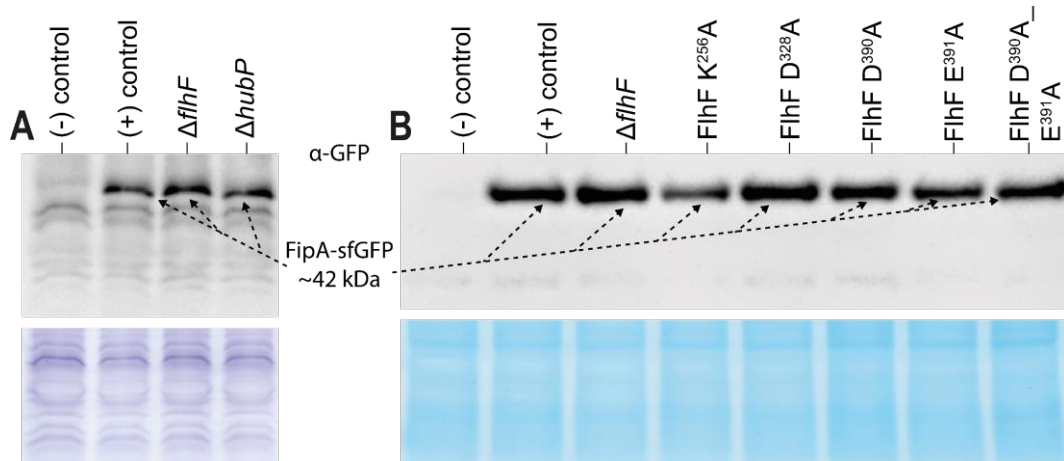
Supplemental figure 41. Expression and stability analysis of *Sp*FipA (Sputcn32_2550) in *flhF* and *hubP* deletion and *Sp*FlhF mutant strains in *S. putrefaciens* CN-32. (A) Western blot and Coomassie stained SDS-PAGE with samples of strains expressing sfGFP tagged *Sp*FipA in a Δ*flhF* and a Δ*hubP* background. **(B)** Western blot and Coomassie stained SDS-PAGE with samples of *Sp*FlhF mutant strains expressing sfGFP tagged *Sp*FipA.
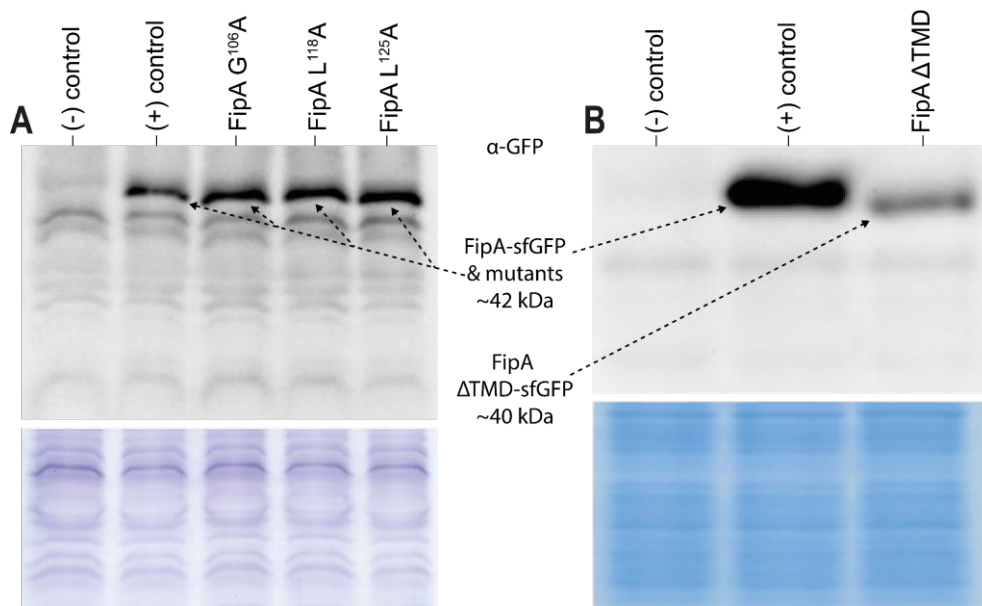
Supplemental figure 42. Expression and stability analysis of *Sp*FipA (Sputcn32_2550) mutants in *S. putrefaciens* CN-32. (A) Western blot and Coomassie stained SDS-PAGE with samples of strains expressing sfGFP tagged *Sp*FipA mutants. **(B)** Western blot and Coomassie stained SDS-PAGE with samples of a strain expressing an sfGFP tagged *Sp*FipA variant with deleted transmembrane domain.
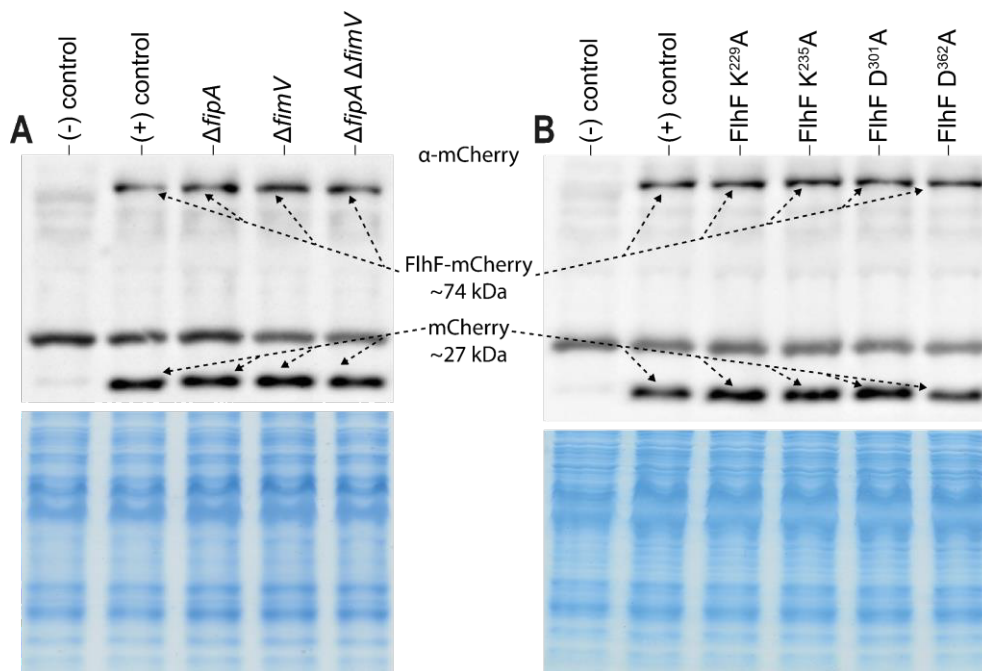
Supplemental figure 43. Expression and stability analysis of wild type *Pp*FlhF (PP_4343) in *fipA* and *fimV* single and double deletion strains and *Pp*FlhF mutants in *P. putida* KT2440. (A) Western blot and Coomassie stained SDS-PAGE with samples of strains expressing mCherry tagged *Pp*FlhF in a Δ*fipA*, Δ*fimV* and Δ*fipA* Δ*fimV* strain. **(B)** Western blot and Coomassie stained SDS-PAGE with samples of strains expressing mCherry tagged *Pp*FlhF mutants.
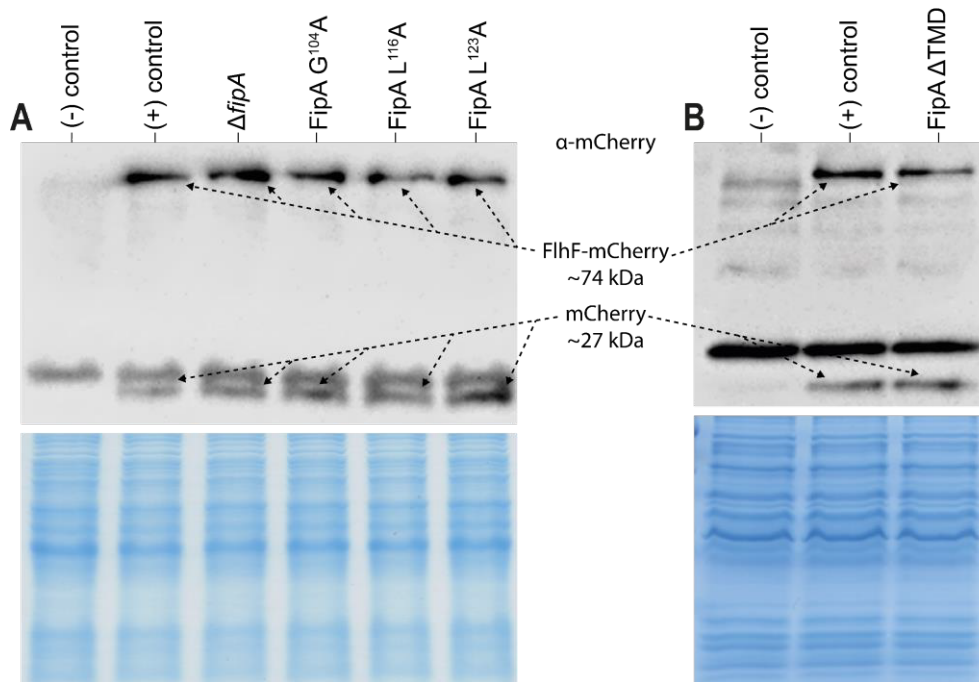
Supplemental figure 44. Expression and stability analysis of wild type *Pp*FlhF (PP_4343) in Δ*fipA* and *Pp*FipA mutant strains in *P. putida* KT2440. (A) Western blot and Coomassie stained SDS-PAGE with samples of strains expressing mCherry tagged *Pp*FlhF in a Δ*fipA* and *Pp*FipA mutant strains. **(B)** Western blot and Coomassie stained SDS-PAGE with samples of a strain carrying a *Pp*FipA variant with deleted transmembrane domain and expressing mCherry tagged *Pp*FlhF.
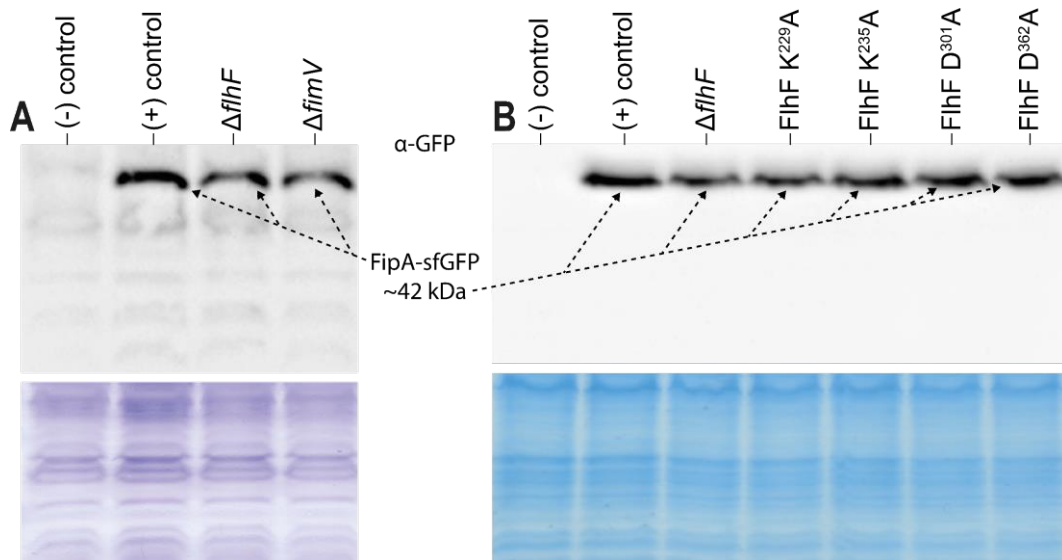
Supplemental figure 45. Expression and stability analysis of wild type *Pp*FipA (PP_4331) in *flhF* and *fimV* deletion and *Pp*FlhF mutant strains in *P. putida* KT2440. (A) Western blot and Coomassie stained SDS-PAGE with samples of strains expressing sfGFP tagged *Pp*FipA in a Δ*flhF* and Δ*fimV* strain. **(B)** Western blot and Coomassie stained SDS-PAGE with samples of *Pp*FlhF mutant strains expressing sfGFP tagged *Pp*FipA.
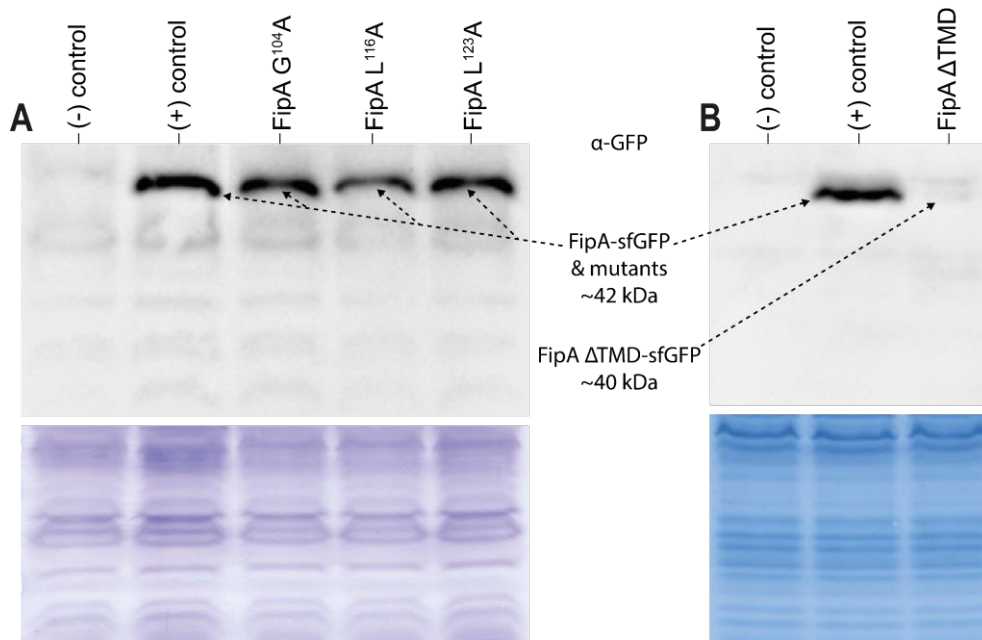
Supplemental figure 46. Expression and stability analysis of *Pp*FipA (PP_4331) mutants in *P. putida* KT2440. (A) Western blot and Coomassie stained SDS-PAGE with samples of strains expressing sfGFP tagged *Pp*FipA mutants. **(B)** Western blot and Coomassie stained SDS-PAGE with samples of a sfGFP tagged *Pp*FipA mutant with deleted transmembrane domain.

Supplemental figure 47. Gene positioning of *fipA* in γ-proteobacteria determined through synteny analysis. (A) Gene positioning of *fipA* on the genome of various bacteria from the *Shewanella* genus. **(B)** Gene positioning of *fipA* on the genome of various bacteria from the *Pseudomonas* genus. **(C)** Gene positioning of *fipA* on the genome of various bacteria from the *Vibrio* genus.
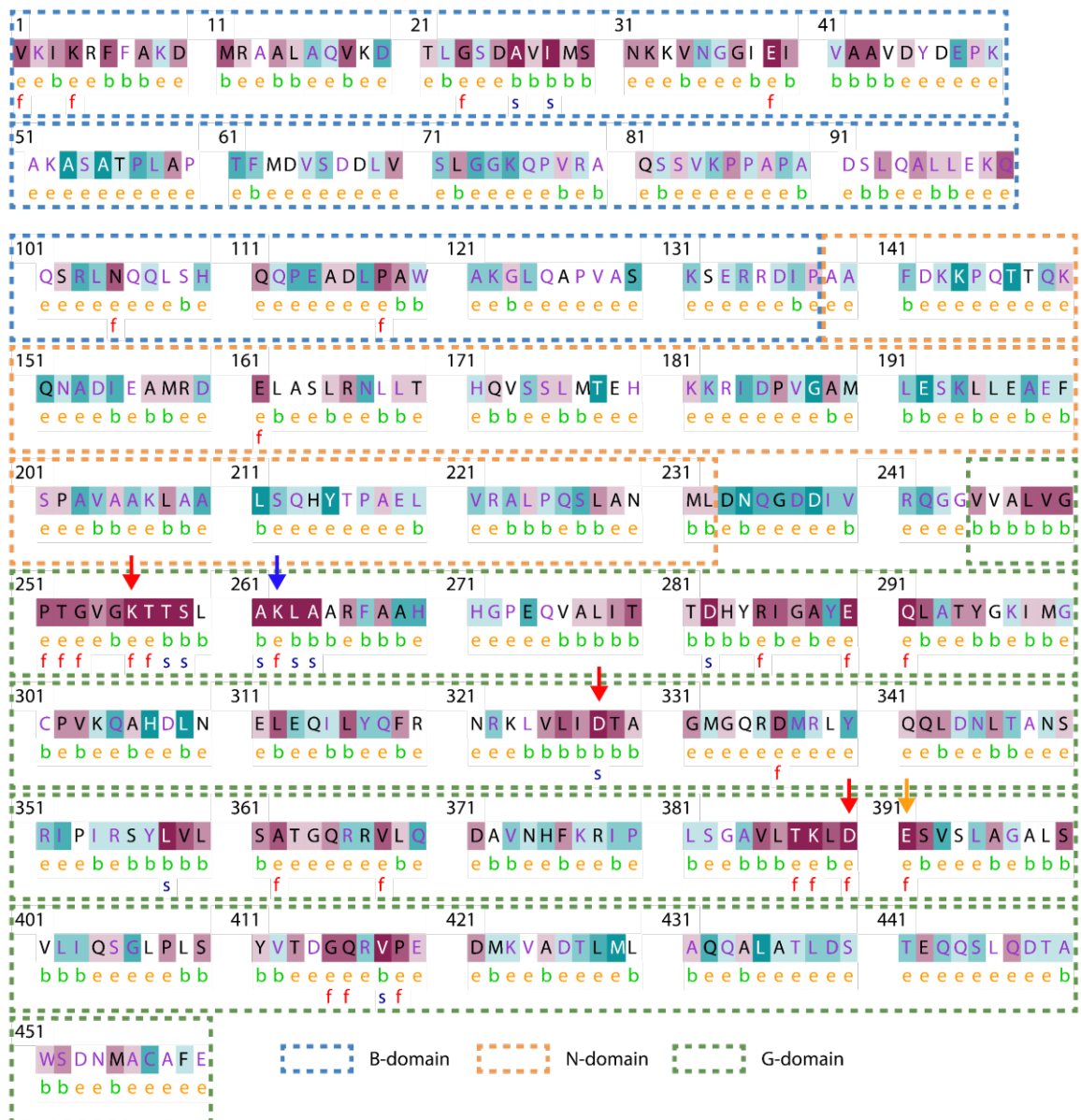
Supplemental figure 48. Amino acid sequence homology and conservation analysis for FlhF conducted with ConSurf [213]**.** Red arrows indicate residues substituted in both *S. putrefaciens* CN-32 and *P. putida* KT2440, whereas the orange arrow indicates a residue substituted in only *S. putrefaciens* CN-32 and the blue arrow indicates a residue substituted only in *P. putida* KT2440.
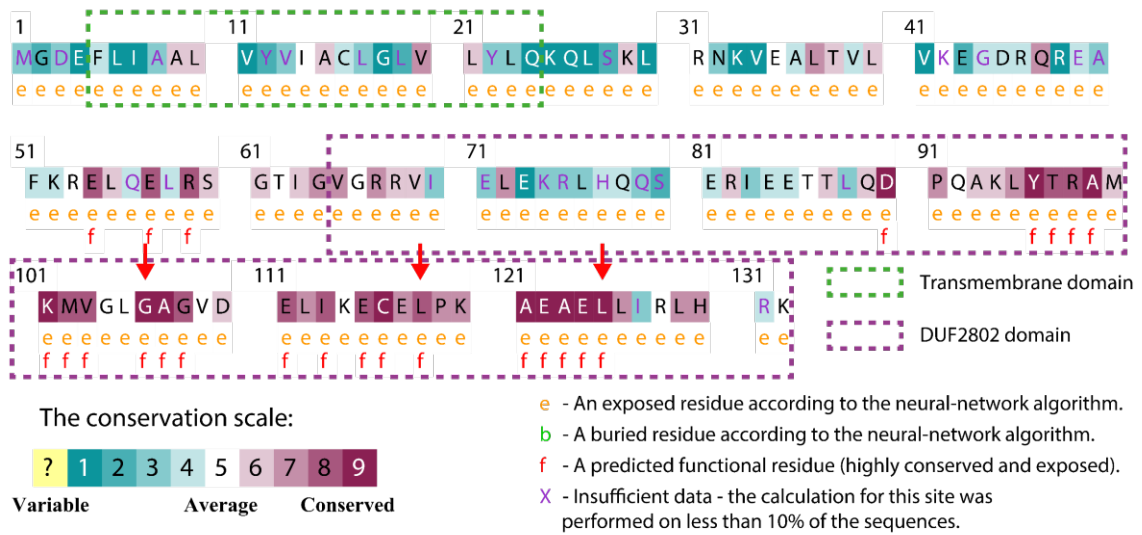
Supplemental figure 49. Amino acid sequence homology and conservation analysis for FipA conducted with ConSurf [213]**.** The red arrows indicate residues substituted in both *S. putrefaciens* CN-32 and *P. putida* KT2440.

7. Abbreviations

AB	antibodies
AP	alkaline phosphatase
Amp	Ampicillin
APS	ammonium peroxydisulfate
Ara	arabinose
Asn	asparagine
a.u.	arbitrary units
BACTH	bacterial adenylate cyclase two-hybrid system
ClusterI	polar flagellar gene cluster of *Shewanella putrefaciens CN-32* (*Sputcn32_2548-2608*)
ClusterII	lateral flagellar gene cluster of *Shewanella putrefaciens CN-32* (*Sputcn32_3444-3485*)
CP	check primer
DAP	2,6-diaminopimelinic acid
ddH$_2$O	double distilled water
DMSO	dimethyl sulfoxide
DNA	desoxyribonucleic acid
E. coli	*Escherichia coli*
EDTA	ethylenediaminetetraacetate
et al.	lat.: *et alii* (and others)
EtBr	ethidium bromide
fT3SS	flagellar type III secretion system
fwd	forward
HRP	horseradish peroxidase
IM	inner membrane

IPTG	isopropyl-β-D-1-thiogalactopyranoside
Kan	Kanamycin
KI	knock in
KO	knock out
LB	lysogeny broth
MCS	multiple cloning site
NEB	New England Biolabs
OD	optical density
OM	outer membrane
PAA	polyacrylamide
PCR	polymerase chain reaction
PMF	proton motive force
Pp	prefix to protein of interest from *Pseudomonas putida* KT2440
PPG	peptidoglycan layer
P. putida	*Pseudomonas putida*
Primer	starter oligonucleotide
Pro	proline
PRR	proline rich region
rev	reverse
RT	room temperature
Suc	sucrose
SDS	sodium dodecyl sulphate
S. putrefaciens	*Shewanella putrefaciens*
SIMIBI	SRP, MinD und BioD (SIMIBI)-type nucleotide triphosphate-binding proteins
SMART	Simple Modular Architecture Research Tool

SP	sequencing primer
Sp	prefix to protein of interest from *Shewanella putrefaciens* CN-32
S. putrefaciens	*Shewanella putrefaciens*
SRP	signal recognition particle
Taq	*Thermus aquaticus*
TEMED	tetramethyl ethylenediamine
TMD	transmembrane domain
v/v	volume per volume
w/v	weight per volume
WT	wild type
X-Gal	5-bromo-4-chloro-3-indolyl-β-D-galactopyranoside

8. References

1. Hook, J. C. *et al.* A Proline-Rich Element in the Type III Secretion Protein FlhB Contributes to Flagellar Biogenesis in the Beta- and Gamma-Proteobacteria. *Front. Microbiol.* **11**, 1–13 (2020).

2. Miyata, M. *et al.* Tree of motility – A proposed history of motility systems in the tree of life. *Genes to Cells* **25**, 6 (2020).

3. Froese, T., Virgo, N. & Ikegami, T. Motility at the origin of life: Its characterization and a model. *Artif. Life* **20**, 55–76 (2014).

4. Jarrell, K. F. & McBride, M. J. The surprisingly diverse ways that prokaryotes move. *Nat. Rev. Microbiol.* **6**, 466–476 (2008).

5. Henrichsen, J. Bacterial surface translocation: a survey and a classification. *Bacteriol. Rev.* **36**, 478 (1972).

6. Harshey, R. M. Bacterial motility on a surface: many ways to a common goal. *Annu. Rev. Microbiol.* **57**, 249–273 (2003).

7. Krell, T. *et al.* Diversity at its best: bacterial taxis. *Environ. Microbiol.* **13**, 1115–1124 (2011).

8. Faguy, D. M. & Jarrell, K. F. A twisted tale: the origin and evolution of motility and chemotaxis in prokaryotes. *Microbiology* 279–281 (1999).

9. Paulick, A. *et al.* Mechanism of bidirectional thermotaxis in Escherichia coli. *Elife* **6**, (2017).

10. Demir, M. & Salman, H. Bacterial Thermotaxis by Speed Modulation. *Biophys. J.* **103**, 1683 (2012).

11. Jékely, G. Evolution of phototaxis. *Philos. Trans. R. Soc. B Biol. Sci.* **364**, 2795 (2009).

12. Müller, F. D., Schüler, D. & Pfeiffer, D. A compass to boost navigation: Cell biology of bacterial magnetotaxis. *J. Bacteriol.* **202**, (2020).

13. Taylor, B. L., Zhulin, I. B. & Johnson, M. S. Aerotaxis and other energy-sensing behavior in bacteria. *Annu. Rev. Microbiol.* **53**, 103–128 (1999).

14. A. J. Merz, M. So, M. P. S. Pilus retraction powers bacterial twitching motility. *Nature* 98–102 (2000).

15. Mattick, J. S. Type IV pili and twitching motility. *Annu. Rev. Microbiol.* **56**, 289–314 (2002).

16. Carbonnelle, E., Helaine, S., Nassif, X. & Pelicic, V. A systematic genetic analysis in Neisseria meningitidis defines the Pil proteins required for assembly, functionality, stabilization and export of type IV pili. *Mol. Microbiol.* **61**, 1510–1522 (2006).

17. Nan, B. Bacterial Gliding Motility: Rolling Out a Consensus Model. *Curr. Biol.* **27**, R154–R156 (2017).

18. Islam, S. T. & Mignot, T. The mysterious nature of bacterial surface (gliding) motility: A focal adhesion-based mechanism in Myxococcus xanthus. *Semin. Cell Dev. Biol.* **46**, 143–154 (2015).

19. Jakobczak, B., Keilberg, D., Wuichet, K. & Søgaard-Andersen, L. Contact- and Protein Transfer-Dependent Stimulation of Assembly of the Gliding Motility Machinery in Myxococcus xanthus. *PLoS Genet.* **11**, (2015).

20. Nan, B. *et al.* Myxobacteria gliding motility requires cytoskeleton rotation powered by proton motive force. *Proc. Natl. Acad. Sci. U. S. A.* **108**, 2498–2503 (2011).

21. Mignot, T., Shaevitz, J. W., Hartzell, P. L. & Zusman, D. R. Evidence that focal adhesion complexes power bacterial gliding motility. *Science (80-.).* **315**, 853–856 (2007).

22. Faure, L. M. *et al.* The mechanism of force transmission at bacterial focal adhesion complexes. *Nature* **539**, 530+ (2016).

23. Wilde, A. & Mullineaux, C. W. Motility in cyanobacteria: polysaccharide tracks and Type IV pilus

motors. *Mol. Microbiol.* **98**, 998–1001 (2015).

24. Walsby, A. E. Mucilage secretion and the movements of blue-green algae. *Protoplasma 1968 651* **65**, 223–238 (1968).

25. Harshey, R. M. & Matsuyama, T. Dimorphic transition in Escherichia coli and Salmonella typhimurium: surface-induced differentiation into hyperflagellate swarmer cells. *Proc. Natl. Acad. Sci. U. S. A.* **91**, 8631 (1994).

26. Alberti, L. & Harshey, R. M. Differentiation of Serratia marcescens 274 into swimmer and swarmer cells. *J. Bacteriol.* **172**, 4322–4328 (1990).

27. Eberl, L., Molin, S. & Givskov, M. Surface motility of Serratia liquefaciens MG1. *J. Bacteriol.* **181**, 1703–1712 (1999).

28. Kawagishi, I., Imagawa, M., Imae, Y., McCarter, L. & Homma, M. The sodium-driven polar flagellar motor of marine Vibrio as the mechanosensor that regulates lateral flagellar expression. *Mol. Microbiol.* **20**, 693–699 (1996).

29. Jones, B. V., Young, R., Mahenthiralingam, E. & Stickler, D. J. Ultrastructure of Proteus mirabilis Swarmer Cell Rafts and Role of Swarming in Catheter-Associated Urinary Tract Infection. *Infect. Immun.* **72**, 3941 (2004).

30. Luchsinger, R. H., Bergersen, B. & Mitchell, J. G. Bacterial Swimming Strategies and Turbulence. *Biophys. J.* **77**, 2377–2386 (1999).

31. Homma, M., Oota, H., Kojima, S., Kawagishi, L. & Lmaet, Y. Chemotactic responses to an attractant and a repellent by the polar and lateral flagellar systems of Vibrio alginolyticus. *Microbiology* **142**, 2777–2783 (1996).

32. Chen, X. & Berg, H. C. Torque-speed relationship of the flagellar rotary motor of Escherichia coli. *Biophys. J.* **78**, 1036–1041 (2000).

33. Berg, H. C. & Brown, D. A. Chemotaxis in Escherichia coli analysed by Three-dimensional Tracking. **239**, 500–504 (1972).

34. Kondoh, H. Tumbling chemotaxis mutants of Escherichia coli: possible gene-dependent effect of methionine starvation. *J. Bacteriol.* **142**, 527 (1980).

35. Brown, D. A. & Berg, H. C. Temporal Stimulation of Chemotaxis in Escherichia coli. *Proc. Natl. Acad. Sci. U. S. A.* **71**, 1388 (1974).

36. Macnab, R. M. & Koshland, D. E. The gradient-sensing mechanism in bacterial chemotaxis. *Proc. Natl. Acad. Sci. U. S. A.* **69**, 2509–2512 (1972).

37. Tsang, N., Macnab, R. & Koshland, D. E. Common mechanism for repellents and attractants in bacterial chemotaxis. *Science* **181**, 60–61 (1973).

38. Son, K., Guasto, J. S. & Stocker, R. Bacteria can exploit a flagellar buckling instability to change direction. *Nat. Phys. 2013 98* **9**, 494–498 (2013).

39. Kühn, M. J., Schmidt, F. K., Eckhardt, B. & Thormann, K. M. Bacteria exploit a polymorphic instability of the flagellar filament to escape from traps. *Proc. Natl. Acad. Sci. U. S. A.* **114**, 6340–6345 (2017).

40. Nakamura, S. Spirochete Flagella and Motility. *Biomol. 2020, Vol. 10, Page 550* **10**, 550 (2020).

41. Duan, Q., Zhou, M., Zhu, L. & Zhu, G. Flagella and bacterial pathogenicity. *J. Basic Microbiol.* **53**, 1–8 (2013).

42. Chaban, B., Hughes, H. V. & Beeby, M. The flagellum in bacterial pathogens: For motility and a whole lot more. *Semin. Cell Dev. Biol.* **46**, 91–103 (2015).

43. McCarter, L. L. Polar flagellar motility of the Vibrionaceae. *Microbiol. Mol. Biol. Rev.* **65**, 445–462 (2001).

44. Martínez-García, E., Nikel, P. I., Chavarría, M. & de Lorenzo, V. The metabolic cost of flagellar

motion in Pseudomonas putida KT2440. *Environ. Microbiol.* **16**, 291–303 (2014).

45. Aiden, T. *Transmission electron micrograph of a singular Campylobacter jejuni bacterium taken at 2200x magnification*.

46. Chao, S. H. *et al.* Lactobacillus capillatus sp. nov., a motile bacterium isolated from stinky tofu brine. *Int. J. Syst. Evol. Microbiol.* **58**, 2555–2559 (2008).

47. Leifson, E. Atlas of bacterial flagellation. *Atlas of bacterial flagellation* 171 https://www.cabdirect.org/cabdirect/abstract/19601101988 (1960).

48. Altegoer, F., Schuhmacher, J., Pausch, P. & Bange, G. From molecular evolution to biobricks and synthetic modules: a lesson by the bacterial flagellum. *Biotechnol. Genet. Eng. Rev.* **30**, 49–64 (2014).

49. Blair, D. F. Flagellar movement driven by proton translocation. *FEBS Lett.* **545**, 86–95 (2003).

50. McCarter, L. L. Dual Flagellar Systems Enable Motility under Different Circumstances. *Microb. Physiol.* **7**, 18–29 (2004).

51. Silhavy, T. J., Kahne, D. & Walker, S. The Bacterial Cell Envelope. *Cold Spring Harb. Perspect. Biol.* **2**, (2010).

52. Kan, W. & Wolgemuth, C. W. The Shape and Dynamics of the Leptospiraceae. *Biophys. J.* **93**, 54–61 (2007).

53. Dombrowski, C. *et al.* The elastic basis for the shape of Borrelia burgdorferi. *Biophys. J.* **96**, 4409–4417 (2009).

54. Charon, N. W., Greenberg, E. P., Koopman, M. B. H. H. & Limberger, R. J. Spirochete chemotaxis, motility, and the structure of the spirochetal periplasmic flagella. *Res. Microbiol.* **143**, 597–603 (1992).

55. Yamaichi, Y. *et al.* A multidomain hub anchors the chromosome segregation and chemotactic machinery to the bacterial pole. *Genes Dev.* **26**, 2348–2360 (2012).

56. Takekawa, N., Kwon, S., Nishioka, N., Kojima, S. & Homma, M. HubP, a Polar Landmark Protein, Regulates Flagellar Number by Assisting in the Proper Polar Localization of FlhG in Vibrio alginolyticus. *J. Bacteriol.* **198**, 3091–3098 (2016).

57. Rossmann, F. *et al.* The role of FlhF and HubP as polar landmark proteins in Shewanella putrefaciens CN-32. *Mol. Microbiol.* **98**, 727–742 (2015).

58. Wehbi, H. *et al.* The peptidoglycan-binding protein FimV promotes assembly of the Pseudomonas aeruginosa type IV pilus secretin. *J. Bacteriol.* **193**, 540–550 (2011).

59. Semmler, A. B. T., Whitchurch, C. B., Leech, A. J. & Mattick, J. S. Identification of a novel gene, fimV, involved in twitching motility in Pseudomonas aeruginosa. 1321–1332 (2000).

60. Wadhams, G. H. & Armitage, J. P. Making sense of it all: bacterial chemotaxis. *Nat. Rev. Mol. Cell Biol.* **5**, 1024–1037 (2004).

61. Kuhlen, L. *et al.* Structure of the core of the type iii secretion system export apparatus. *Nat. Struct. Mol. Biol.* **25**, 583–590 (2018).

62. Johnson, S. *et al.* Molecular structure of the intact bacterial flagellar basal body. *Nat. Microbiol.* **6**, 712 (2021).

63. Santiveri, M. *et al.* Structure and Function of Stator Units of the Bacterial Flagellar Motor. *Cell* **183**, 244-257.e16 (2020).

64. Erhardt, M., Namba, K. & Hughes, K. T. Bacterial nanomachines: the flagellum and type III injectisome. *Cold Spring Harb. Perspect. Biol.* **2**, 1–22 (2010).

65. Ueno, T., Oosawa, K. & Aizawa, S.-I. I. M ring, S ring and proximal rod of the flagellar basal body of Salmonella typhimurium are composed of subunits of a single protein, FliF. *J. Mol. Biol.* **227**, 672–677 (1992).

66. Galán, J. E., Lara-Tejero, M., Marlovits, T. C. & Wagner, S. Bacterial Type III Secretion Systems: Specialized Nanomachines for Protein Delivery into Target Cells. *http://dx.doi.org/10.1146/annurev-micro-092412-155725* **68**, 415–438 (2014).

67. Diepold, A. & Armitage, J. P. Type III secretion systems: the bacterial flagellum and the injectisome. *Philos. Trans. R. Soc. B Biol. Sci.* **370**, (2015).

68. Johnson, S. *et al.* Symmetry mismatch in the MS-ring of the bacterial flagellar rotor explains the structural coordination of secretion and rotation. *Nat. Microbiol.* **5**, 966–975 (2020).

69. Kubori, T., Shimamoto, N., Yamaguchi, S., Namba, K. & Aizawa, S. I. Morphological pathway of flagellar assembly in Salmonella typhimurium. *J. Mol. Biol.* **226**, 433–446 (1992).

70. Ueno, T., Oosawa, K. & Aizawa, S. I. Domain Structures of the MS Ring Component Protein (FliF) of the Flagellar Basal Body of Salmonella typhimurium. *J. Mol. Biol.* **236**, 546–555 (1994).

71. Thomas, D., Morgan, D. G. & DeRosier, D. J. Structures of bacterial flagellar motors from two FliF-FliG gene fusion mutants. *J. Bacteriol.* **183**, 6404–6412 (2001).

72. Grünenfelder, B., Gehrig, S. & Jena, U. Role of the cytoplasmic C terminus of the FliF motor protein in flagellar assembly and rotation. *J. Bacteriol.* **185**, 1624–1633 (2003).

73. Levenson, R., Zhou, H. & Dahlquist, F. W. Structural insights into the interaction between the bacterial flagellar motor proteins FliF and FliG. *Biochemistry* **51**, 5052–5060 (2012).

74. Ogawa, R., Abe-Yoshizumi, R., Kishi, T., Homma, M. & Kojima, S. Interaction of the C-Terminal Tail of FliF with FliG from the Na+-Driven Flagellar Motor of Vibrio alginolyticus. *J. Bacteriol.* **197**, 63 (2015).

75. Brown, P. N., Hill, C. P. & Blair, D. F. Crystal structure of the middle and C-terminal domains of the flagellar rotor protein FliG. *EMBO J.* **21**, 3225–3234 (2002).

76. Irikura, V. M., Kihara, M., Yamaguchi, S., Sockett, H. & Macnab, R. M. Salmonella typhimurium fliG and fliN mutations causing defects in assembly, rotation, and switching of the flagellar motor. *J. Bacteriol.* **175**, 802 (1993).

77. Kihara, M., Miller, G. U. & Macnab, R. M. Deletion analysis of the flagellar switch protein FliG of Salmonella. *J. Bacteriol.* **182**, 3022–3028 (2000).

78. Brown, P. N., Terrazas, M., Paul, K. & Blair, D. F. Mutational Analysis of the Flagellar Protein FliG: Sites of Interaction with FliM and Implications for Organization of the Switch Complex. *J. Bacteriol.* **189**, 305 (2007).

79. Paul, K., Harmon, J. G. & Blair, D. F. Mutational analysis of the flagellar rotor protein FliN: identification of surfaces important for flagellar assembly and switching. *J. Bacteriol.* **188**, 5240–5248 (2006).

80. Sarkar, M. K., Paul, K. & Blair, D. Chemotaxis signaling protein CheY binds to the rotor protein FliN to control the direction of flagellar rotation in Escherichia coli. *Proc. Natl. Acad. Sci. U. S. A.* **107**, 9370–9375 (2010).

81. Bren, A. & Eisenbach, M. The N terminus of the flagellar switch protein, FliM, is the binding domain for the chemotactic response regulator, CheY. *J. Mol. Biol.* **278**, 507–514 (1998).

82. De Mot, R. & Vanderleyden, J. The C-terminal sequence conservation between OmpA-related outer membrane proteins and MotB suggests a common function in both Gram-positive and Gram-negative bacteria, possibly in the interaction of these domains with peptidoglycan. *Mol. Microbiol.* **12**, 333–334 (1994).

83. Lloyd, S. A., Whitby, F. G., Blair, D. F. & Hill, C. P. Structure of the C-terminal domain of FliG, a component of the rotor in the bacterial flagellar motor. *Nat. 1999 4006743* **400**, 472–475 (1999).

84. Zhou, J., Lloyd, S. A. & Blair, D. F. Electrostatic interactions between rotor and stator in the bacterial flagellar motor. *Proc. Natl. Acad. Sci. U. S. A.* **95**, 6436–6441 (1998).

85. Schoenhals, G. J. & Macnab, R. M. FliL is a membrane-associated component of the flagellar

basal body of Salmonella. *Microbiology* **145**, 1769–1775 (1999).

86. Tachiyama, S. *et al.* The flagellar motor protein FliL forms a scaffold of circumferentially positioned rings required for stator activation. *Proc. Natl. Acad. Sci.* **119**, (2022).

87. Minamino, T. & Macnab, R. M. Components of the Salmonella flagellar export apparatus and classification of export substrates. *J. Bacteriol.* **181**, 1388–1394 (1999).

88. Fukumura, T. *et al.* Assembly and stoichiometry of the core structure of the bacterial flagellar type III export gate complex. *PLOS Biol.* **15**, e2002281 (2017).

89. Morimoto, Y. V. *et al.* Assembly and stoichiometry of FliF and FlhA in Salmonella flagellar basal body. *Mol. Microbiol.* **91**, 1214–1226 (2014).

90. Kuhlen, L. *et al.* The substrate specificity switch FlhB assembles onto the export gate to regulate type three secretion. *Nat. Commun.* **11**, 1–10 (2020).

91. Minamino, T. & Macnab, R. M. Domain Structure of *Salmonella* FlhB, a Flagellar Export Component Responsible for Substrate Specificity Switching. *J. Bacteriol.* **182**, 4906–4914 (2000).

92. Ferris, H. U. *et al.* FlhB Regulates Ordered Export of Flagellar Components via Autocleavage Mechanism. *J. Biol. Chem.* **280**, 41236–41242 (2005).

93. Morimoto, Y. V. *et al.* High-resolution pH imaging of living bacterial cells to detect local pH differences. *MBio* **7**, (2016).

94. Erhardt, M., Mertens, M. E., Fabiani, F. D. & Hughes, K. T. ATPase-Independent Type-III Protein Secretion in Salmonella enterica. *PLOS Genet.* **10**, e1004800 (2014).

95. Ward, E. *et al.* Type-III secretion pore formed by flagellar protein FliP. *Mol. Microbiol.* **107**, 94–103 (2018).

96. Minamino, T., Morimoto, Y. V., Hara, N., Aldridge, P. D. & Namba, K. The Bacterial Flagellar Type III Export Gate Complex Is a Dual Fuel Engine That Can Use Both H+ and Na+ for Flagellar Protein Export. *PLOS Pathog.* **12**, e1005495 (2016).

97. Bange, G. *et al.* FlhA provides the adaptor for coordinated delivery of late flagella building blocks to the type III secretion system. *Proc. Natl. Acad. Sci. U. S. A.* **107**, 11295–11300 (2010).

98. Müller, V., Jones, C. J., Kawagishi, I., Aizawa, S. & Macnab, R. M. Characterization of the fliE genes of Escherichia coli and Salmonella typhimurium and identification of the FliE protein as a component of the flagellar hook-basal body complex. *J. Bacteriol.* **174**, 2298–2304 (1992).

99. Saijo-Hamano, Y., Matsunami, H., Namba, K. & Imada, K. Architecture of the bacterial flagellar distal rod and hook of Salmonella. *Biomolecules* **9**, 1–11 (2019).

100. Minamino, T., Yamaguchi, S. & Macnab, R. M. Interaction between FliE and FlgB, a Proximal Rod Component of the Flagellar Basal Body of *Salmonella*. *J. Bacteriol.* **182**, 3029–3036 (2000).

101. Osorio-Valeriano, M., de la Mora, J., Camarena, L. & Dreyfus, G. Biochemical characterization of the flagellar rod components of Rhodobacter sphaeroides: Properties and interactions. *J. Bacteriol.* **198**, 544–552 (2016).

102. Nambu, T., Minamino, T., Macnab, R. M. & Kutsukake, K. Peptidoglycan-hydrolyzing activity of the FlgJ protein, essential for flagellar rod formation in Salmonella typhimurium. *J. Bacteriol.* **181**, 1555–1561 (1999).

103. Jones, C. J., Macnab, R. M., Okino, H. & Aizawa, S.-I. I. Stoichiometric analysis of the flagellar hook-(basal-body) complex of Salmonella typhimurium. *J. Mol. Biol.* **212**, 377–387 (1990).

104. Okino, H. *et al.* Release of flagellar filament-hook-rod complex by a Salmonella typhimurium mutant defective in the M ring of the basal body. *J. Bacteriol.* **171**, 2075–2082 (1989).

105. Jones, C. J. & Macnab, R. M. Flagellar assembly in Salmonella typhimurium: analysis with temperature-sensitive mutants. *J. Bacteriol.* **172**, 1327–1339 (1990).

106. Jones, C. J., Homma, M. & Macnab, R. M. Identification of proteins of the outer (L and P) rings of the flagellar basal body of Escherichia coli. *J. Bacteriol.* **169**, 1489–1492 (1987).

107. Imada, K. Bacterial flagellar axial structure and its construction. *Biophys. Rev.* **10**, 559 (2018).

108. Kühn, M. J. Screw thread motility of polarly flagellated bacteria enhances movement through structured environments. (2019).

109. Xie, L., Altindal, T., Chattopadhyay, S. & Wu, X. L. Bacterial flagellum as a propeller and as a rudder for efficient chemotaxis. *Proc. Natl. Acad. Sci. U. S. A.* **108**, 2246–2251 (2011).

110. Nord, A. L. *et al.* Dynamic stiffening of the flagellar hook. *Nat. Commun. 2022 131* **13**, 1–9 (2022).

111. Kato, T., Makino, F., Miyata, T., Horváth, P. & Namba, K. Structure of the native supercoiled flagellar hook as a universal joint. *Nat. Commun. 2019 101* **10**, 1–8 (2019).

112. Samatey, F. A. *et al.* Structure of the bacterial flagellar hook and implication for the molecular universal joint mechanism. *Nature* **431**, 1062–1068 (2004).

113. Evans, L. D. B., Hughes, C. & Fraser, G. M. Building a flagellum in biological outer space. *Microb. Cell* **1**, 64 (2014).

114. Hirano, T., Yamaguchi, S., Oosawa, K. & Aizawa, S. I. Roles of FliK and FlhB in determination of flagellar hook length in Salmonella typhimurium. *J. Bacteriol.* **176**, 5439–5449 (1994).

115. Fujii, T. *et al.* Identical folds used for distinct mechanical functions of the bacterial flagellar rod and hook. *Nat. Commun. 2017 81* **8**, 1–10 (2017).

116. Ohnishi, K., Ohto, Y., Aizawa, S. I., Macnab, R. M. & Iino, T. FlgD is a scaffolding protein needed for flagellar hook assembly in Salmonella typhimurium. *J. Bacteriol.* **176**, 2272 (1994).

117. Erhardt, M., Singer, H. M., Wee, D. H., Keener, J. P. & Hughes, K. T. An infrequent molecular ruler controls flagellar hook length in Salmonella enterica. *EMBO J.* **30**, 2948–2961 (2011).

118. Ikeda, T., Oosawa, K. & Hotani, H. Self-assembly of the filament capping protein, FliD, of bacterial flagella into an annular structure. *J. Mol. Biol.* **259**, 679–686 (1996).

119. Yonekura, K., Maki-Yonekura, S. & Namba, K. Complete atomic model of the bacterial flagellar filament by electron cryomicroscopy. *Nat. 2003 4246949* **424**, 643–650 (2003).

120. Lino, T. Assembly of Salmonella flagellin in vitro and in vivo. *J. Supramol. Struct.* **2**, 372–384 (1974).

121. Chen, M. *et al.* Length-dependent flagellar growth of vibrio alginolyticus revealed by real time fluorescent imaging. *Elife* **6**, (2017).

122. Sang, S. Y. & Mekalanos, J. J. Decreased potency of the Vibrio cholerae sheathed flagellum to trigger host innate immunity. **76**, 1282–1288 (2008).

123. Brennan, C. A. *et al.* A model symbiosis reveals a role for sheathed-flagellum rotation in the release of immunogenic lipopolysaccharide. *Elife* **3**, (2014).

124. Jones, G. W. & Freter, R. Adhesive properties of Vibrio cholerae: nature of the interaction with isolated rabbit brush border membranes and human erythrocytes. *Infect. Immun.* **14**, 240–245 (1976).

125. Sjoblad, R. D. & Doetsch, R. N. Adsorption of polarly flagellated bacteria to surfaces. *Curr. Microbiol.* **7**, 191–194 (1982).

126. Carpenter, P. B., Hanlon, D. W. & Ordal, G. W. flhF, a Bacillus subtilis flagellar gene that encodes a putative GTP-binding protein. *Mol. Microbiol.* **6**, 2705–2713 (1992).

127. Correa, N. E., Peng, F. & Klose, K. E. Roles of the Regulatory Proteins FlhF and FlhG in the Vibrio cholerae Flagellar Transcription Hierarchy. *J. Bacteriol.* **187**, 6324 (2005).

128. Balaban, M., Joslin, S. N. & Hendrixson, D. R. FlhF and Its GTPase Activity Are Required for

Distinct Processes in Flagellar Gene Regulation and Biosynthesis in Campylobacter jejuni. *J. Bacteriol.* **191**, (2009).

129. Li, X. *et al.* Investigating the role of BN-domains of FlhF involved in flagellar synthesis in Campylobacter jejuni. *Microbiol. Res.* **256**, 126944 (2022).

130. Bourne, H. R., Sanders, D. A. & McCormick, F. The GTPase superfamily: conserved structure and molecular mechanism. **349**, 117–127 (1991).

131. Bourne, H. R., Sanders, D. A. & McCormick, F. The GTPase superfamily: a conserved switch for diverse cell functions. *Nature* **348**, 125–132 (1990).

132. Bange, G. & Sinning, I. SIMIBI twins in protein targeting and localization. *Nat. Struct. Mol. Biol.* **20**, 776–780 (2013).

133. Bange, G., Wild, K. & Sinning, I. Protein Translocation: Checkpoint Role for SRP GTPase Activation. *Curr. Biol.* **17**, R980–R982 (2007).

134. Akopian, D., Shen, K., Zhang, X. & Shan, S. O. Signal Recognition Particle: An essential protein targeting machine. *Annu. Rev. Biochem.* **82**, 693 (2013).

135. Bange, G., Petzold, G., Wild, K., Parlitz, R. O. & Sinning, I. The crystal structure of the third signal-recognition particle GTPase FlhF reveals a homodimer with bound GTP. *Proc. Natl. Acad. Sci. U. S. A.* **104**, 13621–13625 (2007).

136. Green, J. C. D. D. *et al.* Recruitment of the Earliest Component of the Bacterial Flagellum to the Old Cell Division Pole by a Membrane-Associated Signal Recognition Particle Family GTP-Binding Protein. *J. Mol. Biol.* **391**, 679–690 (2009).

137. Bacher, G., Lütcke, H., Jungnickel, B., Rapoport, T. A. & Dobberstein, B. Regulation by the ribosome of the GTPase of the signal-recognition particle during protein targeting. *Nature* **381**, 248–251 (1996).

138. Freymann, D. M., Keenan, R. J., Stroud, R. M. & Walter, P. Structure of the conserved GTPase domain of the signal recognition particle. *Nat. 1997 3856614* **385**, 361–364 (1997).

139. Montoya, G., Svensson, C., Luirink, J. & Sinning, I. Crystal structure of the NG domain from the signal-recognition particle receptor FtsY. *Nat. 1997 3856614* **385**, 365–368 (1997).

140. Wittinghofer, A. & Vetter, I. R. Structure-Function Relationships of the G Domain, a Canonical Switch Motif. *http://dx.doi.org/10.1146/annurev-biochem-062708-134043* **80**, 943–971 (2011).

141. Bange, G. *et al.* Structural basis for the molecular evolution of SRP-GTPase activation by protein. *Nat. Struct. Mol. Biol.* **18**, 1376–1380 (2011).

142. Nagy, G. N. *et al.* Structural Characterization of Arginine Fingers: Identification of an Arginine Finger for the Pyrophosphatase dUTPases. *J. Am. Chem. Soc.* **138**, 15035–15045 (2016).

143. Voigts-Hoffmann, F. *et al.* The structural basis of FtsY recruitment and GTPase activation by SRP RNA. *Mol. Cell* **52**, 643 (2013).

144. Shan, S. O., Schmid, S. L. & Zhang, X. Signal recognition particle (SRP) and SRP receptor: A new paradigm for multi-state regulatory GTPases. *Biochemistry* **48**, 6696 (2009).

145. Egea, P. F. *et al.* Substrate twinning activates the signal recognition particle and its receptor. *Nature* **427**, 215–221 (2004).

146. Shan, S. O., Stroud, R. M. & Walter, P. Mechanism of Association and Reciprocal Activation of Two GTPases. *PLoS Biol.* **2**, (2004).

147. Focia, P. J., Shepotinovskaya, I. V., Seidler, J. A. & Freymann, D. M. Heterodimeric GTPase Core of the SRP Targeting Complex. *Science* **303**, 373 (2004).

148. Dong, H.-J., Shen, X.-L., Li, Y.-D. & Li, Y.-Q. Functional Characterization of Streptomyces coelicolor FtsY. *Protein Pept. Lett.* **14**, 341–345 (2007).

149. Sprang, S. R. G protein mechanisms: Insights from structural analysis. *Annu. Rev. Biochem.* **66**,

639–678 (1997).

150. Terashima, H. *et al.* Assembly mechanism of a supramolecular MS-ring complex to initiate bacterial flagellar biogenesis in Vibrio species. *J. Bacteriol.* **202**, (2020).

151. Millikan, D. S. & Ruby, E. G. FlrA, a σ54-Dependent Transcriptional Activator in Vibrio fischeri, Is Required for Motility and Symbiotic Light-Organ Colonization. *J. Bacteriol.* **185**, 3547 (2003).

152. Jagannathan, A., Constantinidou, C. & Penn, C. W. Roles of rpoN, fliA, and flgR in expression of flagella in Campylobacter jejuni. *J. Bacteriol.* **183**, 2937–2942 (2001).

153. Tsang, J. & Hoover, T. R. Themes and Variations: Regulation of RpoN-Dependent Flagellar Genes across Diverse Bacterial Species. *Scientifica (Cairo).* **2014**, 1–14 (2014).

154. Arroyo-Pérez, E. E. & Ringgaard, S. Interdependent Polar Localization of FlhF and FlhG and Their Importance for Flagellum Formation of Vibrio parahaemolyticus. (2021) doi:10.3389/fmicb.2021.655239.

155. Nascimento dos Santos, R. *et al.* Characterization of C-ring component assembly in flagellar motors from amino acid coevolution. *R. Soc. Open Sci.* **5**, (2018).

156. Rowlett, V. W. & Margolin, W. The Min system and other nucleoid-independent regulators of Z ring positioning. *Front. Microbiol.* **6**, 478 (2015).

157. Blagotinsek, V. *et al.* An ATP-dependent partner switch links flagellar C-ring assembly with gene expression. *Proc. Natl. Acad. Sci. U. S. A.* **117**, 20826–20835 (2020).

158. Schuhmacher, J. S. *et al.* MinD-like ATPase FlhG effects location and number of bacterial flagella during C-ring assembly. *Proc. Natl. Acad. Sci. U. S. A.* **112**, 3092–7 (2015).

159. Gulbronson, C. J. *et al.* FlhG employs diverse intrinsic domains and influences FlhF GTPase activity to numerically regulate polar flagellar biogenesis in Campylobacter jejuni. *Mol. Microbiol.* **99**, 291–306 (2016).

160. Shan, S.-O. ATPase and GTPase Tangos Drive Intracellular Protein Transport. (2016) doi:10.1016/j.tibs.2016.08.012.

161. Dasgupta, N. & Ramphal, R. Interaction of the antiactivator FleN with the transcriptional activator FleQ regulates flagellar number in Pseudomonas aeruginosa. *J. Bacteriol.* **183**, 6636–6644 (2001).

162. Jain, R. & Kazmierczak, B. I. A Conservative Amino Acid Mutation in the Master Regulator FleQ Renders Pseudomonas aeruginosa Aflagellate. *PLoS One* **9**, e97439 (2014).

163. Kondo, S., Homma, M. & Kojima, S. Analysis of the GTPase motif of FlhF in the control of the number and location of polar flagella in Vibrio alginolyticus. *Biophys. Physicobiology* **14**, 173–181 (2017).

164. Minamino, T., Iino, T. & Kutsukake, K. Molecular characterization of the Salmonella typhimurium flhB operon and its protein products. *J. Bacteriol.* **176**, 7630–7637 (1994).

165. Meshcheryakov, V. A., Barker, C. S., Kostyukova, A. S. & Samatey, F. A. Function of FlhB, a Membrane Protein Implicated in the Bacterial Flagellar Type III Secretion System. *PLoS One* **8**, 1–13 (2013).

166. Zarivach, R. *et al.* Structural analysis of the essential self-cleaving type III secretion proteins EscU and SpaS. *Nat. 2008 4537191* **453**, 124–127 (2008).

167. Evans, L. D. B., Poulter, S., Terentjev, E. M., Hughes, C. & Fraser, G. M. A chain mechanism for flagellum growth. *Nature* **504**, 287 (2013).

168. Inoue, Y., Kinoshita, M., Namba, K. & Minamino, T. Mutational analysis of the C-terminal cytoplasmic domain of FlhB, a transmembrane component of the flagellar type III protein export apparatus in Salmonella. *Genes to Cells* **24**, 408–421 (2019).

169. Kodera, N., Uchida, K., Ando, T. & Aizawa, S. I. Two-Ball Structure of the Flagellar Hook-Length

Control Protein FliK as Revealed by High-Speed Atomic Force Microscopy. *J. Mol. Biol.* **427**, 406–414 (2015).

170.   Ho, O. *et al.* Characterization of the Ruler Protein Interaction Interface on the Substrate Specificity Switch Protein in the Yersinia Type III Secretion System. *J. Biol. Chem.* **292**, 3299–3311 (2017).

171.   Kinoshita, M., Aizawa, S. I., Inoue, Y., Namba, K. & Minamino, T. The role of intrinsically disordered C-terminal region of FliK in substrate specificity switching of the bacterial flagellar type III export apparatus. *Mol. Microbiol.* **105**, 572–588 (2017).

172.   Minamino, T. Hierarchical protein export mechanism of the bacterial flagellar type III protein export apparatus. *FEMS Microbiol. Lett.* **365**, 1–9 (2018).

173.   Fraser, G. M. *et al. Substrate specificity of type III flagellar protein export in Salmonella is controlled by subdomain interactions in FlhB. Molecular Microbiology* vol. 48 (2003).

174.   Hirano, T., Mizuno, S., Aizawa, S. I. & Hughes, K. T. Mutations in Flk, FlgG, FlhA, and FlhE that affect the flagellar type III secretion specificity switch in Salmonella enterica. *J. Bacteriol.* **191**, 3938–3947 (2009).

175.   Williams, K. P. *et al.* Phylogeny of Gammaproteobacteria. *J. Bacteriol.* **192**, 2305–2314 (2010).

176.   Fredrickson, J. K. *et al.* Biogenic iron mineralization accompanying the dissimilatory reduction of hydrous ferric oxide by a groundwater bacterium. *Geochim. Cosmochim. Acta* **62**, 3239–3257 (1998).

177.   Min, M., Xu, H., Chen, J. & Fayek, M. Evidence of uranium biomineralization in sandstone-hosted roll-front uranium deposits, northwestern China. *Ore Geol. Rev.* **26**, 198–206 (2005).

178.   Wu, X. *et al.* Shewanella putrefaciens CN32 outer membrane cytochromes MtrC and UndA reduce electron shuttles to produce electricity in microbial fuel cells. *Enzyme Microb. Technol.* **115**, 23–28 (2018).

179.   Bubendorfer, S. *et al.* Specificity of motor components in the dual flagellar system of Shewanella putrefaciens CN-32. *Mol. Microbiol.* **83**, 335–350 (2012).

180.   Bubendorfer, S., Koltai, M., Rossmann, F., Sourjik, V. & Thormann, K. M. Secondary bacterial flagellar system improves bacterial spreading by increasing the directional persistence of swimming. *Proc. Natl. Acad. Sci. U. S. A.* **111**, 11485–90 (2014).

181.   Svenningsen, N. B. *et al.* Pseudomonas putida mt-2 tolerates reactive oxygen species generated during matric stress by inducing a major oxidative defense response. *BMC Microbiol.* **15**, 202 (2015).

182.   Regenhardt, D. *et al.* Pedigree and taxonomic credentials of Pseudomonas putida strain KT2440. *Environ. Microbiol.* **4**, 912–915 (2002).

183.   Bultreys, A., Gheysen, I., Maraite, H. & De Hoffmann, E. Characterization of Fluorescent and Nonfluorescent Peptide Siderophores Produced by Pseudomonas syringae Strains and Their Potential Use in Strain Identification. *Appl. Environ. Microbiol.* **67**, 1718 (2001).

184.   Harwood, C. S., Fosnaugh, K. & Dispensa, M. Flagellation of Pseudomonas putida and analysis of its motile behavior. *J. Bacteriol.* **171**, 4063 (1989).

185.   Navarrete, B. *et al.* Transcriptional organization, regulation and functional analysis of flhF and fleN in Pseudomonas putida. *PLoS One* **14**, e0214166 (2019).

186.   Bouteiller, M. *et al.* Pseudomonas flagella: Generalities and specificities. *Int. J. Mol. Sci.* **22**, 1–28 (2021).

187.   Dasgupta, N., Arora, S. K. & Ramphal, R. fleN, a gene that regulates flagellar number in Pseudomonas aeruginosa. *J. Bacteriol.* **182**, 357–364 (2000).

188.   Pandza, S. *et al.* The G-protein FlhF has a role in polar flagellar placement and general stress response induction in Pseudomonas putida. **36**, 414–423 (2000).

189. Kusumoto, A. *et al.* Regulation of polar flagellar number by the flhF and flhG genes in Vibrio alginolyticus. *J. Biochem.* **139**, 113–121 (2006).

190. Kusumoto, A. *et al.* Collaboration of FlhF and FlhG to regulate polar-flagella number and localization in Vibrio alginolyticus. *Microbiology* **154**, 1390–1399 (2008).

191. Macnab, R. M. How Bacteria Assemble Flagella. *Annu. Rev. Microbiol.* **57**, 77–100 (2003).

192. Cross, T. *et al.* Spheroplast-mediated carbapenem tolerance in Gram-negative pathogens. *Antimicrob. Agents Chemother.* **63**, (2019).

193. Tanaka, M., Ueno, Y., Miyake, T., Sakuma, T. & Okochi, M. Enrichment of membrane curvature-sensing proteins from Escherichia coli using spherical supported lipid bilayers. *J. Biosci. Bioeng.* **133**, 98–104 (2022).

194. Kürner, J., Frangakis, A. S. & Baumeister, W. Cryo-electron tomography reveals the cytoskeletal structure of Spiroplasma melliferum. *Science (80-.).* **307**, 436–438 (2005).

195. Favini-Stabile, S., Contreras-Martel, C., Thielens, N. & Dessen, A. MreB and MurG as scaffolds for the cytoplasmic steps of peptidoglycan biosynthesis. *Environ. Microbiol.* **15**, 3218–3228 (2013).

196. Briegel, A. *et al.* Multiple large filament bundles observed in Caulobacter crescentus by electron cryotomography. *Mol. Microbiol.* **62**, 5–14 (2006).

197. Nanninga, N. Cell Structure, Organization, Bacteria and Archaea. *Ref. Modul. Biomed. Sci.* (2014) doi:10.1016/B978-0-12-801238-3.02309-6.

198. Prouty, M. G., Correa, N. E. & Klose, K. E. The novel sigma54- and sigma28-dependent flagellar gene transcription hierarchy of Vibrio cholerae. *Mol. Microbiol.* **39**, 1595–609 (2001).

199. Moisi, M. *et al.* A novel regulatory protein involved in motility of Vibrio cholerae. *J. Bacteriol.* **191**, 7027–7038 (2009).

200. Williams, A. W. *et al.* Mutations in fliK and flhB affecting flagellar hook and filament assembly in Salmonella typhimurium. *J. Bacteriol.* **178**, 2960–2970 (1996).

201. Miller, V. L. & Mekalanos, J. J. A novel suicide vector and its use in construction of insertion mutations: osmoregulation of outer membrane proteins and virulence determinants in Vibrio cholerae requires toxR. *J. Bacteriol.* **170**, 2575 (1988).

202. Rossmann, F. M. *et al.* The GGDEF Domain of the Phosphodiesterase PdeB in Shewanella putrefaciens Mediates Recruitment by the Polar Landmark Protein HubP. *J. Bacteriol.* **201**, (2019).

203. Nelson, K. E. *et al.* Complete genome sequence and comparative analysis of the metabolically versatile Pseudomonas putida KT2440. *Environ. Microbiol.* **4**, 799–808 (2002).

204. Lassak, J., Henche, A. L., Binnenkade, L. & Thormann, K. M. ArcS, the Cognate Sensor Kinase in an Atypical Arc System of Shewanella oneidensis MR-1. *Appl. Environ. Microbiol.* **76**, 3263 (2010).

205. Karimova, G., Pidoux, J., Ullmann, A. & Ladant, D. A bacterial two-hybrid system based on a reconstituted signal transduction pathway. *Proc. Natl. Acad. Sci. U. S. A.* **95**, 5752–5756 (1998).

206. Kühn, M. J. *et al.* Spatial arrangement of several flagellins within bacterial flagella improves motility in different environments. (2018) doi:10.1038/s41467-018-07802-w.

207. Schindelin, J. *et al.* Fiji: an open-source platform for biological-image analysis. *Nat. Methods* **9**, 676–682 (2012).

208. Hartmann, R., van Teeseling, M. C. F., Thanbichler, M. & Drescher, K. BacStalk: A comprehensive and interactive image analysis software tool for bacterial cell biology. *Mol. Microbiol.* **114**, 140–150 (2020).

209. Laemmli, U. K. Cleavage of structural proteins during the assembly of the head of bacteriophage

T4. *Nature* **227**, 680–5 (1970).

210. Neuhoff, V., Arold, N., Taube, D. & Ehrhardt, W. Improved staining of proteins in polyacrylamide gels including isoelectric focusing gels with clear background at nanogram sensitivity using Coomassie Brilliant Blue G-250 and R-250. *Electrophoresis* **9**, 255–262 (1988).

211. Waterhouse, A. M., Procter, J. B., Martin, D. M. A., Clamp, M. & Barton, G. J. Jalview Version 2-A multiple sequence alignment editor and analysis workbench. *Bioinformatics* **25**, 1189–1191 (2009).

212. Altschul, S. F., Gish, W., Miller, W., Myers, E. W. & Lipman, D. J. Basic local alignment search tool. *J. Mol. Biol.* **215**, 403–410 (1990).

213. Berezin, C. *et al.* ConSeq: the identification of functionally and structurally important residues in protein sequences. *Bioinformatics* **20**, 1322–1324 (2004).

214. Sievers, F. *et al.* Fast, scalable generation of high-quality protein multiple sequence alignments using Clustal Omega. *Mol. Syst. Biol.* **7**, 539 (2011).

215. Schultz, J., Milpetz, F., Bork, P. & Ponting, C. P. SMART, a simple modular architecture research tool: Identification of signaling domains. *Proc. Natl. Acad. Sci. U. S. A.* **95**, 5857–5864 (1998).

216. Blom, J. *et al.* EDGAR: A software framework for the comparative analysis of prokaryotic genomes. (2009) doi:10.1186/1471-2105-10-154.